DI Stefan Krahulec

Enzymology and metabolic engineering of sugar/polyol metabolism in yeast and fungi

Characterization of the system of mannitol dehydrogenases in the human pathogen *Aspergillus fumigatus*, and metabolic pathway engineering for xylose fermentation in *Saccharomyces cerevisiae*

DISSERTATION

zur Erlangung des akademischen Grades eines
Doktor der technischen Wissenschaften

erreicht an der

Technischen Universität Graz

betreut durch:
Univ.-Prof. DI Dr. Bernd Nidetzky
Institut für Biotechnologie und Bioprozesstechnik
Technische Universität Graz

2010

Graz University of Technology

EIDESSTATTLICHE ERKLÄRUNG

Ich erkläre an Eides statt, dass ich die vorliegende Arbeit selbstständig verfasst, andere als die angegebenen Quellen/Hilfsmittel nicht benutzt, und die den benutzten Quellen wörtlich und inhaltlich entnommene Stellen als solche kenntlich gemacht habe.

Graz, am 14.04.2010 ……..
(Unterschrift)

STATUTORY DECLARATION

I declare that I have authored this thesis independently, that I have not used other than the declared sources / resources, and that I have explicitly marked all material which has been quoted either literally or by content from the used sources.

04.14.2010 ……..
(signature)

Acknowledgment

First of all I want to express my gratitude to my supervisor Bernd Nidetzky for providing the topic of this work and excellent mentoring throughout this thesis. I very much appreciate his passion and outstanding approaches in scientific research and his tireless and invaluable support in the composition of scientific articles.

I would like to thank Mario Klimacek for his support as a co-supervisor as well as for excellent collaboration during the preparation of my thesis. Special thanks go to Karin Longus and Valentin Pacher who largely contributed to the generation of data presented herein. I am thankful to Barbara Petschacher and Guilliano Armao for previous work done in the field of xylose fermentation and mannitol metabolism of *A. fumigatus*, respectively. I am grateful to Hansjörg Weber for fruitful collaboration. My sincere thanks go to Mario Müller and Regina Kratzer for scientific and even more for less scientific discussions that brightened up some of my working days. Moreover, I want to thank all members of the Institute of Biotechnology and Biochemical Engineering for the marvelous working atmosphere.

Financial support from the Austrian Science Fund FWF (P18275-B09) is gratefully acknowledged.

Most of all I thank Elisabeth for her loving support and her encouragement in less successful moments of my research. Last but not least I would like to thank my parents and my grandfather for their continuous support and their faith in me.

Abstract

Polyol metabolism has a multitude of physiological functions in fungi, ranging from carbohydrate storage to protection against various stress conditions. It is exploited in numerous biotechnological processes in which microorganisms convert sugars into value-added products. This thesis reports on results of studies on the enzymology of mannitol metabolism in the human pathogenic mold *Aspergillus fumigatus* as well as metabolic engineering to diminish by-product formation in xylose fermentation with recombinant *S. cerevisiae*.

Mannitol metabolism in fungi branches off from glycolysis at fructose 6-phosphate (Fru6*P*), which is converted to mannitol 1-phosphate by a mannitol-1-phosphate 5-dehydrogenase (M1PDH) and further dephosphorylated to mannitol. Catabolism can occur by inversion of this pathway or by oxidation of mannitol to fructose by a mannitol 2-dehydrogenase (M2DH). The polyol-specific long-chain dehydrogenases M2DH and M1PDH from *A. fumigatus* were produced recombinantly in *E. coli* and purified to apparent homogeneity. Detailed biochemical characterizations of the enzymes were performed focusing on substrate specificity and on the kinetic mechanism employing steady-state kinetic analysis for the reaction with unlabeled and deuterium-labeled substrates and coenzymes. Kinetic properties imply that reduction of Fru6*P* with M1PDH is the primary route of mannitol anabolism, while M2DH works in the thermodynamically unfavorable direction of mannitol oxidation *in vivo*.

Xylose fermentation for bio-ethanol production from agricultural waste with *S. cerevisiae* involves introduction of a two step oxidoreductive pathway that converts xylose into xylulose, which is a natural substrate of bakers yeast while xylose is not. Low ethanol yields and high by-product formation (especially xylitol) were ascribed to the different cofactor specificities of the two recombinant enzymes involved. Xylose reductases (XR) prefer NADPH, while

xylitol dehydrogenases (XDH) are NAD^+-dependent. Protein engineering was used to alter the coenzyme specificity of XDH from *Galactocandida mastotermitis*. Combinations of a XDH mutant with suitable variants of the XR from *Candida tenuis* yielded strains in which coenzyme usage by XR and XDH is well balanced. Strain evaluation was carried out in anaerobic bioreactor fermentations, operated in batch or fed-batch mode. Distribution of fermentation products indicates that coenzyme recycling in the steps catalyzed by XR and XDH is a prerequisite for efficient xylose fermentation but is not sufficient for complete suppression of xylitol production.

Zusammenfassung

Polyolmetabolismus hat bei Pilzen viele physiologische Funktionen wie Kohlenhydratspeicherung und Schutz vor Stressfaktoren. In biotechnologischen Prozessen kann dessen Unterdrückung zur Optimierung der Produktausbeute wünschenswert sein. Diese Arbeit berichtet Forschungsergebnisse zur Enzymologie des Mannitolmetabolismus von *Aspergillus fumigatus* und zur Verringerung der Nebenproduktbildung in der Xylosefermentation mit rekombinanter *S. cerevisiae*.

Mannitolmetabolismus in Pilzen erfolgt durch Reduktion von Fruktose-6-Phosphat zu Mannitol-1-Phosphat durch eine Mannitol-1-Phosphat 5-Dehydrogenase (M1PDH) und anschließender Dephosphorylierung zu Mannitol. Der Katabolismus kann durch die Umkehr dieses Weges erfolgen oder durch die Oxidation von Mannitol zu Fruktose mittels einer Mannitol 2-Dehydrogenase (M2DH). Die polyolspezifischen langkettigen Dehydrogenasen M2DH und M1PDH aus *A. fumigatus* wurden rekombinant in *E. coli* hergestellt und gereinigt. Die biochemische Charakterisierung der Enzyme wurde mit Fokus auf Substratspezifität und den kinetischen Mechanismus durch Messungen im Fließgleichgewichtszustand mit unmarkierten und Deuterium-markierten Substraten und Coenzymen durchgeführt. Die kinetischen Eigenschaften implizieren einen Anabolismus von Mannitol primär über die Reduktion von Fruktose-6-Phosphat mittels M1PDH. Die M2DH arbeitet im Organismus hingegen in Mannitoloxidationsrichtung.

Die Xylosefermentation zur Bioethanolproduktion aus Agrarabfällen mittels *S. cerevisiae* erfordert die Integration eines zweistufigen oxidoreduktiven Stoffwechselwegs zur Isomerisierung von Xylose zu Xylulose, welche im Gegensatz zur Xylose ein natürliches Substrat der Bäckerhefe ist. Niedrige Ethanol- und hohe Nebenprodukterträge (v.a. Xylitol) wurden den unterschiedlichen Cofaktorspezifitäten der rekombinanten Enzyme zugeschrieben. Xylosereduktasen (XR) bevorzugen NADPH, während

Xylitoldehydrogenasen (XDH) NAD^+ abhängig sind. Die Cofaktorspezifität der XDH von *Galactocandida mastotermitis* wurde durch Proteinengineering verändert. Die Kombination einer XDH Mutante mit Mutanten der *Candida tenuis* XR ergab Stämme mit einer ausbalancierten Coenzymverwendung von XR und XDH. Die Charakterisierung der Stämme wurde durch anaerobe Bioreaktorfermentationen sowohl im Batch- als auch im Fed-Batch-Betrieb durchgeführt. Die Verteilung der Fermentationsprodukte zeigt, dass die Coenzymregenerierung zwischen XR und XDH eine Voraussetzung für die effiziente Xylosefermentation darstellt, aber nicht ausreichend ist, um eine Xylitolproduktion gänzlich zu unterdrücken.

Table of Contents

Chapter I

Characterization of the system of mannitol dehydrogenases in the human pathogen *Aspergillus fumigatus*

The 6-carbon polyol mannitol is ubiquitous throughout the fungal kingdom and is attributed to be an essential factor of the parasitic lifestyle of several fungal pathogens. The role of mannitol in the protection of fungal parasites against reactive oxygen species generated by infected hosts has caused revived interest in metabolism of this sugar alcohol[1]. The human pathogenic mold *Aspergillus fumigatus* is known to produce enough of this polyol to increase the serum mannitol level of infected animals[2]. However, little is known about mannitol metabolism in *A. fumigatus* and the enzymes involved have not been studied so far.

The proposed routes for mannitol metabolism in fungi involve reduction of D-fructose 6-phosphate (Fru6*P*) to D-mannitol 1-phosphate (Man-ol1*P*) catalyzed by a mannitol-1-phosphate 5-dehydrogenase (M1PDH) und subsequent dephosphorylation to D-mannitol or reduction of D-fructose to D-mannitol by a mannitol 2-dehydrogenase (M2DH). The M2DH and M1PDH from *A. fumigatus* (*Af*M2DH, *Af*M1PDH) were cloned from genomic DNA, expressed in *E. coli a*nd the recombinant proteins were purified to apparent homogeneity. The enzymes displayed the predicted enzymatic functions interconverting fructose to mannitol (*Af*M2DH) and Fru6*P* to Man-ol1*P* (*Af*M1PDH). As expected for members of the family of polyol-specific long-chain dehydrogenases/reductases (PSLDR) both enzymes are monomers in solution (*Af*M2DH ~58 kDa, *Af*M1PDH ~44 kDa), do not require (divalent) metal ions for activity and exhibit a strong preference for NAD^+ over $NADP^+$ (~1000-fold for *Af*M2DH and ~3000-fold for *Af*M1PDH in terms of $k_{cat}/K_{coenzyme}$). Among PSLDRs a conserved lysine (Lys^{213} in *Af*M1PDH) was proposed to serve a role as a general acid-base catalyst for the NAD(H) dependent interconversion of a carbonyl group into a hydroxyl group. Its presumed

key catalytic function was verified for *Af*M1PDH by the substitution of this lysine-residue against an alanine and a concomitant $10^{3.8}$-fold loss of activity. pH profiles for the ketone reduction and alcohol oxidation under substrate saturating (k_{cat}) and substrate limiting ($k_{cat}/K_{substrate}$) conditions with *Af*M2DH and *Af*M1PDH are in line with a key catalytic function of the conserved lysine. However, the complex pH-profiles of *Af*M2DH and *Af*M1PDH clearly indicate that more than one ionizable group is involved in substrate binding and/or catalysis. The k_{cat} profile was usually different from the $k_{cat}/K_{substrate}$ profile, suggesting that more than one step of the enzymatic mechanism is affected by changes in pH. For *Af*M2DH the complex pH profiles might be a reflection of the occurrence of polar amino acids in immediate vicinity of the catalytic lysine.

Detailed kinetic analysis of the reaction mechanism of *Af*M2DH at neutral pH, including primary kinetic isotope effects (KIE), indicates a sequential reaction mechanism where substrate binding and product release occur in a random fashion. For the reduction of fructose the hydride transfer step clearly contributes to the rate limiting step while the rate of mannitol oxidation is strongly governed by the rate of product dissociation. Inhibition studies with adenine nucleotides revealed that the *in vivo* activity of *Af*M2DH is not controlled by the cellular energy charge. It is suggested that *Af*M2DH works in the thermodynamically unfavorable direction of alcohol oxidation under *in vivo* conditions. Besides its activity towards mannitol and fructose *Af*M2DH showed significant activity with the substrate pairs D-arabitol/D-xylulose and D-sorbitol/L-sorbose. The 5-fold higher catalytic efficiency with xylulose than with fructose and the absence of a distinct D-arabitol 4-dehydrogenase proposes a catalytic function of *Af*M2DH in the D-arabitol metabolism of *A. fumigatus*.

Since Man-ol1*P* is a quite costly compound and the synthesis of 5-[²H]-Man-ol1*P* had not been described previously, synthesis of these compounds was a prerequisite for detailed kinetic characterization of *Af*M1PDH. A coupled enzymatic system employing purified formate dehydrogenase from *Candida boidinii* and *Af*M1PDH was used for a NADH

mediated hydrogen transfer from formate or *deuterio* formate to Fru6*P* to yield Man-ol1*P* or the 5-[²H] derivative thereof. Subsequent precipitation as barium salts of *protio* and *deuterio* forms of Man-ol1*P* gave isolated yields of ~90% with purities >95%. Employing the synthesized 5-[²H]-Man-ol1*P* for the reduction of NAD^+ with *Af*M1PDH demonstrated that *Af*M1PDH specifically catalyzes hydrogen transfer to and from the 4*S* position of the nicotinamide moiety of NADH. A high KIE of ~3 on the k_{cat} of Man-ol1*P* oxidation indicates that the hydride transfer is strongly rate determining for the overall reaction rate of Man-ol1*P* oxidation at pH 7.1. In the reverse direction of Fru6*P* reduction product release is strongly rate determining. A sequential reaction mechanism is suggested in which the binding of Fru6*P* and NADH is ordered while the release of Man-ol1*P* and NAD^+ is random and most likely occurs in rapid equilibrium. Kinetic data and thermodynamics of the interconversion of Fru6*P* and Man-ol1*P* with NAD(H) point towards an *in vivo* catalytic function of *Af*M1PDH as a reductase, suggesting that anabolism of mannitol is primarily achieved through the reduction of Fru6*P*. As found for *Af*M2DH the cellular energy charge has no regulatory control on the activity of *Af*M1PDH. However, the presence of intracellular concentrations of adenine nucleotides might half the reaction rate of Man-ol1*P* oxidation. A comparably high thermostability of *Af*M1PDH is in accordance with its recently reported induction under heat shock and might indicate a central role of *Af*M1PDH and hence mannitol production in the stress response of *A. fumigatus*[3].

1. Solomon, P. S.; Waters, O. D.; Oliver, R. P., Decoding the mannitol enigma in filamentous fungi. *Trends Microbiol.* **2007,** 15, (6), 257-62.
2. Wong, B.; Brauer, K. L.; Tsai, R. R.; Jayasimhulu, K., Increased amounts of the *Aspergillus* metabolite D-mannitol in tissue and serum of rats with experimental aspergillosis. *J. Infect. Dis.* **1989,** 160, (1), 95-103.
3. Albrecht, D.; Guthke, R.; Brakhage, A. A.; Kniemeyer, O., Integrative analysis of the heat shock response in *Aspergillus fumigatus*. *BMC Genomics* **2010,** 11, 32.

Available online at www.sciencedirect.com
ScienceDirect
Carbohydrate Research 343 (2008) 1414–1423
Chapter 1.1
Carbohydrate RESEARCH

Characterization of recombinant *Aspergillus fumigatus* mannitol-1-phosphate 5-dehydrogenase and its application for the stereoselective synthesis of *protio* and *deuterio* forms of D-mannitol 1-phosphate

Stefan Krahulec,[a] Guilliano C. Armao,[a] Hansjörg Weber,[b] Mario Klimacek[a,*] and Bernd Nidetzky[a,*]

[a]*Institute of Biotechnology and Biochemical Engineering, Graz University of Technology, Petersgasse 12/I, A-8010 Graz, Austria*
[b]*Institute of Organic Chemistry, Graz University of Technology, Stremayrgasse 16, A-8010 Graz, Austria*

Received 1 February 2008; received in revised form 2 April 2008; accepted 4 April 2008
Available online 10 April 2008

Abstract—A putative long-chain mannitol-1-phosphate 5-dehydrogenase from *Aspergillus fumigatus* (*Af*M1PDH) was overexpressed in *Escherichia coli* to a level of about 50% of total intracellular protein. The purified recombinant protein was a ≈40-kDa monomer in solution and displayed the predicted enzymatic function, catalyzing NAD(H)-dependent interconversion of D-mannitol 1-phosphate and D-fructose 6-phosphate with a specific reductase activity of 170 U/mg at pH 7.1 and 25 °C. NADP(H) showed a marginal activity. Hydrogen transfer from formate to D-fructose 6-phosphate, mediated by NAD(H) and catalyzed by a coupled enzyme system of purified *Candida boidinii* formate dehydrogenase and *Af*M1PDH, was used for the preparative synthesis of D-mannitol 1-phosphate or, by applying an analogous procedure using *deuterio* formate, the 5-[^{2}H] derivative thereof. Following the precipitation of D-mannitol 1-phosphate as barium salt, pure product (>95% by HPLC and NMR) was obtained in isolated yields of about 90%, based on 200 mM of D-fructose 6-phosphate employed in the reaction. In situ proton NMR studies of enzymatic oxidation of D-5-[^{2}H]-mannitol 1-phosphate demonstrated that *Af*M1PDH was stereospecific for transferring the deuterium to NAD^+, producing (4*S*)-[^{2}H]-NADH. Comparison of maximum initial rates for NAD^+-dependent oxidation of *protio* and *deuterio* forms of D-mannitol 1-phosphate at pH 7.1 and 25 °C revealed a primary kinetic isotope effect of 2.9 ± 0.2, suggesting that the hydride transfer was strongly rate-determining for the overall enzymatic reaction under these conditions.

Keywords: D-Mannitol 1-phosphate; D-5-[^{2}H]-Mannitol 1-phosphate; Mannitol-1-phosphate 5-dehydrogenase; *Aspergillus fumigatus*; Biocatalysis; Stereoselective synthesis

1. Introduction

D-Mannitol is one of the most abundant sugar alcohols in nature and ubiquitous throughout the fungal kingdom. Recent evidence supporting a role of mannitol as stress metabolite in the parasitic lifestyle of different fungi has rekindled the interest in the physiological functions fulfilled by mannitol in lower and higher eukaryotes.[1] *Aspergillus niger* utilizes mannitol to protect its conidiospores against the exogenous stress resulting from high temperatures and an oxidative environment.[2] The ability of mannitol to scavenge reactive oxygen species (ROS) is exploited by the human pathogen *Cryptococcus neoformans* and the tobacco pathogen *Alternaria alternata* to suppress the host defense strategies that are based on the generation of ROS against the microbial parasite.[3,4] The wheat pathogen *Stagonospora nodorum* requires mannitol for asexual sporulation.[5] The human pathogen *Aspergillus fumigatus*, which is the most common etiologic agent

* Corresponding authors. Tel.: +43 316 873 8400; fax: +43 316 873 8434 (B.N.); e-mail: bernd.nidetzky@TUGraz.at

0008-6215/$ - see front matter © 2008 Elsevier Ltd. All rights reserved.
doi:10.1016/j.carres.2008.04.011

for invasive aspergillosis in immunosuppressed hosts, produces and releases sufficient amounts of mannitol to raise serum mannitol levels of infected animals.[6,7] Therefore, these findings suggest that the metabolism of mannitol might be a viable target for the development of novel antifungal strategies. The primary biosynthetic route towards mannitol in *Aspergilli* and other fungi is the reduction of D-fructose 6-phosphate (Fru6*P*) to D-mannitol 1-phosphate (Man-ol1*P*) catalyzed by mannitol-1-phosphate 5-dehydrogenase (M1PDH). Man-ol1*P* is subsequently dephosphorylated to mannitol.

According to similarity at the level of the amino acid sequence, almost all the known fungal M1PDHs are classified as polyol-specific long-chain dehydrogenases and reductases (PSLDRs).[8] The PSLDRs constitute a distinct evolutionary lineage of $NAD(P)^+$-dependent secondary alcohol dehydrogenases. These do not require a metal cofactor such as Zn^{2+} for catalysis and are usually active as monomers.[9] The molecular size of PSLDRs varies between 380 and 550 residues, whereby M1PDHs constitute the smallest members of the family. Structure-based sequence analysis has revealed that the currently classified PSLDRs share a common structural organization where the active site is located in a cleft formed by an N-terminal Rossmann-fold coenzyme binding domain and a largely α-helical domain that provides key elements of substrate binding recognition and catalysis. With the exception of the early studies of the enzyme from *A. niger*, little is currently known about the relationships of structure and function of M1PDHs from fungi.[10]

In this paper, we report on the biochemical characterization of a recombinant M1PDH from the human pathogenic mold *A. fumigatus* (*Af*M1PDH, EC 1.1.1.17). Assuming that mannitol constitutes a relevant pathogenic factor of *A. fumigatus*, the biosynthetic M1PDH is a potential drug target. M1PDH-directed inhibition of the microbial parasite should be selective considering that there are no PSLDR orthologues in the human genome. Detailed study of *Af*M1PDH is therefore not only of physiological interest but could also eventually gain a clinical importance.

The analysis of the primary kinetic isotope effect (KIE) resulting from the deuteration of the substrate has provided a valuable insight into the kinetic and catalytic mechanisms utilized by several $NAD(P)^+$-dependent dehydrogenases.[11] The application of a similar KIE strategy to examine *Af*M1PDH requires the synthesis of *protio* and *deuterio* forms of Man-ol1*P*. We describe an enzymatic method (Scheme 1) that allows the preparation of both substrates in high purity and yield. To our knowledge, 5-[^{2}H]-Man-ol1*P* has not been reported in the literature so far.

2. Results and discussion

2.1. Cloning and expression of a putative M1PDH from *A. fumigatus*

The whole genome shotgun sequence of *A. fumigatus* shows an open-reading frame that encodes a putative M1PDH (UniProt/TrEMBL entry Q4X1A4).[12] Because the coding region of the *Af*M1PDH gene is not interrupted by introns, it was possible to amplify the entire gene directly from genomic DNA of *A. fumigatus*. The PCR product thus obtained had the expected size of 1187 bp and was cloned into a pQE-70 plasmid expression vector. The recombinant protein contained at its N-terminus an additional leucine after the initiator methionine that was introduced with the oligonucleotide primer used for PCR. Furthermore, a peptide of eight amino acids (-Arg-Ser-His_6) was fused to the C-terminal end of the protein to facilitate purification. Heterologous

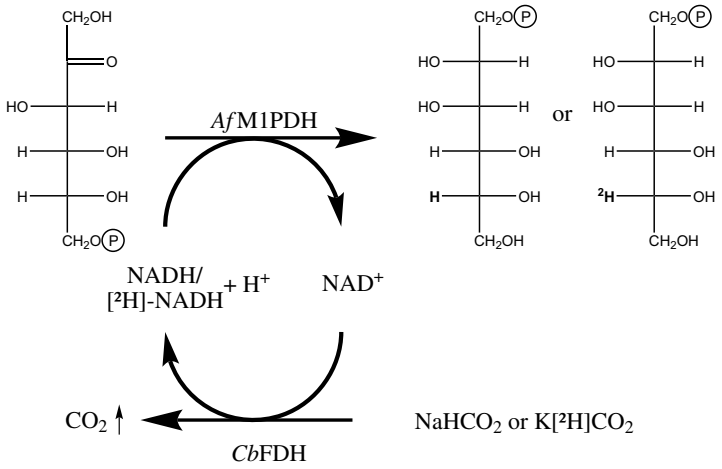

Scheme 1. Enzymatic synthesis of Man-ol1*P* and 5-[^{2}H]-Man-ol1*P* using the coupled enzyme system *Af*M1PDH and *Candida boidinii* formate dehydrogenase (*Cb*FDH).

expression of the *Af*M1PDH gene was carried out in *E. coli* JM109. SDS PAGE of crude bacterial cell extracts revealed an abundant protein band at the position corresponding to the expected molecular mass of ≈44 kDa for the recombinant protein (data not shown). The comparison of specific M1PDH activities in the cell extract (80 U/mg) and the purified enzyme (170 U/mg) indicated that the *Af*M1PDH accounted for about 50% of the total intracellular protein in *E. coli*.

2.2. Purification, and molecular and kinetic characterization of *Af*M1PDH

*Af*M1PDH was purified to apparent homogeneity by a single step of column chromatography, using copper-loaded Chelating Sepharose. A balance of the purification with respect to protein and enzyme activity is given in Table 1. The isolated enzyme migrated as a single protein band in SDS PAGE (Fig. 1). In size exclusion chromatography, it was eluted in a single peak that corresponded to the molecular mass of about 40 kDa and contained all the applied protein and enzyme activity. Therefore, this result suggests that *Af*M1PDH is a functional monomer, like other PSLDRs that have been characterized at the protein level.

The purified *Af*M1PDH displayed the predicted enzymatic function. It showed a specific activity of 169 ± 4 U/mg for the reduction of Fru6*P* by NADH at pH 7.1. In the direction of NAD^+-dependent oxidation of Man-ol1*P* (100 mM glycine/NaOH buffer, pH 10.0), the specific activity was 17.6 ± 1.4 U/mg. Note that the pH values of measurement were chosen in a suitable pH range for mannitol oxidation and fructose reduction (data not shown). Using the same reaction conditions, the specific enzyme activities for Fru6*P* reduction by 0.2 mM NADPH and Man-ol1*P* oxidation by 2.0 mM $NADP^+$ were 0.58 ± 0.05 U/mg and 0.08 ± 0.01 U/mg, respectively. However, it must be emphasized that *Af*M1PDH could not be saturated with reduced and oxidized phosphorylated coenzyme in the steady state, suggesting that the presence of the 2′-phosphate of NADP(H) strongly decreased the binding affinity for the coenzyme.

Michaelis–Menten constants for the reduction of Fru6*P* by NADH and the oxidation of Man-ol1*P* by NAD^+ were determined at neutral pH and are summarized in Table 2. Under the conditions used, the turnover number (k_{cat}) for the direction of Fru6*P* reduction was about 10 times that for the direction of Man-ol1*P* oxidation. The K_m value for NADH was less than one tenth that for NAD^+. By contrast, apparent binding affinity ($1/K_m$) for Man-ol1*P* was higher than that for Fru6*P*. The catalytic efficiencies (k_{cat}/K_m) for reactions with Fru6*P* ($5.9 \times 10^4\ M^{-1}\ s^{-1}$) and Man-ol1*P* ($3.8 \times 10^4\ M^{-1}\ s^{-1}$) in the presence of a saturating concentration of coenzyme were therefore in the same range.

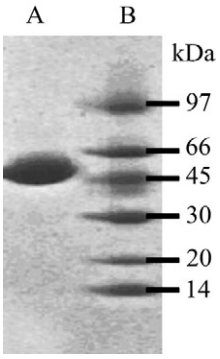

Figure 1. SDS PAGE of purified *Af*M1PDH: (A) *Af*M1PDH purified by metal affinity chromatography; (B) Low molecular weight standard (GE Healthcare).

Table 2. Kinetic constants for purified *Af*M1PDH at 25 °C

	$K_{substrate}$ (mM)	$K_{cofactor}$ (mM)	k_{cat} (s^{-1})
Man-ol1*P*	0.23 ± 0.02	0.75 ± 0.09	8.5 ± 0.4
Fru6*P*	2.1 ± 0.2	0.016 ± 0.001	125 ± 3

Man-ol1*P* oxidation and Fru6*P* reduction were measured in 100 mM Tris/HCl buffer, pH 7.1. See Section 3 for the concentrations of substrates and coenzymes used.

Kinetic data obtained with *Af*M1PDH are well comparable with those for the M1PDH from *A. niger* reported by Kiser and Niehaus.[10] Like *Af*M1PDH, the enzyme from *A. niger* shows a large preference (⩾1000-fold) for the reaction with NAD(H) as compared to NADP(H). The K_m values for substrates and coenzymes are similar for both fungal M1PDHs. The M1PDH from *Escherichia coli* is also a monomer in solution and like the fungal enzymes, it has a higher affinity for NADH than for NAD^+ at neutral pH.[13] It prefers NAD^+ more than 100-fold over $NADP^+$, and its activity appeared to be independent of a metal cofactor.[14]

Table 1. Purification of recombinant *Af*M1PDH expressed in *E. coli*

Purification stage	Total activity (U)	Protein (mg/mL)	Specific activity (U/mg)	Total yield (%)	Purification factor
Crude extract	28 000	50	80	100	1
Affinity chromatography	24 000	4	135	86	1.7
Desalting	21 600	11	169	77	2.1

Results are based on processing 2 g moist bacterial biomass. The *Af*M1PDH activity was assayed in the direction of Fru6*P* reduction at 25 °C using 100 mM Tris/HCl buffer, pH 7.1. The concentrations of Fru6*P* and NADH were 50 mM and 0.2 mM, respectively.

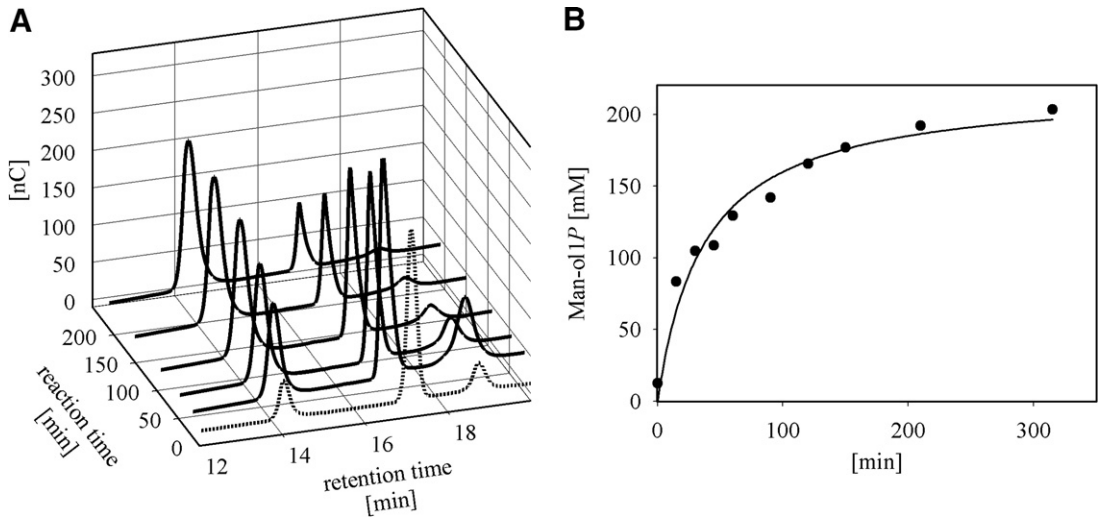

Figure 2. Enzymatic synthesis of Man-ol1*P* monitored by HPAE-PAD: (A) Dashed line: Superimposed traces of authentic standards of Man-ol1*P* (13.7 min), Glc6*P* (16.7 min) and Fru6*P* (18.4 min); Solid lines: Chromatograms for the first 210 min of Man-ol1*P* production from Fru6*P* using *Cb*FDH fraction I for cofactor recycling; (B) time course of Man-ol1*P* production from 200 mM Fru6*P*. The solid line indicates the trend of the data.

Membership of *Af*M1PDH to the PSLDR protein family leads to the suggestion that the catalytic activity of the enzyme is not dependent on a metal cofactor. To verify the structure-derived implication, we incubated purified *Af*M1PDH (0.27 μg/mL) in the presence of 100 mM EDTA for 1 h at room temperature and assayed at various times the residual activity of the enzyme in the direction of Fru6*P* reduction. No loss of activity was observed relative to a control in which EDTA was lacking, as expected for a metal-independent enzyme.

2.3. Enzymatic synthesis of D-mannitol 1-phosphate and 5-[^{2}H]-D-mannitol 1-phosphate

Previously reported routes for the chemical synthesis of Man-ol1*P* started from mannose 6-phosphate or mannitol.[10,15,16] A major drawback of using mannose 6-phosphate is the high cost of the substrate. Phosphorylation of mannitol was performed with phosphorylchloride in pyridinic solution. It required harsh reaction conditions and consumed large amounts of organic solvents. A heterogeneous mixture of mannitol-phosphates was obtained from which 90% pure Man-ol1*P* was recovered through a laborious re-crystallization procedure. The overall yield was therefore only ≈9%.[17] None of the described methods provide a direct access to the deuterated analogue of Man-ol1*P*.

We therefore designed a new synthetic route that is summarized in Scheme 1 and can be flexibly applied for the preparation of Man-ol1*P* or 5-[^{2}H]-Man-ol1*P*. A bi-enzymatic system constituted of *Af*M1PDH and formate dehydrogenase from *Candida boidinii* (*Cb*FDH) was employed. *Af*M1PDH catalyzes the desired synthetic reaction transforming Fru6*P* into Man-ol1*P* via NADH-dependent reduction, and the regeneration of NADH is achieved via NAD^+-dependent oxidation of formate into CO_2 catalyzed by *Cb*FDH.

A typical time course of synthesis of Man-ol1*P* by the coupled action of dehydrogenases is summarized in Figure 2. We used a 2.5-fold excess of *Cb*FDH activity (5 U/mL) over *Af*M1PDH activity (2 U/mL) to ensure that a substantial portion of the total coenzyme, which was added as NAD^+ at the start of the reaction (0.5 mM), was present in the required reduced form. Furthermore, a slight molar excess of formate (250 mM) over Fru6*P* (200 mM) was chosen to ensure the complete conversion of ketose substrate into product. A partially purified preparation of *Cb*FDH with a specific activity of 1.4 U/mg was used in the reaction. High performance anion exchange chromatography with pulsed amperometric detection (HPAE-PAD) was employed for monitoring the progress of the reaction, as shown in panel A of Figure 2. Under the conditions used, more than 99% of the initial Fru6*P* was converted into Man-ol1*P*. Panel B of Figure 2 shows the time course of Man-ol1*P* production. The workup of Man-ol1*P* included the removal of the enzymes by ultrafiltration as the first step. Further purification targeted the elimination of NAD(H) because the contamination of the product with coenzyme could interfere with the planned enzyme kinetic measurements. Because anion exchange chromatography on a MonoQ 5/50 GL (GE Healthcare) column was not successful, we focused on selective precipitation of Man-ol1*P* as barium salt. A screening of conditions for the recovery of product in the highest possible purity revealed that the addition of an equal volume of EtOH to the reaction mixture facilitated precipitation of Man-ol1*P* while NAD(H) and residual formate were retained in the supernatant. After washing and drying the precipitate, Man-ol1*P* was obtained in an isolated yield of 90% and a purity

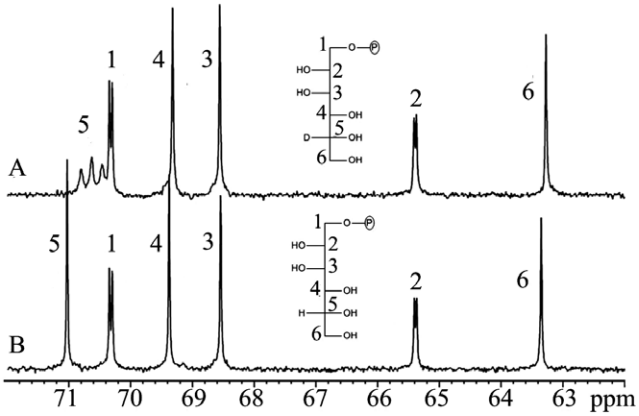

Figure 3. ^{13}C spectra of D-5-[^{2}H]-mannitol 1-phosphate (A) and D-mannitol 1-phosphate (B).

of >95% (determined by HPAE-PAD and NMR). Using NMR analysis, neither NAD^{+} nor NADH could be detected in the isolated product. A possible contamination of the product by Fru6*P*, D-glucose 6-phosphate (Glc6*P*), formate, mannitol, and fructose was ruled out within the limits of detection of the used HPAE-PAD and NMR methods. A ^{13}C NMR spectrum of the final product is shown in Figure 3.

Inspection of the HPAE-PAD traces in Figure 2A shows that immediately after the start of the reaction, a new compound was formed which according to its retention time (16.7 min) could be clearly distinguished from Man-ol1*P* and was identified as Glc6*P*. The Glc6*P* gradually disappeared as the production of Man-ol1*P* progressed. Because no Glc6*P* was added with the substrate, the results imply the presence of an isomerase activity that reversibly interconverts Fru6*P* and Glc6*P*. The only possible source for this activity was the partially purified *Cb*FDH. We therefore measured the activity of phosphoglucose isomerase (PGI) in the used preparation of *Cb*FDH and the *E. coli* cell extract from which it was obtained. The results summarized in Table 3 show that the heat treatment employed in the purification of *Cb*FDH only partially eliminated the PGI activity present in the starting material. A useful consequence of the PGI activity carried over with the *Cb*FDH preparation was that Glc6*P*, which is cheaper than Fru6*P*, could be employed as a substrate for the synthesis of Man-ol1*P* without affecting negatively the space-time yield of the reaction as well as the yield and purity of the final product.

Substitution of formate by [^{2}H]-formate as reductant for the enzymatic conversion of Fru6*P* was expected to provide convenient access to the deuterated analogue of Man-ol1*P*, namely 5-[^{2}H]-D-mannitol 1-phosphate (5-[^{2}H]-Man-ol1*P*). Using reaction conditions otherwise identical to those for Man-ol1*P* production, we observed the complete conversion of ketose substrate but only partial (≈2/3) deuteration of position C–5 in the isolated Man-ol1*P* product. Because the deuterium label in the commercial [^{2}H]-formate had been verified by NMR spectroscopy. We examined rigorously the role of the purity of *Cb*FDH, using for 5-[^{2}H]-Man-ol1*P* synthesis each of the different enzyme preparations shown in Table 3. The highly purified *Cb*FDH obtained after anion exchange chromatography (Fig. 4) was required to synthesize 5-[^{2}H]-Man-ol1*P* with a high degree of deuterium labeling. The isotopic purity of the isolated product was estimated by NMR to be >95% ^{2}H (Fig. 3). To our knowledge, the synthesis of 5-[^{2}H]-Man-ol1*P* has not been reported so far.

We asked the question of whether a causal relationship exists between the removal of PGI activity from the *Cb*FDH preparation and the enhancement of deuterium label in the 5-[^{2}H]-Man-ol1*P* product. A deuterium

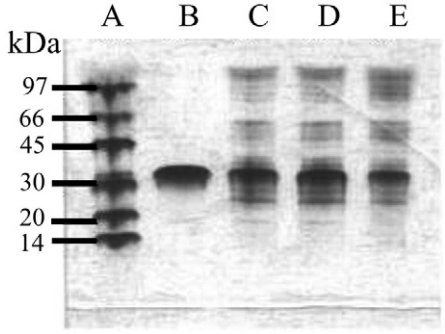

Figure 4. *Cb*FDH purification documented by SDS PAGE analysis: (A) low molecular weight standard (GE Healthcare); (B) purified *Cb*FDH obtained after anion exchange chromatography (fraction III); (C) preparation after heat treatment and desalting (fraction II); (D) preparation after heat treatment (fraction I); (E) crude *E. coli* cell extract.

Table 3. Purification of recombinant *Cb*FDH

Purification stage	Total activity FDH (U)	Protein (mg/mL)	Specific activity FDH (U/mg)	Total yield FDH (%)	Purification factor FDH	Total activity PGI (U)	Specific activity PGI (U/mg)
Crude extract	249	40.6	1.0	100	1.0	317	1.2
Heat denaturation	185	6.4	1.4	74	1.5	232	1.8
Desalting	153	9.4	1.4	62	1.5	203	1.9
Q-Sepharose FF	131	5.22	4.4	53	4.5	<0.06	<0.002

Results are based on processing 3.3 g wet cells of *E. coli*. Desalting was performed by separating the total amount of protein in two batches which was necessary due to the high concentration of formate carried over from the heat treatment. The activities of *Cb*FDH and PGI were assayed as described under Section3.

wash-out experiment was performed in which the completely deuterated 5-[^{2}H]-Man-ol1*P* (75 mM) was incubated at room temperature and pH 7.5 in the presence of the PGI-containing standard preparation of *Cb*FDH (obtained after heat treatment) or a commercial PGI from baker's yeast. Incubation with 2.3 U PGI/mL was done for 22 h and the product was isolated as described above. No deuterium wash-out was observed within the limits of experimental error of ^{13}C NMR analysis. Further examination of the interesting reaction that leads to partial deuteration of Man-ol1*P* was beyond the remit of this study and is left for consideration in the future.

2.4. Stereochemical course of hydrogen transfer catalyzed by *Af*M1PDH

NAD(P)$^+$-dependent dehydrogenases are usually highly stereoselective with regard to transfer of hydrogen from the prochiral C–4 of the nicotinamide moiety of NADH or NADPH. These are classified according to stereochemical preference as pro-*R* or pro-*S* specific. To determine the stereochemical course of the reaction catalyzed by *Af*M1PDH, we incubated the purified enzyme in the presence of 5-[^{2}H]-Man-ol1*P* and NAD$^+$ and monitored by using in situ ^{1}H NMR analysis the formation of the deuterated, hence chiral NADH product. The results in Figure 5 reveal that (4*S*)-[^{2}H]-NADH was produced upon the enzymatic oxidation of 5-[^{2}H]-Man-ol1*P*. The stereoselectivity of the reduction of NAD$^+$ was absolute within the limits of detection of the chosen analytical method. Therefore, these results imply that the *Af*M1PDH belongs to the group of pro-*S* specific dehydrogenases, a functional classification that the fungal enzyme shares with M1PDHs from the bacteria *Aerobacter aerogenes* and *E. coli*.[9,18,19] The stereoselectivity of biocatalytic hydrogen transfer to NAD$^+$ reflects the relative orientation of substrate and coenzyme upon their binding to the enzyme. It is dictated by the protein structure and therefore expected to be conserved among evolutionary related dehydrogenases. The pro-*S* stereoselectivity of *Af*M1PDH is consistent with the proposed membership of the enzyme to the family of PSLDRs.[20,21]

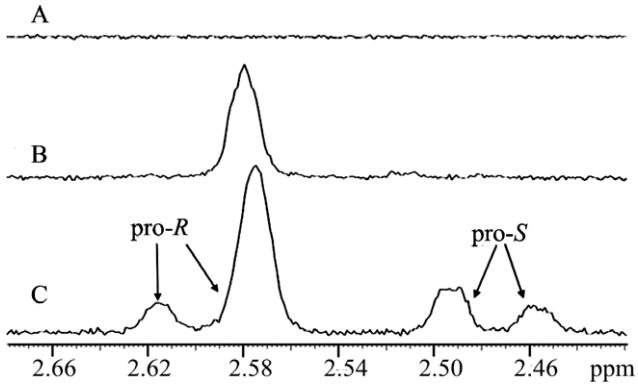

Figure 5. Stereospecificity of hydrogen transfer to the nicotinamide moiety of NAD(H) catalyzed by *Af*M1PDH: (A) 5-[^{2}H]-Man-ol1*P* and NAD$^+$ before enzymatic conversion; (B) formation of (4*S*)-[^{2}H]-NADH after enzymatic reaction for 30 min; incubations in (A) and (B) were carried out using 2 mM NAD$^+$, 5 mM 5-[^{2}H]-Man-ol1*P* in 30 mM Tris/HCl, p^{2}H 7.1; (C) formation of NADH and (4*S*)-[^{2}H]-NADH after 15 min of enzymatic reaction using 5 mM NAD$^+$ and 5 mM of a 2:1 mixture of 5-[^{2}H]-Man-ol1*P*/Man-ol1*P* in 50 mM Tris/HCl, p^{2}H 9.8.

2.5. KIE on NAD$^+$-dependent enzymatic oxidation of D-mannitol 1-phosphate

Figure 6 compares time courses of the enzymatic oxidation of Man-ol1*P* and 5-[^{2}H]-Man-ol1*P* obtained under conditions in which the concentrations of the substrate (6 mM) and NAD$^+$ (6 mM) were saturating in the steady state and therefore maximum initial rates (V_{max}) are measured. It shows that substrate deuteration caused a significant slowing down of the reaction catalyzed by *Af*M1PDH. Because the molar enzyme concentration was identical in the two experiments, the slopes of linear plots of the concentration of reduced coenzyme against the reaction time could be directly used to calculate the KIE, which is the ratio of the slopes measured with *protio* and *deuterio* substrate and had a value of 2.9 ± 0.2. The degree of rate reduction expressed in the value of KIE depends on how much the isotope-sensitive step of hydride transfer contributes to the overall reaction. Under the V_{max} conditions used, the substrate binding steps are not relevant kinetically. However, microscopic reaction steps comprised in the value of V_{max} include kinetic isomerizations of substrate-bound enzyme forms, the chemical conversion steps, and the release of product and NADH to regenerate the free enzyme. The dissociation of the NAD(P)H product constitutes the rate-determining step in reactions catalyzed by many

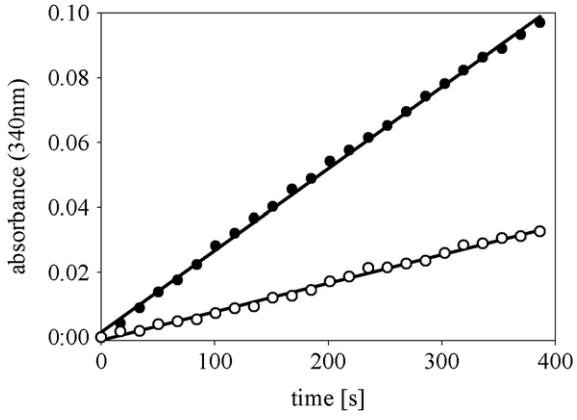

Figure 6. Primary deuterium isotope effect on k_{cat} of Man-ol1*P*/5-[^{2}H]-Man-ol1*P* oxidation: initial rates of Man-ol1*P* oxidation (●) and 5-[^{2}H]-Man-ol1*P* oxidation (○). The concentrations of substrate and NAD$^+$ were 6 mM each.

$NAD(P)^+$-dependent dehydrogenases, reflected by a KIE on V_{max} that is equal to or not much larger than unity.[11] In *Af*M1PDH, by contrast, the chemical step of hydride transfer strongly governs the maximum rate of Man-ol1*P* oxidation by NAD^+ at pH 7.1.

Summarizing, we have functionally expressed the M1PDH from *A. fumigatus* in *E. coli* and performed a biochemical characterization of the recombinant enzyme. A new method of synthesis of Man-ol1*P* and its *deuterio* analogue 5-[^{2}H]-Man-ol1*P* was established. Using the KIE approach thus made possible, we determined that hydride transfer to NAD^+ is a slow step in the overall oxidation of Man-ol1*P* and product release is not rate-determining.

3. Experimental

3.1. Materials

Fructose 6-phosphate (Fru6*P*), D-mannitol 1-phosphate (Man-ol1*P*), β-nicotinamide adenine dinucleotides ($NAD(P)^+$, NAD(P)H), sodium formate, potassium [^{2}H]-formate, salts and buffer reagents were from Sigma–Aldrich (St. Louis, MO, USA). T4-Ligase, restriction enzymes and *Taq* DNA polymerases were from Fermentas (Burlington, Canada). The pQE70-vector was obtained from Qiagen (Hilden, Germany). PWO-polymerase was a product of PEQLAB (Erlangen, Germany). Oligonucleotides were obtained from VBC-Biotech (Vienna, Austria). Genomic DNA of *A. fumigatus* was kindly provided by Dr. Hubertus Haas (Division of Molecular Biology, Medical University of Innsbruck, Austria).

3.2. D-Mannitol 1-phosphate

Enzymatic conversion of Fru6*P* or Glc6*P* (200 mM) to Man-ol1*P* was carried out in a 30 mM Tris/HCl buffer, pH 7.5, containing 250 mM sodium formate, 0.5 mM NAD^+, 5 U/mL partially purified *Cb*FDH (fraction I; see Section 3.6), and 2 U/mL purified *Af*M1PDH. Enzyme activities of *Cb*FDH (NAD^+-dependent oxidation of formate) and *Af*M1PDH (NADH-dependent reduction of Fru6*P*) were measured at 25 °C under conditions in which the concentrations of substrate and coenzyme were saturating (*Cb*FDH: 250 mM formate, 2 mM NAD^+; *Af*M1PDH: 50 mM Fru6*P*, 0.2 mM NADH). The enzyme assays were performed in 30 mM Tris/HCl, pH 7.5.

The synthesis of Man-ol1*P* was carried out in a batch reaction at room temperature, typically for 20 h. The working volume was 10 mL. The pH of the reaction was controlled at a value of 7.5 through the addition of diluted HCl. Gentle mixing with a magnetic stirrer was used before taking samples or while adjusting the pH. A pH of 7.5 was chosen because both *Af*M1PDH and *Cb*FDH show good activity and stability under these conditions. After the reaction, enzymes were removed by ultrafiltration using Vivaspin 6 MWCO 10 kDa microconcentrator tubes (Sartorius AG, Goettingen, Germany) at 4500 g. Man-ol1*P* was precipitated through the addition of an equimolar amount of $BaSO_4$ followed by the dilution of the reaction mixture with the same volume of absolute EtOH. Precipitation was allowed to proceed for 2 h at 4 °C. The precipitate was collected by filtration and washed exhaustively with absolute EtOH. The barium salt of Man-ol1*P* was dried over night at 40 °C. ^{1}H NMR (D_2O): ppm 3.81 (m, 2H), 3.71 (m, 2H), 3.63 (m, 3H), 3.49 (dd, 1H, J_1 11.7 Hz, J_2 5.3 Hz); ^{13}C NMR (D_2O): ppm 71.0 (C-5), 70.3 (C-1, d, J_{C-P} 5.8 Hz), 69.4 (C-4), 68.5 (C-3), 65.4 (C-2, d, J_{C-P} 4.8 Hz), 63.4 (C-6). The isolated product showed the same retention time in HPAE-PAD (13.7 min) as the authentic Man-ol1*P* standard obtained from Sigma–Aldrich.

3.3. 5-[^{2}H]-D-Mannitol 1-phosphate

The synthesis of 5-[^{2}H]-Man-ol1*P* used the analogous procedure employed for the production of Man-ol1*P* except that potassium [^{2}H]-formate served as the reductant and a purified preparation of *Cb*FDH (fraction III; see Section 3.6) was utilized. ^{1}H NMR (D_2O): ppm 3.81 (m, 2H), 3.71 (m, 2H), 3.63 (m, 2H), 3.49 (d, 1H, *J* 11.7 Hz); ^{13}C NMR (D_2O): 70.6 (C-5, t, J_{C-D} 22.5 Hz), 70.3 (C-1, d, J_{C-P} 5.8 Hz), 69.3 (C-4), 68.6 (C-3), 65.4 (C-2, d, J_{C-P} 4.8 Hz), 63.3 (C-6). The 5-[^{2}H]-Man-ol1*P* eluted in HPAE-PAD at the same retention time (13.7 min) as the authentic Man-ol1*P* standard.

3.4. Analytical methods

3.4.1. Protein analysis. Purification of *Cb*FDH and *Af*M1PDH was monitored by SDS PAGE using the Phast System (GE Healthcare, Chalfont St. Giles, United Kingdom). Staining of protein bands was done with Coomassie Brilliant Blue. Size exclusion chromatography of purified *Af*M1PDH was carried out on a Superdex 200 HR 10/30 gel filtration column (GE Healthcare). The column was calibrated with a gel filtration standard from Bio-Rad Laboratories (Hercules, USA).

3.4.2. Assays. Photometric measurements were carried out with a DU800 spectrophotometer from Beckman Coulter Inc. (Fullerton, CA, USA). The activities of *Cb*FDH and *Af*M1PDH were determined from initial rate measurements in which the production or consumption of NADH at a wavelength of 340 nm ($\varepsilon = 6.22\ cm^{-1}\ mM^{-1}$) was measured. Unless otherwise indicated, the activity of *Af*M1PDH was assayed at 25 °C either in the direction of NADH-dependent reduction of Fru6*P* using a 100 mM Tris/HCl buffer, pH 7.1,

or in the direction of NAD^+-dependent oxidation of Man-ol1*P* using a 100 mM glycine/NaOH buffer, pH 10.0. The concentrations of Fru6*P* and NADH were 50 mM and 0.2 mM, respectively. The concentrations of Man-ol1*P* and NAD^+ were 0.5 mM and 2 mM, respectively. The activity of *Cb*FDH was assayed in the direction of NAD^+-dependent oxidation of formate at 30 °C using 100 mM potassium phosphate buffer, pH 7.5. The concentrations of formate and NAD^+ were 162 mM and 2 mM, respectively.

PGI activity was measured in a coupled enzymatic assay at 30 °C essentially as described by Ruijter and Visser except that *Af*M1PDH was used instead of the M1PDH from *A. nidulans*.[22] The principle of the assay is that Glc6*P* is isomerised by PGI to Fru6*P*, which is in turn reduced by *Af*M1PDH. Therefore, PGI activity is measured as the decrease in the absorbance of NADH at 340 nm. The assay was performed in 100 mM potassium phosphate buffer, pH 7.5, and contained 20 mM Glc6*P*, ≈4 U/mL *Af*M1PDH, and 0.2 mM NADH.

Protein concentrations were measured with the Bio-Rad Protein Assay, which is based on the method of Bradford and was calibrated against BSA.[23] Man-ol1*P* and 5-[^{2}H]-Man-ol1*P* were quantified enzymatically using *Af*M1PDH in 100 mM glycine/NaOH buffer, pH 10.0, containing 2 mM NAD^+. Concentrations were calculated from the formed NADH using appropriate calibration of the assay with authentic Man-ol1*P* in the range of 0.04–0.20 mM.

3.4.3. Carbohydrate analysis. High performance anion exchange chromatography with pulsed amperometric detection (HPAE-PAD) was utilized to measure the concentration of Fru6*P*, Glc6*P*, and Man-ol1*P* or 5-[^{2}H]-Man-ol1*P* in samples taken from enzymatic conversions. The analysis was performed using a Dionex BioLC system (Dionex Corporation, Sunnyvale, CA, USA) equipped with a CarboPac PA10 column (4 × 250 mm) and an Amino Trap guard column (4 × 50 mm) thermostated at 30 °C. Phosphorylated sugars were detected with an ED50A electrochemical detector using a gold working electrode and a silver/silver chloride reference electrode by applying the predefined waveform for carbohydrates. Elution was carried out at a flow rate of 1 mL/min based on a previously described method with a linear gradient from 50 to 275 mM NaOAc applied within 22 min in an isocratic background of 4 mM NaOH.[24] Column was flushed 5 min with 800 mM NaOAc (+4 mM NaOH) and 15 min with the starting conditions before the next sample was injected.

3.4.4. NMR. Measurements were carried out on a Varian INOVA 500 MHz spectrometer (Varian Inc., Palo Alto, CA, USA) at 22 °C in D_2O (99.9% D) using the VNMR 6.1c software. ^{1}H NMR spectra were measured at 499.98 MHz and ^{13}C NMR at 125.69 MHz. For ^{13}C NMR spectra of Man-ol1*P* and 5-[^{2}H]-Man-ol1*P* 15 000 scans were accumulated and 1 Hz line broadening was used for sensitivity enhancement prior to Fourier transformation. Enzymatic conversions of NAD^+ (2 mM or 5 mM) into [^{2}H]-NADH and NADH with *Af*M1PDH (≈1 μM) using Man-ol1*P*/5-[^{2}H]-Man-ol1*P* (5 mM) in 30 mM Tris/HCl, p^{2}H 7.1, or 50 mM Tris/HCl, p^{2}H 9.8, were performed directly in the NMR sample tube, which is placed in the magnet. Proton NMR spectra were recorded by acquiring 30272 data points and accumulation of 200 scans.

3.5. Gene cloning, and production and purification of recombinant *Af*M1PDH

The intron-less open-reading frame encoding *Af*M1PDH was amplified from genomic DNA of *A. fumigatus Af*293 using PCR with PWO-polymerase and the following pair of oligonucleotide primers:

forward primer: 5′-GATCTAGCATGCTAGGAAAG-AAGGCTATCCAGTTTG-3′,
reverse primer: 5′-GATCTAAGATCTCTTGCTGTC-CTTCTGCACCTT-3′.[12]

The PCR product was digested with SphI and BglII and inserted into the plasmid vector pQE70 previously treated with the same restriction enzymes. The obtained construct was transformed into *E. coli* JM109. Cells harboring pQE70-*Af*M1PDH were cultivated at 37 °C in LB-Lennox-medium containing 115 mg/L ampicillin. Expression of recombinant *Af*M1PDH was induced by IPTG (125 μM) in mid-exponential growth phase after the temperature was decreased to 25 °C. After about 20 h post-induction, *E. coli* biomass was harvested by centrifugation (4400 g, 20 min, 4 °C) and disrupted twice with a French Press at 1500 psi cell pressure. Debris of bacterial cells were removed by ultracentrifugation at 80 000 g for 45 min at 4 °C. The crude cell extract was then applied on a column of copper-loaded Chelating Sepharose Fast Flow (XK 16 column from GE Healthcare; 1.6 × 6.2 cm) equilibrated with a 50 mM Tris/HCl buffer, pH 7.1, that contained 300 mM sodium chloride and glycerol (10% v/v). Competitive elution was achieved using a linear gradient of imidazole in the range of 0–220 mM which was applied over eight column volumes while employing a constant flow rate of 1.5 mL/min. Imidazole, sodium chloride and glycerol were afterwards removed using a HiPrep 26/10 prepacked desalting column (GE Healthcare).

3.6. Gene cloning, and production and purification of recombinant *Cb*FDH

C. boidinii ATCC 18810 was grown on YPD medium (10 g/L yeast extract, 20 g/L peptone and 20 g/L

glucose), and its genomic DNA was isolated using the Wizard® Genomic DNA Purification Kit from Promega (Madison, WI, USA). The gene encoding *Cb*FDH (EC 1.2.1.2) was amplified by PCR with the High Fidelity PCR Enzyme Mix from Fermentas (Burlington, Canada) and the following pair of oligonucleotide primers:

forward primer: 5′-GATCTAGAATTCATGAAGATCGTTTTAGTCTTATATGATGCTG-3′,
reverse primer: 5′-GATCTACTGCAGTTATTTCTTATCGTGTTTACCGTAAGCTTTAG-3′.

The PCR product was digested with EcoRI and PstI and inserted into the plasmid vector pBTac1 (Boehringer Mannheim, Germany) previously cleaved with the same restriction enzymes. Identity of the primary amino acid sequence with the *Cb*FDH described by Sakai et al. (UniProt/TrEMBL entry O93968) was confirmed by DNA sequencing.[25] Expression of recombinant *Cb*FDH was done in *E. coli* JM109, using the procedure described under Section 3.5. Purification of *Cb*FDH was performed using slight modifications of the protocol described by Slusarczyk et al. for the isolation of FDH1 from *C. boidinii* (UniProt/TrEMBL entry O13437).[26] Briefly, the crude *E. coli* extract (obtained as described under 3.5) was incubated in the presence of 10% w/v formate or [^{2}H]-formate at 60 °C for 5 min. Precipitated proteins were removed by centrifugation (11 200 g, 10 min, 4 °C). The supernatant (fraction I) was desalted in two batches using a pre-packed desalting column (see Section 3.5). The desalted protein solution (fraction II) was loaded on a column of Q-Sepharose Fast Flow (XK 16 column from GE Healthcare; 1.6 × 9.0 cm) equilibrated with 10 mM potassium phosphate buffer, pH 7.5. At a flow of 10 mL/min the column was flushed with 4.5 column volumes of the phosphate buffer before adding up to 150 mM NaCl in a linear gradient of 50 column volumes. Purified *Cb*FDH was stabilized by the addition of either 200 mM sodium formate or potassium [^{2}H]-formate (fraction III).

3.7. Characterization of *Af*M1PDH

To redissolve the barium salts of Man-ol1*P* and 5-[^{2}H]-Man-ol1*P*, we added an equimolar amount of Na_2SO_4 to the product. The formed $BaSO_4$ was removed by centrifugation (10 min at 11 200 g). The actual concentrations of dissolved Man-ol1*P* and 5-[^{2}H]-Man-ol1*P* were determined enzymatically as described under 3.4. Kinetic parameters of *Af*M1PDH for NAD^+-dependent oxidation of Man-ol1*P* were measured at 25 °C in 100 mM Tris/HCl buffer, pH 7.1, using varied concentrations of NAD^+ (0.04–8.8 mM) or Man-ol1*P* (0.03–3.4 mM) while keeping the concentration of the respective other substrate constant and saturating (Man-ol1*P*: 4.3 mM; NAD^+: 5.8 mM). Similarly, kinetic parameters for NADH-dependent reduction of Fru6*P* were obtained using concentrations of NADH between 0.002 and 0.2 mM or Fru6*P* between 0.5 and 40 mM, while keeping the other substrate constant and saturating (45 mM Fru6*P*; 0.2 mM NADH). The enzyme was appropriately diluted in the corresponding reaction buffer. Reactions were started with enzyme and initial rates were recorded photometrical as described in Section 3.4. Steady state kinetic parameters were determined by fitting the Michaelis–Menten equation to the experimental data using Sigma Plot 9.0 (SYSTAT Software Inc., San Jose, CA, USA). The kinetic turnover numbers (k_{cat}) were calculated from the maximal initial velocities using the molecular mass of 44.2 kDa as derived from the unprocessed amino acid sequence of recombinant *Af*M1PDH. Primary deuterium KIE on k_{cat} in the direction of alcohol oxidation was obtained by using saturating concentration of Man-ol1*P* or 5-[^{2}H]-Man-ol1*P* (6 mM) and NAD^+ (6 mM), employing otherwise identical reaction conditions as described above for Man-ol1*P* oxidation.

Acknowledgments

We are especially grateful to Dr. Hubertus Haas (Division of Molecular Biology, Medical University of Innsbruck, Austria) for providing genomic DNA of *A. fumigatus*. We thank Eva Glaumann for assistance in cloning of *Cb*FDH. Financial support from the Austrian Science Fund FWF (P18275-B09) is gratefully acknowledged.

References

1. Solomon, P. S.; Waters, O. D.; Oliver, R. P. *Trends Microbiol.* **2007**, *15*, 257–262.
2. Ruijter, G. J.; Bax, M.; Patel, H.; Flitter, S. J.; van de Vondervoort, P. J.; de Vries, R. P.; vanKuyk, P. A.; Visser, J. *Eukaryot. Cell* **2003**, *2*, 690–698.
3. Jennings, D. B.; Ehrenshaft, M.; Pharr, D. M.; Williamson, J. D. *Proc. Natl. Acad. Sci. U.S.A.* **1998**, *95*, 15129–15133.
4. Chaturvedi, V.; Wong, B.; Newman, S. L. *J. Immunol.* **1996**, *156*, 3836–3840.
5. Solomon, P. S.; Waters, O. D.; Jorgens, C. I.; Lowe, R. G.; Rechberger, J.; Trengove, R. D.; Oliver, R. P. *Biochem. J.* **2006**, *399*, 231–239.
6. Latgé, J. P. *Clin. Microbiol. Rev.* **1999**, *12*, 310–350.
7. Wong, B.; Brauer, K. L.; Tsai, R. R.; Jayasimhulu, K. *J. Infect. Dis.* **1989**, *160*, 95–103.
8. Nidetzky, B.; Klimacek, M. Fungal mannitol 2-dehydrogenases and mannitol-1-phosphate 5-dehydrogenases constitute novel branches in the protein family of polyol-specific long-chain dehydrogenases and reductases. In *Enzymology and Molecular Biology of Carbonyl Metabolism*; Weiner, H., Maser, E., Lindahl, R., Plapp, B., Eds.; Purdue University Press: West Lafayette, 2007; Vol. 13, pp 305–322.

9. Klimacek, M.; Kavanagh, K. L.; Wilson, D. K.; Nidetzky, B. *Chem. Biol. Interact.* **2003**, *143-144*, 559–582.
10. Kiser, R. C.; Niehaus, W. G., Jr. *Arch. Biochem. Biophys.* **1981**, *211*, 613–621.
11. Cook, P. F. Kinetic and regulatory mechanisms of enzymes from isotope effects. In *Enzyme Mechanism from Isotope Effects*; Cook, P. F., Ed., 1st ed.; CRC Press: Boca Raton, Ann Arbor, Boston, London, 1991; pp 203–231.
12. Nierman, W. C.; Pain, A.; Anderson, M. J.; Wortman, J. R.; Kim, H. S.; Arroyo, J.; Berriman, M.; Abe, K.; Archer, D. B.; Bermejo, C.; Bennett, J.; Bowyer, P.; Chen, D.; Collins, M.; Coulsen, R.; Davies, R.; Dyer, P. S.; Farman, M.; Fedorova, N.; Feldblyum, T. V.; Fischer, R.; Fosker, N.; Fraser, A.; García, J. L.; García, M. J.; Goble, A.; Goldman, G. H.; Gomi, K.; Griffith-Jones, S.; Gwilliam, R.; Haas, B.; Haas, H.; Harris, D.; Horiuchi, H.; Huang, J.; Humphray, S.; Jimenez, J.; Keller, N.; Khouri, H.; Kitamoto, K.; Kobayashi, T.; Konzack, S.; Kulkarni, R.; Kumagai, T.; Lafon, A.; Latgé, J. P.; Li, W.; Lord, A.; Lu, C.; Majoros, W. H.; May, G. S.; Miller, B. L.; Mohamoud, Y.; Molina, M.; Monod, M.; Mouyna, I.; Mulligan, S.; Murphy, L.; O'Neil, S.; Paulsen, I.; Peñalva, M. A.; Pertea, M.; Price, C.; Pritchard, B. L.; Quail, M. A.; Rabbinowitsch, E.; Rawlins, N.; Rajandream, M. A.; Reichard, U.; Renauld, H.; Robson, G. D.; Rodriguez de Córdoba, S.; Rodríguez-Peña, J. M.; Ronning, C. M.; Rutter, S.; Salzberg, S. L.; Sanchez, M.; Sánchez-Ferrero, J. C.; Saunders, D.; Seeger, K.; Squares, R.; Squares, S.; Takeuchi, M.; Tekaia, F.; Turner, G.; Vazquez de Aldana, C. R.; Weidman, J.; White, O.; Woodward, J.; Yu, J. H.; Fraser, C.; Galagan, J. E.; Asai, K.; Machida, M.; Hall, N.; Barrell, B.; Denning, D. W. *Nature* **2005**, *438*, 1151–1156.
13. Teschner, W.; Serre, M. C.; Garel, J. R. *Biochimie* **1990**, *72*, 33–40.
14. Novotny, M. J.; Reizer, J.; Esch, F.; Saier, M. H., Jr. *J. Bacteriol.* **1984**, *159*, 986–990.
15. Wolff, J. B.; Kaplan, N. O. *J. Biol. Chem.* **1956**, *218*, 849–869.
16. Klungøsyr, L. *Biochim. Biophys. Acta* **1966**, *128*, 55–62.
17. Klungsøyr, L. *Biochim. Biophys. Acta* **1967**, *146*, 10–17.
18. do Nascimento, K. H.; Davies, D. D. *Biochem. J.* **1975**, *149*, 553–557.
19. Alizade, M. A.; Gaede, K.; Brendel, K. *Hoppe-Seyler's Z. Physiol. Chem.* **1976**, *357*, 1163–1169.
20. Slatner, M.; Nidetzky, B.; Kulbe, K. D. *Biochemistry* **1999**, *38*, 10489–10498.
21. Kavanagh, K. L.; Klimacek, M.; Nidetzky, B.; Wilson, D. K. *J. Biol. Chem.* **2002**, *277*, 43433–43442.
22. Ruijter, G. J.; Visser, J. *Biochimie* **1999**, *81*, 267–272.
23. Bradford, M. M. *Anal. Biochem.* **1976**, *72*, 248–254.
24. de Bruijn, S. M.; Visser, R. G. F.; Vreugdenhil, D. *Phytochem. Anal.* **1999**, *10*, 107–112.
25. Sakai, Y.; Murdanoto, A. P.; Konishi, T.; Iwamatsu, A.; Kato, N. *J. Bacteriol.* **1997**, *179*, 4480–4485.
26. Slusarczyk, H.; Felber, S.; Kula, M. R.; Pohl, M. *Eur. J. Biochem.* **2000**, *267*, 1280–1289.

Contents lists available at ScienceDirect

Chemico-Biological Interactions

journal homepage: www.elsevier.com/locate/chembioint

Polyol-specific long-chain dehydrogenases/reductases of mannitol metabolism in *Aspergillus fumigatus*: Biochemical characterization and pH studies of mannitol 2-dehydrogenase and mannitol-1-phosphate 5-dehydrogenase

Stefan Krahulec, Guilliano C. Armao, Patricia Bubner, Mario Klimacek*, Bernd Nidetzky**

Institute of Biotechnology and Biochemical Engineering, Graz University of Technology, Petersgasse 12/I, A-8010 Graz, Austria

ARTICLE INFO

Article history:
Available online 15 October 2008

Keywords:
Polyol-specific long-chain dehydrogenases/reductases
Mannitol
Mannitol 1-phosphate
Mannitol metabolism
Catalytic mechanism
pH profile analysis

ABSTRACT

Functional genomics data suggests that the metabolism of mannitol in the human pathogen *Aspergillus fumigatus* involves the action of two polyol-specific long-chain dehydrogenases/reductases, mannitol-1-phosphate 5-dehydrogenase (M1PDH) and mannitol 2-dehydrogenase (M2DH). The gene encoding the putative M2DH was expressed in *Escherichia coli*, and the purified recombinant protein was characterized biochemically. The predicted enzymatic function of a NAD^+-dependent M2DH was confirmed. The enzyme is a monomer of 58 kDa in solution and does not require metals for activity. pH profiles for M2DH and the previously isolated M1PDH were recorded in the pH range 6.0–10.0 for the oxidative and reductive direction of the reactions under conditions where substrate was limiting (k_{cat}/K) or saturating (k_{cat}). The pH-dependence of log k_{cat} was usually different from that of log(k_{cat}/K), suggesting that more than one step of the enzymatic mechanism was affected by changes in pH. The greater complexity of the pH profiles of log(k_{cat}/K) for the fungal enzymes as compared to the analogous pH profiles for M2DH from *Pseudomonas fluorescens* may reflect sequence changes in vicinity of the conserved catalytic lysine.

1. Introduction

Aspergillus species, *Aspergillus fumigatus* in particular, are the etiologic agents of many infections in humans, either alone or in association with other opportunistic fungi. These organisms therefore cause multiple diseases including invasive pulmonary aspergillosis, aspergilloma, and numerous forms of hypersensitivity diseases [1]. It has been estimated on the basis of environmental surveys that all humans inhale at least several hundreds of *A. fumigatus* conidia per day [2]. Immunocompetent individuals are rarely affected by the inhaled conidia as these are eliminated by innate immune mechanisms [3]. However, because of the increase in immunosuppressed patients and the degree of severity of modern immunosuppressive therapies, *A. fumigatus* has become the currently most prevalent fungal pathogen [4]. Infections by *Aspergillus* are usually fatal in immunocompromised hosts and are reported to be the major cause of death in leukemia treatment centers and transplantation units [4,5]. Among a number of virulence factors of *Aspergillus* that have been described, the ability of the fungus to effectively scavenge free radicals produced by the host phagocytes has been previously emphasized [6].

The acyclic hexitol D-mannitol (Man-ol) fulfils a role as a free radical scavenger and through that capacity, it is thought to assist in suppressing the reactive oxygen species-mediated defense of the host's immune system [6,7]. It was shown, for example, that Man-ol produced by the human pathogen *Cryptococcus neoformans* and by the tobacco pathogen *Alternaria alternata* functions in scavenging reactive oxygen species generated as result of the defense mechanism of the host [8,9]. *A. fumigatus*, interestingly, produces and releases sufficient amounts of Man-ol to raise serum levels of Man-ol in infected animals [10]. This indicates an essential role of Man-ol in the parasitic life style of *A. fumigatus*.

The metabolism of Man-ol in fungi is assumed to take place primarily via two routes. The biosynthetic pathway involves reduction of D-fructose 6-phosphate (Fru6*P*) to D-mannitol 1-phosphate (Man-ol1*P*) catalyzed by a mannitol-1-phosphate 5-dehydrogenase (M1PDH) and subsequent dephosphorylation of Man-ol1*P* to Man-ol catalyzed by a phosphatase [11]. Mobilization of Man-ol that has accumulated intracellularly can occur by reversal of the described anabolic route whereby conversion of Man-ol to Man-ol1*P* depends on ATP and is catalyzed by a kinase. Alternatively,

* Corresponding author.
** Corresponding author. Tel.: +43 316 873 8400; fax: +43 316 873 8434.
E-mail address: bernd.nidetzky@TUGraz.at (B. Nidetzky).

0009-2797/$ – see front matter © 2008 Elsevier Ireland Ltd. All rights reserved.
doi:10.1016/j.cbi.2008.10.001

Man-ol may be oxidized to D-fructose (Fru) catalyzed by mannitol 2-dehydrogenases (M2DH). The Fru would then be phosphorylated to Fru6*P*.

Generally, M1PDHs and M2DHs are secondary alcohol dehydrogenases that utilize NAD(P)$^+$ as co-substrate and oxidizing reagent. The M2DHs are evolutionary quite diverse. Based on similarities in the amino acid sequence and according to the size of the polypeptide chain, M2DHs from different sources have been categorized as member of one of the three main superfamilies of alcohol dehydrogenases: the short-chain dehydrogenases/reductases (~250 amino acids), the medium-chain dehydrogenases/reductases (~350 amino acids), and the long-chain dehydrogenases/reductases (~360–550 amino acids) [12–14]. Almost all of the known M1PDHs, by contrast, share a clear evolutionary relationship and have been classified into the family of polyol-specific long-chain dehydrogenases/reductases (PSLDRs) [15]. Only one open-reading frame encoding for a putative M1PDH (*Af*M1PDH) and one encoding for a putative M2DH (*Af*M2DH) were identified within the whole genome shotgun sequence of *A. fumigatus* [16]. From their deduced amino acid sequences, both enzymes belong to the family of PSLDRs [15]. Considering the absence of PSLDR orthologues in the human genome, *Af*M1PDH and *Af*M2DH might be interesting targets for selective inhibition in new strategies developed against *A. fumigatus*.

The PSLDRs comprise proteins from prokaryotic and eukaryotic origin. They are clustered into 7 sub-families which in turn are defined by a minimum of 30% internal amino acid identity [17]. Fungal PSLDRs are either M2DHs or M1PDHs [15]. PSLDRs fold into monomers, vary in size between 380 and 550 amino acid residues, and catalyze the metal independent oxidation of secondary alcohol groups in polyol substrates using NAD(P)$^+$ as the coenzyme. A common structural organization was suggested for PSLDRs where the active site is located in a cleft formed by two domains: a N-terminal Rossmann-fold domain that binds the coenzyme, and a largely α-helical C-terminal domain that provides key elements of substrate binding, recognition and catalysis [18,19]. With a typical size of about 360 amino acids, M1PDHs are the smallest among the PSLDRs. However, they retain the core elements of secondary structure that are present in all members of the family [18].

The predicted catalytic function of *Af*M1PDH was recently confirmed in a study of the recombinant enzyme produced in *E. coli* [20]. However, no biochemical data is available for *Af*M2DH so far. We have therefore cloned and expressed the coding gene in *E. coli* and report here on the functional properties of the purified protein. The proposed annotation of the protein as NAD$^+$-dependent M2DH was corroborated. Additionally, we determined pH profiles of kinetic parameters for the oxidative and reductive direction of the reactions catalyzed by *Af*M2DH and *Af*M1PDH. Comparison of these pH-dependencies with relevant pH profiles for the well-characterized M2DH from *Pseudomonas fluorescens* (*Ps*M2DH) provides novel insights into structure-function relationships for the fungal enzymes [21,22].

2. Materials and methods

2.1. Materials

2.1.1. Chemicals

Fru, Fru6*P*, Man-ol, albumin from bovine serum (BSA, Cohn fraction V), salts and buffer reagents were from Sigma–Aldrich (St. Louis, MO, USA). β-Nicotinamide adenine dinucleotides (NAD$^+$ and sodium salts of NADP$^+$, NADH, NADPH; minimum purity 97%) were obtained from Roth (Karlsruhe, Germany). Man-ol1*P* was synthesized enzymatically as described elsewhere [20].

2.1.2. Molecular biology reagents

T4-Ligase, restriction enzymes as well as *Pfu* and *Taq* DNA polymerases were from Fermentas (Burlington, Canada). The plasmid expression vector pQE-70 was obtained from Qiagen (Hilden, Germany). *Pwo* DNA polymerase was a product of PEQLAB (Erlangen, Germany). Oligonucleotides were obtained from VBC-Biotech (Vienna, Austria). A preparation of genomic DNA of *A. fumigatus* was kindly provided by Dr. Hubertus Haas (Division of Molecular Biology, Medical University of Innsbruck, Austria). DNA sequencing was performed by VBC-Biotech.

2.1.3. Enzymes

*Af*M1PDH was produced and purified as described in a recent publication [20].

2.2. Recombinant Af*M2DH*

The intron-less open-reading frame encoding the putative *Af*M2DH was amplified from genomic DNA of *A. fumigatus* using the following pair of oligonucleotide primers: forward primer: 5′-GATCTAGCATGCCACCTCTCAAGCTCAATAGC-3′, reverse primer: 5′-GATCTAAGATCTGTTAATGTACTTGGGGAG-3′ [16]. The procedures used for gene cloning as well as for production and purification of recombinant protein were identical to the ones used by Krahulec et al. in the preparation of recombinant *Af*M1PDH [20]. Purification was checked by SDS PAGE. Concentrated solutions of purified protein (2.6 mg/mL) were prepared using Vivaspin 20 (10 kDa MWCO) microconcentrator tubes (Sartorius AG, Goettingen, Germany). One mg/mL BSA was added for stabilization and protein solutions were stored at −20 °C in a 50-mM Tris/HCl buffer, pH 7.1.

Protein concentrations were measured with the Bio-Rad Protein Assay (Bio-Rad Laboratories; Hercules, USA) referenced against BSA. M2DH activity was routinely assayed in the direction of NADH dependent reduction of Fru at 25 °C using 100 mM Tris/HCl buffer, pH 7.1. The concentrations of Fru and NADH were 800 and 0.2 mM, respectively.

2.3. Biochemical characterization of Af*M2DH*

2.3.1. Molecular mass determination

Size exclusion chromatography (SEC) of purified *Af*M2DH was carried out on a Superdex 200 HR 10/30 gel filtration column (GE Healthcare; Chalfont St. Giles, UK) using a 50 mM potassium phosphate buffer, pH 7.0, which contained 100 mM NaCl. The column was calibrated with a gel filtration standard from Bio-Rad Laboratories at a constant flow rate of 0.5 mL/min. Two hundred microliters of *Af*M2DH solution (1 mg/mL) were applied on the column using the same flow rate. Protein elution was detected by absorbance at 280 nm using a GE-Healthcare Äkta FPLC system.

2.3.2. Kinetic parameters

Initial rate measurements were performed with a DU800 spectrophotometer from Beckman Coulter, Inc., (Fullerton, CA, USA), recording the formation or depletion of NAD(P)H at a wavelength of 340 nm ($\varepsilon_{NAD(P)H}$ = 6.22 cm^{-1} mM^{-1}). Enzymatic reactions were carried out at 25 °C in 100 mM Tris/HCl buffer (pH 7.1; Fru reduction) or 100 mM glycine/NaOH buffer (pH 10.0; Man-ol oxidation). Initial rates were recorded under conditions where the concentration of NAD$^+$ (0.02–1.0 mM) and NADH (0.002–0.2 mM) was varied and the concentration of Man-ol (400 mM) and Fru (800 mM) was constant and saturating, respectively. They were likewise measured under conditions where the concentrations of Man-ol (3.0–400 mM) and Fru (2.0–250 mM) were varied and the

concentrations of NAD^+ (2.0 mM) and NADH (0.2 mM) were constant and saturating, respectively. Rate measurements using $NADP^+$ and NADPH as coenzyme were carried out using variable concentrations of $NADP^+$ (0.02–2.5 mM) and NADPH (0.002–0.1 mM) at constant concentrations of Man-ol (400 mM) and Fru (1.5 M), respectively. Variable concentrations of Man-ol (4.0–400 mM) and Fru (0.01–1.0 M) were used with constant concentrations of $NADP^+$ (2.0 mM) and NADPH (0.2 mM), respectively.

2.4. Site-directed replacement of Lys^{213} by Ala in Af*M1PDH*

A two stage PCR protocol was used to substitute Lys^{213} of *Af*M1PDH by Ala [23]. The previously described pQE-70 expression vector harboring the *Af*M1PDH gene was used as the template [20]. Note that amino acid numbering of *Af*M1PDH starts with the initiator methionine as 1 and does not consider the additional leucine that is present at the N-terminus of the recombinant protein [20]. *Pfu* DNA polymerase and a complementary pair of oligonucleotide primers were applied, with the sequence of the direct primer being 5′-CCTACATCGAACGCGCGCTCTTCACCGTCAACACCG-3′. After digestion of the template DNA with DpnI the circular gapped product was electro-transformed into *E. coli* JM109 cells. The mutated *Af*M1PDH (K213A) was produced and purified exactly as reported for the wild-type enzyme [20]. SDS PAGE was used to verify over-expression of K213A and to monitor purification thereof. Purified K213A was assayed for activity using Man-ol1*P* (0.50 mM) and NAD^+ (2.00 mM) as the substrates and applying a 100-mM glycine/NaOH buffer, pH 10.0. The chosen substrate concentrations are saturating for wild-type *Af*M1PDH under the reaction conditions used [20].

2.5. pH studies

Initial rates catalyzed by *Af*M1PDH and *Af*M2DH were recorded at variable pH in the oxidative and reductive direction of the respective enzymatic reaction using a three-component buffer mixture of 50 mM MES, 100 mM Tris and 50 mM glycine that ensured a constant ionic strength over the measured pH range from about 5.5 to 10.4 [24]. At each pH, rates were obtained under conditions where the substrate concentration was varied while the concentration of NAD^+ or NADH was constant and saturating, usually at 2.0 and 0.2 mM, respectively (see Section 3). Man-ol1*P* was dissolved from its solid barium salt as described elsewhere and the actual concentration of substrate stock solutions was verified enzymatically [20].

2.6. Data processing

Data analysis was performed by using the program Sigma Plot 9.0 (Systat Software, Inc., San Jose, CA, USA). Kinetic parameters were obtained by fitting the Michaelis–Menten equation to experimental initial rates using unweighted non-linear least squares regression analysis. The kinetic turnover number (k_{cat}) was calculated from the estimated maximum initial rate and the molarity of the enzyme solution used which in turn was determined from the measured protein concentration and the molecular mass of recombinant *Af*M1PDH (44.2 kDa) or *Af*M2DH (57.6 kDa). The pH-dependencies of k_{cat} and k_{cat}/K were analyzed using kinetic parameters in logarithmic form. The pH profiles were fitted with Eqs. (1)–(5). Eq. (1) describes a pH-dependence where $\log Y$ ($Y = k_{cat}$ or k_{cat}/K) increases with a slope of +1 below pK_1 and is level above pK_1. Eq. (2) describes a pH-rate profile where $\log Y$ is level below pK_1 and decreases with a slope of −1 above pK_1. Eq. (3) describes a bell shaped pH profile that decreases below pK_1 and above pK_2. Eq. (4) is used to describe a pH profile where activity decreases with a slope of +2 at low pH, implying the presence of two ionizable groups of pK_1 and pK_2. This pH profile is level above the two pK values. Eq. (5) expands Eq. (3) to include the additional feature that activity decreases in a wavelike form at high pH from a high constant value (C_H) to a lower constant value (C_L) [25]. In Eqs. (1)–(5), C is the pH independent value of Y, K is a proton dissociation constant, and $[H^+]$ is the proton concentration.

$$\log Y = \log\left[\frac{C}{1+[H^+]/K_1}\right] \quad (1)$$

$$\log Y = \log\left[\frac{C}{1+K_1/[H^+]}\right] \quad (2)$$

$$\log Y = \log\left[\frac{C}{1+[H^+]/K_1+K_2/[H^+]}\right] \quad (3)$$

$$\log Y = \log\left[\frac{C}{1+[H^+]/K_2+[H^+]^2/(K_1K_2)}\right] \quad (4)$$

$$\log Y = \log\left[\frac{C_H}{1+[H^+]/K_1+K_2/[H^+]}+\frac{C_L}{1+[H^+]/K_2}\right] \quad (5)$$

3. Results

3.1. Cloning and expression of the gene encoding Af*M2DH*

The whole genome shotgun sequence of *A. fumigatus* contains an open-reading frame that encodes a putative M2DH of the PSLDR type (EC 1.1.1.67, UniProt/TrEMBL entry Q4WQY4) [16]. Because the coding region of this gene is not interrupted by introns, it was possible to amplify the entire *Af*M2DH gene directly from genomic DNA of *A. fumigatus*. The PCR product thus obtained had the expected size of 1526 bp and was cloned into a pQE-70 plasmid expression vector. The deduced amino acid sequence of the recombinant protein contained at its N-terminus after the initiator Met, a Pro residue instead of the authentic Ala which was introduced with the oligonucleotide primer used for PCR. Furthermore, a peptide of eight amino acids (-Arg-Ser-His_6) was fused to the C-terminal end of the protein to facilitate purification.

Heterologous expression of the *Af*M2DH gene harboring the modifications described above was carried out in *E. coli* JM109 using the conditions previously employed for production of recombinant *Af*M1PDH [20]. A specific M2DH activity of 14 U/mg was measured in the bacterial cell extract. Apart from a NADH oxidase activity which accounts for about 0.4% of the activity measured in the crude extract, no basal level of activity towards Fru reduction with NADH could be detected in the *E. coli* JM109 strain. Analysis by SDS PAGE showed an abundant protein band at a position in the gel that corresponded to the expected molecular mass of ≈58 kDa for recombinant *Af*M2DH (Fig. 1A, lane 1).

3.2. Purification and biochemical properties of Af*M2DH*

*Af*M2DH was purified to apparent homogeneity using affinity chromatography with copper-loaded Chelating Sepharose. Table 1 summarizes the purification protocol and provides a balance with respect to total protein and enzyme activity. The isolated enzyme migrated as a single protein band of ≈58 kDa mass in SDS PAGE (Fig. 1A, lane 2). Panel B of Fig. 1 shows that *Af*M2DH eluted as a single protein peak in SEC. The molecular mass of the enzyme estimated from the elution volume was 53 kDa, suggesting that *Af*M2DH is a functional monomer in solution like *Af*M1PDH and all other members of the PSLDR family that have so far been characterized at the protein level [15,20].

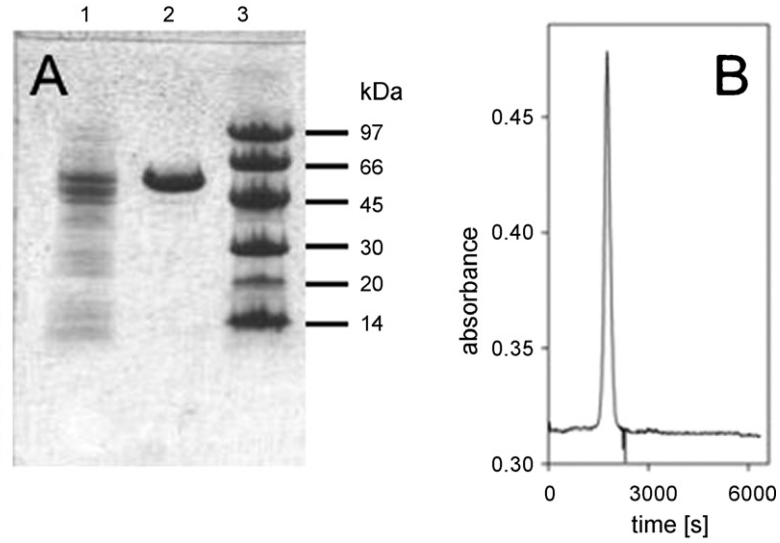

Fig. 1. Purification of *Af*M2DH documented by SDS PAGE (A) and analysis of the purified protein by size exclusion chromatography (B): in panel A, lanes 1–3 show the crude cell extract of *E. coli* JM109 expressing the gene encoding for the recombinant *Af*M2DH, *Af*M2DH purified by metal affinity chromatography, and the molecular mass marker proteins, respectively.

Table 1
Purification of recombinant *Af*M2DH expressed in *E. coli* JM109. Results are based on processing 3.7 g moist bacterial biomass. *Af*M2DH activity was assayed in the direction of Fru reduction at 25 °C using 100 mM Tris/HCl buffer, pH 7.1. The concentrations of Fru and NADH were 800 and 0.2 mM, respectively.

Purification stage	Total activity (U)	Protein (mg/mL)	Specific activity (U/mg)	Total yield (%)	Purification factor
Crude extract	2530	16.4	14	100	1
Affinity chromatography	1370	1.0	68	54	4.9
Desalting	840	0.6	94	33	6.7

Purified *Af*M2DH had a specific activity of 94 ± 5 U/mg for Fru reduction with NADH at pH 7.1. In the direction of NAD^+-dependent oxidation of Man-ol at pH 10.0, the specific activity was 220 ± 3 U/mg. The corresponding specific activities measured with $NADP^+$ and NADPH were about 3.8 and 19 U/mg, respectively (note that the enzyme could not be saturated with the coenzyme concentrations used). Activities for the reactions with Man-ol1*P* (60 mM) and Fru6*P* (120 mM) with NAD^+ (2 mM) and NADH (0.2 mM) under otherwise identical conditions were below values that could have resulted from small impurities (<0.02% of Man-ol in Man-ol1*P*; <0.3% of Fru in Fru6*P*) in the substrates used. Considering that the catalytic action of PSLDRs is not dependent on a metal cofactor, we tested the effect of the metal chelator EDTA on the activity of *Af*M2DH [15]. The purified enzyme (23 μM) was incubated in the presence of a large molar excess of EDTA (100 mM) for up to 1 h at 0 °C, and residual M2DH activity was assayed at various times. No loss of activity was observed relative to a control which lacked EDTA, suggesting that *Af*M2DH is a metal-independent enzyme.

3.3. *Kinetic characterization of* Af*M2DH*

Kinetic parameters for Man-ol oxidation by NAD^+ and $NADP^+$ at pH 10.0 and for Fru reduction by NADH and NADPH at pH 7.1 are summarized in Table 2. *Af*M2DH was a much poorer enzyme when it employed $NADP^+$ and NADPH as compared to NAD^+ and NADH. The initial rate of Man-ol oxidation displayed a linear dependence on the concentration of $NADP^+$ in the range 0.02–2.50 mM, indicating that unlike NAD^+ the enzyme could not be saturated with $NADP^+$ in the steady state under the conditions used. The same observation was made for Fru reduction by NADPH (0.002–0.100 mM). The affinity of *Af*M2DH for binding $NADP^+$ and NADPH is clearly much lower than that for binding NAD^+ and NADH. Catalytic efficiencies for reaction with $NADP^+$ and NADPH were obtained from linear plots of the enzymatic rates against the coenzyme concentration and are shown in Table 2. These efficiencies were three ($NADP^+$) and two (NADPH) orders of magnitude lower than the corresponding k_{cat}/K values for reactions with NAD^+ and NADH. Despite the fact that *Af*M2DH is a dual specific, namely NAD^+ and $NADP^+$ dependent,

Table 2
Apparent kinetic constants for purified *Af*M2DH at 25 °C: Man-ol oxidation was measured in 100 mM glycine/NaOH buffer pH 10.0 and Fru reduction in 100 mM Tris/HCl buffer, pH 7.1. See Section 2 for the concentrations of substrates and coenzymes used.

	$K_{substrate}$ (mM)	$K_{cofactor}$ (mM)	k_{cat} (s^{-1})	$k_{cat}/K_{substrate}$ (s^{-1} mM^{-1})	$k_{cat}/K_{cofactor}$ (s^{-1} mM^{-1})
Man-ol/NAD^+	13 ± 1	0.15 ± 0.02	212 ± 3	17 ± 1	1400 ± 100
Fru/NADH	60 ± 7	0.019 ± 0.002	86 ± 5	1.4 ± 0.2	4700 ± 500
Man-ol/$NADP^+$	82 ± 12[a]	n.a.[b]	3.6 ± 0.2[a]	0.04 ± 0.01[a]	1.20 ± 0.02
Fru/NADPH	159 ± 19[a]	n.a.[b]	18 ± 1[a]	0.12 ± 0.02[a]	57 ± 4

[a] Note that the constant concentrations of NADPH (200 μM) and $NADP^+$ (2 mM) used were not saturating.
[b] Not applicable (see Section 3).

enzyme, it displays a strong preference for reaction with NAD(H). Michaelis constants for Man-ol and Fru determined at a constant concentration of $NADP^+$ (2.00 mM) and NADPH (0.200 mM) were elevated 6.5- and 2.6-fold as compared to the corresponding K_m values obtained under otherwise identical conditions using NAD^+ and NADH. However, the concentrations of NAD^+ and NADH were saturating while the same concentrations of $NADP^+$ and NADPH were not. The catalytic efficiencies for Man-ol and Fru were also decreased 381- and 12-fold when $NADP^+$ and NADPH replaced NAD^+ and NADH, respectively.

3.4. pH effects on kinetic parameters

The pH-dependencies of k_{cat} and $k_{cat}/K_{substrate}$ were determined for the forward and reverse direction of the reactions catalyzed by *Af*M2DH and *Af*M1PDH. NAD^+ and NADH were used as coenzymes. The experimental pH profiles are shown in Fig. 2 along with the corresponding pH profiles for *Ps*M2DH that are taken from literature [21,22]. The pH-dependencies seen in the three enzymes were strikingly different. Results of control experiments revealed that the Michaelis constant of *Af*M1PDH for NAD^+ increased from a value of 10 μM at pH 10.0 to a higher value of 800 μM at pH 7.1. Initial rate measurements carried out in the pH range 6.9–7.4 therefore employed a constant NAD^+ concentration of 10.0 mM (instead of the normally used 2.00 mM). Each pH profile was fitted with the appropriate equation, and the results are summarized in Table 3. Correlation coefficients (R^2) associated with the regression analysis were ≥0.99 (*Af*M2DH) and ≥0.93 (*Af*M1PDH), indicating that the fit was generally good. Estimates for the pH independent value of k_{cat} or k_{cat}/K at the optimum state of protonation, that is, C and C_H in Eqs. (3) and (5), often were afflicted with a large statistical error. There was generally a strong correlation between the estimated value of C (or C_H) and the corresponding pK values. Considering that C values represent the levels in the pH profiles, it is clearly understood that C becomes increasingly ill-defined when pK_2 approaches or falls below pK_1 (for detailed discussion, see [26]). We noted that in cases where pK_1 > pK_2, there was even a slight dependence of the final estimate for C (or C_H) on the initial parameter value chosen during non-linear least squares regression analysis, indicating problems with the search for a global minimum of residual least squares. However, the relevant numbers reported in Table 3 are robust estimates and the overall conclusions are not affected by the high statistical error associated with C or C_H.

3.5. Site directed mutagenesis of Lys^{213} in Af*M1PDH*

Evidence from high-resolution structures and results of site-directed mutagenesis studies have established that Lys^{295} serves a role as general acid–base catalyst of NAD(H)-dependent interconversion of Man-ol and Fru by *Ps*M2DH [19,27]. Lys^{295} (*Ps*M2DH numbering) is strictly conserved among the known PSLDRs [15,17]. The pH profiles for k_{cat}/K of *Ps*M2DH are thought to reveal the ionization of the side chain of Lys^{295} which must be unprotonated for Man-ol oxidation and protonated for Fru reduction. To verify the presumed key catalytic function of the homologous residue in *Af*M1PDH, we substituted the relevant Lys^{213} by Ala. A homogeneous preparation of K213A was obtained (data not shown) using protocols established previously during studies of the wild-type enzyme [20]. Using 2.9 μM of the purified K213A in the enzymatic assay (0.50 mM Man-ol1*P*, 2.00 mM NAD^+, pH 10.0), a residual activity with a turnover frequency of about 0.0019 s^{-1} was found for the mutated *Af*M1PDH. The loss of activity caused by the replacement of the side chain of Lys^{213} by the side chain of Ala was therefore $10^{3.8}$-fold, consistent with the proposed catalytic function of the lysine.

4. Discussion

4.1. Biochemical properties of Af*M2DH*

4.1.1. General

The amino acid sequence of *Af*M2DH is 43.3% identical to the sequence of *Ps*M2DH. Based on evolutionary relationship analysis, *Af*M2DH was previously classified as a member of the PSLDR sub-family 1, the M2DHs [15]. The categorization was performed in the absence of biochemical data for *Af*M2DH, and results of this work now provide a clear-cut functional annotation of the gene product. We showed that the recombinant enzyme produced in *E. coli* displays the predicted enzymatic function, catalyzing the stereospecific interconversion of Man-ol and Fru. *Af*M2DH is distinct from the second enzyme of Man-ol metabolism in *A. fumigatus*, namely *Af*M1PDH which is related to *Af*M2DH by membership to the family of PSLDRs but differs from it with respect to sub-family categorization. *Af*M1PDH is a member of the sub-family 7 and shows only low sequence identity with *Af*M2DH (14%) and *Ps*M2DH (12%) [15]. Activities for the reactions of *Af*M2DH with Man-ol1*P* and Fru6*P* were below values that could have resulted from small impurities (<0.02% of Man-ol in Man-ol1*P*; <0.3% of Fru in Fru6*P*) in the substrates used. This finding is consistent with the proposed structure–function relationships for PSLDR subfamilies 1 and 7. The monomeric structure in solution and the independence of the enzymatic activity on (divalent) metal ions are features that *Af*M2DH shares with other members of the PSLDR family [15,17].

4.1.2. Coenzyme and substrate specificities

The three dimensional structure of *Ps*M2DH complexed with NAD^+ provided an explanation for the ≈130-fold (k_{cat}/K_{NAD^+}) preference of this enzyme for reaction with NAD^+ as compared to $NADP^+$ [19,21]. Recent results from mutational analysis of the coenzyme binding pocket of *Ps*M2DH confirmed the structure-derived suggestion that the side chain of Asp^{69} prevents accommodation of the 2′-phosphate group of $NADP^+$ [28]. Asp^{69} of *Ps*M2DH is conserved in *Af*M2DH (Fig. 3), suggesting that the fungal enzyme should also prefer NAD^+ over $NADP^+$ [15]. Biochemical data are consistent with this notion. The observed preference for NAD^+ of *Af*M2DH is in the same range as that of *Ps*M2DH. The apparent affinity of *Af*M2DH for binding NADH at pH 7.1 is 10 times that of *Ps*M2DH under the same conditions [21]. Likewise, k_{cat}/K for NADH was 10-fold higher in *Af*M2DH as compared to *Ps*M2DH. Michaelis constants for NAD^+ at pH 10.0 are almost similar for fungal and bacterial enzymes [22]. Considering that release of NADH is the rate-determining step of Man-ol oxidation by *Ps*M2DH at pH 10.0, it is noteworthy that the k_{cat} of *Af*M2DH is 5 times that of the bacterial enzyme [22]. The result suggests that under the conditions examined, the rate of dissociation of NADH is significantly higher in *Af*M2DH than in *Ps*M2DH. k_{cat} values for Fru reduction at pH 7.1 are similar in the two M2DHs [21].

Molecular interactions responsible for substrate binding in *Ps*M2DH are known from the crystal structure of the enzyme bound with NAD^+ and Man-ol [18,19]. It is interesting that despite the fact that all of the nine residues that make non-covalent contacts with bound Man-ol in *Ps*M2DH are completely conserved in the sequence of *Af*M2DH (Fig. 3), the Michaelis constants of the fungal enzyme for Man-ol and Fru are 30- and 2.5-fold larger than the corresponding constants for *Ps*M2DH [15,21,22]. However, the interpretation must consider that for an enzymatic reaction involving two substrates and two products the K_M value is a kinetically complex parameter that includes steps not directly implicated in binding of the substrate [29]. The work of Grimshaw

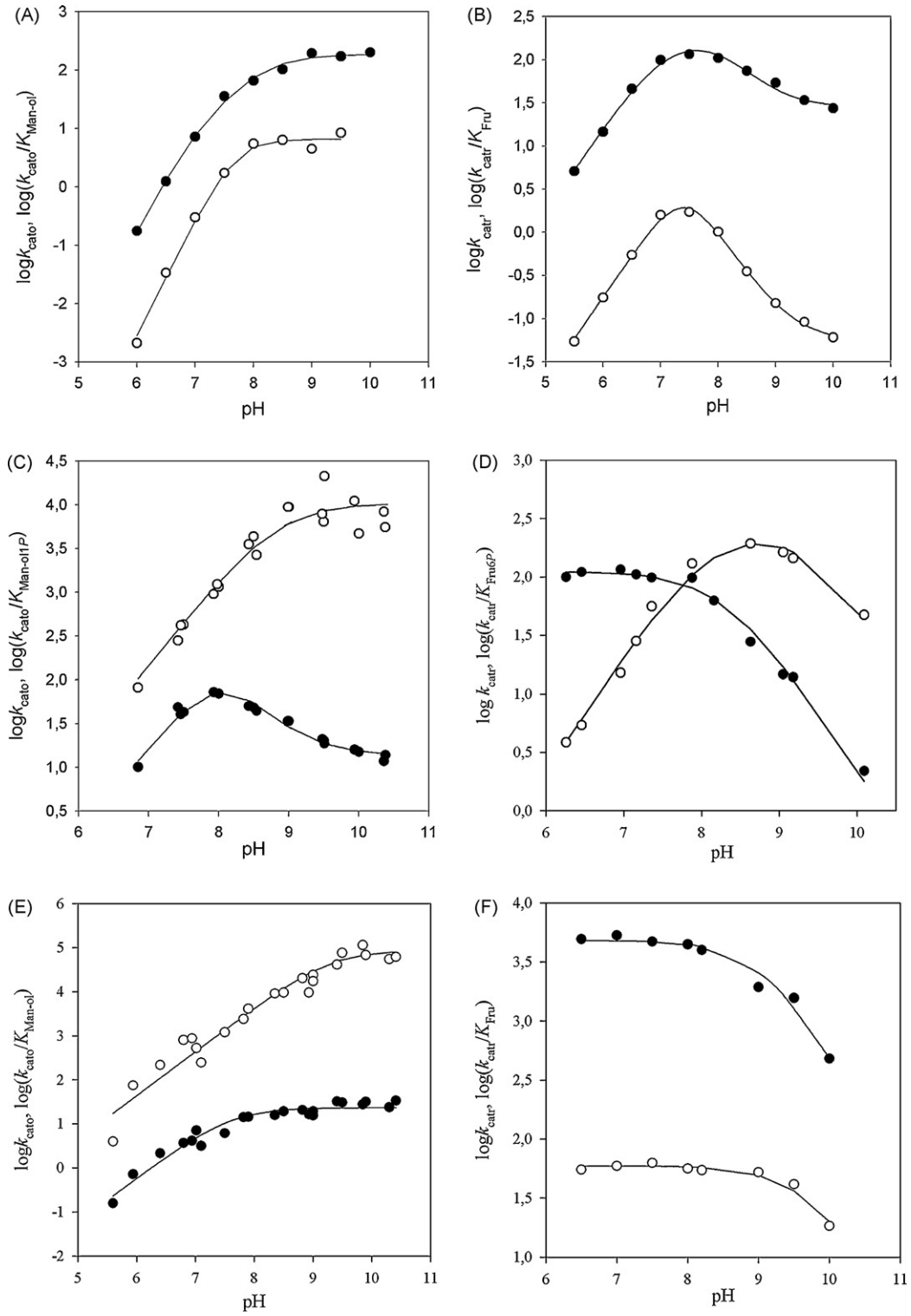

Fig. 2. pH profiles of *Af*M2DH (A and B), *Af*M1PDH (C and D) and *Ps*M2DH (E and F): (●) log k_{cat} and (○) log(k_{cat}/K). Data is given in units of s^{-1} (k_{cat}) and s^{-1} mM^{-1} (k_{cat}/K_M). Panels (A and E) and (B and F) show Man-ol oxidation and Fru reduction, respectively. Panels (C) and (D) show Man-ol1*P* oxidation and Fru6*P* reduction, respectively. Data in panels (E) and (F) are from the literature [21,22].

et al. on human aldose reductase provides an interesting example where it was shown that by increasing (≈9-fold) the otherwise limiting rate of release of the $NADP^+$ product through a single point mutation of Cys^{298} into Ala, the Michaelis constant for the substrate xylose was enhanced significantly (≈37-fold) [30].

4.2. Mechanistic deductions from pH profile analysis for Af*M1PDH and* Af*M2DH*

The pH profiles of log(k_{cat}/K) for *Ps*M2DH decrease below p*K* 9.2 in the direction of Man-ol oxidation by NAD^+ and above p*K* 9.3 in the direction of Fru reduction by NADH [21,22]. These profiles

Table 3
p*K* values from pH profiles of *Af*M1PDH and *Af*M2DH.

Parameter	Eq. fitted	pK_1	pK_2	C
*Af*M1PDH				
$\log k_{cato}$	(5)	8.3 ± 0.5	7.8 ± 0.4	$C_H = 300 \pm 190\ s^{-1}$; $C_L = 14 \pm 1\ s^{-1}$
$\log(k_{cato}/K_{Man\text{-}ol1P})$	(1)	8.9 ± 0.3		$10000 \pm 1400\ s^{-1}\ mM^{-1}$
$\log k_{catr}$	(2)	8.3 ± 0.1		$112 \pm 8\ s^{-1}$
$\log(k_{catr}/K_{Fru6P})$	(3)	8.1 ± 0.2	9.3 ± 0.1	$291 \pm 100\ s^{-1}\ mM^{-1}$
*Af*M2DH				
$\log k_{cato}$	(4)	6.8 ± 0.1	8.2 ± 0.2	$188 \pm 17\ s^{-1}$
$\log(k_{cato}/K_{Man\text{-}ol})$	(4)	8.3 ± 0.5	7.1 ± 0.4	$6.6 \pm 1.0\ s^{-1}\ mM^{-1}$
$\log k_{catr}$	(5)	7.1 ± 0.1	8.1 ± 0.3	$C_H = 200 \pm 40\ s^{-1}$; $C_L = 28 \pm 3\ s^{-1}$
$\log(k_{catr}/K_{Fru})$	(5)	8.0 ± 0.3	6.8 ± 0.2	$C_H = 15 \pm 7\ s^{-1}\ mM^{-1}$; $C_L = 0.053 \pm 0.004\ s^{-1}\ mM^{-1}$

suggest, as Man-ol and Fru do not ionize in the probed pH range, that deprotonation/protonation of a single group on enzyme-NAD$^+$ and enzyme-NADH controls the sequence of steps from binding of the substrate (Man-ol, Fru) to the release of the first product. The ordered kinetic mechanism of *Ps*M2DH implies that Man-ol or Fru are released before NADH or NAD$^+$, respectively. Mutational analysis of Lys^{295} revealed that the observed p*K* values most probably reflect the pH-dependent ionization of the ε-amino group of the catalytic lysine [27]. The p*K* in the pH profiles of $\log k_{cat}$ are displaced outward by about 1.5 and 0.4 pH units relative to the corresponding pH profiles of $\log(k_{cat}/K)$ in Man-ol oxidation and Fru reduction, respectively [21,22]. The up or down shift in the p*K* value may result because non-covalent bonding between the enzyme and the substrate affects the p*K* or it may simply mirror the effect of kinetic complexity on the observable p*K* in the pH profile of $\log k_{cat}$. Microscopic steps not included in k_{cat}/K like the release of NADH during Man-ol oxidation, are known to contribute to k_{cat} of *Ps*M2DH [21]. The proposed pH-dependence for the reaction mechanism of *Ps*M2DH serves as a point of departure for analyzing the more complex pH profiles of *Af*M2DH and *Af*M1PDH.

4.2.1. Af*M2DH*

The pH profiles of $\log(k_{cat}/K)$ and $\log k_{cat}$ for Man-ol oxidation by *Af*M2DH decrease with a slope of +2 at low pH. From fits of Eq. (4) to the data, two molecular dissociation constants pK_1 and pK_2 are calculated. The p*K* values are only about 1.4/1.2 pH units apart one from another, suggesting that they cannot be treated as completely independent ionizations. It should be noted that in the pH profile $\log(k_{cat}/K)$, the pK_2 is significantly smaller than the pK_1. This implies that proton binding is strongly cooperative and a scenario is supported where the second proton to dissociate from enzyme-NAD$^+$ does so more readily than the first [26]. Cooperativity of proton

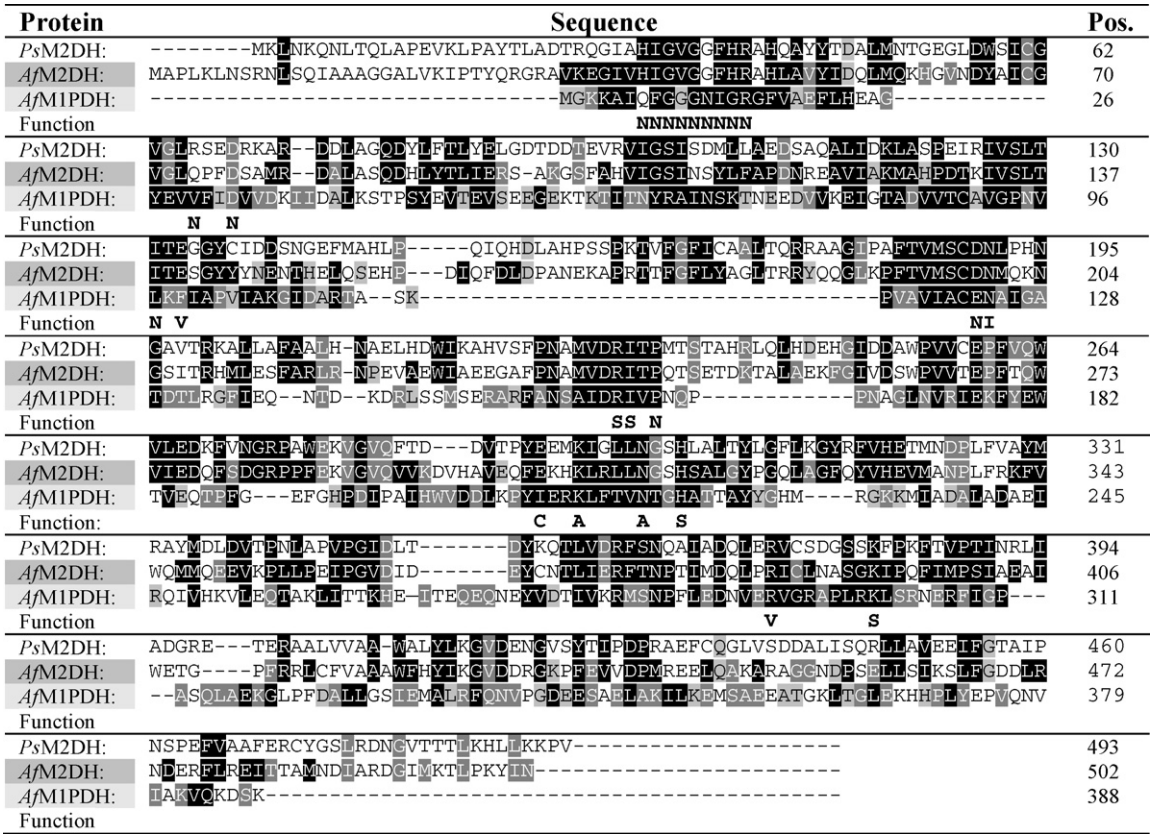

Fig. 3. Sequence comparison for *Af*M2DH, *Af*M1PDH, and *Ps*M2DH using results from a family-wide multiple sequence alignment [15]: boxes show the level of residue conservation within the sub-family (1: M2DH; 7: M1PDH) and according to their origin from prokaryotic or eukaryotic organisms as 100% (black), ≥80% (grey, white labels) and ≥60% (grey, black label). The function line highlights residues important for enzyme activity where N stands for coenzyme binding; S stands for substrate binding; C stands for catalysis. Further, V means function as N and S; A means function as S and C; I means function as N, S and C.

binding appears to have been weakened markedly under conditions of a saturating concentration of Man-ol (k_{cat}). The observed pH-dependencies also indicate that *Af*M2DH must be doubly deprotonated for activity in the direction of Man-ol oxidation. Because essentially the same p*K* values are found in the pH-rate profile under conditions when substrate is limiting (k_{cat}/K) or saturating (k_{cat}), we believe that the ionizable groups in *Af*M2DH that are responsible for pK_1 and pK_2 are important for catalysis rather than substrate binding. The assignment of p*K* values to groups is certainly not straightforward in *Af*M2DH. However, sequence changes for *Af*M2DH as compared to *Ps*M2DH in immediate neighborhood of the catalytic lysine (Fig. 3) could perhaps explain the different pH-dependencies in the two enzymes. The residue preceding the Lys in the sequence is a His in *Af*M2DH whereas it is a Met in *Ps*M2DH. It is plausible that the His would have to be unprotonated for activity and that changes in the protonation state of the His would also affect the ionization of the nearby Lys and *vice versa*. Whatever p*K* of the binary complex of *Af*M2DH with NAD^+ might represent the deprotonation of Lys^{307}, it is considerably lower than the p*K* found for Lys^{295} in the binary complex of *Ps*M2DH with NAD^+. The drop in p*K* is possibly due to the presence of basic amino acids in immediate vicinity of Lys^{307}, namely Lys^{305} and Arg^{309}.

The pH profile of $\log(k_{cat}/K)$ in Fru reduction displays a decrease at low pH where the activity is lost with a slope of +1. Furthermore, $\log(k_{cat}/K)$ decreases in a wavelike dependence from a high constant value at around neutral pH to a lower constant value at high pH. Two p*K* values describe this pH profile, implying that there are two ionizable groups in enzyme-NADH of which one must be unprotonated for substrate binding or catalysis and another should be protonated for optimum activity. While the requirement for a monoprotonated *Af*M2DH is clearly suggested by the data, the pH profile does not tell which of the two apparent groups of the enzyme must be deprotonated. The p*K* values obtained from fits of Eq. (5) to the data yield pK_2 < pK_1, reflecting positive cooperativity in proton binding to enzyme-NADH. The observed pH-dependence for $\log(k_{cat}/K)$ would be consistent with the involvement of His^{306} and Lys^{307} as ionizable groups but cannot prove it. Furthermore the level at high pH of the $\log(k_{cat}/K_{Fru})$ profile indicate a residual, although highly truncated activity that is left after deprotonation of the catalytic acid–base. This may be due to the other basic amino acids found in the neighborhood of Lys^{307}. The pH profile of $\log k_{cat}$ is overall similar to the pH profile of $\log(k_{cat}/K)$ except that pK_2 > pK_1. Therefore, like seen in the pH-dependencies of *Af*M2DH in the direction of Man-ol oxidation, the cooperativity in proton binding under conditions when Fru is limiting appears to have been decreased significantly in the presence of a saturating substrate concentration.

4.2.2. Af*M1PDH*

The pH profile of $\log(k_{cat}/K)$ for Man-ol1*P* oxidation decreases with a slope of +1 below p*K* 8.9. The pK_2 of sugar phosphates is typically in the pH range between 5.8 and 6.6 suggesting that Man-ol1*P* is unlikely to show a p*K* as high as 8.9 in solution [31]. The results indicate that a single group on the enzyme-NAD^+ complex, likely Lys^{213}, must be deprotonated for substrate binding and/or catalysis. Results of mutational analysis showing a $10^{3.8}$-fold reduction of activity in the direction of Man-ol1*P* oxidation at pH 10.0 upon replacement of the lysine by alanine support an important role for Lys^{213} in the catalytic mechanism of *Af*M1PDH. The pH profile of $\log k_{cat}$ has a similar appearance as the pH-dependencies for Fru reduction by *Af*M2DH. Fits of the data with Eq. (5) yielded two p*K* values whereby pK_2 was smaller than pK_1. We have recently shown that hydride transfer is rate limiting for k_{cat} of Man-ol1*P* oxidation by *Af*M1PDH at pH 7.1 [20]. The different pH-dependencies of $\log k_{cat}$ and $\log(k_{cat}/K)$ for Man-ol oxidation suggest that there is a change in rate limitation from hydride transfer to another step in the enzymic mechanism in response to elevation of pH.

The pH profile of $\log(k_{cat}/K)$ for Fru6*P* reduction by *Af*M1PDH is bell-shaped and shows decreases in the high and low pH region with slope values of +1 and −1, respectively. Therefore, this implies that the pH-dependence in reduction is controlled by the ionization of two groups of which one must be protonated and the other must be deprotonated for substrate binding and/or catalysis. The calculated p*K* values are separated by only 1.2 pH units, indicating that they cannot be treated as completely independent ionizations. Interestingly, the pH profile of $\log k_{cat}$ appears to be controlled by only a single ionization. It is level at low pH and decreases with a slope of −1 above p*K* 8.3. The ionizable group must be protonated for activity and is tentatively assigned to Lys^{213}, acting as general catalytic acid for carbonyl group reduction. p*K*-to-group assignment for the pH profile of $\log(k_{cat}/K)$ for Fru6*P* reduction is not clearly possible with the data available. However, it is probable that one of the observable p*K* values reflects the ionization of Lys^{213}. Considering that k_{cat} conditions eliminate one of the two p*K* values seen in the pH-dependence under conditions where the concentration of Fru6*P* was limiting (k_{cat}/K), it is reasonable to assume that the ionizable group other than Lys^{213} is required for substrate binding. Considering its pK_2 of 6.1 in solution, the phosphate group of Fru6*P* is not a likely candidate to be responsible for one of the observable p*K* values in the pH profile of $\log(k_{cat}/K)$ [31].

Summarizing, results of pH profile analysis for *Af*M2DH and *Af*M1PDH suggest that the conserved active-site lysine plays a major role in determining the pH-dependencies of the two fungal enzymes. However, when compared with *Ps*M2DH where the pH-dependencies in forward and reverse direction are simple and reflect protonation and deprotonation of Lys^{295}, respectively, the pH profiles of *Af*M2DH and *Af*M1PDH are often complex and controlled by the ionization of more than just a single enzyme group. Sequence changes in the fungal enzymes relative to *Ps*M2DH place additional ionizable residues in the immediate neighborhood of the catalytic lysine. These residues are likely to not only influence (sometimes cooperatively) the ionization behavior of the lysine but also contribute to the pH-dependence of the activity overall.

Acknowledgments

Valentin Pacher is thanked for expert technical assistance. We are grateful to Dr. Hubertus Haas (Division of Molecular Biology, Medical University of Innsbruck, Austria) for providing genomic DNA of *Aspergillus fumigatus*. Financial support from the Austrian Science Fund FWF (P18275-B09 to B.N.) is gratefully acknowledged.

References

[1] J.P. Latgé, *Aspergillus fumigatus* and aspergillosis, Clin. Microbiol. Rev. 12 (2) (1999) 310–350.
[2] V. Chazalet, J.P. Debeaupuis, J. Sarfati, J. Lortholary, P. Ribaud, P. Shah, M. Cornet, H. Vu Thien, E. Gluckman, G. Brücker, J.P. Latgé, Molecular typing of environmental and patient isolates of *Aspergillus fumigatus* from various hospital settings, J. Clin. Microbiol. 36 (6) (1998) 1494–1500.
[3] A. Schaffner, H. Douglas, A. Braude, Selective protection against conidia by mononuclear and against mycelia by polymorphonuclear phagocytes in resistance to *Aspergillus*. Observations on these two lines of defense in vivo and in vitro with human and mouse phagocytes, J. Clin. Invest. 69 (3) (1982) 617–631.
[4] D.W. Denning, Invasive aspergillosis, Clin. Infect. Dis. 26 (4) (1998) 781–805.
[5] F. Derouin, Special issue on aspergillosis, Pathol. Biol. 42 (7) (1994) 625–736.
[6] D.A. Stevens, R.B. Moss, V.P. Kurup, A.P. Knutsen, P. Greenberger, M.A. Judson, D.W. Denning, R. Crameri, A.S. Brody, M. Light, M. Skov, W. Maish, G. Mastella, Allergic bronchopulmonary aspergillosis in cystic fibrosis—state of the art: Cystic Fibrosis Foundation Consensus Conference, Clin. Infect. Dis. 37 (Suppl. 3) (2003) 225–264.
[7] B. Shen, R.G. Jensen, H.J. Bohnert, Mannitol protects against oxidation by hydroxyl radicals, Plant. Physiol. 115 (2) (1997) 527–532.

[8] D.B. Jennings, M. Ehrenshaft, D.M. Pharr, J.D. Williamson, Roles for mannitol and mannitol dehydrogenase in active oxygen-mediated plant defense, Proc. Natl. Acad. Sci. U.S.A. 95 (25) (1998) 15129–15133.
[9] V. Chaturvedi, B. Wong, S.L. Newman, Oxidative killing of *Cryptococcus neoformans* by human neutrophils. Evidence that fungal mannitol protects by scavenging reactive oxygen intermediates, J. Immunol. 156 (10) (1996) 3836–3840.
[10] B. Wong, K.L. Brauer, R.R. Tsai, K. Jayasimhulu, Increased amounts of the *Aspergillus* metabolite D-mannitol in tissue and serum of rats with experimental aspergillosis, J. Infect. Dis. 160 (1) (1989) 95–103.
[11] P.S. Solomon, O.D. Waters, R.P. Oliver, Decoding the mannitol enigma in filamentous fungi, Trends Microbiol. 15 (6) (2007) 257–262.
[12] H. Jörnvall, B. Persson, M. Krook, S. Atrian, R. Gonzalez-Duarte, J. Jeffery, D. Ghosh, Short-chain dehydrogenases/reductases (SDR), Biochemistry 34 (18) (1995) 6003–6013.
[13] B. Persson, J.S. Zigler Jr., H. Jörnvall, A super-family of medium-chain dehydrogenases/reductases (MDR). Sub-lines including zeta-crystallin, alcohol and polyol dehydrogenases, quinone oxidoreductase enoyl reductases, VAT-1 and other proteins, Eur. J. Biochem. 226 (1) (1994) 15–22.
[14] B. Persson, J. Jeffery, H. Jörnvall, Different segment similarities in long-chain dehydrogenases, Biochem. Biophys. Res. Commun. 177 (1) (1991) 218–223.
[15] B. Nidetzky, M. Klimacek, Fungal mannitol 2-dehydrogenases and mannitol-1-phosphate 5-dehydrogenases constitute novel branches in the protein family of polyol-specific long-chain dehydrogenases and reductases, in: H. Weiner, E. Maser, R. Lindahl, B. Plapp (Eds.), Enzymology and Molecular Biology of Carbonyl Metabolism, Purdue University Press, West Lafayette, 2007, pp. 305–322.
[16] W.C. Nierman, A. Pain, M.J. Anderson, J.R. Wortman, H.S. Kim, J. Arroyo, M. Berriman, K. Abe, D.B. Archer, C. Bermejo, J. Bennett, P. Bowyer, D. Chen, M. Collins, R. Coulsen, R. Davies, P.S. Dyer, M. Farman, N. Fedorova, T.V. Feldblyum, R. Fischer, N. Fosker, A. Fraser, J.L. García, M.J. García, A. Goble, G.H. Goldman, K. Gomi, S. Griffith-Jones, R. Gwilliam, B. Haas, H. Haas, D. Harris, H. Horiuchi, J. Huang, S. Humphray, J. Jimenez, N. Keller, H. Khouri, K. Kitamoto, T. Kobayashi, S. Konzack, R. Kulkarni, T. Kumagai, A. Lafon, J.P. Latgé, W. Li, A. Lord, C. Lu, W.H. Majoros, G.S. May, B.L. Miller, Y. Mohamoud, M. Molina, M. Monod, I. Mouyna, S. Mulligan, L. Murphy, S. O'Neil, I. Paulsen, M.A. Peñalva, M. Pertea, C. Price, B.L. Pritchard, M.A. Quail, E. Rabbinowitsch, N. Rawlins, M.A. Rajandream, U. Reichard, H. Renauld, G.D. Robson, S. Rodriguez de Córdoba, J.M. Rodríguez-Peña, C.M. Ronning, S. Rutter, S.L. Salzberg, M. Sanchez, J.C. Sánchez-Ferrero, D. Saunders, K. Seeger, R. Squares, S. Squares, M. Takeuchi, F. Tekaia, G. Turner, C.R. Vazquez de Aldana, J. Weidman, O. White, J. Woodward, J.H. Yu, C. Fraser, J.E. Galagan, K. Asai, M. Machida, N. Hall, B. Barrell, D.W. Denning, Genomic sequence of the pathogenic and allergenic filamentous fungus *Aspergillus fumigatus*, Nature 438 (7071) (2005) 1151–1156.
[17] M. Klimacek, K.L. Kavanagh, D.K. Wilson, B. Nidetzky, *Pseudomonas fluorescens* mannitol 2-dehydrogenase and the family of polyol-specific long-chain dehydrogenases/reductases: sequence-based classification and analysis of structure–function relationships, Chem. Biol. Interact. 143–144 (2003) 559–582.
[18] K.L. Kavanagh, M. Klimacek, B. Nidetzky, D.K. Wilson, Crystal structure of *Pseudomonas fluorescens* mannitol 2-dehydrogenase: evidence for a very divergent long-chain dehydrogenase family, Chem. Biol. Interact. 143–144 (2003) 551–558.
[19] K.L. Kavanagh, M. Klimacek, B. Nidetzky, D.K. Wilson, Crystal structure of *Pseudomonas fluorescens* mannitol 2-dehydrogenase binary and ternary complexes. Specificity and catalytic mechanism, J. Biol. Chem. 277 (45) (2002) 43433–43442.
[20] S. Krahulec, G.C. Armao, H. Weber, M. Klimacek, B. Nidetzky, Characterization of recombinant *Aspergillus fumigatus* mannitol-1-phosphate 5-dehydrogenase and its application for the stereoselective synthesis of protio and deuterio forms of D-mannitol 1-phosphate, Carbohydr. Res. 343 (9) (2008) 1414–1423.
[21] M. Slatner, B. Nidetzky, K.D. Kulbe, Kinetic study of the catalytic mechanism of mannitol dehydrogenase from *Pseudomonas fluorescens*, Biochemistry 38 (32) (1999) 10489–10498.
[22] M. Klimacek, B. Nidetzky, Examining the relative timing of hydrogen abstraction steps during NAD(+)-dependent oxidation of secondary alcohols catalyzed by long-chain D-mannitol dehydrogenase from *Pseudomonas fluorescens* using pH and kinetic isotope effects, Biochemistry 41 (31) (2002) 10158–10165.
[23] W. Wang, B.A. Malcolm, Two-stage PCR protocol allowing introduction of multiple mutations, deletions and insertions using QuikChange site-directed mutagenesis, Biotechniques 26 (4) (1999) 680–682.
[24] K.J. Ellis, J.F. Morrison, Buffers of constant ionic strength for studying pH-dependent processes, Methods Enzymol. 87 (1982) 405–426.
[25] K. Brocklehurst, D. Kowlessur, G. Patel, W. Templeton, K. Quigley, E.W. Thomas, C.W. Wharton, F. Willenbrock, R.J. Szawelski, Consequences of molecular recognition in the S1–S2 intersubsite region of papain for catalytic-site chemistry. Change in pH-dependence characteristics and generation of an inverse solvent kinetic isotope effect by introduction of a P1–P2 amide bond into a two-protonic-state reactivity probe, Biochem. J. 250 (3) (1988) 761–772.
[26] K.F. Tipton, H.B. Dixon, Effects of pH on enzymes, Methods Enzymol. 63 (1979) 183–234.
[27] M. Klimacek, K.L. Kavanagh, D.K. Wilson, B. Nidetzky, On the role of Brønsted catalysis in *Pseudomonas fluorescens* mannitol 2-dehydrogenase, Biochem. J. 375 (1) (2003) 141–149.
[28] P. Bubner, M. Klimacek, B. Nidetzky, Structure-guided engineering of the coenzyme specificity of *Pseudomonas fluorescens* mannitol 2-dehydrogenase to enable efficient utilization of NAD(H) and NADP(H), FEBS Lett. 582 (2) (2008) 233–237.
[29] B.V. Plapp, On calculation of rate and dissociation constants from kinetic constants for the ordered Bi Bi mechanism of liver alcohol dehydrogenase, Arch. Biochem. Biophys. 156 (1) (1973) 112–114.
[30] C.E. Grimshaw, K.M. Bohren, C.J. Lai, K.H. Gabbay, Human aldose reductase: subtle effects revealed by rapid kinetic studies of the C298A mutant enzyme, Biochemistry 34 (44) (1995) 14366–14373.
[31] I.C. Schneider, P.J. Rhamy, R.J. Fink-Winter, P.J. Reilly, High-performance anion-exchange chromatography of sugar and glycerol phosphates on quaternary ammonium resins, Carbohydr. Res. 322 (1–2) (1999) 128–134.

Enzymes of mannitol metabolism in the human pathogen *Aspergillus fumigatus*: kinetic properties of mannitol 2-dehydrogenase and mannitol-1-phosphate 5-dehydrogenase, and their physiological implications

Stefan Krahulec, Guilliano Cem Armao, Mario Klimacek, Bernd Nidetzky[§]

Institute of Biotechnology and Biochemical Engineering, Graz University of Technology, Petersgasse 12/I, A-8010 Graz, Austria

[§]Corresponding author

Editorial correspondence to:

Dr. Bernd Nidetzky

Institute of Biotechnology and Biochemical Engineering, Graz University of Technology, Petersgasse 12/I, 8010 Graz, Austria

E-mail: bernd.nidetzky@TUGraz.at

Phone: +43-316-873-8400; Fax: +43-316-873-8434

Abbreviations: Man-ol: D-mannitol, Man-ol1*P*: D-mannitol 1-phosphate, Fru: D-fructose, Fru6*P*: D-fructose 6-phosphate, M1PDH: mannitol-1-phosphate 5-dehydrogenase, *Af*M1PDH: M1PDH from *Aspergillus fumigatus*, M2DH: mannitol 2-dehydrogenase, *Af*M2DH: M2DH from *Aspergillus fumigatus*, *Ps*M2DH: M2DH from *Pseudomonas fluorescens*, KIE: kinetic isotope effect

Keywords: mannitol, mannitol metabolism, *Aspergillus fumigatus*, mannitol-1-phosphate 5-dehydrogenase, mannitol 2-dehydrogenase

Subdivision: Enzymes and catalysis

Summary

The sugar alcohol mannitol is ubiquitous in fungi and ascribed to fulfill a central role in stress response. While mannitol metabolism is well studied on an organism basis, little is known about the molecular properties of the enzymes involved. In the human pathogen *Aspergillus fumigatus* two polyol-specific long-chain dehydrogenases/reductase participate in mannitol metabolism, a mannitol-1-phosphate 5-dehydrogenase (*Af*M1PDH) and a mannitol 2-dehydrogenase (*Af*M2DH). Analysis of initial velocity patterns and primary kinetic isotope effects on the apparent kinetic parameters for the forward and reverse reaction show that *Af*M2DH has a random bi-bi mechanism at pH 7.1. Hydride transfer clearly contributes to the rate determine step of fructose reduction while product release limits the reaction rate of mannitol oxidation. *Af*M1PDH has a sequential bi-bi mechanism at neutral pH, where NADH and fructose 6-phosphate (Fru6*P*) binding is ordered with NADH binding first while release of mannitol 1-phosphate (Man-ol1*P*) and NAD^+ is random and most likely occurs in rapid equilibrium. The release of products is the major rate limiting step for Fru6*P* reduction, while the reaction rate of Man-ol1*P* oxidation is strongly governed by the hydride transfer. *Af*M2DH works in the thermodynamically unfavorable direction of mannitol oxidation *in vivo* and might fulfill an additional function in D-arabinitol metabolism, working as a D-arabinitol 4-dehydrogenase. *Af*M1PDH primarily acts as a reductase *in vivo*, establishing that anabolism of mannitol in *A. fumigatus* is achieved by the reduction of Fru6*P* and subsequent dephosphorylation of Man-ol1*P*. *Af*M1PDH is in contrast to the M1PDH from *E. coli* not controlled by the cellular energy charge, which may facilitate a higher flux from Fru6*P* to Man-ol1*P* and thereby the accumulation of mannitol. The thermostability of *Af*M1PDH at elevated temperatures is in line with a central role of mannitol as a stress metabolite in *A. fumigatus*.

Introduction

D-mannitol is ubiquitous throughout the fungal kingdom and one of the most abundant polyols in nature. Over the past decades a multitude of functions have been ascribed to the accumulation of mannitol in fungi. Some of the described functions could not be verified for the fungi studied, including the role as an essential carbohydrate reserve and a central contribution of mannitol metabolism in regeneration of NADPH [1]. However, the role of mannitol as a stress metabolite and especially its function in the parasitic lifestyle of several fungi has recently revived interest in the physiological function and metabolism of this polyol. Initially mannitol metabolism was proposed to function as a cycle which branches off from glycolysis at fructose 6-phosphate (Fru6*P*) and involves a mannitol-1-phosphate 5-dehydrogenase (M1PDH) interconverting Fru6*P* to mannitol 1-phosphate (Man-ol1*P*), a mannitol 1-phosphate phosphatase yielding mannitol, a mannitol 2-dehydrogenase (M2DH) that converts mannitol to fructose and a hexokinase activity to regain Fru6*P* [2]. Recent studies based on reversed genetic approaches now strongly suggest that mannitol metabolism is not operating as a cycle [1, 3-5]. The major route for mannitol production is generally believed to occur via reduction of Fru6*P* to Man-ol1*P* and subsequent dephosphorylation. Interestingly, the reverse of this pathway has been suggested to fulfill a central role in mannitol catabolism [1, 3-5].

Hence, disruption of the gene encoding for M1PDH in *Aspergillus niger*, the wheat pathogen *Phaeosphaeria nodorum* (*Stagonospora nodorum*) and the tobacco pathogen *Alternaria alternata* resulted in the absence of mannitol in the mycelium of *A. niger* and a 5-fold and 10-fold reduction in the intracellular mannitol content of *P. nodorum* and *A. alternata*, respectively [3-5]. Mannitol deficiencies revealed its requirement for thermal and osmotic stress tolerance in *A. niger* and in asexual sporulation of *P. nodorum* [3, 5]. Severity of tobacco infection strongly correlates with the mannitol content of *A. alternata* and the transcripts of the gene encoding M1PDH and M2DH increase in response to host plant cell

extract [6, 7]. Moreover, the infected plant excretes a mannitol 1-dehydrogenase (oxidizes mannitol to mannose) in response to fungal infection. Overexpression of a mannitol 1-dehydrogenase from celery in tobacco was therefore a successful strategy to enhance the resistance against *A. alternata*, strengthening the notion that mannitol is a central factor of plant pathogenicity [6-8]. Increasing levels of mannitol were noted for other interactions of fungal pathogens (e.g. *Uromyces fabae*, *Cladosporium fulvum*) and their hosts, indicating that the important role of mannitol is clearly not limited to *A. alternata* [9, 10]. In accordance with the studies on plant pathogens it was reported that the human pathogen *Cryptococcus neoformans* produces large amounts of mannitol in infected hosts which protects the organism against reactive oxygen species (ROS) generated by phagocytes [11, 12]. A mannitol low producer mutant was more susceptible to growth inhibition and killing by heat, high salt concentrations and human polymorphonuclear neutrophils and was thereby 5000-fold less pathogenic than the wild type strain [12, 13]. In line with these reports on the central role of mannitol in fungal pathogenicity, it was found that *Aspergillus fumigatus* excretes enough mannitol to raise serum mannitol levels of infected animals [14].

The pathogenic and allergenic mold *A. fumigatus* is regarded as the most common agent to cause invasive aspergillosis in immunosuppressed hosts [15]. One of the traits assigned to pathogenicity is its high thermotolerance, surviving temperatures up to 70°C. Lately it was found that M1PDH from *A. fumigatus* (*Af*M1PDH) is up regulated at the transcriptional level upon heat shock and a concomitant increase in the protein product has been identified [16]. A role of *Af*M1PDH and hence mannitol metabolism in the thermotolerance of *A. fumigatus* is in good accordance with the findings that mannitol is necessary for *A. niger* and *C. neoformans* to cope with heat shock. Besides other virulence factors, the ability to suppress ROS generated by the host phagocytes has been described for *A. fumigatus* [17]. Overall it can be concluded that mannitol metabolism might be a viable target for novel antifungal strategies.

Besides early studies on M1PDH from *A. niger*, little is known about the enzymatic properties of fungal M1PDHs [18]. Detailed kinetic analysis of the enzymes is however a prerequisite to understand the *in vivo* function of enzymes involved in the mannitol metabolism. To date these data are not available for the enzymes related to mannitol metabolism of *A. fumigatus*. Recently we described molecular cloning, overexpression in *E. coli* and purification of a *Af*M2DH and *Af*M1PDH, which were both classified as members of the polyol-specific long-chain dehydrogenases/reductases (PSLDR) family [19, 20]. Since there are no PSLDR orthologous in the human genome, *Af*M2DH and *Af*M1PDH might be potential targets for selective inhibition in antifungal strategies. Herein we now report on detailed kinetic analysis of the two enzymes and their physiological implications.

Results

Substrate specificity of *Af*M1PDH and *Af*M2DH

Substrate range for *Af*M2DH was tested with a variety of sugars and sugar alcohols (see the experimental section for details). *Af*M2DH showed significant activities (≥ 1% in comparison to D-mannitol/D-fructose) only with the substrate pairs D-arabinitol/D-xylulose and D-sorbitol/L-sorbose. Apparent kinetic parameters for these substrates are summarized in Table 1. For fructose and xylulose substrate inhibition was noted at high substrate concentrations. Taking account for substrate inhibition did not significantly alter the apparent kinetic constants compared to parameters obtained from fitting the Michaelis-Menten equation to data points below the occurrence of substrate inhibition (see Table 1). Unless otherwise noted, subsequent determinations of kinetic parameters in the direction of fructose reduction were carried out below an inhibiting substrate concentration. As expected for a member of the PSLDR sub-family 1, the D-*arabo* configuration of polyol substrates is necessary for activity with *Af*M2DH [21]. As observed for M2DH from *Pseudomonas fluorescens* (*Ps*M2DH) the C2 (*R*) configuration (D-mannitol) is preferred over the C2 (*S*)

configuration (D-sorbitol). It can be assumed from the crystal structure of *Ps*M2DH that carbonyl substrates bind to the active site of *Af*M2DH in their open chain form [22]. Hence, the lower K_M value for xylulose than for fructose can be explained by a much higher abundance of the open-chain tautomere for xylulose (~20% [23]) than for fructose (~1% [24]). Based on the free carbonyl form in solution, the K_M for fructose is 2.8-fold lower than for xylulose.

Table 1: Kinetic constants for the substrate spectrum of *Af*M2DH

Values in brackets are those obtained when substrate inhibition is taken into account (see the Results for details).

Substrate	k_{cat} [s^{-1}]	K_m [mM]	k_{cat}/K_m [$s^{-1}mM^{-1}$]
D-fructose	86 ± 5 (93 ±9)	60 ± 7 (65 ± 8)	1.4 ± 0.2 (1.4 ± 0.2)
D- xylulose	64 ±1 (70 ±1)	8.3 ± 0.4 (9.6 ± 0.3)	7.7 ± 0.4 (7.3 ± 0.3)
L-sorbose	ND	ND	0.0022 ± 0.0001
D-mannitol	212 ± 3	13 ± 1	17 ± 1
D-arabinitol	162 ± 5	163 ± 13	0.99 ± 0.08
D-sorbitol	60 ± 1	680 ± 30	0.088 ± 0.004

Unlike M2DHs, M1PDHs (PSLDR sub-family 7) are highly specific for their natural substrate pair Man-ol1*P* and Fru6*P* [18, 25]. Activity of *Af*M1PDH was probed with a variety of phosphorylated and unphosphorylated sugars and sugar alcohols (see the experimental section for details). Activity with all substrate was < 1% than the activity with the natural substrate pair which is in good accordance with the substrate specificity of other members of the PSLDR sub-family 7. M1PDH from *Aspergillus niger* was reported to be inactive (< 0.1%)

with a variety of phosphorylated sugars (glucose 6-phosphate, fructose 1-phosphate, ribose 5-phosphate, glucitol 6-phosphate) [18] and out of D-glucose 6-phosphate, D-fructose 1-phosphate, D-mannose 6-phosphate, L-sorbose 6-phosphate, D-tagatose 6-phosphate, D-ribulose 5-phosphate and D-sedoheptulose 7-phosphate *E. coli* M1PDH showed only detectable activity with D-glucose 6-phosphate (10%) [25].

Both enzymes have a high preference for NAD^+ over $NADP^+$. In terms of $k_{cat}/K_{coenzyme}$ a ~3000 and ~1000-fold preference for NAD^+ was measured for *Af*M1PDH (data not shown) and *Af*M2DH ([20]), respectively. This is in good accordance with a ~850-fold preference for NAD^+ reported for *Ps*M2DH ([26]). It was suggested by the crystal structure of *Ps*M2DH complexed with NAD^+ [22] and confirmed by mutational analysis [26] that the side chain of Asp^{69} prevents accommodation of the 2'-phosphate group of $NADP^+$, which is conserved in *Af*M2DH and *Af*M1PDH.

Initial velocity patterns from full kinetic studies

Initial rates for NADH-dependent reduction of Fru6*P* and fructose as well as NAD^+-dependent Man-ol1*P* and mannitol oxidation with *Af*M1PDH and *Af*M2DH, were recorded at pH 7.1. Varying substrate concentrations were employed at different constant cofactor concentrations (see the experimental section for details). Double reciprocal plots gave intersecting patterns for the forward and reverse reactions of both enzymes (Figure 1). This is consistent with a sequential reaction mechanism were both, substrate and coenzyme, have to bind to the enzyme to form a ternary complex before a product is released. For reduction of Fru6*P* with *Af*M1PDH data were analyzed considering an ordered mechanism of reactant binding (Eq (3)). Data for the oxidation of Man-ol1*P* with *Af*M1PDH as well as for the forward and reverse reaction of *Af*M2DH were analyzed accounting for a random mechanism (Eq (4)) (see the discussion for details). Kinetic parameters obtained from full kinetic studies are summarized in Table 2. Note that the rather small value for K_{iNADH} of Fru6*P* oxidation

was difficult to determine and may be afflicted with a rather large error. Internal consistency of the constants for *Af*M1PDH and *Af*M2DH in Table 2 was verified with the Haldane relationship for a sequential bi-bi kinetic mechanism Eq. (5) where app K_{eq} is the apparent equilibrium constant at pH 7.1. For *Af*M1PDH kinetic constants gave an app K_{eq} of 0.0055. This value corresponds to a pH independent thermodynamic K_{eq} of 4.3×10^{-10} M which is in perfect agreement with a previously determine K_{eq} of 4.9×10^{-10} M [25]. Likewise a pH independent K_{eq} of 4.3×10^{-9} M was calculated for *Af*M2DH. This value is in good accordance with previously reported K_{eq} values of 8.2×10^{-9} M and 5.3×10^{-9} M determined from kinetic constants and experimentally [27]. Equilibrium constants reveal that the direction of Man-ol1*P* oxidation is thermodynamically ~10-times less favored than the oxidation of mannitol.

Table 2: Kinetic parameters for the natural substrate pair of *Af*M1PDH and *Af*M2DH

Data was obtained using varying substrate concentrations at different constant cofactor concentrations in 100 mM Tris/HCl pH 7.1 (see the experimental section). Experimental data were fitted to a) Eq. (3) or b) Eq. (4).

	k_{cat} [s^{-1}]	$K_{cofactor}$ [mM]	$K_{substrate}$ [mM]	K_{iA} [µM]	α
			***Af*M1PDH**		
Fru6*P* / NADH [a]	112 ± 7	0.042 ± 0.005	3.5 ± 0.4	3.4 ± 2.1	
Man-ol1*P* / NAD^+ [b]	8.9 ± 0.6	0.82 ± 0.32	0.13 ± 0.05		1.6 ± 0.8
			***Af*M2DH**		
Fru / NADH [b]	94 ± 4	0.015 ± 0.008	41 ± 24		1.4 ± 0.9
Man-ol / NAD^+ [b]	14.2 ± 0.3	0.11 ± 0.02	11 ± 2		2.0 ± 0.4

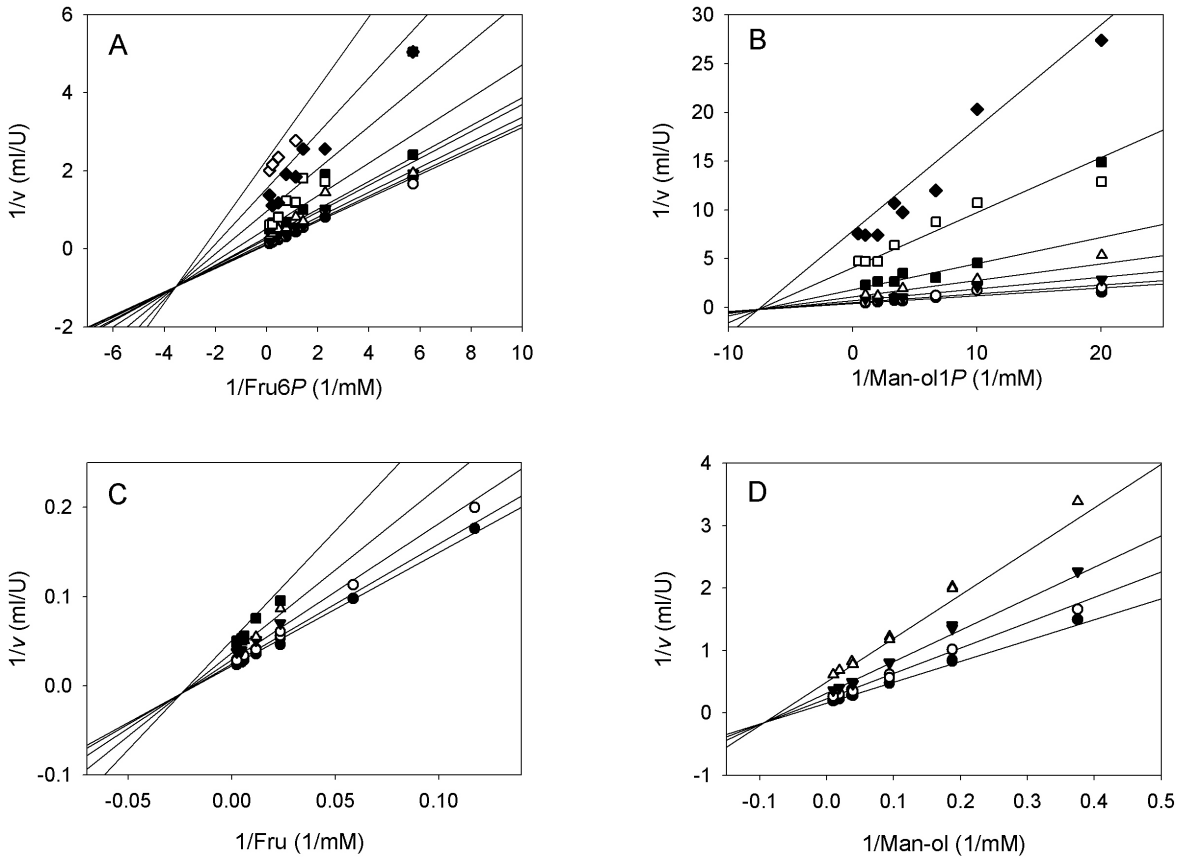

Figure 1: Double reciprocal plots of initial rate measurements with *Af*M1PDH (panel A and B) and *Af*M2DH (panel C and D) at pH 7.1.

Panels A and B show initial rates for reduction of varying Fru6*P* concentrations (A) and oxidation of varying Man-ol1*P* concentrations (B) at several constant NADH (A) and NAD^+ (B) concentrations (full circles: (A) 160 µM (B) 5.9 mM; empty circles: (A) 80 µM (B) 2.9 mM; full triangles: (A) 40 µM (B) 1.2 mM; empty triangles: (A) 20 µM (B) 0.59 mM; full squares: (A) 8 µM (B) 0.29 mM; empty squares (A) 4µM (B) 0.12 mM; full diamonds: (A) 2.4 µM (B) 0.059 mM; empty diamonds (A) 1.6 µM). Panels C and D display initial rates for reduction of varying fructose concentrations (C) and oxidation of varying mannitol concentrations (D) at several constant NADH (C) and NAD^+ (D) concentrations (full circles: (C) 200 µM (D) 1.4 mM; empty circles: (C) 100 µM (D) 0.34 mM; full triangles: (C) 50 µM (D) 0.17 mM; empty triangles: (C) 25 µM (D) 0.085 mM; full squares: (C) 14 µM).

Control of enzyme activities by the cellular energy charge

An inhibition study with adenine nucleotides was performed to evaluate the control of the cellular energy charge over the enzymatic activity of M1PDH and M2DH and hence on the flux to and from mannitol. Inactivation patterns of ATP, ADP and AMP were recorded for both enzymes in forward and reverse reaction using a constant and saturating concentration of the substrates while cofactors were varied at different constant concentrations of the adenine nucleotides. Plots of reciprocal reaction rates against reciprocal cofactor concentrations are shown in Supplementary Figure 1 (*Af*M1PDH) and Supplementary Figure 2 (*Af*M2DH). Inhibition with adenine nucleotides was best described by a competitive binding to the enzymes between the inhibitors and the cofactors. Inhibition constants (K_i^{EI}) were therefore obtained by fitting Eq. (6) to the experimental data. Resulting K_i^{EI} values are presented in Table 3. No inhibitory effect of ATP on NAD^+ and NADH binding could be detected for mannitol reduction and fructose oxidation with *Af*M2DH.

Table 3: Inhibition constants of adenine nucleotides for *Af*M1PDH and *Af*M2DH

Data was obtained using varying cofactor concentrations at different constant adenine nucleotide concentrations in 100 mM Tris/HCl pH 7.1, keeping the substrate concentration constant and saturating (see the experimental section).

	***Af*M1PDH**		***Af*M2DH**	
	Fru6*P* reduction	Man-ol1*P* oxidation	Fru reduction	Man-ol oxidation
$K_i^{EI}{}_{AMP}$ [mM]	4.6 ± 0.6	1.5 ± 0.1	2.9 ± 0.7	5.6 ± 0.5
$K_i^{EI}{}_{ADP}$ [mM]	5.6 ± 1.9	2.0 ± 0.2	4.8 ± 1.3	5.7 ± 0.4
$K_i^{EI}{}_{ATP}$ [mM]	6.5 ± 1.4	1.4 ± 0.1	ND	ND

Kinetic isotope effects

Kinetic isotope effects (KIE) were determined for the forward and reverse reaction of *Af*M1PDH and *Af*M2DH at pH 7.1 by comparing initial rates recorded with unlabeled and the deuterium labeled cofactor (4*S*)-[²H]-NADH as well as by comparing rates for unlabeled and labeled forms of Man-ol1*P* and mannitol, respectively. Isotope effects on k_{cat}, $k_{cat}/K_{cofactor}$ and $k_{cat}/K_{substrate}$ are summarized in Table 4. KIEs for reduction of Fru6*P*, oxidation of Man-ol1*P*/5-[²H]-Man-ol1*P* with *Af*M1PDH and oxidation of mannitol/2-[²H]-D-mannitol with *Af*M2DH were calculated by fitting Eq. (7) to the experimental data. Note that the symmetry of mannitol results in a deuterated fraction (F_i) of 0.5 for 2-[²H]-mannitol. Substrate inhibition that occurred for *Af*M2DH at high fructose concentrations (molar range) with NADH was absent with (4*S*)-[²H]-NADH. Therefore, KIE on k_{cat} in the direction of fructose oxidation was determined by fitting Eq. (7) to the experimental initial rates using varied fructose concentrations below occurrence of substrate inhibition and by direct comparison of k_{cat} values for (4*S*)-[²H]-NADH and NADH taking account for substrate inhibition. $^{D}k_{cat}$ for fructose reduction in Table 4 (2.0 ± 0.3) represents a mean value and SD for 3 independent experiments evaluated in either way described above. $^{D}k_{cat}/K_{Fru}$ was calculated by fitting Eq. (8) to initial rates recorded below a fructose concentration of 40 mM. $^{D}k_{cat}/K_{NADH}$ was calculated according to $^{D}k_{cat}/(K_{NADH}/K_{(4S)\text{-}[^2H]\text{-}NADH})$. Note that K_{NADH} was constant for a broad range of fructose concentrations (0.020 – 0.018 mM at 40 to 800 mM fructose).

Table 4: Kinetic isotope effects for forward and reverse reaction of *Af*M1PDH and *Af*M2DH

Data was obtained from initial rate measurements of protio and deuterio forms of the sugar alcohols and NADH at pH 7.1.

***Af*M1PDH**			
$^{D}k_{cat}$	2.9 ± 0.2	$^{D}k_{cat}$	1.5 ± 0.1
$^{D}(k_{cat}/K_{Man\text{-}ol1P})$	2.4 ± 0.5	$^{D}(k_{cat}/K_{Fru6P})$	3.1 ± 0.4
$^{D}(k_{cat}/K_{NAD})$	2.4 ± 0.4	$^{D}(k_{cat}/K_{NADH})$	0.8 ± 0.2
***Af*M2DH**			
$^{D}k_{cat}$	1.0 ± 0.1	$^{D}k_{cat}$	2.0 ± 0.3
$^{D}(k_{cat}/K_{Man\text{-}ol})$	1.2 ± 0.2	$^{D}(k_{cat}/K_{Fru})$	1.9 ± 0.2
$^{D}(k_{cat}/K_{NAD})$	1.6 ± 0.2	$^{D}(k_{cat}/K_{NADH})$	1.6 ± 0.3

Thermal stability of *Af*M1PDH and *Af*M2DH

Stability of *Af*M1PDH was investigated at 30°C, 40°C and 50°C in 100 mM Tris/HCl pH 7.1. Due to a fast inactivation above 30°C, thermal stability of *Af*M2DH was followed at 0°C, 25°C and 30°C using the same buffer. Semi logarithmic plots of normalized residual activities revealed a first order activity decay (Supplementary Figure 3). Half life times (τ_H) are summarized in Table 5. At 30°C *Af*M1PDH showed a more than two orders of magnitude higher half life time than *Af*M2DH. In contrast to *Af*M2DH, *Af*M1PDH is quite stable at elevated temperatures. Stability of *Af*M1PDH is almost independent on the protein concentration (τ_H at 6 µg/ml is at least 60% of the τ_H at 0.23 mg/ml). Half life times for *A. niger* M1PDH and *A. parasiticus* M1PDH at pH 7.0 and 30°C were reported to be greater than 4.7 h and 2 h, respectively [28], hence about one order of magnitude smaller than for *Af*M1PDH. Heat treatment (10 minutes, 50°C in 50 mM Tris/HCl pH 7.5) of M1PDH from *Spatoglossum pacificum* resulted in a complete inactivation [29]. Comparison with these M1PDHs indicates a remarkable thermal stability of the enzyme from *A. fumigatus*.

Table 5: Thermal stability of *Af*M1PDH and *Af*M2DH

τ_H is the half life time of the enzyme under the indicated conditions.

***Af*M1PDH**			***Af*M2DH**		
Temperature	$\tau_{H\ (0.23\ mg/ml)}$ [h]	$\tau_{H\ (6\ \mu g/ml)}$ [h]	Temperature	$\tau_{H\ (0.5\ mg/ml)}$ [h]	$\tau_{H\ (3\ \mu g/ml)}$ [h]
30°C	43 ± 4	31 ± 1	0°C	93 ± 7	15 ± 1
40°C	23 ± 1	18 ± 2	25°C	3.6 ± 0.2	0.64 ± 0.03
50°C	0.26 ± 0.03	0.16 ± 0.02	30°C	0.42 ± 0.04	0.06 ± 0.01

Discussion

Substrate recognition

A crystal structure of the ternary complex of *Ps*M2DH indicated 8 residues which are directly interacting with the hydroxyl-groups of mannitol [22]. All of them are conserved in *Af*M2DH and *Af*M1PDH including Lys^{381} (*Ps*M2DH numbering) which interacts with the C6-OH group of mannitol (the position of the phosphate group in Man-ol1*P*). Another amino acid (Glu^{133}) interacting with mannitol via a water molecule is conserved in *Af*M2DH but replaced against Phe in *Af*M1PDH. It was postulated that exchange of Glu^{133} (interacting with Lys^{381} via a second water molecule) and Phe^{385} (located parallel to the side chain of Lys^{381}) to Phe and Asn, respectively, causes conformational changes involving Lys^{381} and provide binding and recognition for Man-ol1*P* [30]. Oxidation of a broad range of aldose sugars was assayed with *Af*M2DH and *Af*M1PDH to test the possibility of replacing the C6-OH group of mannitol or the phosphate group of Man-ol1*P* by an aldehyde moiety and hence oxidation of the C5-OH /C4-OH group of hexoses and pentoses. None of them showed significant activity (> 1% than the activity with the natural substrate) rejecting the possibility that *Af*M2DH or *Af*M1PDH have a hexose 5-oxidoreductase or pentose 4-oxidoreductase activity.

The substrate range of *Af*M2DH is in good accordance with the substrate specificity of a previously characterized bacterial PSLDR, *Ps*M2DH [27]. Apparent substrate binding

affinities for fructose and sorbitol are in the same range for the bacterial and the fungal enzyme (2.5-fold higher $K_{fructose}$ und 1.5-fold higher $K_{sorbitol}$ for *Af*M2DH) [27]. Affinities for the polyols mannitol and arabinitol were markedly decreased in *Af*M2DH (33- and 12-fold, respectively) while the affinity for xylulose was 16-fold increased [27, 31]. Turn over numbers were generally slightly higher for the fungal enzyme (1.6-fold for fructose, 2.5-fold for xylulose, 5-fold for mannitol, 3.4-fold for arabinitol and 4.7-fold for sorbitol) [27, 31]. Note that parameters for *Ps*M2DH with sorbitol and arabinitol were measured at pH 9.0 [27]. The almost 40-fold increase in the catalytic efficiency on xylulose for *Af*M2DH is interesting since the genomic sequence of *A. fumigatus* suggests that a distinct D-arabinitol 4-dehydrogenase (EC 1.1.1.11), catalyzing the reduction of D-xylulose to D-arabinitol is absent in this organism [32]. This suggests that *Af*M2DH might, besides oxidation of mannitol, fulfill a role in D-arabinitol metabolism of *A. fumigatus*. In this respect, the role of a putative enzyme annotated as D-arabinitol dehydrogenase but assigned to the EC Nr. 1.1.1.69 (gluconate 5-dehdrogenase) is currently unclear [32]. However, this protein shows low sequence identity to D-arabinitol 4-dehydrogenase (≤ 12.1 % to the enzyme from *Klebsiella pneumoniae*, *Yersinia pestis* and *Ralstonia solanacearum*). In turn it must be noted that a putative protein of *A. fumigatus* that is currently classified as a Sou1-like, sorbitol/xylulose reductase (UniProt/TrEMBL entry Q4WZX5) might have a function as a short chain $NADP^+$-dependent M2DH [30].

Mechanistic deductions for *Af*M2DH and *Af*M1PDH

Full kinetic studies in oxidative and reductive direction revealed a sequential mechanism for *Af*M1PDH and *Af*M2DH. For *Af*M1PDH an isotope effect for k_{cat}/K_{NADH} that is unity within the experimental error and an isotope effect of ~3 for k_{cat}/K_{Fru6P} reveals that binding of Fru6*P* and NADH is ordered, where NADH has to bind before Fru6*P* to form the ternary complex. Finite and equal KIEs on k_{cat}/K_{NAD} and $k_{cat}/K_{Man\text{-}ol1P}$ suggest that release of Man-ol1*P* and

NAD^+ from the ternary complex is random and most likely occur in rapid equilibrium [33]. It is interesting to note that in addition to equal isotope effects on catalytic efficiencies *Af*M1PDH has even a lower affinity for NAD^+ than for Man-ol1*P* binding at pH 7.1. The same observations, random binding and $K_{NAD} > K_{Man\text{-}ol1P}$, were made for M1PDH from *A. niger* [18]. The suggested catalytic mechanism for *Af*M1PDH is summarized graphically in Figure 2A. The somewhat lower isotope effect of k_{red} than for k_{red}/K_{Fru6P} implies that product release contributes significantly to the rate determine step in the overall reaction of Fru6*P* reduction. In contrast, a high $^{D}k_{cat}$ of ~3 was noted for Man-ol1*P* oxidation illustrating that hydride transfer strongly governs the reaction rate for Man-ol1*P* oxidation under substrate saturated conditions [19]. Considering a ~20-fold higher turn over number for Fru6*P* reduction than for Man-ol1*P* oxidation leads to the conclusion that the hydride transfer from NADH to the ketose substrate is much faster than from the alcohol to NAD^+.

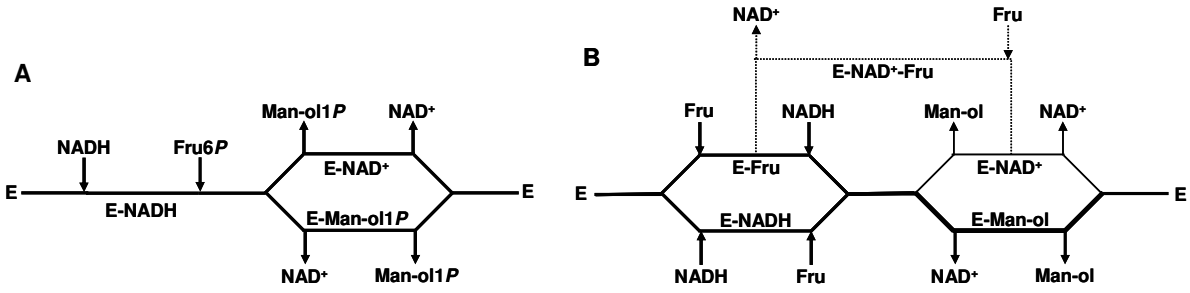

Figure 2: Suggested reaction mechanisms for *Af*M1PDH (A) and *Af*M2DH (B) at pH 7.1.

The thin and thick lines for product release in panel B shows the preference for NAD^+ to dissociate before mannitol. To account for the observed substrate inhibition pattern the formation of an abortive E-NAD^+-Fru complex is suggested and indicated by a dotted line (see the Discussion section for details).

Isotope effects measured with *Af*M2DH in the forward and reverse reaction suggest that substrate binding and product release occur in a random fashion (Figure 2B). α factors > 1 indicate that binding of the first substrate does not support binding of the second substrate. Almost equal and statistically not significantly different isotope effects on k_{cat}/K_{Fru} and on k_{cat}/K_{NADH} indicate almost equal chances for the formation of the enzyme-NADH and enzyme-fructose complexes, with maybe a slight preference for the formation of the E-NADH complex. Due to a higher KIE for k_{cat}/K_{NAD} than for $k_{cat}/K_{Man\text{-}ol}$ release of NAD^+ before mannitol seems to be preferred. $k_{cat}/K_{Man\text{-}ol}$ can within the experimental error even be unity which would point towards reactant release in an ordered fashion, where NAD^+ has to dissociate first from the Michaels-complex. Substrate inhibition for fructose reduction was noted for saturating and subsaturating concentrations of NADH (0.25 – 0.025 mM). Inhibition was however absent with (4*S*)-[²H]-NADH. Substrate inhibition was further noted for xylulose reduction with NADH with a somewhat lower inhibition constant, reflecting the lower K_M for xylulose than for fructose. These observations highly disfavor explanation of substrate inhibition based on diffusion limitation at higher viscosities (molar fructose concentrations). Inhibition solely based on the slower formation of the ternary complex via E-fructose seems unlikely since the inhibition pattern was not altered significantly (data not shown) at varying NADH concentrations. We therefore suggest that the observed effect might be best described by the formation of an abortive E-NAD^+-fructose complex which dissociates at a rate that can limit the overall reduction of fructose with NADH but is not limiting for the ~2-times slower reduction with (4*S*)-[²H]-NADH. Formation of this abortive complex necessitates occurrence of an E-NAD^+ complex which further strengthens the notion that product release is not strictly ordered. However, substrate inhibition at molar concentrations of fructose seems to be unlikely to influence the enzyme action *in vivo*. $^{D}k_{cat} \geq {}^{D}k_{cat}/K_{NADH}$ and $^{D}k_{cat}/K_{Fru}$ suggest that in the direction of fructose reduction product release form the ternary complex is fast and has little control about the overall reaction rate

whereas hydride transfer clearly contributes to the rate limiting step. An isotope effect on k_{cat} for mannitol oxidation which is unity indicates that product dissociation is completely rate limiting for the overall reaction in direction of substrate oxidation.

Enzymatic properties controlling flux to and from mannitol *in vivo*

Almost equal and relatively high K_i values for adenine nucleotide inhibition of Fru6*P* reduction with *Af*M1PDH (Table 3) are in a remarkable contrast to the inhibition pattern of the bacterial M1PDH from *E. coli* (K_i of ATP ~0.06 mM, K_i of AMP ~0.8 mM [34]). While at high ATP concentrations (aerobic conversion of glucose), the reduction of Fru6*P* is strongly inhibited in *E. coli*, no regulation of Fru6*P* reduction due to the cellular energy charge is expected for *Af*M1PDH. This suggests a significantly different role of M1PDH and hence mannitol metabolism in *A. fumigatus* than in *E. coli* and is in line with accumulation of this polyol in *A. fumigatus*. Regulation of *Af*M1PDH and mannitol metabolism is more likely to occur at the transcriptional or translational level (e.g. M1PDH production is induced by heat shock [16]). Likewise it was found for *A. niger* that the expression of the gene encoding M1PDH was higher in conidiating mycelium and that M1PDH activity increased more than six fold in sporulating mycelium. This correlates with a 4.5-fold higher mannitol concentration in spores than in mycelia indicating that mannitol production in *A. niger* is at least partially controlled by the transcription or translation of the gene encoding the M1PDH activity [3]. In the reverse direction of Man-ol1*P* oxidation the K_i values of ATP and AMP are similar for both (*E. coli* and *A. fumigatus*) M1PDHs and approximately equal for both adenine nucleotides [34]. Like for Fru6*P* reduction with *Af*M1PDH, there is apparently no control of the Man-ol1*P* oxidation by the energy charge for both M1PDHs. However adenine nucleotides might reduce the reaction rate for Man-ol1*P* oxidation with *Af*M1PDH under *in vivo* substrate concentrations (applying intracellular metabolite concentration determined for

A. niger – see the following paragraph: turn over uninhibited 0.8 s^{-1} and inhibited 0.4 s^{-1}, according to Eq. (4) and Eq. (10), respectively).

Relevant intracellular concentrations to estimate the enzymatic action of M1PDH *in vivo* have been described by Ruijter and coworkers for the closely related fungi *A. niger* in the exponential growth phase of aerobically glucose grown mycelium (ATP 2.6 mM, ADP 0.5 mM, AMP 0.09 mM, NAD^+ 0.83 mM, NADH 0.01 mM, Fru6*P* 0.23 mM [35] and Man-ol1*P* 0.05 mM [3] - internal cell volume determined by the same authors in [35] was taken to calculated mM from µM/g CDW). Assuming comparable intracellular concentrations for *A. fumigatus*, a ~5-fold higher turn over for the reduction of Fru6*P* (4.4 s^{-1}) than for oxidation of Man-ol1*P* (0.8 s^{-1}) is calculated using Eq. (3) and Eq. (4), respectively. Taking account for inhibition by adenine nucleotides (Eq. (9) and Eq. (10)) increases the preference for the reduction of Fru6*P* to ~10-fold (Fru6*P* reduction: 4.1 s^{-1}; Man-ol1*P* oxidation: 0.4 s^{-1}). Disregarding possible product inhibition, this strongly indicates that *Af*M1PDH works as a reductase *in vivo*. While intracellular concentration of Fru6*P*, NAD^+ and adenine nucleotides determined for *A. niger* are in good accordance with data for other organisms (e.g. *Penicillium chrysogenum* [36, 37]) the reported intracellular concentration of NADH is subject to a high error (10 ± 10 µM) and is rather low compared to reports for other organisms [35, 38, 39]. Moreover the intracellular Man-ol1*P* concentration might change from fungi to fungi and may change with growth conditions. We therefore evaluated the change in the net turn over (k_{net}, which is the turn over for Fru6*P* reduction minus the turn over for Man-ol1*P* oxidation), depending on varying NADH and Man-ol1*P* concentrations (Figure 3A and B). For both cases, including (Figure 3B) or excluding (Figure 3A) inhibition by adenine nucleotides, *Af*M1PDH seems to work as a reductase over the entire concentration range considered (NADH 5 to 150 µM, Man-ol1*P* 10 to 500 µM). Applying the equilibrium constant for Man-ol1*P* oxidation of 4.9×10^{-10} M as determined by Wolff and Kaplan [25], reveals a ~9-fold deviation from equilibrium at the postulated *in vivo* concentrations, implying an enzymatic

action in the reductive direction. Dependency on Man-ol1*P* and NADH concentrations as described above is demonstrated in Figure 3C and supports the notion that *Af*M1PDH primarily works as a reductase *in vivo* and hence facilitates a net flux from Fru6*P* to Man-ol1*P*.

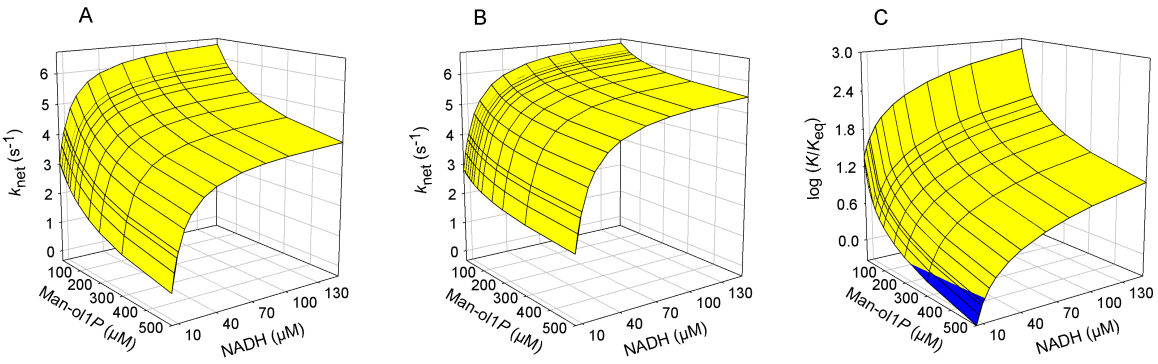

Figure 3: Predicted *in vivo* direction for interconversion of Fru6*P* and Man-ol1*P* with *Af*M1PDH.

Yellow parts show conditions were *Af*M1PDH works as a reductase while blue parts denote for enzymatic action in the direction of Man-ol1*P* oxidation. Panel A shows k_{net} against reactant concentrations of NADH and Man-ol1*P*, calculated according to Eq. (3) and (4) applying constants from Table 2. Panel B displays k_{net} when inhibition by adenine nucleotides is taken into account (Eq. (9) and Eq. (10)). In panel C direction of reaction is predicted based on the ratio of reactant concentrations to the equilibrium constant ($K_{eq} = 4.9\times10^{-10}$ M [25]) at pH 7.1. *In vivo* concentrations of Fru6*P*, NAD^+ and adenine nucleotides were taken from studies of *A. niger* [3, 35].

This is in line with the observations that disruption of the gene encoding for the M1PDH activity in *A. alternata*, *A. niger* and *P. nodorum* results in a ≥ 70% reduced intracellular mannitol content [3-5]. The central role of M1PDHs in the production of mannitol is thereby fully corroborated. Interestingly, knock-out of M2DH in *A. alternate* resulted in normal growth on mannitol while the M1PDH mutant grew poorly [4]. Similarly it was found that a M2DH knock-out of *P. nodorum* grew on mannitol with a lower rate but no growth was

evident when M1PDH was disrupted [5] (note that this study might have overlooked the existence of a second M2DH in *P. nodorum* [30]). These results suggest that M1PDH can have a central role in mannitol catabolism, when used as the sole carbon source. However, knock–out studies do not give an answer, whether intracellularly stock piled mannitol is utilized via oxidation of Man-ol1*P*. Thermodynamics of the interconversion of Fru6*P* and Man-ol1*P* with NAD(H) necessitates an increase in the Man-ol1*P* to Fru6*P* and/or NADH to NAD^+ ratio to facilitate enzymatic conversion in the oxidative direction. Under these conditions (maybe when mannitol is used as carbon source) *Af*M1PDH might also function as an oxidase.

For *Af*M2DH, no inhibition was observed with ATP for mannitol oxidation and fructose reduction. Inhibition constants for AMP and ADP are in both directions more than one order of magnitude higher than the expected *in vivo* concentrations of these adenine nucleotides. Therefore, it can be concluded that *Af*M2DH is not significantly inhibited by adenine nucleotides *in vivo*. In an early study on *A. fumigatus* metabolites a mannitol content of about ~1% was determined [40]. Assuming the same intracellular volume than for *A. niger* this results in an intracellular mannitol concentration of ~ 50 mM. For *A. niger* an internal mannitol content of ~120 mM (mycelia) and ~500 mM (spores) is calculated [3]. Mannitol concentrations in the range of 50 mM or above and a NAD^+ concentration of ~0.8 mM imply that *Af*M2DH is saturated (> 4.5-fold K_M) with mannitol and NAD^+ (~ 7.5-fold K_M) *in vivo*. Based on cofactor concentrations determined for *A. niger* and the equilibrium constant for fructose reduction (8.1×10^{-9} M) [27] a nine-fold higher intracellular fructose than mannitol content would be necessary to thermodynamically facilitate a net reduction of fructose. Even though no literature on internal fructose concentration is (to our knowledge) available, fructose concentrations exceeding the mannitol content are highly unlikely to occur in the fungal cell. Hence, it can be concluded that *Af*M2DH works in the thermodynamically unfavorable direction of alcohol oxidation *in vivo*.

Thermal resistance of *Af*M1PDH might be linked to heat shock

A. fumigatus thermotolerance (surviving up to 70°C) is regarded as one of the pathogenicity factors of this human-pathogenic mold. Thermoresistance is polygenic and heat shock response is largely controlled by the transcription factors Hsf 1, Msn 2/4 and Hac 1 [16]. Recently it was shown that expression of *Af*M1PDH is regulated by Hsf1 and an up regulation of M1PDH at the transcriptional level as well as a corresponding increase of the protein product at a shift from 30 to 48°C has been identified [16]. Furthermore it was outlined that heat shock goes along with enhanced oxygen respiration. Thereby an increase in ROS formation occurs which causes activation of the oxidative stress response which would be in line with the importance of mannitol to scavenge ROS [41]. The thermostability shown for *Af*M1PDH (τ_H ~20 h at 40°C) is in accordance with its induction at elevated temperature which can be found in infected hosts and may indicate the importance of *Af*M1PDH in the parasitic life style of *A. fumigatus*.

Experimental procedures

Materials

Recombinant *Af*M1PDH and *Af*M2DH were produced in *E. coli* and purified as descript recently [19, 20]. Enzymatic production of D-mannitol 1-phosophate and 5-[²H]-D-mannitol 1-phosphate was carried out as described elsewhere in full detail [19]. D-Xylulose was produced by microbial oxidation of D-arabinitol according to a published protocol [42]. (4*S*)-[²H]-NADH was prepared using glucose dehydrogenase from *Bacillus megaterium* and employing 1-[²H]-D-glucose. Deutero NADH was purified by MonoQ anion-exchange chromatography following previously reported protocols [27, 43, 44]. Stereochemistry of (4*S*)-[²H]-NADH and degree of deuteration (95 ± 1 %) were analyzed by ^{1}H NMR and MS, respectively. 2-[²H]-mannitol was prepared by enzymatic conversion of D-fructose and

purified as described recently [31, 45]. Isotopic purity of 2-[²H]-mannitol was determined by MS (> 99%). No residual fructose, NAD^+ or NADH were detected by ^{13}C NMR. D-mannitol, D-fructose, D-fructose 6-phosphate, β-nicotinamide adenine dinucleotides (NAD^+, NADH) and adenine nucleotides (ATP, ADP, AMP) at a purity ≥ 95 % were obtained from commercial sources.

Assay conditions

Unless otherwise indicated, all assays for carbonyl reduction were carried out at 25°C in a 100 mM Tris/HCl buffer (pH 7.1) employing a constant concentration of NADH (0.2mM). Alcohol oxidation was determined in a 100 mM glycine/NaOH buffer (pH 10.0) at 25°C using 2.0 mM NAD^+. Initial rate measurements were recorded with a DU800 spectrophotometer (Beckman Coulter, Inc; Fullerton, CA, USA), following the formation or depletion of NADH at 340 nm (ε_{NADH} = 6.22 $cm^{-1}mM^{-1}$). The enzymes were appropriately diluted in the corresponding reaction buffers. Stability of the two enzymes were determined at two different protein concentrations (*Af*M1PDH: 0.23 mg/ml, 6 µg/ml; *Af*M2DH: 0.5 mg/ml, 3 µg/ml) and at three temperatures (*Af*M1PDH: 30°C, 40°C, 50°C; *Af*M2DH: 0°C, 25°C, 30°C).

Substrate specificity of *Af*M2DH and *Af*M1PDH was assayed with a varied of sugars and sugar alcohols using a substrate concentration of 300 mM. Alcohol oxidation with *Af*M2DH was performed with D-mannitol, D-xylitol, L-arabinitol, D-arabinitol, D -ribitol, D-sorbitol, D-xylose, L-xylose, D -glucose, D-ribose, D-galactose, L-fucose, 2-deoxy-D-galactose, L-arabinose, D-arabinose, D-lyxose, 2-deoxy-D-glucose and D-mannose. Carbonyl reduction with *Af*M2DH was investigated with D-fructose, L-sorbose, D-xylulose and dihydroxyaceton. Substrate spectrum of *Af*M1PDH was ascertained for the oxidation of D-mannitol 1-phosphate (1mM), D-mannitol, D-sorbitol, D-ribitol, D-xylitol, D-xylose, L-xylose, D-glucose, D-mannose, L-arabinose, D-arabinose, D-galactose, L-fucose, D-lyxose and reduction of D-

fructose, L-sorbose, D-xylulose, D-fructose 1,6-bisphosphate, D-fructose 6-phosphate (100 mM) as well as for D-glucose 6-phosphate and D-glucose 1-phosphate (both at 150 mM). Apparent kinetic parameters for designated substrates of *Af*M2DH were measured using varying concentrations of D-fructose (2 - 1000 mM), D-xylulose (0.5 – 450 mM), L-sorbose (20 – 1000 mM), D-mannitol (1 – 400 mM), D-arabinitol (3 – 1300 mM) and D-sorbitol (30 – 1600mM).

Full kinetic studies for *Af*M1PDH and *Af*M2DH were carried out in 100 mM Tris/HCl pH 7.1. For *Af*M1PDH varying concentrations of Fru6*P* (0.17 – 8.7 mM) and Man-ol1*P* (0.02-2.3 mM) were used at several constant concentrations of NADH from 0.0016 to 0.16 mM and NAD^+ from 0.06 to 5.9 mM, respectively. Data for *Af*M2DH were recorded for varying concentrations of fructose (8.5 – 430 mM) and mannitol (3 – 110 mM) at constant concentrations of NADH from 0.014 to 0.20 mM and NAD^+ from 0.085 to 1.4 mM, respectively. Inhibition studies with adenine nucleotides were performed at constant substrate concentrations (*Af*M1PDH: 30 mM Fru6*P* or 1mM Man-ol1*P*; *Af*M2DH: fructose 1.5 M or mannitol 0.2 M) in 100 mM Tris/HCl, pH 7.1. Cofactor concentrations were varied for carbonyl reduction between 0.008 to 0.25 mM NADH and between 0.05 to 2.5 mM NAD^+ for alcohol oxidation at constant concentrations of AMP, ADP or ATP (0.63 - 5.0 mM).

Primary deuterium isotope effects on apparent kinetic parameters of *Af*M1PDH and *Af*M2DH were determined at neutral pH (100 mM Tris/HCl, pH 7.1) by comparison of initial rates recorded with unlabeled or deuterium-labeled substrates or coenzymes. For *Af*M1PDH the NAD^+-dependent oxidation of Man-ol1*P* and 5-[²H]-Man-ol1*P* was assayed using varying concentrations of NAD^+ (0.08 - 8 mM) or Man-ol1*P*/5-[²H]-Man-ol1*P* (0.04 – 6.2 mM) while keeping the concentration of the other substrate constant and saturating (NAD^+: 5.7 mM; Man-ol1*P*/5-[²H]-Man-ol1*P*: 1.0 mM). Parameters for Fru6*P* reduction were recorded using concentrations of NADH/(4*S*)-[²H]-NADH between 0.002 and 0.2 mM or Fru6*P* between 0.45 and 45 mM at a constant and saturating concentration of the second substrate (0.2 mM

NADH/(4*S*)-[²H]-NADH, 45 mM Fru6*P*). Likewise, parameters for alcohol oxidation with *Af*M2DH were measured varying mannitol/5-[²H]-mannitol from 0.9 to 180 mM and NAD^+ between 0.08 and 4 mM using a constant concentration of NAD^+ (4 mM) and mannitol/5-[²H]-mannitol (260 mM), respectively. For ketose reduction fructose was used between 4 and 840 mM and NADH/(4*S*)-[²H]-NADH from 0.002 to 0.2 mM at a constant concentration of NADH/(4*S*)-[²H]-NADH (0.25 mM) or fructose (800 mM).

Data Processing

Kinetic parameters were determined by fitting Eq. (1)-(8) to the experimental data using unweighted non-linear least-squares regression analysis with Sigma Plot 9.0 (SYSTAT Software Inc., San Jose, CA; USA). Initial rates measured under condition where a single substrate concentration was varied were fitted to Eq. (1) or in case of substrate inhibition to Eq. (2). In Eq. (1) and (2) v is the initial rate, k_{cat} the kinetic turnover number, E and S the molar concentrations of enzyme (molar mass for recombinant *Af*M1PDH: 44.2 kDa and *Af*M2DH: 57.6 kDa) and substrate, K_M the apparent Michaelis constant and K_{iS} the substrate inhibition constant. Data from full kinetic analysis were fitted with Eq. (3) or (4). Eq. (3) was used when substrate binding is assumed to occur in an ordered fashion with cofactor binding first while Eq. (4) was employed when reactants can bind in a random fashion (see Results on KIEs for details). In Eq. (3) and (4) A and B are the molar concentrations of coenzyme and substrate, K_A and K_B the corresponding binding constants and K_{iA} the apparent dissociation constant of the coenzyme. α is a factor describing how binding of one substrate changes the dissociation constant for the other substrate. The apparent equilibrium constant (app K_{eq}) was calculated according to the Haldane equation for an ordered bi bi mechanism (Eq. (5)). In Eq. (5) k_{ox} and k_{red} are the turnover numbers for alcohol oxidation and ketose reduction, respectively. K_{iNADH} and K_{iNAD} are the dissociation constants for NADH and NAD^+ while K_{RO} and K_{ROH} are the binding constants for the ketose and ployol substrates. In case of a random

fashion of substrate binding K_i values were substituted by $\alpha \times K_A$. Inhibition constants (K_i^{EI}) for adenine nucleotides were obtained from fits of Eq. (6) (describing competitive inhibition against coenzyme) to initial rate data. KIEs on apparent kinetic parameters were calculated by fitting Eq. (7) and (8) to the experimental data [46]. E_V and $E_{V/K}$ are the isotope effects minus 1 on k_{cat} and k_{cat}/K_M, respectively. F_i is the fraction of deuterium in the labeled substrate. Eq. (7) describes isotope effects on k_{cat} and k_{cat}/K_M while Eq. (8) solely considers an isotope effect on k_{cat}/K_M. Eq. (8) was used to calculate $E_{V/K}$ from the linear dependency of the initial rate on the substrate concentration in the case where substrate inhibition occurs at high concentrations. Eq. (9) and Eq. (10) were derived from Eq. (3) and (4), respectively, accounting for competitive inhibition of adenine nucleotides against coenzymes when $K_i^{EI}{}_{ATP} \sim K_i^{EI}{}_{ADP} \sim K_i^{EI}{}_{AMP}$.

(1) $v = k_{cat} \times E \times S/(K_M + S)$

(2) $v = k_{cat} \times E \times S/[K_M + S \times (1 + S/K_{iS})]$

(3) $v = k_{cat} \times E \times A \times B/(K_{iA} \times K_B + K_A \times B + K_B \times A + A \times B)$

(4) $v = k_{cat} \times E \times A \times B/(A \times B + \alpha \times K_A \times B + \alpha \times K_B \times A + \alpha \times K_A \times K_B)$

(5) app $K_{eq} = k_{ox} \times K_{iNADH} \times K_{RO}/(k_{red} \times K_{iNAD} \times K_{ROH})$

(6) $v = k_{cat} \times E \times S/[K_M \times (1 + I/K_i^{EI}) + S]$

(7) $v = k_{cat} \times E \times S/[K_M \times (1 + F_i \times E_{V/K}) + S \times (1 + F_i \times E_V)]$

(8) $v = k_{cat} \times E \times S/[K_M \times (1 + F_i \times E_{V/K}) + S]$

(9) $v = k_{cat} \times E \times A \times B/\{K_{iA} \times K_B + K_A \times [1 + (AMP + ADP + ATP)/K_i^{EI}{}_{ATP}] \times B + K_B \times A + A \times B\}$

(10) $v = k_{cat} \times E \times A \times B/\{A \times B + \alpha \times K_A \times [1 + (AMP + ADP + ATP)/K_i^{EI}{}_{ATP}] \times B + \alpha \times K_B \times A + \alpha \times K_A \times [1 + (AMP + ADP + ATP)/K_i^{EI}{}_{ATP}) \times K_B\}$

Acknowledgment

Valentin Pacher and Karin Longus are thanked for expert technical assistance. We are grateful to Dr. Michael Murkovic (Institute of Biochemistry, Graz University of Technology) and Dr. Hansjörg Weber (Institute of Organic Chemistry, Graz University of Technology) for MS and NMR measurements, respectively. Finical support from the Austrian Science Fund FWF (P18275-B09 to B.N.) is gratefully acknowledged.

References

1. Solomon PS, Waters OD & Oliver RP (2007) Decoding the mannitol enigma in filamentous fungi. *Trends Microbiol* **15**, 257-262.
2. Hult K & Gatenbeck S (1978) Production of NADPH in the mannitol cycle and its relation to polyketide formation in *Alternaria alternata*. *Eur J Biochem* **88**, 607-612.
3. Ruijter GJ, Bax M, Patel H, Flitter SJ, van de Vondervoort PJ, de Vries RP, vanKuyk PA & Visser J (2003) Mannitol is required for stress tolerance in *Aspergillus niger* conidiospores. *Eukaryot Cell* **2**, 690-698.
4. Vélëz H, Glassbrook NJ & Daub ME (2007) Mannitol metabolism in the phytopathogenic fungus *Alternaria alternata*. *Fungal Genet Biol* **44**, 258-268.
5. Solomon PS, Waters OD, Jorgens CI, Lowe RG, Rechberger J, Trengove RD & Oliver RP (2006) Mannitol is required for asexual sporulation in the wheat pathogen *Stagonospora nodorum* (glume blotch). *Biochem J* **399**, 231-239.
6. Vélëz H, Glassbrook NJ & Daub ME (2008) Mannitol biosynthesis is required for plant pathogenicity by *Alternaria alternata*. *FEMS Microbiol Lett* **285**, 122-129.
7. Jennings DB, Ehrenshaft M, Pharr DM & Williamson JD (1998) Roles for mannitol and mannitol dehydrogenase in active oxygen-mediated plant defense. *Proc Natl Acad Sci USA* **95**, 15129-15133.
8. Cheng FY, Zamski E, Guo WW, Pharr DM & Williamson JD (2009) Salicylic acid stimulates secretion of the normally symplastic enzyme mannitol dehydrogenase: a possible defense against mannitol-secreting fungal pathogens. *Planta* **230**, 1093-1103.
9. Voegele RT, Hahn M, Lohaus G, Link T, Heiser I & Mendgen K (2005) Possible roles for mannitol and mannitol dehydrogenase in the biotrophic plant pathogen *Uromyces fabae*. *Plant Physiol* **137**, 190-198.
10. Joosten MHAJ, Hendrickx LJM & De Wit PJGM (1990) Carbohydrate composition of apoplastic fluids isolated from tomato leaves inoculated with virulent or avirulent races of *Cladosporium fulvum* (syn. *Fulvia fulva*). *Neth J Pl Path* **96**, 103-112.
11. Smirnoff N & Cumbes QJ (1989) Hydroxyl radical scavenging activity of compatible solutes. *Phytochemistry* **28**, 1057-1060.
12. Chaturvedi V, Flynn T, Niehaus WG & Wong B (1996) Stress tolerance and pathogenic potential of a mannitol mutant of *Cryptococcus neoformans*. *Microbiology (Reading, England)* **142 (Pt 4)**, 937-943.
13. Chaturvedi V, Wong B & Newman SL (1996) Oxidative killing of *Cryptococcus neoformans* by human neutrophils. Evidence that fungal mannitol protects by scavenging reactive oxygen intermediates. *J Immunol* **156**, 3836-3840.

14. Wong B, Brauer KL, Tsai RR & Jayasimhulu K (1989) Increased amounts of the *Aspergillus* metabolite D-mannitol in tissue and serum of rats with experimental aspergillosis. *J Infect Dis* **160**, 95-103.
15. Latgé JP (1999) *Aspergillus fumigatus* and aspergillosis. *Clin Microbiol Rev* **12**, 310-350.
16. Albrecht D, Guthke R, Brakhage AA & Kniemeyer O (2010) Integrative analysis of the heat shock response in *Aspergillus fumigatus*. *BMC genomics* **11**, 32.
17. Stevens DA, Moss RB, Kurup VP, Knutsen AP, Greenberger P, Judson MA, Denning DW, Crameri R, Brody AS, Light M, Skov M, Maish W & Mastella G (2003) Allergic bronchopulmonary aspergillosis in cystic fibrosis--state of the art: Cystic Fibrosis Foundation Consensus Conference. *Clin Infect Dis* **37(Suppl. 3)**, 225-264.
18. Kiser RC & Niehaus WG, Jr. (1981) Purification and kinetic characterization of mannitol-1-phosphate dehydrogenase from *Aspergillus niger*. *Arch Biochem Biophys* **211**, 613-621.
19. Krahulec S, Armao GC, Weber H, Klimacek M & Nidetzky B (2008) Characterization of recombinant *Aspergillus fumigatus* mannitol-1-phosphate 5-dehydrogenase and its application for the stereoselective synthesis of protio and deuterio forms of D-mannitol 1-phosphate. *Carbohydr Res* **343**, 1414-1423.
20. Krahulec S, Armao GC, Bubner P, Klimacek M & Nidetzky B (2009) Polyol-specific long-chain dehydrogenases/reductases of mannitol metabolism in *Aspergillus fumigatus*: biochemical characterization and pH studies of mannitol 2-dehydrogenase and mannitol-1-phosphate 5-dehydrogenase. *Chem Biol Interact* **178**, 274-282.
21. Klimacek M, Kavanagh KL, Wilson DK & Nidetzky B (2003) *Pseudomonas fluorescens* mannitol 2-dehydrogenase and the family of polyol-specific long-chain dehydrogenases/reductases: sequence-based classification and analysis of structure-function relationships. *Chem Biol Interact* **143-144**, 559-582.
22. Kavanagh KL, Klimacek M, Nidetzky B & Wilson DK (2002) Crystal structure of *Pseudomonas fluorescens* mannitol 2-dehydrogenase binary and ternary complexes. Specificity and catalytic mechanism. *J Biol Chem* **277**, 43433-43442.
23. Wu J, Serianni AS & Vuorinen T (1990) Furanose ring anomerization: kinetic and thermodynamic studies of the D-2-pentuloses by 13C-n.m.r. spectroscopy. *Carbohydr Res* **206**, 1-12.
24. Collins P & Ferrier R (1995) *Monosaccharides: Their Chemistry and Their Roles in Natural Products* Wiley, Chichester.
25. Wolff JB & Kaplan NO (1956) D-Mannitol 1-phosphate dehydrogenase from *Escherichia coli*. *J Biol Chem* **218**, 849-869.
26. Bubner P, Klimacek M & Nidetzky B (2008) Structure-guided engineering of the coenzyme specificity of *Pseudomonas fluorescens* mannitol 2-dehydrogenase to enable efficient utilization of NAD(H) and NADP(H). *FEBS letters* **582**, 233-237.
27. Slatner M, Nidetzky B & Kulbe KD (1999) Kinetic study of the catalytic mechanism of mannitol dehydrogenase from *Pseudomonas fluorescens*. *Biochemistry* **38**, 10489-10498.
28. Foreman JE & Niehaus WG, Jr. (1985) Zn2+-induced cooperativity of mannitol-1-phosphate dehydrogenase from Aspergillus parasiticus. *J Biol Chem* **260**, 10019-10022.
29. Ikawa T, Watanabe T & Nisizawa K (1972) Enzymes involved in the last steps of the biosynthesis of mannitol in brown algae. *Plant Cell Physiol* **13**, 1017-1029.
30. Nidetzky B & Klimacek M (2007) Fungal mannitol 2-dehydrogenases and mannitol-1-phosphate 5-dehydrogenases constitute novel branches in the protein family of polyol-specific long-chain dehydrogenases and reductases. In *Enzymology and Molecular Biology of Carbonyl Metabolism* (Weiner H, Maser E, Lindahl R & Plapp B, eds), pp. 305-322. Purdue University Press, West Lafayette.

31. Klimacek M & Nidetzky B (2002) Examining the relative timing of hydrogen abstraction steps during NAD(+)-dependent oxidation of secondary alcohols catalyzed by long-chain D-mannitol dehydrogenase from *Pseudomonas fluorescens* using pH and kinetic isotope effects. *Biochemistry* **41**, 10158-10165.
32. Nierman WC, Pain A, Anderson MJ, Wortman JR, Kim HS, Arroyo J, Berriman M, Abe K, Archer DB, Bermejo C, Bennett J, Bowyer P, Chen D, Collins M, Coulsen R, Davies R, Dyer PS, Farman M, Fedorova N, Feldblyum TV, Fischer R, Fosker N, Fraser A, García JL, García MJ, Goble A, Goldman GH, Gomi K, Griffith-Jones S, Gwilliam R, Haas B, Haas H, Harris D, Horiuchi H, Huang J, Humphray S, Jimenez J, Keller N, Khouri H, Kitamoto K, Kobayashi T, Konzack S, Kulkarni R, Kumagai T, Lafon A, Latgé JP, Li W, Lord A, Lu C, Majoros WH, May GS, Miller BL, Mohamoud Y, Molina M, Monod M, Mouyna I, Mulligan S, Murphy L, O'Neil S, Paulsen I, Peñalva MA, Pertea M, Price C, Pritchard BL, Quail MA, Rabbinowitsch E, Rawlins N, Rajandream MA, Reichard U, Renauld H, Robson GD, Rodriguez de Córdoba S, Rodríguez-Peña JM, Ronning CM, Rutter S, Salzberg SL, Sanchez M, Sánchez-Ferrero JC, Saunders D, Seeger K, Squares R, Squares S, Takeuchi M, Tekaia F, Turner G, Vazquez de Aldana CR, Weidman J, White O, Woodward J, Yu JH, Fraser C, Galagan JE, Asai K, Machida M, Hall N, Barrell B & Denning DW (2005) Genomic sequence of the pathogenic and allergenic filamentous fungus *Aspergillus fumigatus*. *Nature* **438**, 1151-1156.
33. Cook PF (1991) Kinetic and Regulatory Mechanisms of Enzymes from Isotope Effects. In *Enzyme Mechanism from Isotope Effects* (Cook PF, eds), pp. 203-231. CRC Press, Inc., Boca Raton, Ann Arbor, Boston, London.
34. Klungsøyr L (1967) The binding of adenine nucleotides to the mannitol-I-phosphate dehydrogenase of Escherichia coli. *Biochim Biophys Acta* **146**, 10-17.
35. Ruijter GJG & Visser J (1996) Determination of intermediary metabolites in *Aspergillus niger*. *J Microbiol Methods* **25**, 295-302.
36. Packer HL, Keshavarz-Moore E, Lilly MD & Thomas CR (1992) Estimation of cell volume and biomass of *Penicillium chrysogenum* using image analysis. *Biotechnol Bioeng* **39**, 384-391.
37. Nasution U, van Gulik WM, Kleijn RJ, van Winden WA, Proell A & Heijnen JJ (2006) Measurement of intracellular metabolites of primary metabolism and adenine nucleotides in chemostat cultivated *Penicillium chrysogenum*. *Biotechnol Bioeng* **94**, 159-166.
38. Nissen TL, Anderlund M, Nielsen J, Villadsen J & Kielland-Brandt MC (2001) Expression of a cytoplasmic transhydrogenase in *Saccharomyces cerevisiae* results in formation of 2-oxoglutarate due to depletion of the NADPH pool. *Yeast (Chichester, England)* **18**, 19-32.
39. Pollak N, Dölle C & Ziegler M (2007) The power to reduce: pyridine nucleotides--small molecules with a multitude of functions. *Biochem J* **402**, 205-218.
40. Yamamoto Y, Nitta K, Tango K, Saito T & Tsuchimuro M (1965) Studies on the metabolic products of a strain of *Aspergillus fumigatus* (DH 413). I. Isolation and chemical structures of metabolites. *Chem Pharm Bull (Tokyo)* **13**, 935-941.
41. Sugiyama K, Izawa S & Inoue Y (2000) The Yap1p-dependent induction of glutathione synthesis in heat shock response of *Saccharomyces cerevisiae*. *J Biol Chem* **275**, 15535-15540.
42. Mayer G, Kulbe KD & Nidetzky B (2002) Utilization of xylitol dehydrogenase in a combined microbial/enzymatic process for production of xylitol from D-glucose. *Appl Biochem Biotechnol* **98-100**, 577-589.
43. Mostad SB & Glasfeld A (1993) Using High Field NMR to Determine Dehydrogenase Stereospecificity with Respect to NADH. *J Chem Educ* **70**, 504-506.
44. Orr GA & Blanchard JS (1984) High-performance ion-exchange separation of oxidized and reduced nicotinamide adenine dinucleotides. *Anal Biochem* **142**, 232-234.

45. Klimacek M & Nidetzky B (2010) The oxyanion hole of *Pseudomonas fluorescens* mannitol 2-dehydrogenase: a novel structural motif for electrostatic stabilization in alcohol dehydrogenase active sites. *Biochem J* **425**, 455-463.
46. Blanchard JS & Cleland WW (1980) Kinetic and chemical mechanisms of yeast formate dehydrogenase. *Biochemistry* **19**, 3543-3550.

Chapter II

Metabolic pathway engineering for xylose fermentation in *Saccharomyces cerevisiae*

Green house gases, high oil prices and supply instability have led to an increased emphasis on renewable sources of energy. Bio-ethanol is a CO_2-neutral alternative to fossil fuels and has become a billion dollar business. Currently bio-ethanol is mainly produced from agricultural products with high starch or sucrose content (1st generation). Lignocellulosic material from agricultural waste would be a cost efficient alternative carbon source that could eliminate the concerns about raw material utilization in biofuel production (2nd generation). Beside hexoses, pentoses (especially xylose) account for a significant fraction of the carbohydrates present in lignocellulosic hydrolysates. *Saccharomyces cerevisiae* displays a high productivity and ethanol tolerance, yet is unable to utilize xylose. Insertion of a heterologous pathway consisting of xylose reductase (XR) and xylitol dehydrogenase (XDH) enables isomerization of xylose into xylulose which is in turn phosphorylated by xylulose kinase (XK) and enters the pentose phosphate pathway. The major downside is the different cofactor specificity of XR and XDH. XR prefers NADPH over NADH while XDH is NAD^+-dependent leading to an accumulation of NADH at the expense of NADPH, the formation of xylitol as by-product and a reduced ethanol yield.

Protein engineering was used to craft the area of the coenzyme binding pocket responsible for accommodation of the phosphate moiety of $NADP^+$ in the *silverleaf whitefly* ketose reductase on the coenzyme binding pocket of the XDH from *Galactocandida mastotermitis* (*Gm*XDH), resulting in the exchange of the peptide Asp^{202}-Leu-Val-Glu-Ser^{206} into Ala^{202}-Arg-Ser-Pro-Arg^{206}. A “sloppy” PCR reaction was useful to generate a series of mutants in which one or two amino acids of the introduced peptide were deleted. The highest specific activity with

$NADP^+$ (~70% of the specific activity of the wild type with NAD^+) was found for the Ala^{202}-Δ-Δ-Pro-Arg^{206} (where Δ is a one amino acid deletion) variant (*Gm*XDH-V2K1). According to catalytic efficiencies, this mutant shows a 4-fold preference for the utilization of $NADP^+$. This is close to the preferences, NADPH compared with NADH, in the previously described mutants of the XR from *Candida tenuis* (*Ct*XR-ND Asn^{276}→Asp (4-fold) and *Ct*XR-DM Lys^{274}→Arg Asn^{276}→Asp (0.8-fold))[1]. Therefore, a combination of the XDH and XR mutants could be expected to support well balanced coenzyme utilization for the isomerization of xylose into xylulose. Consequently, two novel yeast strains were constructed by chromosomal integration of the genes encoding the *Gm*XDH-V2K1 mutant and either the *Ct*XR-DM (BP11001) or *Ct*XR-ND (BP11002) mutant along with an additional copy of the endogenous xylulose kinase. Performance of these yeast strains were evaluated in xylose conversion studies and compared with the previously constructed strains BP000 (expressing the wild type of *Gm*XDH and *Ct*XR) and BP10001 (expressing the wild type *Gm*XDH and the *Ct*XR-DM mutant)[2]. Oxygen-limited xylose conversions (20 g/L) in shake flasks revealed a 36% and 43% reduced glycerol yield for BP11001 and BP11002 in comparison to BP000. However, the xylitol and ethanol yields were unchanged for BP11001 as compared to BP000. For BP11002 the ethanol yield was even lower and the xylitol yield was higher (both 14%) than for the reference strain expressing the wild type enzymes. Anaerobic conversion of 20 g/L xylose in a bioreactor with BP11001 showed a markedly reduced glycerol yield (52%) and a 13% reduced xylitol yield while the ethanol yield was not changed compared to BP000. Overall BP11001 and BP11002 resemble BP10001 in terms of glycerol yield but BP10001 is clearly superior regarding ethanol yield and xylitol yield (42% enhanced and 52% reduced compared to BP000)[2]. Combining concentrations of internal metabolites with kinetic parameters of the *Gm*XDH enzymes suggests that under *in vivo* conditions the *Gm*XDH mutant is a significantly slower enzyme (~1/10) than the wild type. The observed product distribution for BP11001 and BP11002 might therefore be due to an unfavourable ratio

between the *in vivo* activities of the *Ct*XR and *Gm*XDH mutants. Thus, further studies on external factors that limit the xylose uptake rate (q_{xylose}) under xylose only and mixed glucose-xylose substrate conditions were performed with the previously constructed strain BP10001[2]. An increase in xylose concentration from 10 to 50 g/L resulted in an acceleration of substrate uptake by BP10001 (0.05 - 0.14 g/g CDW/h) and a concomitant decrease in the xylitol yield (0.28 - 0.15 g/g), revealing an overall improvement in the distribution of fermentation products from BP000 to BP10001 in response to an increase in the initial xylose concentration. Both strains converted a mixture of glucose and xylose (10 g/L each) sequentially with glucose being the preferred substrate. While product yields in the glucose phase were similar, BP10001 showed an enhanced ethanol yield (~30%) and decreased yields of xylitol (~28%) and glycerol (~68%) in the xylose phase. Both strains showed a detectable xylose uptake at low glucose concentrations (< 4 g/L) and a substantially higher q_{xylose} at concentrations < 2 g/L glucose than under conditions when only xylose is present. A fed batch process employing an exponential glucose feed to keep $q_{glucose}$ at a constant level (~0.7 g/g CDW/h) and the residual glucose concentration in the reactor below 0.3 g/L resulted in an initial q_{xylose} of 0.30 ± 0.04 g/g CDW/h (at 48 g/L xylose). The ~2-fold increase in q_{xylose} indicates that design of process conditions can complement genetic approaches which aim to enhance q_{xylose}. A gain of q_{xylose} at a low glucose influx can be explained by the accumulation of glycolytic and pentose phosphate intermediates that facilitates “pull” of xylose into the metabolism, through the law of mass action as well as by inducing a global cellular response. A lowering of the xylitol yield in co-fermentation of glucose and xylose was reported for other yeast strains and explained as a consequence of enhanced coenzyme recycling by the increased flux through glycolysis when glucose is present[3]. Interestingly, with BP10001 the xylitol yield on xylose was not reduced in fed batch co-fermentation compared to the corresponding xylose batch fermentation. This may indicate that the coenzyme utilization of XR and XDH is well balanced and hence that *Ct*XR-DM works as a solely NADH-dependent

reductase *in vivo*. This is further supported by the notion that the molar yield of "redox sink" metabolites, namely glycerol and xylitol, was identical in glucose only and glucose-xylose fed batch fermentations. Even though flux balance analysis (FBA) using a constrained genome-scale metabolic model of *S. cerevisiae*[4] could tolerate a surprisingly broad range of coenzyme preferences of the *Ct*XR-DM (xylose batch: 0-36% NADPH; glucose –xylose fed batch 0-86%), unrealistically high fluxes from pyruvate to oxaloacetate at increasing NADPH-reactivity of *Ct*XR-DM strongly favor a highly NADH-preferring XR reaction.

1. Petschacher, B.; Leitgeb, S.; Kavanagh, K. L.; Wilson, D. K.; Nidetzky, B., The coenzyme specificity of *Candida tenuis* xylose reductase (AKR2B5) explored by site-directed mutagenesis and X-ray crystallography. *Biochem. J.* **2005,** 385, (Pt 1), 75-83.
2. Petschacher, B.; Nidetzky, B., Altering the coenzyme preference of xylose reductase to favor utilization of NADH enhances ethanol yield from xylose in a metabolically engineered strain of *Saccharomyces cerevisiae*. *Microb. Cell Fact.* **2008,** 7, 9.
3. Karhumaa, K.; Fromanger, R.; Hahn-Hägerdal, B.; Gorwa-Grauslund, M. F., High activity of xylose reductase and xylitol dehydrogenase improves xylose fermentation by recombinant *Saccharomyces cerevisiae*. *Appl. Microbiol. Biotechnol.* **2007,** 73, (5), 1039-46.
4. Kuepfer, L.; Sauer, U.; Blank, L. M., Metabolic functions of duplicate genes in *Saccharomyces cerevisiae*. *Genome Res.* **2005,** 15, (10), 1421-30.

Biotechnology Journal

DOI 10.1002/biot.200800334

Biotechnol. J. 2009, 4, 684–694

Research Article

Engineering of a matched pair of xylose reductase and xylitol dehydrogenase for xylose fermentation by *Saccharomyces cerevisiae*

Stefan Krahulec, Mario Klimacek and Bernd Nidetzky*

Institute of Biotechnology and Biochemical Engineering, Graz University of Technology, Graz, Austria

Received 3 December 2008
Revised 12 March 2009
Accepted 24 March 2009

Metabolic engineering of *Saccharomyces cerevisiae* for xylose fermentation has often relied on insertion of a heterologous pathway consisting of nicotinamide adenine dinucleotide (phosphate) NAD(P)H-dependent xylose reductase (XR) and NAD^+-dependent xylitol dehydrogenase (XDH). Low ethanol yield, formation of xylitol and other fermentation by-products are seen for many of the *S. cerevisiae* strains constructed in this way. This has been ascribed to incomplete coenzyme recycling in the steps catalyzed by XR and XDH. Despite various protein-engineering efforts to alter the coenzyme specificity of XR and XDH individually, a pair of enzymes displaying matched utilization of NAD(H) and NADP(H) was not previously reported. We have introduced multiple site-directed mutations in the coenzyme-binding pocket of *Galactocandida mastotermitis* XDH to enable activity with $NADP^+$, which is lacking in the wild-type enzyme. We describe four enzyme variants showing activity for xylitol oxidation by $NADP^+$ and NAD^+. One of the XDH variants utilized $NADP^+$ about 4 times more efficiently than NAD^+. This is close to the preference for NADPH compared with NADH in mutants of *Candida tenuis* XR. Compared to an *S. cerevisiae*-reference strain expressing the genes for the wild-type enzymes, the strains comprising the gene encoding the mutated XDH in combination with a matched XR mutant gene showed up to 50% decreased glycerol yield without increase in ethanol during xylose fermentation.

Keywords: Coenzyme preference · Enzyme engineering · Redox engineering · Xylitol dehydrogenase · Xylose utilization

1 Introduction

The Kyoto protocol, high oil prices and supply instability have led policy-makers to put increased emphasis on renewable sources of energy. Conversion of lignocellulosic biomass into liquid fuels has therefore drawn a strongly revived interest in recent years. Bioethanol is currently produced from starch or sucrose, rekindling the controversial debate about food and feed versus energy [1]. The use of lignocellulose-based feedstocks would eliminate the concern over raw material utilization in biofuel production. It is a widely held notion that lignocellulosic ethanol constitutes a sustainable trans-

Correspondence: Dr. Bernd Nidetzky, Institute of Biotechnology and Biochemical Engineering, Graz University of Technology, Petersgasse 12/I, 8010 Graz, Austria
E-mail: bernd.nidetzky@TUGraz.at
Fax: +43-316-873-8434

Abbreviations: ***Ct*XR**, *Candida tenuis* xylose reductase; ***Ct*XR-Dm**, $K^{274}\rightarrow R$ $N^{276}\rightarrow D$ mutant of *Ct*XR; ***Ct*XR-ND**, $N^{276}\rightarrow D$ mutant of *Ct*XR; ***Gm*XDH**, *Galactocandida mastotermitis* xylitol dehydrogenase; ***Gm*XDH-V2K1**, $D^{202}LVES^{206}\rightarrow A^{202}\Delta\Delta PR^{206}$ mutant of *Gm*XDH; ***Gm*XDH-V2K2**, $D^{202}LVES^{206}\rightarrow A^{202}RSPR^{206}$ mutant of *Gm*XDH; **NAD**, nicotinamide adenine dinucleotide; **NAD(P)**, nicotinamide adenine dinucleotide (phosphate); ***Ps*XDH**, *Pichia stipitis* xylitol dehydrogenase; ***Wf*KR**, *silverleaf whitefly* ketose reductase; **XDH**, xylitol dehydrogenase; **XI**, xylose isomerase; **XK**, xylulose kinase; **XKS1**, gene of *S. cerevisiae* encoding xylulose kinase; **XR**, xylose reductase

* Additional corresponding author: Dr. Mario Klimacek
E-mail: mario.klimacek@TUGraz.at

portation fuel and that biomass-to-ethanol processes may become economically viable within the next 5–10 years.

The yeast *Saccharomyces cerevisiae* is among the preferred organisms for fermentation of D-glucose and other hexoses as it naturally has a high productivity and ethanol tolerance. Furthermore, *S. cerevisiae* is relatively resistant to the low pH and the overall composition of lignocellulose hydrolyzates [2]. Despite these clear advantages, there is, however, the drawback that *S. cerevisiae* in its wild-type form cannot ferment D-xylose and L-arabinose due to lack of active catabolic pathways for the two sugars. The two pentoses are abundant in hemicellulose hydrolyzates [3] where they constitute ≥80% of the total sugar. Their conversion, in particular that of xylose, is therefore considered a requirement for lignocellulosic ethanol to be economically viable. With the use of recombinant DNA technology, *S. cerevisiae* has been engineered for fermentation of xylose. The approaches chosen differed according to whether the heterologous pathway utilized in the conversion of xylose into xylulose comprised two sequential redox-transformations, as in yeasts and fungi, or a direct isomerization, as in bacteria [4]. Xylulose is a natural substrate of *S. cerevisiae* and enters the pentose phosphate pathway as xylulose 5-phosphate.

A fundamental problem of the oxidoreductive pathway is that xylose reductase (XR) and xylitol dehydrogenase (XDH) display different preferences for using nicotinamide adenine dinucleotide (phosphate) [NAD(P)(H) and NAD(H)] in their respective reaction. While XDH in its natural form is highly specific for NAD^+, the XR utilizes NADPH and NADH with variable selectivities depending on the source of the enzyme. Incomplete coenzyme recycling in the steps catalyzed by XR and XDH was considered the main reason for an ethanol yield far below the theoretical (0.51 g/g; see Eq. 1 [5]) and formation of fermentation by-products, mainly xylitol but also glycerol, in large amounts [1, 2, 6–9]. Kuyper *et al*. [5] have predicted the metabolic balance for a situation when XR shows equal utilization of NADPH and NADH (Eq. 2). At an *in vivo* utilization ratio (NADPH/NADH) of XR greater than 1, formation of glycerol was proposed to reflect the additional requirement for redox balancing under the typically non-growing conditions of xylose fermentation by *S. cerevisiae* [10].

$$6 \text{ xylose} \rightarrow 10 \text{ ethanol} + 10\ CO_2 + 10 \text{ ATP} \quad (1)$$

$$12 \text{ xylose} \rightarrow 9 \text{ ethanol} + 12\ CO_2 + 9 \text{ ATP} + 6 \text{ xylitol} \quad (2)$$

A number of studies show that the redox imbalances generated during xylose assimilation can be alleviated, however, not removed entirely at points elsewhere in the overall metabolism [11–15]. Following the identification of a long sought xylose isomerase (XI) that could be expressed functionally in *S. cerevisiae*, a platform of yeast strains was therefore constructed where the XR-XDH route was replaced by direct XI-catalyzed isomerization of xylose (*e.g*. [5, 16, 17]). Genetic optimization of strains harboring XI included deletion of the GRE3 gene that encodes a nonspecific aldehyde reductase capable of promoting NADPH-dependent reduction of xylose as well as overexpression of genes encoding enzymes of the non-oxidative pentose phosphate pathway [17]. These adaptations of the yeast resulted in a strain, which as expected from Eq. (1), did marginally produce xylitol (0.003 g/g) and gave a good ethanol yield (0.43 g/g) [17].

Protein engineering of XR and XDH is a clear alternative strategy with which to overcome the problem of coenzyme imbalance. Site-directed mutagenesis of XR to produce enzyme variants showing enhanced utilization of NADH compared with NADPH was reported for reductases from *Candida tenuis* [18], *Pichia stipitis* [19-21], and *Hansenula polymorpha* [22]. Engineering of XDH focused on the enzyme from *P. stipitis* and addressed enhancement of the activity with $NADP^+$ [23, 24]. *S. cerevisiae* strains harboring mutated XR or XDH fermented xylose significantly (≤40%) better than the corresponding reference strain that comprised the wild-type enzymes [21, 25-28]. These results led us to speculate that by using a perfectly matched pair of XR and XDH, xylose fermentation could be taken one step closer to the optimum situation described by Eq. (1). Unfortunately, this presumably ideal combination of enzymes has not yet been described. The quest for a suitable combination of XR and XDH has received strong support from a recent study in which was compared the efficiency of xylose fermentation by two isogenic strains of *S. cerevisiae*, one expressing *Pyromyces* sp. XI and another expressing *Pichia stipitis* XR and XDH. While the xylitol yield was lower and the ethanol yield was higher in the strain expressing XI, the strain expressing XR and XDH was superior in terms of both xylose consumption rate and specific productivity of ethanol [16].

We report here on the design of a series of variants of *Galactocandida mastotermitis* XDH (*Gm*XDH) that harbored multiple site-directed substitutions in the putative binding pocket for the 2′-hydroxyl of NAD^+ and unlike the wild-type enzyme, displayed activity with $NADP^+$. The ratio of

specific activities for xylitol oxidation by $NADP^+$ and NAD^+ was between 4 and 4×10^2 in these *Gm*XDH variants. The mutated XDH showing the best match with existing variants of *Candida tenuis* XR (*Ct*XR) [17] was selected, and an XR-XDH pair is described, in which the coenzyme preference, NADP(H) compared with NAD(H), was exactly balanced at a value of 4. We define "coenzyme preference" as the ratio of catalytic efficiencies ($V_{max}/K_{coenzyme}$) for reaction with NADP(H) and NAD(H). Two novel strains of *S. cerevisiae* expressing a relevant combination of mutated XR and XDH genes were characterized in xylose fermentation experiments. The product distribution resulting from anaerobic conversion of xylose by these strains is benchmarked against the previously described reference strain that harbors XR and XDH in their respective NAD(P)H and NAD^+-utilizing wild-type forms [25]. The results suggest that coenzyme recycling between the XR and XDH reactions is on its own not sufficient to achieve high ethanol yields. They therefore support the notion [29–32] that the individual intracellular activities of XR and XDH have to be considered in the optimization of xylose-fermenting strains of *S. cerevisiae*.

2 Materials and methods

2.1 Materials

Unless otherwise indicated, all strains, media, chemicals, molecular biology kits and reagents were the same as described elsewhere in full detail [25]. Oligonucleotide primers were obtained from VBC-Biotech (Vienna, Austria).

2.2 Preparation of $NADP^+$-active variants of *Gm*XDH

2.2.1 Mutation

The plasmid vector pBTac1 harboring the gene encoding wild-type *Gm*XDH was used as the template for PCR-based mutagenesis [33]. A previously described inverse PCR protocol was employed [34, 35]. Briefly, the PCR was performed using hot start (65°C), 25 amplification cycles (denaturation 95°C 40 s, annealing 55°C 40 s, elongation 72°C 8 min) and finally another 15 min at 72°C. *Pfu* DNA polymerase (Fermentas, Burlington, Canada) and the following pair of oligonucleotide primers were employed in the PCR reaction: forward primer: 5′-CCACGTAGACTTAACCTTGCCAAGGAG-3′, reverse primer: 5′-AGAACGAGCAATAATAG-TAACAGATTCAGCAC-3′. The mismatched bases are underlined and in the case of perfect priming, would result in the replacement of the peptide $D^{202}LVES^{206}$ by $A^{202}RSPR^{206}$ in a single PCR step. However, it was expected from experience that PCR amplification would rather yield an array of gene variants where different combinations of multiple-site mutations are introduced in the region D^{202} to S^{206}. A plasmid mixture obtained by PCR was transformed into competent cells of *Escherichia coli* JM109 using electroporation. Single-colony transformants were picked and evaluated in a medium-throughput screening for enzyme activity with NAD^+ and $NADP^+$.

2.2.2 Medium-throughput screening

Clones were cultivated in 300 mL baffled shake flasks at 37°C and 120 rpm containing 30 mL of LB-medium and 150 mg/L of ampicillin. Protein expression was induced with IPTG (200 μM) in the mid-exponential growth phase after the temperature had been decreased to 25°C. After 4 h, the cells were harvested by centrifugation (4400 × *g*, 15 min, 4°C). Crude cell extract was obtained by treating about 150 mg of the wet pellet with 0.5 mL B-PER (Pierce; Rockford, IL). Cell debris was removed by centrifugation, and samples were analyzed for protein content and xylitol dehydrogenase activity using NAD^+ or $NADP^+$ (see Section 2.5). Plasmids from clones showing clear enzyme activity in the presence of $NADP^+$ were sequenced (VBC-Biotech).

2.3 Construction of yeast integration vectors and transformation

The previously described cloning strategy was employed [25]. Preparation of the yeast integration vectors started with amplification of the genes encoding the Asn^{276}→Asp mutant of *Ct*XR (*Ct*XR-ND; [18]) and the XDH mutant (*Gm*XDH-V2K1) to be described later. The amplified genes were each subcloned into the vector pRS416GPD to fuse the ORF to the TDH3 (formerly named GPD) promoter and CYC1 terminator (Table 1). In the next step, the reported plasmid Y*Ct*XR-Dm/*Gm*XDH-Wt/XKS1 [25] was used to replace the gene cassette (including promoter and terminator) for *Ct*XR-Dm by the corresponding gene cassette for *Ct*XR-ND (see Table 1 for details), resulting in Y*Ct*XR-ND/*Gm*XDH-Wt/XKS1. *Ct*XR-Dm and *Gm*XDH-Wt stands for genes encoding the Lys^{274}→Arg Asn^{276}→Asp [18] double mutant of *Ct*XR and the wild-type enzyme of *Gm*XDH, respectively. XKS1 is the endogenous gene of *S. cerevisiae* encoding xylulose kinase (XK; [25]). A further exchange of *Gm*XDH-Wt by *Gm*XDH-V2K1 (including promoter and terminator) using the plasmids Y*Ct*XR-

ND/*Gm*XDH-Wt/XKS1 and Y*Ct*XR-Dm/*Gm*XDH-Wt/XKS1 yielded the plasmids Y*Ct*XR-ND/*Gm*XDH-V2K1/XKS1 and Y*Ct*XR-Dm/*Gm*XDH-V2K1/XKS1, respectively.

Integration vectors Y*Ct*XR-Dm/*Gm*XDH-V2K1/XKS1 and Y*Ct*XR-ND/*Gm*XDH-V2K1/XKS1 were linearized with *Sda*I and transformed into *S. cerevisiae* CEN.PK 113-5D, using a protocol described recently [25]. The resulting strains were termed BP11001 (*Ct*XR-Dm/*Gm*XDH-V2K1/XKS1) and BP11002 (Y*Ct*XR-ND/*Gm*XDH-V2K1/XKS1) and stored in 15% glycerol at –80 °C. The previously described strains BP000 (Y*Ct*XR-Wt/*Gm*XDH-Wt/XKS1) and BP10001 (Y*Ct*XR-Dm/*Gm*XDH-Wt/XKS1) were used as references [25].

2.4 Xylose fermentation studies

These were performed in shaken flasks as well as in a Braun Biostat C stirred bioreactor. The experimental set-up and the procedures used have been described elsewhere in full detail [25]. Briefly, the xylose concentration was 20 g/L, and the initial biomass concentration was 3.2 g cell dry weight (CDW)/L. All shake flask experiments were carried out in quadruplicates at an initial pH of 6.5, and results are given as mean value and SD. The concentration of dissolved O_2 in shake flask cultures was controlled each time a sample was taken. It never exceeded 20 µM. Anaerobic reaction conditions in the bioreactor were achieved by gassing the medium with N_2 at a flow rate of 0.16 vvm. Operation of the bioreactor was exactly as reported previously [25].

2.5 Analyses

2.5.1 Preparation of cell extracts

Cells of *E. coli* were disintegrated using B-Per (Pierce). About 150 mg wet cell mass was suspended in 500 µL lysis reagent, mixed well, and incubated for 1 min. Insoluble material was removed by centrifugation (15 700 × *g*, 15 min, 4°C), and the supernatant was used further. Yeast biomass was disrupted by using a French Press. Cells were suspended to a concentration of ~70 g/L in 12 mL, and the sample was passed three times through an Aminco (Silver Spring, MD) pressure chamber/cell operated at 1500 psi. The soluble fraction was recovered by centrifugation (80 000 × *g*, 45 min, 4°C). Alternatively, yeast cells were disrupted using the Y-Per lysis reagent (Pierce) according to instruction of the supplier. Total protein in cell extracts obtained in either way was determined using the Bio-Rad Protein Assay (Bio-Rad, Richmond, CA) referenced against known concentrations of BSA.

Table 1. Construction of the yeast integration plasmids Y*Ct*XR-ND/*Gm*XDH-V2K1/XKS1 and Y*Ct*XR-Dm/*Gm*XDH-V2K1/XKS1

	Target sequence	Template plasmid	Primers	Target plasmid	Restriction sites	Resulting plasmid
1	*Ct*XR-ND gene	pET1I-*Ct*XR-ND [a]	Fwd: 5'-GGTGGTGGATCCATGAGCGCAAGTATCCCAGAC-3' Rev: 5'-CTAGTGGGTCGACTTAAACGAAGATTGGAATGTTGT-3'	pRS416GPD	*BamHI SalI*	pRS416GPD-*Ct*XR-ND
	*Gm*XDH-V2K1 gene	pBTacI-*Gm*XDH-V2K1	Fwd: 5'-GGTGGTGGATCCATGTCTACTCCTGAAAACTTATCT-3' Rev: 5'-GGTGGTGTCGACTTACTCAGGGCCGTTAATGATG-3'	pRS416GPD	*BamHI SalI*	pRS416GPD-*Gm*XDH-V2K1
2	Gene cassette *Ct*XR-ND	pRS416GPD-*Ct*XR-ND	Fwd: 5'-GGTGGTGAATTCAGTTTATCATTATCAATACTCGCCATTTC-3' Rev: 5'-GGTGGTGAATTCGGCCGCAAATTAAAGCCTTCG-3'	Y*Ct*XR-Dm/*Gm*XDH-Wt/XKSI [b]	*EcoRI*	Y*Ct*XR-ND/*Gm*XDH-Wt/XKSI
3	Gene cassette *Gm*XDH-V2K1	pRS416GPD-*Gm*XDH-V2K1	Fwd: 5'-CATGGTATCGATAGTTTATCATTATCAATACTCGCCATTTC-3' Rev: 5'-CATGGTATCGATGGCCGCAAATTAAAGCCTTCG-3'	Y*Ct*XR-ND/*Gm*XDH-Wt/XKSI Y*Ct*XR-Dm/*Gm*XDH-Wt/XKSI [b]	*ClaI*	Y*Ct*XR-ND/*Gm*XDH-V2K1/XKSI [c] Y*Ct*XR-Dm/*Gm*XDH-V2K1/XKSI [d]

a) See ref. [18]. Resulting genotypes after integration into *S. cerevisiae* CEN.PK 113-5D.
b) CEN.PK 113-5D ura3::(GPDp-XKSI-CYCIt, GPDp-*Ct*XR-Dm-CYCIt, GPDp-*Gm*XDH-Wt-CYCIt) – strain BP10001 [25].
c) CEN.PK 113-5D ura3::(GPDp-XKSI-CYCIt, GPDp-*Ct*XR-ND-CYCIt, GPDp-*Gm*XDH-V2K1-CYCIt) – strain BP11002.
d) CEN.PK 113-5D ura3::(GPDp-XKSI-CYCIt, GPDp-*Ct*XR-Dm-CYCIt, GPDp-*Gm*XDH-V2K1-CYCIt) – strain BP11001.

2.5.2 Enzyme activity measurements

Enzyme-catalyzed initial rates were acquired with a DU800 spectrophotometer from Beckman Coulter (Fullerton, CA), recording at 25°C the increase or decrease in absorbance at 340 nm resulting from formation or depletion of NAD(P)H ($\varepsilon_{NAD(P)H}$ = 6.22 cm^{-1} mM^{-1}). Time courses were typically recorded for up to 10 min, and the rate was obtained from linear plots of absorbance against time. The experimental reaction rates were usually in the range 0.004–0.2 ΔAbs/min. XDH activity was measured in 50 mM Tris/HCl buffer, pH 9.0, using 140 mM xylitol and 2 mM NAD^+ (or $NADP^+$) as the substrates. Activities of XR and XK were measured using the reported assays [25].

2.5.3 Steady-state kinetic analysis

We used crude cell extract obtained from *S. cerevisiae* biomass grown aerobically for about 12 h at 30°C. The previously described media (pH 6.5) [25] was used with the exception that 20 g/L glucose replaced xylose, and ergosterol and Tween 80 were lacking. The French Press was used for cell disruption. Initial rates of xylitol oxidation were recorded under conditions where the concentration of NAD^+ or $NADP^+$ was varied in the range 0.45–3.0 mM at two constant concentrations of substrate (50 or 150 mM). A 100-mM potassium phosphate buffer, pH 7.0, was used. Data were plotted as initial rate against the coenzyme concentration. Kinetic parameters (V_{max}, K_m) were obtained from non-linear fits of the Michaelis-Menten equation to the data. In the case that saturation in NAD^+ or $NADP^+$ was not achieved, the catalytic efficiency (V_{max}/K_m) was obtained from the part of the plot where the initial rate was linearly dependent on the coenzyme concentration. V_{max}/K_m corresponds to the slope value. The program Sigma Plot 9.0 (Systat Software, San Jose, CA) was used for linear and non-linear least squares regression analysis.

2.5.4 Monitoring xylose conversion

Samples were taken at suitable times from xylose fermentations performed in shake flasks and in the bioreactor. Immediate work-up involved centrifugation of a suitable portion of the sample (10 min, 15 700 × *g*, 4°C) and storage of the supernatant at –20°C. Unless otherwise mentioned, cell growth was recorded as increase in optical density at 600 nm measured using the remainder of the sample. To determine CDW, 40 mL of culture broth was filtered through a 0.45-μm Polyethersulfone membrane filter (47-mm diameter; Sartorius, Göttingen, Germany) that had been dried for 10 min in a 750 W Moulinex Micro-Chef microwave oven operated at the lowest power level. The filter cake was washed thoroughly using 0.9% NaCl solution and again dried in the microwave (20 min).

An IN1313 acoustic gas analyzer (Innova AirTechInstruments, Ballerup, Denmark) was used to measure the concentrations of ethanol and CO_2 in the bioreactor off gas. The instrument was calibrated with a reference gas containing 0.1% ethanol and 5.0% CO_2, the remainder being N_2 (Linde, Stadl-Paura, Austria). Relevant components of the culture supernatant (xylose, xylitol, glycerol, acetate, ethanol, pyruvate) were analyzed by HPLC using the reported protocol [25].

The carbon balance for the conversion of xylose was calculated by taking all measured compounds (see above) into account. For shake flask experiments where CO_2 formation was not quantitated, it was assumed that 1 mol of CO_2 was formed per each mol of acetate and ethanol. The amount of CO_2 and ethanol carried out with the off-gas of the bioreactor was measured and considered in the carbon balance.

3 Results

3.1 $NADP^+$-active variants of *Gm*XDH

3.1.1 Mutant design

The amino acid sequence of *Gm*XDH is 43 and 53% identical to the sequences of *silverleaf whitefly* ketose reductase (*Wf*KR) and *P. stipitis* XDH (*Ps*XDH), respectively. *Wf*KR is naturally dependent on NADP(H) whereas *Ps*XDH requires NAD(H) for activity. A crystal structure of *Wf*KR in the unliganded apo-form revealed a phosphate molecule bound at the position presumably occupied by the 2′-phosphate of NADP(H) in the enzyme-coenzyme complex [36]. Figure 1 shows a partial multiple sequence alignment of *Gm*XDH, *Ps*XDH and *Wf*KR, comparing the region in the primary structures, which in *Wf*KR is thought to accommodate the 2′-phosphate group of the coenzyme. The putative binding pocket for the 2′-OH of NAD(H) in *Ps*XDH was remodeled by site-directed mutagenesis to introduce residues Ala^{199}, Arg^{200}, Ser^{201} and Arg^{204} of *Wf*KR at the corresponding positions of the yeast enzyme [23]. In k_{cat}/K_m terms, the resulting mutant XDH preferred $NADP^+$ about 33-fold over NAD. We therefore targeted the region Asp^{202}-Leu-Val-Glu-Ser^{206} in *Gm*XDH using a mutagenesis experiment, in which PCR with the chosen oligonucleotide primers would, in the case of ideal priming, introduce the sequence Ala^{202}-Arg-Ser-Pro-Arg^{206} as in *Wf*KR. However, it was considered that the exonuclease activity of the DNA polymerase as well as imperfect priming of the oligonu-

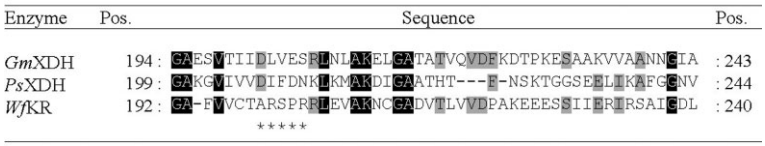

Figure 1. Partial multiple alignment of the amino acid sequences in *Gm*XDH, *Ps*XDH and *Wf*KR thought to accommodate the 2'-OH of NAD(H) in the xylitol dehydrogenases and the 2'-phosphate of NADP(H) in the ketoreductase: The degree of residue conservation is shown as 100% (white label, black box) and 67% (black label, grey box). Asterisks mark the residues of *Wf*KR potentially involved in the binding of the 2'-phosphate group of $NADP^+$.

cleotide might lead to a series of alternatively mutated genes that could encode interesting variants of *Gm*XDH.

3.1.2 Selection

An activity-based screening was therefore used to select *Gm*XDH mutants capable of oxidizing xylitol in the presence of $NADP^+$. From a series of positive clones, we chose four candidates that displayed higher activity with $NADP^+$ than NAD^+. Sequencing revealed the *Gm*XDH variants summarized in Table 2, and specific activities of these enzymes utilizing NAD^+ and $NADP^+$ are shown. Mutants for which the expressed level of activity was lower than 2 U/mg were not further pursued. Considering the coenzyme selectivity of the available mutants of *Ct*XR, the gene encoding *Gm*XDH-V2K1 was selected for yeast strain engineering.

3.2 Construction of *S. cerevisiae* strains expressing mutated XR and XDH genes

We obtained two novel yeast strains, termed BP11001 and BP11002, by inserting the vector Y*Ct*XR-Dm/*Gm*XDH-V2K1/XKS1 and Y*Ct*XR-ND/*Gm*XDH-V2K1/XKS1 into the URA3-locus of the parent strain CEN.PK 113-5D, respectively (Table 1). Genomic integration of the respective gene cassette was verified by measurement of specific enzyme activities in cell extracts of glucose-grown BP11001 and BP11002, as shown in Table 3. Catalytic efficiencies of wild-type and mutated *Gm*XDH for reaction with NAD^+ and $NADP^+$ were determined using the crude enzyme preparations. Results are shown in Table 4. The V2K1 mutant of *Gm*XDH showed a linear dependence of the enzymatic reaction rate on the concentration of NAD^+ and $NADP^+$ irrespective of whether the constant xylitol concentration was 50 or 150 mM. By contrast, when determined at 50 and 150 mM xylitol, the K_m of the wild-type enzyme for NAD^+ was 0.9 (± 0.2) and 0.5 (± 0.1) mM, respectively. A threefold increase in xylitol concentration from 50 to 150 mM caused enhancement of $V_{max}/K_{NAD(P)^+}$ for V2K1 by about the same factor, suggesting that apparent binding of xylitol was also weakened in V2K1 as compared to the wild-type enzyme whose K_m for xylitol (at pH 7.5) is 12 mM [34]. Consistent with the reported K_m, V_{max}/K_{NAD^+} of the wild-type enzyme increased only moderately, by a factor of 1.7, as result of the increase of the xylitol concentration from 50 to 150 mM. Kinetic data in Table 4 suggest that the combination of *Ct*XR-ND (k_{cat}/K_{NADPH} = 2.2 $s^{-1}\mu M^{-1}$; k_{cat}/K_{NADH} = 0.54 $s^{-1}\mu M^{-1}$; $(k_{cat}/K_{NADPH})/(k_{cat}/K_{NADH})$ = 4 [18]) and *Ct*XR-Dm (k_{cat}/K_{NADPH} = 0.23 $s^{-1}\mu M^{-1}$; k_{cat}/K_{NADH} = 0.29 $s^{-1}\mu M^{-1}$; $(k_{cat}/K_{NADPH})/(k_{cat}/K_{NADH})$ = 0.8 [18]) with *Gm*XDH-V2K1 should support efficient recycling of NAD(P)H coenzymes in the conversion of xylose into xylulose. The relative utilization of NADPH and NADH by *Ct*XR-ND and *Ct*XR-Dm was previously determined experimentally under "simulated *in vivo* conditions". Reported intracellular concentrations ([37] and references therein) of NADPH (508 µM), NADH (185 µM) and xylose (113 mM) were employed in the assay. The molar ratio of NADPH and

Table 2. $NAD(P)^+$-dependent variants of *Gm*XDH and their specific xylitol dehydrogenase activities: Section 2.5 reports on the experimental procedures used. SD was ≤ 20%; Δ represents a one-amino acid deletion

Name	Mutation	Specific activity NAD^+ (U/mg)	Specific activity $NADP^+$ (U/mg)	Selectivity $NADP^+/NAD^+$
*Gm*XDH-Wt	TIIDLVESRLN	15	0.036	0.0024
*Gm*XDH-V2K1	TIIAΔΔPRRLN	2.6	10.3	4
*Gm*XDH-V2K2	TIIARSPRRLN	0.00048	0.20	425
*Gm*XDH-V1K7 [a)]	TIIARSΔΔRLN	0.025	0.42	17
*Gm*XDH-V1K8 [b)]	TIIARSΔRRLN	0.057	1.2	21

a) $D^{202}LVES^{206} \rightarrow A^{202}RS\Delta\Delta^{206}$ mutant of *Gm*XDH.
b) $D^{202}LVES^{206} \rightarrow A^{202}RS\Delta R^{206}$ mutant of *Gm*XDH.

Table 3. Specific activities of XR, XDH and XK in crude cell extracts of xylose-fermenting strains of *S. cerevisiae*: Cells were grown aerobically in basal media [25] containing 20 g/L glucose and disrupted by using a French Press. The SD on reported values was ≤ 20%

Strain	Coenzyme	XR activity (U/mg)	XDH activity (U/mg)	XK activity (U/mg)
BP11001	NAD(H)	0.16	0.27	0.32
	NADP(H)	0.27	0.62	
BP11002	NAD(H)	0.18	0.23	0.39
	NADP(H)	0.40	0.51	
BP10001 [a)]	NAD(H)	0.18	0.62	0.42
	NADP(H)	0.26		
BP000 [a)]	NAD(H)	0.18	0.73	0.43
	NADP(H)	0.23		

a) Previously described reference strains [25]. Crude extracts were prepared using Y-Per disruption of cells obtained from xylose fermentations in shaken flasks. While specific activities of XR and XDH are in good (XR) and reasonable (XDH) agreement with literature [25], the levels of XK are ~fivefold lower than those reported earlier. We noted XK to be extremely sensitive to dilution and show fast decay of its activity over time (unpublished results from this laboratory, 2009). It is possible, therefore, that different times between cell disruption and activity measurement explain the variation in XK specific activities reported here and elsewhere [25]. However, the levels of XK in the different yeast strains used in this study are clearly well comparable.

NADH used for xylose reduction was 7 for *Ct*XR-ND and 1.5 for *Ct*XR-Dm [37].

3.3 Oxygen-limited conversion of xylose in shake-flask cultures

Strains BP11001 and BP11002 as well as the reference strains BP000 and BP10001 were grown on glucose. Washed yeast biomass was used to inoculate shake flasks containing mineral medium in which 20 g/L xylose was the sole carbon source. Figure 2 shows time courses of xylose conversion by BP11001 and BP11002 under conditions where the concentration of dissolved O_2 was limiting (≤ 20 μM). The physiological parameters characterizing the fermentations are summarized in Table 5. No biomass was formed from xylose within limits of the experimental error. In a carbon balance calculated from the data in Table 5 whereby CO_2 was inferred from the ethanol and acetate values, only ≤ 7% of the total carbon from xylose remained unaccounted for. Results obtained for strains BP000 und BP10001 are in good agreement with literature [25]. Compared to BP000, the glycerol yield in strains BP11001 and BP11002 was decreased 36 and 43%, respectively, whereas acetate yields were correspondingly increased (Table 5). The yields of ethanol and xylitol in BP11001 were unchanged relative to the corresponding yields in BP000. In BP11002, however, the ethanol yield was lower and the xylitol yield was higher (both 14%) than the corresponding yields in BP000.

3.4 Fermentation of xylose in the anaerobic bioreactor

Strain BP11001 was used. Figure 3 shows the time course of xylose conversion, and Table 5 summarizes the fermentation parameters along with previously reported data for strains BP10001 and BP000. The carbon balance was closed, implying that the measurements were internally consistent. BP11001 showed similar specific rates for xylose uptake as the reference strains. The yield of

Table 4. Catalytic efficiencies of wild-type and mutated forms of *Gm*XDH at 25 °C: Kinetic data was measured using cell extracts of *S. cerevisiae* expressing the gene encoding for *Gm*XDH in wild-type or V2K1 mutated form. A 100-mM potassium phosphate buffer, pH 7.0, was used. See Section 2.5 for further details. The S.D. on reported values was ≤ 20%

	Xylitol (mM)	V_{max}/K_{NADP^+} (U/mg/mM)	V_{max}/K_{NAD^+} (U/mg/mM)	V_{max}/K_{NADP^+} / V_{max}/K_{NAD^+}	$V_{phys(NADP^+)}$ (U/mg) [c)]	$V_{phys(NAD^+)}$ (U/mg) [e)]	$V_{phys(NADP^+)}/V_{phys(NAD^+)}$
*Gm*XDH-Wt	150	7×10^{-4} [a)]	0.38 [b)]	2×10^{-3}	7×10^{-5} [d)]	0.14 [f)]	5×10^{-4}
*Gm*XDH-Wt	50	6×10^{-4} [a)]	0.22 [b)]	3×10^{-3}	6×10^{-5} [d)]	0.11 [f)]	5×10^{-4}
*Gm*XDH-V2K1	150	0.067 [a)]	0.017 [a)]	4	7×10^{-3} [d)]	0.020 [d)]	0.3
*Gm*XDH-V2K1	50	0.028 [a)]	6×10^{-3} [a)]	4	3×10^{-3} [d)]	8×10^{-3} [d)]	0.4

a) Calculated from the linear dependence of the initial rate on the coenzyme concentration.
b) Calculated from V_{max} and K_{NAD^+} values that were obtained by fitting the Michaelis-Menten equation to the experimental data.
c) An *in vivo* concentration for $NADP^+$ of 0.1 mM [41] was used in the calculation of $V_{phys(NADP^+)}$.
d) Calculated using the term $(V_{max}/K_{NAD(P)^+}) \times [NAD(P)^+]$ considering that $[NAD(P)^+] < K_{NAD(P)^+}$.
e) An *in vivo* concentration for NAD^+ of 1.2 mM [41] was used in the calculation of $V_{phys(NAD^+)}$.
f) Calculated using the Michaelis-Menten equation.

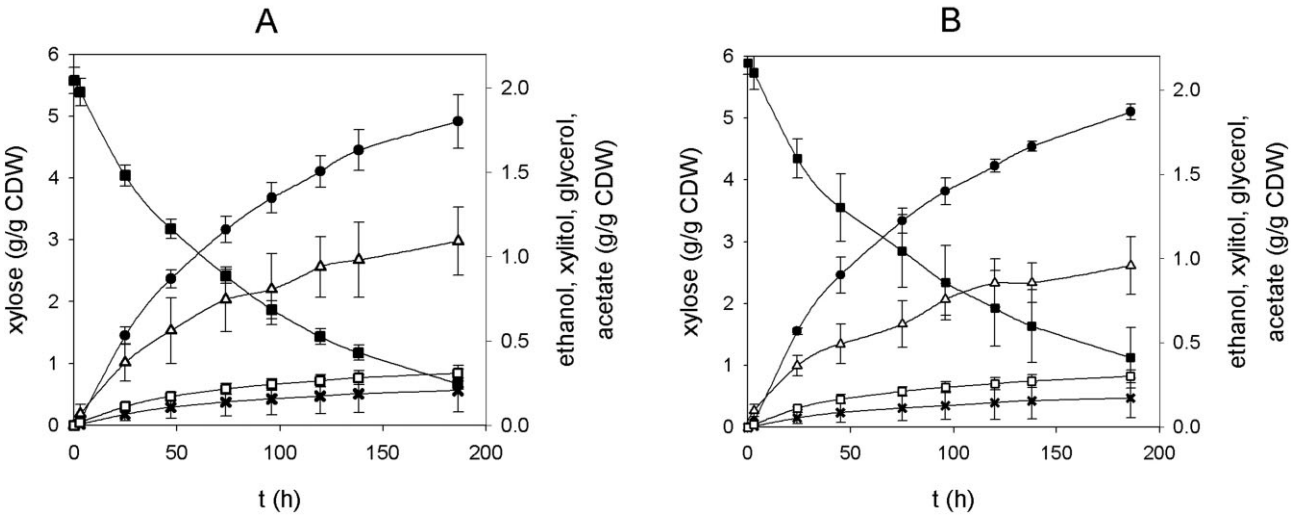

Figure 2. Xylose conversion in shake flasks: Panels A and B show results for BP11001 and BP11002, respectively. The symbols indicate xylose (full squares), xylitol (circles), ethanol (triangles), acetate (empty squares) and glycerol (stars). The shown results are mean values from quadruplicate fermentation experiments with error bars indicating the SD.

ethanol in BP11001 was identical to that in BP000, however, it was clearly lower than in BP10001. The new strain BP11001 produced 52% less glycerol than BP000, thus resembling BP10001 with respect to the glycerol yield. Unlike BP10001 in which formation of xylitol was reduced by about 50% as compared to BP000, the new strain BP11001 displayed a xylitol yield just 13% lower than that for the reference strain expressing wild-type XR and XDH genes. Acetate production on the other hand was about two times that of BP000. Therefore, although the values of the yield coefficients for glycerol and acetate differed between the two experiments, the overall product distribution seen for xylose fermentation by BP11001 in shake flasks was largely confirmed under the bioreactor conditions.

4 Discussion

The XR and XDH have previously been engineered individually to alter their coenzyme preference towards enhanced utilization of NADH and $NADP^+$, respectively [18–23]. The best-improved XR enzyme is about 13-times more efficient in the reaction with NADH, as compared to NADPH [20]. An $NADP^+$-dependent variant of XDH has also been described [23], and metabolic consequences in *S. cerevisiae* resulting from the change in XR or XDH coenzyme preference have been evaluated in xylose fermentation studies [21, 25–28]. The current evidence supports a scenario where coenzyme recycling in the steps catalyzed by XR and XDH contributes to a comprehensive improvement of the

Table 5. Comparison of xylose fermentation by different strains of *S. cerevisiae*

	Shake flask (oxygen limited)				Bioreactor (anaerobic)		
	BP000[c]	BP10001[c]	BP11001[c]	BP11002[c]	BP000[d]	BP10001[d]	BP11001
q_{xylose}[a]	0.09 ± 0.01	0.08 ± 0.01	0.06 ± 0.01	0.06 ± 0.01	0.06	0.08	0.06
$Y_{ethanol}$[b]	0.23 ± 0.03	0.30 ± 0.01	0.23 ± 0.03	0.20 ± 0.01	0.24	0.34	0.24
$Y_{xylitol}$[b]	0.36 ± 0.02	0.23 ± 0.02	0.37 ± 0.05	0.41 ± 0.04	0.39	0.19	0.34
$Y_{glycerol}$[b]	0.073 ± 0.007	0.051 ± 0.014	0.046 ± 0.016	0.041 ± 0.009	0.048	0.021	0.023
$Y_{acetate}$[b]	0.049 ± 0.002	0.046 ± 0.006	0.068 ± 0.004	0.070 ± 0.004	0.019	0.020	0.044
C-recovery	95%[e]	93%[e]	97%[e]	94%[e]	101%	96%	99%

a) Xylose uptake rates (q_{xylose}) are given in g/(g CDW h) calculated from time-course data obtained in the first 24 h of the fermentation.
b) Yield coefficients (Y) are given in g/g xylose; they were calculated using data obtained after a reaction time of 75 h (shake flasks) or 121 h (bioreactor).
c) Mean values and SD from quadruplicate experiments are given.
d) Values are taken from ref. [25].
e) For calculation of the carbon balance it was assumed that one mol CO_2 was formed per mol of ethanol or acetate.

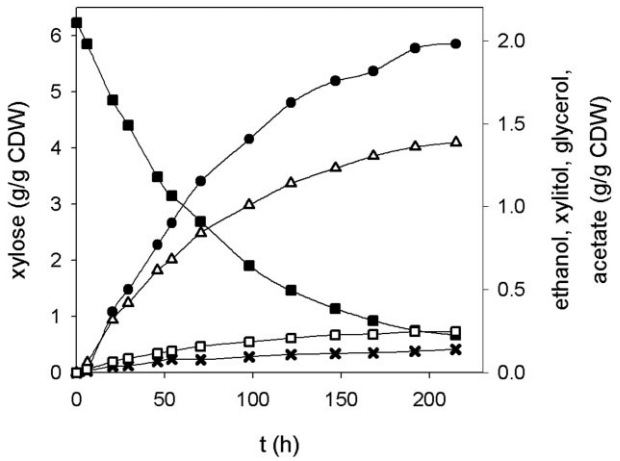

Figure 3. Xylose conversion by BP11001 under anaerobic conditions in a bioreactor: The symbols indicate xylose (full squares), xylitol (circles), ethanol (triangles), acetate (empty squares) and glycerol (stars).

distribution of fermentation products from xylose [5]. Because a well matched pair of XR and XDH is so far not available, we describe here adjustment of the coenzyme preference of *Gm*XDH towards optimum compatibility with one of the known *Ct*XR enzymes, wild type or mutant. This is the first report in which mutated XR and XDH were combined in a xylose-fermenting strain of *S. cerevisiae*.

4.1 Engineering of *Gm*XDH for enhanced utilization of NADP+

Sequence similarity was used to identify the region of the *Gm*XDH primary structure likely involved in the binding of the ribosyl 2′-OH of NAD+ (see Fig. 1). *Gm*XDH is a member of medium-chain dehydrogenase/reductase superfamily of proteins [33, 38] and has a Rossmann-fold coenzyme-binding domain. A „sloppy" PCR reaction was useful to introduce a set of multiple mutations, spatially restricted to the area of presumed functional relevance in the translated protein. Several interesting enzyme variants were selected in a screening for NADP+-dependent xylitol dehydrogenase activity. Substitution of the peptide Asp[202]-Leu-Val-Glu-Ser[206] by the corresponding peptide Ala[199]-Arg-Ser-Pro-Arg[203] from *Wf*KR resulted in a marked, 2×10^5-fold alteration in the ratio of specific activities, NADP+ compared with NAD+, from 0.0024 in the wild-type enzyme to 425 in the *Gm*XDH-V2K2 mutant. However, the change in selectivity for the quintuple mutant V2K2 was overwhelmingly due to a disruption of the reaction with NAD+, implying that *Gm*XDH-V2K2 was clearly not a good NADP+-dependent catalyst for xylitol oxidation. Deletion of Pro[202] from the *Wf*KR motif as in the V1K7 and V1K8 mutants of *Gm*XDH complemented the NAD+-dependent activity of V2K2 about 100-fold and also caused a slight enhancement of the rate of the enzymatic reaction with NADP+.

However, in terms of the level of NADP+-dependent activity that determines the flux of carbon from xylitol to xylulose, only the V2K1 mutant that harbors the *Wf*KR motif truncated by deletions of Arg200 and Ser201 appeared to be useful. When assayed with NADP+, *Gm*XDH-V2K1 displayed about 70% of the activity of the wild-type enzyme with NAD+. The mutated XDH was a promiscuous enzyme capable of utilizing NADP+ and NAD+ with efficiencies clearly significant when compared to the corresponding value of V_{max}/K_m for the wild-type enzyme using NAD+. This finding was unexpected because not only is it suggested from the crystal structure of *Wf*KR that the diad of Arg and Ser bind the 2′-phosphate group on NADP+ [35], but it was also considered from results of previous studies of dehydrogenases belonging to the Rossmann fold family that Asp[202] would be a key residue required for the interaction of *Gm*XDH with NAD+ [39]. The *Gm*XDH-V2K1 mutant lacks either element of coenzyme specificity in the primary structure, indicating a complex structure-function relationship for this enzyme that is not fully understood. However, a role of Arg[200] and Ser[201] of *Wf*KR in discriminating against the use of NAD+ is corroborated by the results for *Gm*XDH.

4.2 Analysis of metabolic consequences resulting from the engineered XR-XDH pathway in a novel xylose-fermenting strain of *S. cerevisiae*

Coenzyme preferences have been reported for crude and isolated protein preparations of wild-type and mutated forms of XR and XDH [18–23, 33]. Aggregate data from *in vitro* measurements suggests that yeast strains harboring engineered *Ct*XR and wild-type XDH will recycle in the XDH step maximally half of the coenzyme utilized in the XR reaction [37]. The strain BP10001 producing the doubly mutated variant of *Ct*XR surpassed the reference strain harboring wild-type *Ct*XR in terms of ethanol yield (+42%) as well as in xylitol (-52%) and glycerol (-57%) yields (see ref. [25] and Table 5).

Considering that naturally occurring XR usually display a ≥ threefold (according to $k_{cat}/K_{NAD(P)H}$) preference for reaction with NADPH compared with NADH [18, 40], wild-type XR and NADP+-dependent XDH should present an excellent pair of enzymes with which to optimize coenzyme recycling during xylose assimilation. However, a recent comparison of two isogenic strains of *S. cerevisiae*

harboring a *P. stipitis* xylose pathway that contained XDH in NAD^+-dependent wild-type or $NADP^+$-dependent mutated form revealed only modest enhancement (≈ 10%; 0.36 g/g) of the ethanol yield from xylose resulting from the change in XDH coenzyme preference [27]. Results obtained here by using strains BP11001 and BP11002 are therefore important to address the key question of how significant is coenzyme recycling in the steps of XR and XDH relative to other factors such as the overall flux through the pathway, for example.

In spite of the fact that according to *in vitro* data, BP11001 and BP11002 provide a better match in coenzyme preference of XR and XDH than BP10001, their performance during xylose fermentation in shake flasks was clearly worsened when judged on the basis of ethanol and xylitol yields. BP11002 did not even reach the benchmark level presented by the reference strain expressing the genes for wild-type XR and XDH. A notable difference of both novel strains as compared to BP000 was the decreased yield of glycerol. The extent to which glycerol formation was suppressed in BP11001 and BP11002 was comparable to that observed in BP10001. If as suggested by van Maris *et al*. [10] glycerol serves as reporter of excess NADH generated in the xylose pathway under the typically non-growing conditions of xylose fermentation by *S. cerevisiae*, strains BP10001, BP11001 and BP11002 are similar in their ability to avoid this type of coenzyme imbalance. The product distribution resulting from anaerobic conversion of xylose by BP11001 was confirmed in bioreactor experiments. What is then the reason for the relatively high yield of xylitol (and the low yield of ethanol) in BP11001 as compared to BP10001 when it can be assumed that perturbation of the coenzyme balance due to xylose assimilation was smaller in the former strain?

We think that the overall flux through the xylose pathway may not be the same for the different yeast strains, and it should be relevant to consider these changes in a rigorous evaluation. With the assumption that the intracellular concentration of $NADP^+$ is just about one-twelfth that of NAD^+ (2.9 µmol NAD^+/g CDW; measured for anaerobic conversion of glucose [41]), we can estimate using V_{max}/K_m in Table 4 that the overall reaction rate of *Gm*XDH-V2K1 with $NADP^+$ and NAD^+ is smaller by a factor of 5 (150 mM xylitol) to 11 (50 mM xylitol) than the corresponding rate of the wild-type enzyme. As a result, the effective ratio of XDH and XR activities is also 5- to 11-fold lower in BP11001 than in BP10001. Previous studies have shown that the activity of XDH can cause a kinetic bottleneck that manifests itself in xylitol excretion [29–32]. The important advantage of BP11002 and in particular BP11001 lies in the fact that flux optimization can now be performed under conditions where coenzyme is efficiently recycled between XR and XDH.

Karin Longus, Veronika Milocco and Valentin Pacher are thanked for their expert technical assistance. Financial support from the Austrian Science Fund FWF (P18275-B09 to B.N. and J2698 to M.K.) is gratefully acknowledged.

The authors have declared no conflict of interest.

5 References

[1] Hahn-Hägerdal, B., Galbe, M., Gorwa-Grauslund, M. F., Lidén, G., Zacchi, G., Bio-ethanol – the fuel of tomorrow from the residues of today. *Trends Biotechnol.* 2006, *24*, 549–556.

[2] Hahn-Hägerdal, B., Karhumaa, K., Fonseca, C., Spencer-Martins, I., Gorwa-Grauslund, M. F., Towards industrial pentose-fermenting yeast strains. *Appl. Microbiol. Biotechnol.* 2007, *74*, 937–953.

[3] Aristidou, A., Penttilä, M., Metabolic engineering applications to renewable resource utilization. *Curr. Opin. Biotechnol.* 2000, *11*, 187–198.

[4] Jeffries, T. W., Utilization of xylose by bacteria, yeasts, and fungi. *Adv. Biochem. Eng. Biotechnol.* 1983, *27*, 1–32.

[5] Kuyper, M., Winkler, A. A., van Dijken, J. P., Pronk, J. T., Minimal metabolic engineering of *Saccharomyces cerevisiae* for efficient anaerobic xylose fermentation: a proof of principle. *FEMS Yeast Res.* 2004, *4*, 655–664.

[6] Otero, J. M., Panagiotou, G., Olsson, L., Fueling industrial biotechnology growth with bioethanol. *Adv. Biochem. Eng. Biotechnol.* 2007, *108*, 1–40.

[7] Chu, B. C., Lee, H., Genetic improvement of *Saccharomyces cerevisiae* for xylose fermentation. *Biotechnol. Adv.* 2007, *25*, 425–441.

[8] Hahn-Hägerdal, B., Karhumaa, K., Jeppsson, M., Gorwa-Grauslund, M. F., Metabolic engineering for pentose utilization in *Saccharomyces cerevisiae*. *Adv. Biochem. Eng. Biotechnol.* 2007, *108*, 147–177.

[9] Jeffries, T. W., Engineering yeasts for xylose metabolism. *Curr. Opin. Biotechnol.* 2006, *17*, 320–326.

[10] van Maris, A. J., Winkler, A. A., Kuyper, M., de Laat, W. T., *et al.*, Development of efficient xylose fermentation in *Saccharomyces cerevisiae*: xylose isomerase as a key component. *Adv. Biochem. Eng. Biotechnol.* 2007, *108*, 179–204.

[11] Bro, C., Regenberg, B., Förster, J., Nielsen, J., In silico aided metabolic engineering of *Saccharomyces cerevisiae* for improved bioethanol production. *Metab. Eng.* 2006, *8*, 102–111.

[12] Jeppsson, M., Johansson, B., Hahn-Hägerdal, B., Gorwa-Grauslund, M. F., Reduced oxidative pentose phosphate pathway flux in recombinant xylose-utilizing *Saccharomyces cerevisiae* strains improves the ethanol yield from xylose. *Appl. Environ. Microbiol.* 2002, *68*, 1604–1609.

[13] Roca, C., Nielsen, J., Olsson, L., Metabolic engineering of ammonium assimilation in xylose-fermenting *Saccharomyces*

cerevisiae improves ethanol production. *Appl. Environ. Microbiol.* 2003, *69*, 4732–4736.

[14] Sonderegger, M., Schumperli, M., Sauer, U., Metabolic engineering of a phosphoketolase pathway for pentose catabolism in *Saccharomyces cerevisiae*. *Appl. Environ. Microbiol.* 2004, *70*, 2892–2897.

[15] Verho, R., Londesborough, J., Penttila, M., Richard, P., Engineering redox cofactor regeneration for improved pentose fermentation in *Saccharomyces cerevisiae*. *Appl. Environ. Microbiol.* 2003, *69*, 5892–5897.

[16] Karhumaa, K., Garcia Sanchez, R., Hahn-Hägerdal, B., Gorwa-Grauslund, M. F., Comparison of the xylose reductase-xylitol dehydrogenase and the xylose isomerase pathways for xylose fermentation by recombinant *Saccharomyces cerevisiae*. *Microb. Cell Fact.* 2007, *6*, 5.

[17] Kuyper, M., Hartog, M. M., Toirkens, M. J., Almering, M. J. *et al.*, Metabolic engineering of a xylose-isomerase-expressing *Saccharomyces cerevisiae* strain for rapid anaerobic xylose fermentation. *FEMS Yeast Res.* 2005, *5*, 399–409.

[18] Petschacher, B., Leitgeb, S., Kavanagh, K. L., Wilson, D. K., Nidetzky, B., The coenzyme specificity of *Candida tenuis* xylose reductase (AKR2B5) explored by site-directed mutagenesis and X-ray crystallography. *Biochem. J.* 2005, *385*, 75–83.

[19] Kostrzynska, M., Sopher, C. R., Lee, H., Mutational analysis of the role of the conserved lysine-270 in the *Pichia stipitis* xylose reductase. *FEMS Microbiol. Lett.* 1998, *159*, 107–112.

[20] Liang, L., Zhang, J., Lin, Z., Altering coenzyme specificity of *Pichia stipitis* xylose reductase by the semi-rational approach CASTing. *Microb. Cell. Fact.* 2007, *6*, 36.

[21] Watanabe, S., Abu Saleh, A., Pack, S. P., Annaluru, N. *et al.*, Ethanol production from xylose by recombinant *Saccharomyces cerevisiae* expressing protein-engineered NADH-preferring xylose reductase from *Pichia stipitis*. *Microbiology* 2007, *153*, 3044–3054.

[22] Dmytruk, O. V., Dmytruk, K. V., Abbas, C. A., Voronovsky, A. Y., Sibirny, A. A., Engineering of xylose reductase and overexpression of xylitol dehydrogenase and xylulokinase improves xylose alcoholic fermentation in the thermotolerant yeast *Hansenula polymorpha*. *Microb. Cell. Fact.* 2008, *7*, 21.

[23] Watanabe, S., Kodaki, T., Makino, K., Complete reversal of coenzyme specificity of xylitol dehydrogenase and increase of thermostability by the introduction of structural zinc. *J. Biol. Chem.* 2005, *280*, 10340–10349.

[24] Metzger, M. H., Hollenberg, C. P., Amino acid substitutions in the yeast *Pichia stipitis* xylitol dehydrogenase coenzyme-binding domain affect the coenzyme specificity. *Eur. J. Biochem.* 1995, *228*, 50–54.

[25] Petschacher, B., Nidetzky, B., Altering the coenzyme preference of xylose reductase to favor utilization of NADH enhances ethanol yield from xylose in a metabolically engineered strain of *Saccharomyces cerevisiae*. *Microb. Cell Fact.* 2008, *7*, 9.

[26] Jeppsson, M., Bengtsson, O., Franke, K., Lee, H., *et al.*, The expression of a *Pichia stipitis* xylose reductase mutant with higher K_M for NADPH increases ethanol production from xylose in recombinant *Saccharomyces cerevisiae*. *Biotechnol. Bioeng.* 2006, *93*, 665–673.

[27] Matsushika, A., Watanabe, S., Kodaki, T., Makino, K., *et al.*, Expression of protein engineered $NADP^+$-dependent xylitol dehydrogenase increases ethanol production from xylose in recombinant *Saccharomyces cerevisiae*. *Appl. Microbiol. Biotechnol.* 2008, *81*, 243–255.

[28] Hou, J., Shen, Y., Li, X. P., Bao, X. M., Effect of the reversal of coenzyme specificity by expression of mutated *Pichia stipitis* xylitol dehydrogenase in recombinant *Saccharomyces cerevisiae*. *Lett. Appl. Microbiol.* 2007, *45*, 184–189.

[29] Walfridsson, M., Anderlund, M., Bao, X., Hahn-Hägerdal, B., Expression of different levels of enzymes from the *Pichia stipitis* XYL1 and XYL2 genes in *Saccharomyces cerevisiae* and its effects on product formation during xylose utilisation. *Appl. Microbiol. Biotechnol.* 1997, *48*, 218–224.

[30] Jin, Y. S., Jeffries, T. W., Changing flux of xylose metabolites by altering expression of xylose reductase and xylitol dehydrogenase in recombinant *Saccharomyces cerevisiae*. *Appl. Biochem. Biotechnol.* 2003, *105–108*, 277–286.

[31] Karhumaa, K., Fromanger, R., Hahn-Hägerdal, B., Gorwa-Grauslund, M. F., High activity of xylose reductase and xylitol dehydrogenase improves xylose fermentation by recombinant *Saccharomyces cerevisiae*. *Appl. Microbiol. Biotechnol.* 2007, *73*, 1039–1046.

[32] Eliasson, A., Hofmeyr, J. S., Pedler, S., Hahn-Hägerdal, B., The xylose reductase/xylitol dehydrogenase/xylulokinase ratio affects product formation in recombinant xylose-utilising *Saccharomyces cerevisiae*. *Enzyme Microb. Technol.* 2001, *29*, 288–297.

[33] Habenicht, A., Motejadded, H., Kiess, M., Wegerer, A., Mattes, R., Xylose utilisation: cloning and characterisation of the xylitol dehydrogenase from *Galactocandida mastotermitis*. *Biol. Chem.* 1999, *380*, 1405–1411.

[34] Nidetzky, B., Helmer, H., Klimacek, M., Lunzer, R., Mayer, G., Characterization of recombinant xylitol dehydrogenase from *Galactocandida mastotermitis* expressed in *Escherichia coli*. *Chem. Biol. Interact.* 2003, *143–144*, 533–542.

[35] Klimacek, M., Nidetzky, B., A catalytic consensus motif for D-mannitol 2-dehydrogenase, a member of a polyol-specific long-chain dehydrogenase family, revealed by kinetic characterization of site-directed mutants of the enzyme from *Pseudomonas fluorescens*. *Biochem. J.* 2002, *367*, 13–18.

[36] Banfield, M. J., Salvucci, M. E., Baker, E. N., Smith, C. A., Crystal structure of the NADP(H)-dependent ketose reductase from *Bemisia argentifolii* at 2.3 Å resolution. *J. Mol. Biol.* 2001, *306*, 239–250.

[37] Petschacher, B., Nidetzky, B., Engineering *Candida tenuis* Xylose reductase for improved utilization of NADH: antagonistic effects of multiple side chain replacements and performance of site-directed mutants under simulated in vivo conditions. *Appl. Environ. Microbiol.* 2005, *71*, 6390–6393.

[38] Lunzer, R., Mamnun, Y., Haltrich, D., Kulbe, K. D., Nidetzky, B., Structural and functional properties of a yeast xylitol dehydrogenase, a Zn^{2+}-containing metalloenzyme similar to medium-chain sorbitol dehydrogenases. *Biochem. J.* 1998, *336*, 91–99.

[39] Carugo, O., Argos, P., NADP-dependent enzymes. I: Conserved stereochemistry of cofactor binding. *Proteins* 1997, *28*, 10–28.

[40] Verduyn, C., Van Kleef, R., Frank, J., Schreuder, H., *et al.*, Properties of the NAD(P)H-dependent xylose reductase from the xylose-fermenting yeast *Pichia stipitis*. *Biochem. J.* 1985, *226*, 669–677.

[41] Nissen, T. L., Anderlund, M., Nielsen, J., Villadsen, J., Kielland-Brandt, M. C., Expression of a cytoplasmic transhydrogenase in *Saccharomyces cerevisiae* results in formation of 2-oxoglutarate due to depletion of the NADPH pool. *Yeast* 2001, *18*, 19–32.

MICROBIAL CELL FACTORIES
Chapter 2.2

RESEARCH Open Access

Fermentation of mixed glucose-xylose substrates by engineered strains of *Saccharomyces cerevisiae*: role of the coenzyme specificity of xylose reductase, and effect of glucose on xylose utilization

Stefan Krahulec, Barbara Petschacher, Michael Wallner, Karin Longus, Mario Klimacek, Bernd Nidetzky*

Abstract

Background: In spite of the substantial metabolic engineering effort previously devoted to the development of *Saccharomyces cerevisiae* strains capable of fermenting both the hexose and pentose sugars present in lignocellulose hydrolysates, the productivity of reported strains for conversion of the naturally most abundant pentose, xylose, is still a major issue of process efficiency. Protein engineering for targeted alteration of the nicotinamide cofactor specificity of enzymes catalyzing the first steps in the metabolic pathway for xylose was a successful approach of reducing xylitol by-product formation and improving ethanol yield from xylose. The previously reported yeast strain BP10001, which expresses heterologous xylose reductase from *Candida tenuis* in mutated (NADH-preferring) form, stands for a series of other yeast strains designed with similar rational. Using 20 g/L xylose as sole source of carbon, BP10001 displayed a low specific uptake rate q_{xylose} (g xylose/g dry cell weight/h) of 0.08. The study presented herein was performed with the aim of analysing (external) factors that limit q_{xylose} of BP10001 under xylose-only and mixed glucose-xylose substrate conditions. We also carried out a comprehensive investigation on the currently unclear role of coenzyme utilization, NADPH compared to NADH, for xylose reduction during co-fermentation of glucose and xylose.

Results: BP10001 and BP000, expressing *C. tenuis* xylose reductase in NADPH-preferring wild-type form, were used. Glucose and xylose (each at 10 g/L) were converted sequentially, the corresponding $q_{substrate}$ values being similar for each strain (glucose: 3.0; xylose: 0.05). The distribution of fermentation products from glucose was identical for both strains whereas when using xylose, BP10001 showed enhanced ethanol yield (BP10001 0.30 g/g; BP000 0.23 g/g) and decreased yields of xylitol (BP10001 0.26 g/g; BP000 0.36 g/g) and glycerol (BP10001 0.023 g/g; BP000 0.072 g/g) as compared to BP000. Increase in xylose concentration from 10 to 50 g/L resulted in acceleration of substrate uptake by BP10001 (0.05 - 0.14 g/g CDW/h) and reduction of the xylitol yield (0.28 g/g - 0.15 g/g). In mixed substrate batches, xylose was taken up at low glucose concentrations (< 4 g/L) and up to fivefold enhanced xylose uptake rate was found towards glucose depletion. A fed-batch process designed to maintain a "stimulating" level of glucose throughout the course of xylose conversion provided a q_{xylose} that had an initial value of 0.30 ± 0.04 g/g CDW/h and decreased gradually with time. It gave product yields of 0.38 g ethanol/g total sugar and 0.19 g xylitol/g xylose. The effect of glucose on xylose utilization appears to result from the enhanced flux of carbon through glycolysis and the pentose phosphate pathway under low-glucose reaction conditions.

Conclusions: Relative improvements in the distribution of fermentation products from xylose that can be directly related to a change in the coenzyme preference of xylose reductase from NADPH in BP000 to NADH in BP10001

* Correspondence: bernd.nidetzky@tugraz.at
Institute of Biotechnology and Biochemical Engineering, Graz University of Technology, Petersgasse 12/I, A-8010 Graz, Austria

increase in response to an increase in the initial concentration of the pentose substrate from 10 to 50 g/L. An inverse relationship between xylose uptake rate and xylitol yield for BP10001 implies that xylitol by-product formation is controlled not only by coenzyme regeneration during two-step oxidoreductive conversion of xylose into xylulose. Although xylose is not detectably utilized at glucose concentrations greater than 4 g/L, the presence of a low residual glucose concentration (< 2 g/L) promotes the uptake of xylose and its conversion into ethanol with only moderate xylitol by-product formation. A fed-batch reaction that maintains glucose in the useful concentration range and provides a constant $q_{glucose}$ may be useful for optimizing q_{xylose} in processes designed for co-fermentation of glucose and xylose.

Background

A substantial metabolic engineering effort has been directed towards development of strains of *Saccharomyces cerevisiae* capable of fermenting both the hexoses (mainly D-glucose) and pentoses (mainly D-xylose and L-arabinose) present in lignocellulose hydrolysates [1-5]. The repertoire of substrates utilized by *S. cerevisiae* in wild-type form does not include either pentose. Expression of heterologous pathways for conversion of D-xylose and L-arabinose has yielded strains showing the required substrate scope [1,4]. However, production of ethanol from the pentoses is by far less efficient in terms of specific productivity as compared to the fermentation of glucose. There is clearly not a single limiting step in pentose fermentation by *S. cerevisiae* and therefore, strain engineering for enhanced flux from substrate to ethanol remains a challenge. Depending on the route explored for conversion of D-xylose and L-arabinose into D-xylulose, maintenance of a balanced ratio for oxidized and reduced forms of $NADP^+$ and NAD^+ constitutes a fundamental issue of strain physiology during pentose fermentation. Utilization of (mainly) NADPH for reduction when NAD^+ is exclusively employed for oxidation results in a poor recycling of redox cofactors in the initial steps of pentose metabolism which in turn leads to a highly unfavourable distribution of fermentation products in which by-products like xylitol are formed in excess [1,5-7].

Protein engineering to alter the coenzyme specificity of xylose reductase (XR) or xylitol dehydrogenase (XDH) such that a reasonably matched pair of NAD^+ or $NADP^+$-utilizing enzymes is obtained, respectively, was a useful strategy towards generation of yeast strains with improved capabilities for fermentation of xylose [8-13]. The role of coenzyme recycling in the steps of XR and XDH is well demonstrated for conditions in which xylose is the sole source of carbon [8,10-12]. However, the situation is less clear for co-fermentation of glucose and xylose. Imbalance resulting from the two-step isomerization of xylose into xylulose may be alleviated through metabolism of glucose via the oxidative pentose phosphate pathway as this produces, hence regenerates NADPH [14,15]. Despite a number of studies, the impact of glucose on fermentation of xylose by *S. cerevisiae* strains harbouring engineered forms of XR or XDH clearly necessitates clarification.

High concentrations of glucose have been known to suppress utilization of xylose by engineered strains of *S. cerevisiae*, explicable on account of the specificity of sugar transporters naturally available to this organism [16-19]. However, it was also observed that xylose uptake was enhanced at low concentrations of glucose as compared to otherwise identical reaction conditions lacking glucose [15,17,20]. The physiological basis for acceleration of xylose consumption when glucose is present is not entirely clear. Notwithstanding, a fed-batch reaction in which a constant promoting level of glucose is maintained throughout the course of sugar conversion was considered a potentially useful process option for pentose fermentation [17]. It was also shown recently that the fed-batch reaction can be realized practically in a process of "simultaneous saccharification and fermentation", in short SSF. The SSF starts from a lignocellulose substrate in which using suitable pretreatment, most of the hemicellulose has already been degraded to soluble sugars, mainly pentoses, while the cellulose remains polymeric. The glucose is then released continuously by the action of cellulases ("saccharification"), resulting in an enhanced co-fermentation of glucose and the pentoses, especially xylose [21].

Using a pair of previously described xylose-fermenting strains of *S. cerevisiae* in which one (BP000) expresses the gene encoding *Ct*XR in the NADPH-preferring wild-type form and another (BP10001) expresses the gene for a doubly mutated NADH-preferring variant of this enzyme [8], we herein performed a comprehensive examination of how improved recycling of NADH in the steps of XR and XDH affects sugar fermentation for a mixed glucose-xylose substrate. The NAD^+-specific XDH from the yeast *Galactocandida mastotermitis* was used. The results show that benefits in terms of ethanol yield resulting from the use of an engineered XR are realized *fully* under co-fermentation conditions, which is a novel finding. We also analysed (external) factors that limit q_{xylose} of BP10001 under xylose-only and mixed glucose-xylose substrate conditions. An inverse

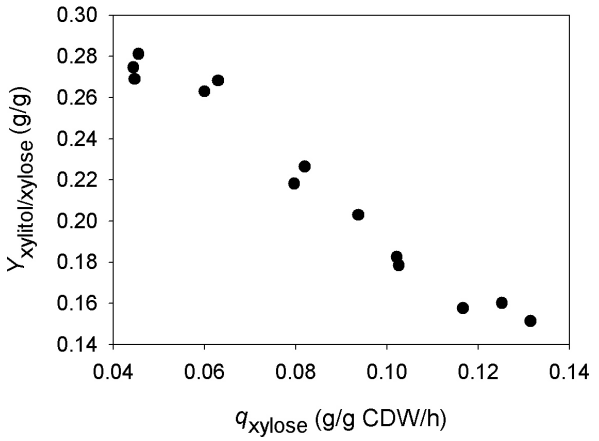

Figure 1 Xylitol yield ($Y_{xylitol}$) for xylose fermentations by strain BP10001 depends on the specific rate of xylose uptake (q_{xylose}). Data for q_{xylose} and $Y_{xylitol}$ are from the first 48 h of substrate conversion in 5 independent fermentations using varying initial xylose concentrations of 10 g/L (*this work*; xylose phase in mixed glucose-xylose fermentation; Table 1), 15 g/L (*unpublished results*), 20 g/L ([8]), and 50 g/L (*this work*).

Table 1 Physiological parameters for BP000 and BP10001 obtained from batch fermentations of a mixed glucose-xylose substrate (10 g/L each)

	Glucose phase[b]		Xylose phase[d]	
	BP000	**BP10001**	**BP000**	**BP10001**
q [g/g CDW/h][a]	3.0	2.9	0.05	0.05
$Y_{ethanol}$ [g/g]	0.36	0.36	0.23	0.30
$Y_{xylitol}$ [g/g]	0.006	ND[c]	0.36	0.26
$Y_{glycerol}$ [g/g]	0.12	0.11	0.072	0.023
$Y_{acetate}$ [g/g]	0.009	0.010	0.028	0.044
C-recovery [%]	101	97	108	107

a) $q_{glucose}$ and q_{xylose} were determined from data acquired in the first 6 h of the glucose phase and in the first 50 h of the xylose phase respectively. S.D.s on uptake rates were ≤ 12%;

b) Yield coefficients (g/g glucose and xylose consumed) were calculated using data obtained after a reaction time of 6 h. Except for $Y_{xylitol}$ where calculation of S.D. was not applicable, S.D.s were ≤ 14%.

c) ND - not detectable

d) Yield coefficients (g/g xylose consumed) represent mean values for the initial 100 hours of the xylose utilization phase. S.D.s were ≤ 11%.

relationship between xylose uptake rate and yield of xylitol is suggested for BP10001 (see Figure 1 and later in text), supporting conceptually novel thinking that coenzyme regeneration is *per se* not sufficient to prevent the by-product formation completely. We further show using a new design of fed-batch reaction that glucose (< 2 g/L) can be used to substantially enhance the xylose uptake of BP10001.

Results

Anaerobic conversion of a mixed glucose-xylose substrate

Figure 2 shows time courses of fermentation of a mixed glucose-xylose substrate (10 g/L each) by BP000 (panels A,B) and BP10001 (panels C,D). Both strains used the two substrates sequentially, glucose prior to xylose (Figure 2A,C). For reason of clarity, the glucose consumption phase of the fermentation by BP000 and BP10001 is depicted in Figures 2B and 2D, respectively, separated from the corresponding xylose consumption phase. Physiological parameters calculated from the data are summarized in Table 1. Closed carbon balances for conversion of glucose and xylose indicate that the yield coefficients for product formation from each of the two sugars are internally consistent.

With the exception that a tiny amount of xylitol was produced by BP000 during the "glucose phase", the performance of the two yeast strains in glucose fermentation was identical within limits of experimental error. However, use of BP10001 resulted in enhanced ethanol production from xylose (~30%) as compared to BP000. In the "xylose phase" of the fermentation, formation of xylitol and glycerol was decreased by about 28% and 68%, respectively. Acetate formation occurred at a very low level in each strain. It was increased by ~57% in BP10001 as compared to BP000. While at face value, this difference in acetate yield would seem to hint at a substantial physiological distinction between BP000 and BP10001, it is important to consider that $Y_{acetate}$ for both strains varied, with no recognisable trend, between 0.02 and 0.05 in different experimental settings (e.g. shake flask, bioreactor, substrate concentration) (see refs [8,9]. and this work). Although we cannot, therefore, offer an explanation for the variability of $Y_{acetate}$ at this time, we do believe that the observed acetate formation is not a clear and interpretable reporter of metabolic consequences resulting from the change in XR coenzyme specificity between BP000 and BP10001.

Effect of a high xylose uptake on performance of strain BP10001

In a previous study of xylose fermentation by BP10001, a yield coefficient of 0.19 g/g was reported for xylitol which is much lower than $Y_{xylitol}$ in Table 1. Besides use of a mixed glucose-xylose substrate here while pure xylose was applied in the earlier work, the initial uptake rate (24 hours) in this study (0.05 g/g CDW/h) differed from the one found previously (~0.10 g/g CDW/h). To determine the uptake rate and xylitol yield at high xylose concentrations, we performed a batch fermentation experiment in which 50 g/L xylose was used as the substrate. The results are shown in Figure 3A and physiological parameters are summarized in Table 2. $Y_{ethanol}$ and $Y_{xylitol}$ (over ~120 hours) were identical within limits of error to the corresponding yield coefficients obtained when using 20 g/L xylose. However, $Y_{glycerol}$ increased with fermentation time from 0.025 g/g (18 h) to 0.038 g/g (116 h) and was overall higher than the glycerol yield seen in

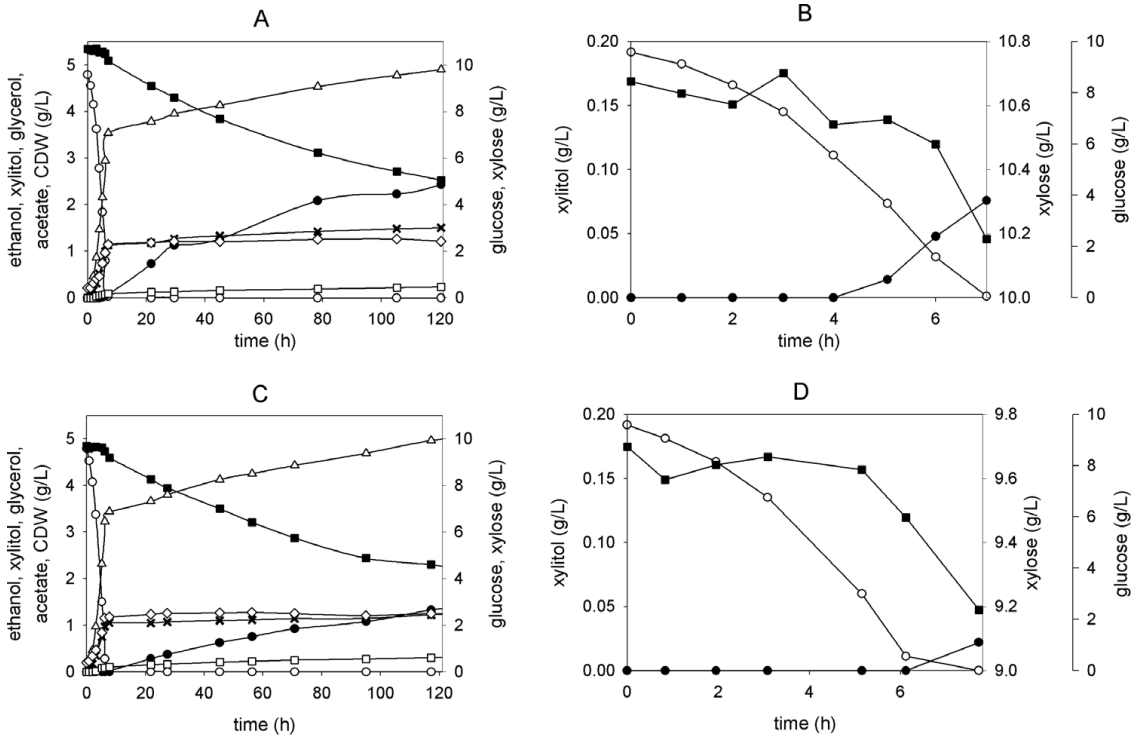

Figure 2 Batch fermentations using a mixed glucose-xylose substrate. Full time courses of conversion of glucose and xylose (10 g/L each) are shown for BP000 and BP10001 in panels A and C, respectively. Panels B and D are close-up representations of the "glucose phases" for BP000 and BP10001, respectively. Symbols: glucose (empty circles), xylose (full squares), xylitol (full circles), ethanol (empty triangles), acetate (empty squares), glycerol (stars) and CDW (empty diamonds).

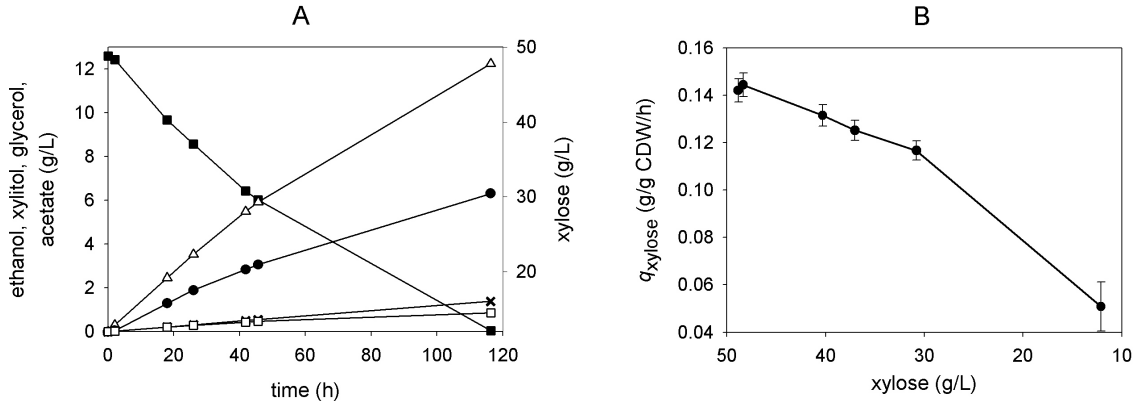

Figure 3 Batch fermentation of xylose (50 g/L) by BP10001. Symbols: xylose (full squares), xylitol (full circles), ethanol (empty triangles), acetate (empty squares) and glycerol (stars). Panel B shows the change of the specific uptake rate with xylose concentration.

fermentations using 20 g/L xylose (0.021 g/g) [8]. Data from xylose fermentations at 10 g/L (Table 1) and 50 g/L (Table 2) suggest that the specific xylose uptake rate increases, about threefold, in response to a fivefold change in the initial xylose concentration (see Additional file 1). Moreover, five independent xylose fermentations starting with different initial xylose concentrations (10 to 50 g/L), including experiments from a previous study with BP10001 [8], indicate an inverse correlation between the specific rate of xylose uptake in the range of 0.05 - 0.12 g/g CDW/h and the xylitol yield (0.28 g/g - 0.15 g/g) (Figure 1).

The decrease in q_{xylose} that occurs in the course of xylose consumption (Figure 3B) may be a consequence of depletion of the xylose substrate. It was confirmed that neither BP10001 nor BP000 lost a substantial

Table 2 Physiological parameters for BP10001 under different fermentation conditions

	Xylose Batch	Glucose Fed-Batch	Glucose/Xylose Fed-Batch
$q_{glucose}$ [g/g CDW/h][a]		0.79	0.65
q_{xylose} [g/g CDW/h][a]	0.14		0.30 - 0.19[c]
$Y_{ethanol}$ [g/g][b]	0.33	0.39	0.38
$Y_{xylitol}$ [g/g][b]	0.17		0.05/0.19[d]
$Y_{glycerol}$ [g/g][b]	0.038	0.070	0.029
$Y_{acetate}$ [g/g][b]	0.023	<0.001	<0.001
C-recovery [%]	99	100	94

a) Uptake rates were determined from data acquired in the first 20 h. S.D.s on uptake rates were < 10%.

b) Yield coefficients (g/g sugar consumed) were calculated using data after a reaction time of 120 h (batch) or 20 h (fed batch). S.D.s were < 10% (except $Y_{glycerol}$: < 20%). $Y_{acetate}$ in fed-batch reactions was too low for an S.D. to be determined.

c) q_{xylose} decreased over the initial 20 hours of fermentation (see also Figure 5B).

d) Yield coefficients are based on either the sum of consumed glucose and xylose or on consumed xylose alone.

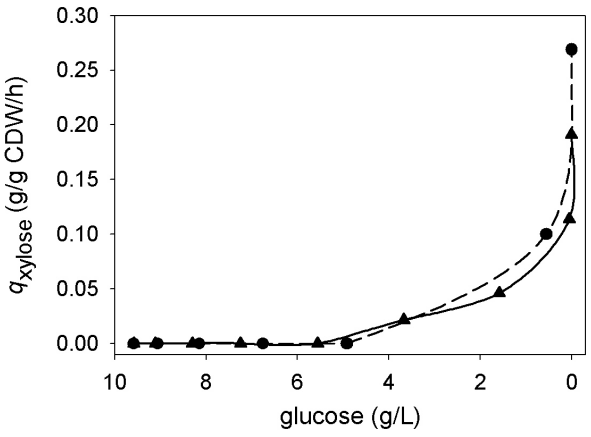

Figure 4 Specific rate of xylose uptake in the "glucose phase" of batch fermentations using a mixed glucose-xylose substrate. Data for BP000 and BP10001 are shown as triangles and circles, respectively. For determination of q_{xylose}, see the Methods.

amount (< 25%) of cell viability, measured as colony forming units in samples taken over time, during xylose fermentation for up to 120 h. It was likewise found (data not shown) that the activities of xylose reductase, xylitol dehydrogenase and xylulose kinase in crude *S. cerevisiae* cell extracts did not change significantly over time, implying that the observed decrease in q_{xylose} does not result because of inactivation of enzymes involved in the initial steps of xylose assimilation. In fact, the value for q_{xylose} of about 0.05 g/g CDW/h at 12 g/L xylose (Figure 3B; after 120 hours) agrees very well with the q_{xylose}-xylose correlation shown in Additional file 1. However, one has to consider that loss of q_{xylose} after extended fermentation times is probably a complex phenomenon, which in addition to the effect of substrate depletion could also report on the inhibition by fermentation products as well as on overall changes in cell physiology due to incubation under non-growth conditions.

Effect of low glucose levels on the xylose uptake rate

Figure 4 shows the change in q_{xylose} in the transient phase of a mixed sugar substrate fermentation by BP10001 and BP000 (Figure 2) where after depletion of about 60% of the initial glucose concentration, xylose starts to become co-utilized with glucose. The results reveal that q_{xylose} was raised to a detectable level at glucose concentrations lower than 4 g/L. Interestingly, when the glucose concentration further dropped to below 2 g/L, q_{xylose} reached a value substantially higher than the reference uptake rate (~0.05 g/g CDW/h at 10 g/L xylose) measured under conditions when only xylose was present. We emphasize that determination of q_{xylose} in the presence of glucose must be done with caution, considering that the analysis necessitates measurement of small changes in the concentration of xylose and the number of data points that can be collected in the relevant "window" of glucose concentrations is clearly limited. However, the findings suggest that control of the glucose concentration in a range where q_{xylose} is positively affected might be a useful strategy to improve the productivity of ethanol production from xylose by BP10001.

Fed-batch process maintaining a low glucose concentration throughout the course of xylose conversion

A fed-batch process was designed in which $q_{glucose}$ was constant (~0.7 g/g CDW/h) and the concentration of glucose was maintained at a level (< 0.3 g/L) known from Figure 4 to enhance q_{xylose}. The required glucose feed (F_t) was controlled as described under Methods.

Figure 5A shows relevant product time courses from the fed-batch experiment, and Table 2 summarizes physiological parameters calculated from the data. Results from a control experiment in which the glucose feed constituted the sole source of carbon are also shown in Table 2. Figure 5B shows that q_{xylose} decreased over time from an initial value of ~0.30 g/g CDW/h (at 48 g/L xylose) to ~0.19 g/g CDW/h (at 35 g/L xylose) after 20 h. Gradual depletion of xylose in the course of the fed-batch process (Figure 5A) may be partly responsible for the observed drop of q_{xylose}. Despite this decrease, q_{xylose} was always larger than the reference value of q_{xylose} (0.14 g/g CDW/h at 48 g/L xylose; 0.12 g/g CDW/h at 30 g/L xylose) from the fermentation in which xylose was the sole carbon source. $Y_{xylitol}$ was constantly at a low level (0.19 ± 0.02 g/g xylose) throughout the course

of the fed-batch reaction, indicating that the xylitol yield was independent of q_{xylose} under these conditions. Note that Figure 1 is consistent with these observations as it suggests that $Y_{xylitol}$ levels out at high q_{xylose}. The difference between $Y_{xylitol}$ (≈ 0.15 g/g xylose) expected from Figure 1 and the measured data might be ascribed to co-utilization of glucose and xylose in the fed-batch reaction. Small amounts of extracellular succinate (Y = 0.002 g/g sugar) and lactate (Y = 0.012 g/g sugar) were also formed in the reaction. Comparison of the total amount glucose and xylose utilized after 20 hours reveals that about 28 sugar mol% were derived from xylose.

Flux balance analysis (FBA)

The analysis was performed using a constrained genome-scale metabolic model of *S. cerevisiae* that included the steps catalyzed by XR and XDH (see the Methods for details). The purpose of the FBA was to obtain a detailed interpretation of the physiological response of BP10001 to a change in external substrate conditions and to determine the effect of cosubstrate usage by XR on the overall metabolism. Results of the FBA were in excellent agreement with the observed distribution of extracellular fermentation products and therefore verify the internal consistency of the experimental data applied in the analysis. Figure 6 shows the flux distribution in the central carbon metabolism of BP10001 under conditions used in the fed-batch fermentations (glucose-xylose; glucose alone) and in the batch conversion of xylose. Additional file 2 gives a complete summary of the flux calculations. Production of fumarate, which was not analyzed in the experiments described, was a requirement of the metabolic flux model to account for biomass formation during fermentation of glucose. Literature shows that fumarate and some malate is formed from glucose in anaerobic culture of *S. cerevisiae* [22]. Interestingly, therefore, the model did not predict malate production except for conditions in which during conversion of glucose-xylose and xylose alone, it was assumed that XR utilizes only NADPH (see Figure 6). FBA in which the rates of substrate uptake and product release were used as constant parameters gave yield coefficients for biomass formation from glucose (Y_{XS} = 0.045) and glucose-xylose (Y_{XS} = 0.086) that were significantly lower than the corresponding coefficients measured experimentally (Additional file 3). When instead $q_{ethanol}$ (glucose-xylose) or q_{CO_2} (glucose) was allowed to be variable, the model predictions were in excellent agreement with the observed Y_{XS} values (Additional file 3). The corresponding estimates for $q_{ethanol}$ and q_{CO_2} still agreed with the measured values within the limits of experimental error (see Additional file 3).
Consistent with observations, the model did not predict biomass formation for the fermentation using xylose as the sole carbon source. Using q_{CO_2} as the objective function for FBA, formation of extracellular products was well accounted for by the model. When alternatively $q_{ethanol}$ was employed as objective function, the calculated value of 0.050 g/g CDW/h for $q_{ethanol}$ (equivalent to $Y_{ethanol}$ = 0.37 g/g) was unrealistically high, and it was confirmed by the experiment that q_{CO_2} was greater than $q_{ethanol}$ (Additional file 3).

The calculated flux distribution in the central carbon metabolism of BP10001 for conditions of the glucose fed-batch is in excellent agreement with findings of others, applying different approaches of FBA (genome-scale metabolic model [23]; central-carbon metabolic models [14,24]; METAFOR-^{13}C-constraint metabolic flux ratio analysis [25]) to *S. cerevisiae* fermenting glucose as the limiting substrate. The reader is referred to Additional file 2 for a complete summary. However, by

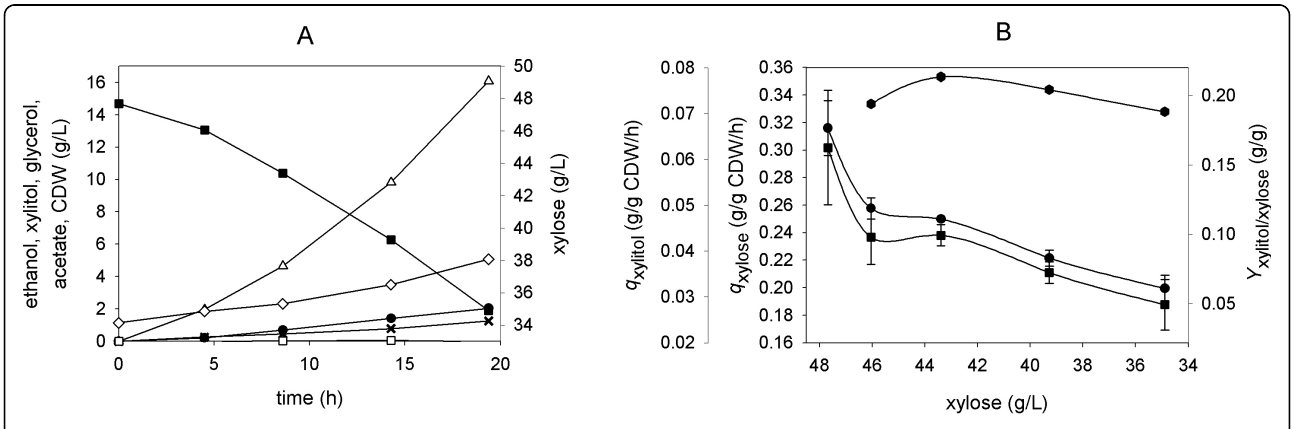

Figure 5 Co-fermentation of glucose and xylose by BP10001 in a fed-batch bioreactor experiment. The symbols in panel A show: xylose (full squares), xylitol (full circles), ethanol (empty triangles), acetate (empty squares), glycerol (stars), CDW (empty diamonds). Panel B shows dependencies of specific rates (q_{xylose}, squares; $q_{xylitol}$, circles) and the xylitol yield coefficient (hexagons) on xylose concentration.

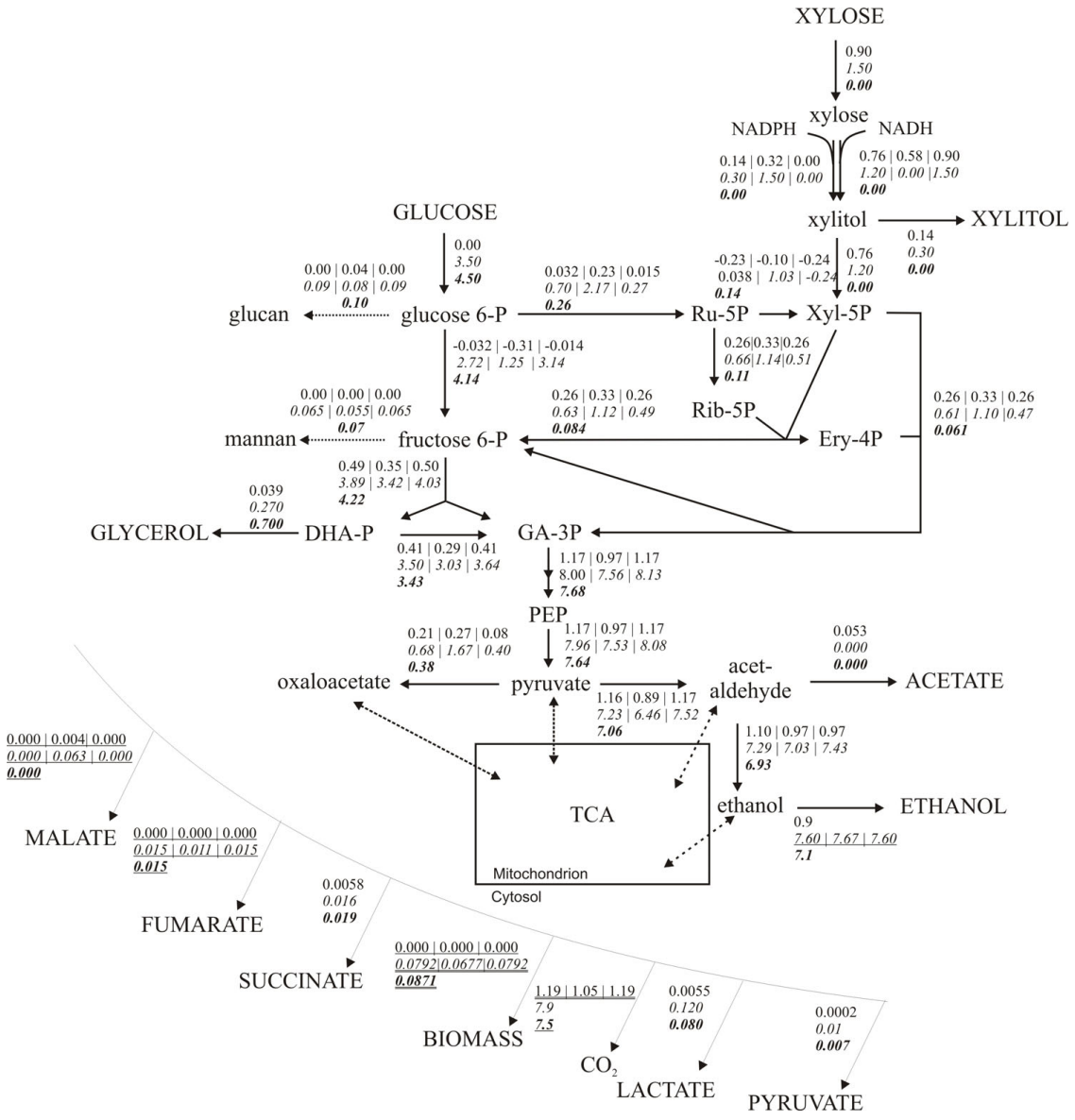

Figure 6 Central metabolic flux map for BP10001 under different fermentation conditions. Substrates and extracellular products are shown in capital letters. Flux distributions were calculated for the batch fermentation using xylose alone (numbers on top) as well as for fed-batch fermentations using glucose-xylose (numbers in italic; middle) and glucose alone (numbers in bold; bottom). The data used in FBA are from Additional file 3. Objective functions and unrestricted product release rates are underlined twice and once, respectively. Flux distributions were calculated for the assumption that q_{NADPH} for xylose reduction = $q_{xylitol}$ (left in row) or for the upper (middle in row) and lower (right in row) limits of NADPH utilization by XR. Only the relevant part of the central carbon metabolism is displayed for reasons of clarity. Flux values are given in mmol/g CDW/h and values for biomass are displayed in gram.

way of comparison, the flux of glucose entering the oxidative pentose phosphate pathway (this work: 0.057 mol/mol; FBA from literature: 0.016 - 0.06 mol/mol; METAFOR: 0.05 mol/mol) and the flux from cytosolic pyruvate to oxalacetate (this work: 0.084 mol/mol; FBA from literature: 0.034 - 0.085 mol/mol; METAFOR: 0.05 mol/mol) validate the results of FBA performed herein.

The metabolic flux model could tolerate a surprisingly broad range of coenzyme preferences of the doubly mutated XR. Unless "forced" to use NADPH for xylose reduction, the model would always employ NADH in the XR reaction. Very interestingly, therefore, the acceptable range of NADPH compared with NADH usage by the enzyme was clearly dependent on the fermentation conditions used. When xylose served as the sole source

of carbon, it was predicted that XR could use between no and 36% NADPH for xylose reduction, with the remainder of the total xylose consumed being derived from the NADH-dependent reaction. Note that the "physiological" specificity of XR thus implied ($rate_{NADPH}/rate_{NADH} \leq 0.53$) is in useful agreement with data from *in vitro* characterization of the isolated enzyme [26]. It is striking that the model was almost insensitive to variable coenzyme usage by XR when glucose-xylose was employed as the substrate. XR could use between 0 and 86% NADPH without affecting the patterns of extracellular metabolites and biomass. A coenzyme preference of XR exceeding 86% NADPH, however, resulted in a decrease in biomass yield, maximally 15% when xylose reduction took place as a strictly NADPH-dependent reaction. These results imply that FBA cannot be used to determine NADPH compared with NADH utilization by XR under the *in vivo* conditions unless further constraints are applied in the analysis. Figure 6 shows results of FBA for conditions corresponding to the upper and lower limits of XR coenzyme preference. A third flux distribution is displayed in Figure 6 which is based on FBA made with the assumption that $q_{xylitol}$ equals q_{NADPH} of the XR reaction. Using this additional constraint, the predicted specificity of XR (NADPH/NADH) is ~0.2, an almost perfect reflection of the biochemical properties of the enzyme [26].

Discussion

Novel and generally relevant findings for the xylose-fermenting *S. cerevisiae* strain BP10001 are: a direct correlation showing that $q_{xylitol}$ decreases in response to an increase in q_{xylose}; high tolerance of a genome-scale metabolic flux model of *S. cerevisiae* to large variations in the usage of NADPH and NADH for xylose reduction; strong evidence that the mutated XR (from *C. tenuis*) works as a NADH-dependent reductase under the physiological reaction conditions. Furthermore, a detailed analysis of glucose-xylose co-fermentation by BP10001 is presented.

Fermentation of mixed glucose-xylose substrates by BP000 and BP10001

The largely sequential utilization of substrates, glucose prior to xylose, by BP000 and BP10001 is in agreement with previous studies of xylose-fermenting strains of *S. cerevisiae* and is thought to reflect, among other effects, the substrate selectivity of the transport systems involved in uptake of the two sugars [17,19,27,28]. A specific xylose transport rate ($q_{TRxylose}$) of about 0.8 - 0.9 g/g CDW/h was previously determined for *S. cerevisiae* at 20 g/L xylose [18,29]. This $q_{TRxylose}$ surpasses q_{xylose} for BP000 and BP10001 by one order of magnitude, suggesting that xylose transport is not a limiting factor for the overall xylose conversion rate in the two strains under conditions where xylose is the sole carbon source. This notion is fully corroborated by findings of others, showing for recombinant yeast strains having either PUA or CEN.PK genetic background that xylose transport has little control over the xylose utilization rate unless there is substantial improvement in the rate of xylose metabolic steps located downstream of xylose uptake [18,28-30]. Positive effects on the distribution of fermentation products from xylose (increase in $Y_{ethanol}$, decrease in $Y_{xylitol}$; see Table 1) that result from use of the mutated, NADH-preferring XR as compared to the NADPH-preferring wild-type enzyme were retained upon changing the reaction conditions from xylose (20 g/L) as the sole source of carbon [8] to a mixed glucose-xylose substrate (10 g/L each; *this work*). However, one must exercise caution in comparing the two fermentations directly, especially in terms of $Y_{xylitol}$ because the ~2-fold enhancement of q_{xylose} resulting from a doubling of the xylose concentration from 10 g/L to 20 g/L caused a decrease in $Y_{xylitol}$ by 27% from 0.26 g/g to 0.19 g/g (Table 1 and [8]). The clear correlation between $Y_{xylitol}$ and q_{xylose} established for BP10001 (Figure 1) implies that xylitol by-product formation is controlled not only by the extent to which XR is matched with XDH in respect to coenzyme usage (see later). Moreover, the results (Table 1, Figure 2) validate BP10001 as a useful strain for ethanol production from mixed glucose-xylose substrates.

Is coenzyme recycling between XR and XDH still a limiting factor for xylose fermentation by BP10001?

Despite the fact that results of FBA were inconclusive regarding the coenzyme preference of the mutated XR under physiological reaction conditions, a number of indirect experimental observations suggest that mainly NADH is used for xylose reduction. Engineered strains of *S. cerevisiae* expressing the genes for *Pichia stiptis* XR and XDH formed less xylitol when glucose-xylose was offered instead of xylose alone [17,31]. The lowering of $Y_{xylitol}$ was plausibly explained as a consequence of enhanced coenzyme recycling that results because of the increased glycolytic flux when glucose is present [31]. For BP10001, however, the xylitol yield in fed-batch co-fermentation of glucose and xylose was identical to $Y_{xylitol}$ of the corresponding batch reaction in which the same concentration (50 g/L) of xylose was employed as sole source of carbon. These findings would be consistent with balanced coenzyme usage by XR and XDH in BP10001.

Comparison of fed-batch fermentations using glucose and glucose-xylose as the substrate reveals a lowered yield coefficient for glycerol under conditions of the mixed sugar carbon source. Interestingly, even the total

amount of "redox sink" products, that is glycerol + xylitol, was smaller during utilization of glucose-xylose (~0.11 mol/mol total sugar consumed) than the glycerol produced from glucose alone (~0.14 mol/mol). The low value of $Y_{acetate}$ (< 0.001 g/g) in either fed-batch fermentation indicates that production of NADPH via the acetate pathway was negligible. Release of CO_2 was similar in both fermentations, suggesting that formation of NADPH in the oxidative pentose phosphate pathway cannot have been significantly elevated in the presence of glucose-xylose as compared to glucose alone. There is, therefore, no evidence of formation of excess NADH in the conversion of xylose to xylulose by BP10001, supporting the notion that the XR used functions as an NADH-dependent enzyme *in vivo*.

Novel lessons from FBA using a genome-scale metabolic model

It is interesting to compare the results of FBA for upper and lower boundary conditions with respect to the consumption of NADPH for xylose reduction (Figure 6). In the batch fermentation of xylose, usage of 36% NADPH by XR resulted in a high flux (0.3 mol/mol xylose) from pyruvate to oxalacetate. In the fed-batch co-fermentation of glucose and xylose, the assumption of a solely NADPH-dependent reaction of XR was reflected by a similarly high flux (0.33 mol/mol sugar) towards oxalacetate. The flux pyruvate→ oxalacetate was decreased when it was assumed that $q_{xylitol}$ equaled q_{NADPH} in the XR reaction. The lowest flux towards oxalacetate (< 0.10 mol/mol sugar) was calculated for the condition of an NADH-specific XR. Wahlbom et al. used *S. cerevisiae* strain TMB 3001, which is similar to our strain BP000 in that it overexpresses genes (from *P. stipitis*) encoding NAD(P)H-dependent XR and NAD^+-dependent XDH, and applied data from chemostat fermentations of glucose (20 g/L) and glucose-xylose (5 and 15 g/L; 10 g/L each) to FBA using a condensed metabolic model [14]. It is unfortunately not clear how these authors handled the issue of XR coenzyme preference in the FBA. However, the flux pyruvate→ oxalacetate was low (< 0.10 mol/mol sugar) for strain TMB 3001 irrespective of the substrate conditions used ([14]) and corresponded to the flux calculated for BP10001 with the assumption of an NADH-dependent XR. Pitkänen et al. applied FBA to *S. cerevisiae* strain H2490 which like TMB 3001 overexpresses wild-type genes for *P. stipitis* XR and XDH [15]. Using a fixed 1:1 ratio for NADPH and NADH usage by XR, these authors calculated a similarly low flux pyruvate→ oxalacetate (0.02 mol/mol) [15]. In agreement with Wahlbom et al. [14], we find that the relative flux towards oxalacetate was identical for fed-batch fermentations using glucose or glucose-xylose (NADH-dependent XR).

Strains TMB 3001 [14] and H2490 [15] displayed enhanced flux through the oxidative pentose phosphate pathway when xylose was present in the medium, an effect ascribed to the requirement for regeneration of the NADPH used up in the XR reaction. Consistent with this notion, application of a mutated XR (from *P. stipitis*) that showed a higher preference for NADH than the wild-type enzyme [32], resulted in a comparatively lowered flux from glucose 6-phosphate to ribulose 5-phosphate. However, the FBA shown in Figure 6 predicts that only 2 - 5 mol% of total sugar is metabolized by BP10001 via the oxidative pentose phosphate pathway when it is assumed that XR utilizes NADH only. The relative flux through the oxidative pentose phosphate pathway increases dramatically to 40% under conditions of the fed-batch co-fermentation of glucose and xylose, assuming XR to be dependent on NADPH. The relevant figure is 14% given that $q_{xylitol}$ equaled q_{NADPH} in the XR reaction. A positive correlation between the predicted fluxes glucose 6-phosphate→ ribulose 5-phosphate and pyruvate→ oxalacetate was noted, probably indicating that the CO_2 lost in the oxidative pentose phosphate pathway is *formally* re-incorporated through synthesis of oxalacetate. This suggestion from FBA is very unlikely to reflect the true *in vivo* situation, and we conclude therefore that results in Figure 6 are most consistent with an XR reaction that depends on NADH.

Beyond coenzyme recycling: the role of q_{xylose}

Figure 1 implies that in BP10001, the distribution of fermentation products from xylose is favourably affected by an increase in q_{xylose}. We have shown in a recent paper that *S. cerevisiae* strain BP11001 expressing an engineered pair of XR (from *C. tenuis*) and XDH (from *G. mastotermitis*) having almost completely matched *in vitro* coenzyme specificities fermented xylose less efficiently in terms of both yield and productivity than BP10001 [9]. The tentative explanation, now corroborated by Figure 1, was that the mutated XDH, which was just ~1/10 as active as the wild-type enzyme, introduced an extra kinetic bottleneck that irrespective of the presumed near-perfect recycling of NAD(P)H during conversion of xylose into xylulose caused $Y_{xylitol}$ to increase as compared to strain BP10001 [9]. Like coenzyme recycling, kinetic "pull" to remove xylitol, the thermodynamically favoured intermediate product of the two-step oxidoreductive isomerization of xylose into xylulose, appears to be an additional critical factor that controls $Y_{xylitol}$. The importance for XDH to be present in excess (≥ 10-fold) over XR was recognized by Hahn-Hägerdal and co-workers before [33].

We observed herein and in previous works that q_{xylose} decreased slowly during the course of conversion of xylose [8,9]. Loss of cell viability and inactivation of

xylose pathway enzymes (XR, XDH, XK) were ruled out as possible causes for the drop in xylose consumption rate (*this work*). Xylose transport could be an issue although there is currently no clear evidence suggesting its importance as a rate-determining factor in BP10001. A plausible, yet speculative explanation is that because of its high K_m for xylose (~100 mM) [34], the XR is difficult to saturate with substrate and therefore becomes an increasingly less efficient catalyst for xylose reduction as the fermentation progresses. However, despite supporting findings from the work of other groups, a quantitative relationship between the level of XR activity and q_{xylose} remains to be demonstrated [29,35]. Notwithstanding, further optimization of xylose-fermenting strains of *S. cerevisiae* should consider q_{xylose} (see below). Moreover, interpretation of experimental yield coefficients (e.g. $Y_{xylitol}$) should not disregard the possibility that observations may be complex manifestations of the combined effects of the intracellular redox balance and the substrate consumption rate.

Enhancement of q_{xylose} at low levels of glucose: observations and process-related opportunities

Results for BP10001 confirm the notion from a number of prior studies on xylose-fermenting strains of *S. cerevisiae* that glucose inhibits the utilization of xylose (e.g. [17,19,27]). Fewer studies, however, have so far addressed the role of a low glucose level on *enhancing* q_{xylose} [15,17,20]. Measurement of xylose consumption in the presence of a small concentration of glucose presents a challenge to both the experimental set-up and the analytical tools used. Despite notable efforts (e.g. [15]), therefore, the q_{xylose}-stimulating effect of glucose has not been fully analyzed and its occurrence is sometimes related to a glucose concentration "greater than zero". Suggestions for its molecular interpretation include the induction of relevant sugar transport proteins in *S. cerevisiae* at low glucose and the proposal that in order to drive xylose assimilation via the pentose phosphate pathway the cell needs to maintain a certain amount of glycolytic flux (see later) [17,36].

It was determined herein from results of a controlled fed-batch fermentation in which glucose was available in a q_{xylose}-enhancing concentration of below 0.3 g/L that xylose uptake by BP10001 was accelerated about twofold as compared to reference reaction using xylose alone. The value of 0.30 ± 0.04 g/g CDW/h obtained for q_{xylose} under the fed-batch conditions was identical with limits of error to the xylose uptake rate of 0.29 g/g CDW/h reported for strain TMB 3415 in a batch fermentation of 60 g/L xylose [37]. Unlike BP10001, TMB 3415 incorporates a substantial history of strain optimization including overexpression of genes encoding all enzymes of the non-oxidative pentose phosphate pathway and deletion of GRE3 (a non-specific NADPH-dependent aldose reductase that reduces xylose) [37]. Therefore, design of process conditions could complement genetic approaches of strain engineering that aim at optimizing q_{xylose}. It is also worth noting that conditions used in the fed-batch process may not be too different from the situation encountered during SSF of pretreated lignocellulose [21,38]. The often used high-temperature pretreatment at mildly acidic conditions liberates most of the xylan fraction as xylose while leaving the cellulose unhydrolysed. The relatively slow action of subsequently added cellulases provides the "glucose feed" for glucose-xylose co-fermentation by the ethanologenic yeast. Innovative strategies for controlling the release of glucose in SSF include pulsed addition of substrate or feeding of cellulases [39,40]. Maintenance of a constant glucose release rate is expected to ensure constant glucose uptake by the yeast cells, which normally do not grow in lignocellulose hydrolysates used. The fed-batch scheme developed herein presents a novel and significant addition to the overall concept of enhancing q_{xylose} by a low concentration of glucose. It is conducive to the accurate determination of q_{xylose} at a constant $q_{glucose}$ under conditions in which yeast cells are growing. We expect that for obvious practical reasons, an initial evaluation of novel yeast strains will always be done in synthetic media based on soluble substrates. We hope therefore that others will find the results in Figure 5 useful with respect to an application-oriented physiological characterization of their yeast strains. An interesting finding for BP10001 is that the molar ratio (2.6 : 1) of glucose and xylose utilized in the fed-batch fermentation nicely matches the relative content of these sugars in common lignocellulosic feedstocks (e.g. corn stover, 2.2 : 1; rice straw, 2.5 : 1 [41]).

The results of FBA (Figure 6; NADH-dependent XR) provide a useful picture about the flux changes in BP10001 that may result upon switch from xylose fermentation in batch to glucose-xylose co-fermentation in the fed-batch. The presence of a low glucose concentration is predicted to bring about substantial enhancement of flux through different steps of the pentose phosphate pathway (non-oxidative: ~2-fold; oxidative: ~10-fold) and glycolysis (~10-fold) as compared to xylose-only reaction conditions. Furthermore, it prevents a small "back-flux" from fructose 6-phosphate to glucose 6-phosphate, occurring when only xylose is present, from taking place. Figure 6 is in line with the idea that accumulation of glycolytic and pentose phosphate intermediates facilitates "pull" of xylose into the metabolism, through the law of mass action as well as by inducing a global cellular response that affects both the level of transcription of key metabolic genes (e.g. hexose transporters [36], glycolytic and ethanologenic enzymes [17,42]) and the protein level [20]. Studies employing

various "omics" techniques have demonstrated that *S. cerevisiae* recognizes glucose very differently from xylose as substrate for alcoholic fermentation [17,18,20,36,37,43,44]. However, the major rate-limiting factors in xylose fermentation are unfortunately still elusive.

Conclusions

Relative improvements in the distribution of fermentation products from xylose that can be directly related to a change in the coenzyme preference of XR from NADPH in BP000 to NADH in BP10001 increase in response to an increase in the initial concentration of the pentose substrate from 10 to 50 g/L. Because q_{xylose} is also enhanced at high xylose levels, a relationship between q_{xylose} and $Y_{xylitol}$ is therefore suggested. Although xylose is not detectably utilized by BP10001 and BP000 at glucose concentrations greater than 4 g/L, the presence of a low residual glucose concentration (< 2 g/L) promotes the uptake of xylose, with q_{xylose} being about twofold enhanced as compared to a xylose-only reference reaction. From FBA, increased flux through glycolysis and the pentose phosphate pathway could be responsible for the stimulating effect of glucose on q_{xylose}. The low-glucose conditions also facilitate xylose conversion into ethanol at only moderate xylitol by-product formation. A fed-batch reaction that maintains a constant glucose uptake rate and a low residual glucose concentration is a useful method to quantify the effect of glucose on q_{xylose}, providing relevant information for further process design.

Methods

Materials

Unless otherwise indicated, chemicals and strains were those reported elsewhere in full detail [8]. Mineral media for shake flask precultures and bioreactor experiments were as described by Jeppsson et. al. [11] except that no extra riboflavin and folic acid were supplied. Ten mg/L of ergosterol, 0.42 g/L of Tween-80 and 250 μl/L of Antifoam 204 (Sigma-Aldrich, St. Louis, MO, USA) were added to media used in anaerobic reactions. Anaerobic batch and fed-batch conversions of mixed glucose and xylose substrates were carried out in a Braun Biostat CT bioreactor (Sartorius AG, Goettingen, Germany). Two six bladed disc impellers were used for stirring at 200 rpm. The ratio of impeller to reactor diameter was 0.4. The pH was kept constant at 5.0 by automatic addition of 1 M NaOH. The reactor was sparged with nitrogen at a constant flow rate of 0.65 L/min and the temperature was kept constant at 30°C.

Anaerobic batch and fed-batch cultivations in the bioreactor

Batch conversions in the Braun Biostat CT bioreactor were described previously in full detail [8]. Anaerobic batch conversion of mixed sugar substrates contained 10 g/L of xylose and 10 g/L glucose. An initial CDW of ~0.2 g/L was used. A batch conversion of xylose (50 g/L) was carried out using a CDW of ~3 g/L.

Fed-batch experiments using BP10001 were carried out in the same bioreactor operated as in the batch mode, except that the initial CDW was ~1 g/L. The media contained or lacked 50 g/L xylose, and glucose was supplied from an external pump (Knauer Smartline 1000, Berlin, Germany). An approximate exponential flow rate was used that ensured maintenance of a constant glucose concentration during the reaction. The required glucose feed (F_t) was controlled according to equation (1) where $\mu_{glucose}$ is the specific growth rate, Δ [Glc] is the difference in glucose concentration in the feed (333 g/L) and the reactor set point (~10 mg/L), Y_{XS} is the yield coefficient for biomass formation from glucose which was assumed from data in Figure 2 to be 0.10 (g/g), X_0 (= 1.0 g/L) and V_0 (= 4.0 L) are biomass concentration and reactor volume at the time of the feed start, respectively, and t is the reaction time.

$$F_t = (\mu_{glucose} / \Delta[Glc] Y_{XS}) X_0 V_0 \exp(\mu_{glucose} t) \quad (1)$$

Using a reported Monod constant for *S. cerevisiae* fermenting glucose (25 mg/L; [45]), we calculated that $\mu_{glucose}$ of BP10001 should be 0.083 (1/h) under the conditions used. Note: μ_{max} of BP10001 fermenting glucose was determined as 0.29 (1/h), and Y_{XS} from glucose was assumed to be identical under batch and fed-batch fermentation conditions [24]. The feed solution was sparged with N_2 and substrate feed over 26 h resulted in the addition of about 0.9 L volume. It was shown that the level of glucose was always below 0.3 g/L.

Analytic of external metabolites

Immediate work-up of samples taken from the bioreactor involved centrifugation of 1 mL of broth (10 min, 15700 g, 4°C) and storage of the supernatant at - 20°C. Cell growth was recorded as increase in optical density at 600 nm. CDW was determined as described elsewhere [9]. Off gas analysis (measuring CO_2 and ethanol) was done using an Innova 1313 acoustic gas analyzer (Ballerup, Denmark) that was calibrated with reference gas containing 0.1% ethanol and 5.0% CO_2, the remainder being N_2 (Linde, Stadl-Paura, Austria).

Relevant components of the culture supernatant (xylose, xylitol, glycerol, acetate, ethanol, pyruvate, succinate and lactate) were routinely analyzed by HPLC using an Aminex HPX-87H column (Biorad, Hercules, USA) according to a previously reported protocol [8]. Samples containing glucose and xylose were additionally measured by HPLC using an Aminex HPX-87C column (Biorad) operated at 85°C. Elution of analytes was done

at a flow rate of 0.4 mL/min using distilled water as the mobile phase (for details on enhanced phosphate, glucose and xylose separation see Additional file 4). The residual glucose in fed-batch experiments was too low (< 0.3 g/L) to be measured by HPLC. It was therefore determined enzymatically using a glucose-UV kit from DIPROmed (Weigelsdorf, Austria). Measurements were referenced against known concentrations of glucose.

Constrained flux balance analysis (FBA)

Data for strain BP10001 (Additional file 3) was applied to FBA. A recently reported genome-scale metabolic model of *S. cerevisiae* (iLL672) was used in a slightly modified form [46] (see Additional file 2). The model was expanded for import of xylose and export of xylitol as well as for the reactions of XR and XDH (see Figure 6). Considering the dual coenzyme specificity of XR from *C. tenuis*, it was necessary to define two reactions: xylose + NADPH $\leftarrow\rightarrow$ xylitol + $NADP^+$; xylose + NADH $\leftarrow\rightarrow$ xylitol + NAD^+ [26]. The flux ratio for the XR reaction utilizing NADPH and NADH was varied manually between 0 (100% NADH) and 1 (100% NADPH) to define the range of XR specificity that was still compatible with the experimental observations. Results are shown for upper and lower limits of NADPH utilization as well as for assumed conditions in which the rate of NADPH consumption was equal to the rate of xylitol formation.

The flux model was constrained by eliminating (flux = 0) for reactions reported to be inactive during fermentation of glucose and xylose. Briefly, for fed-batch reactions using glucose or glucose-xylose as substrate, CIT3, IDP2, ICL1, GND2, ADH2, NDE1, YMR118c, COX12, FDH1, 2, POX, FOX2, FAA2, INO1, YPL27w, AGX1, CTA1, CTT1, GRE2 and SFC1 [47,48] were not considered. For the batch fermentation of xylose, ACS1, CYB2, BTS1, PHO89, JEN1 were additionally eliminated [49,50]. Unless mentioned otherwise, all specific rates in Additional file 3 were fixed in the optimization. Biomass and CO_2 were used as objective functions for fed-batch and batch fermentations, respectively, and linear optimization was carried out with the LINDO API 5.0 solver. Rates of formation of fumarate and malate were estimated by the solver because no experimental data were available for these products.

Calculations

For batch fermentations, the yield coefficients were calculated from analyte concentrations measured in g/L. Data for CO_2 and ethanol carried out with the bioreactor off-gas were normalized to 1 L of fermentation broth, considering the volume change due to withdrawal of samples. The carbon balance was calculated by taking all measured compounds (external metabolites, biomass, CO_2 and ethanol in off-gas) into account. A value of 26.4 g/C-mol biomass [51] was used to calculate the amount of carbon transformed into biomass. Glucose and xylose uptake rates as well as product formation rates were determined by plotting concentrations against reaction time. For non-growing cells (xylose as sole carbon source), data could be fit by linear equations. For growing cells (glucose-xylose), data were fit with a three-parameter exponential growth function. The first derivative of the resulting equation was used to calculate uptake and production rates at the time of withdrawal of sample, normalized with CDW.

In fed-batch fermentations, the actual reactor volume at each time of withdrawing a sample was calculated by taking account volumes of feed and added base as well as the sample volume. The total mass of each analyte (including the biomass) was determined from the actual reactor volume and the analyte concentration measured in the sample, considering the amount of analytes withdrawn with previous samples. The mass of glucose supplied was calculated from feed volume added × feed concentration of glucose. Product yields and carbon balances were calculated from mass data. Specific rates are normalized on the actual amount of CDW present at the time of withdrawing sample.

Additional file 1: Dependence of q_{xylose} on xylose concentration for strain BP10001. Data are from 5 independent fermentations using varied initial concentrations of xylose. q_{xylose} was determined from the first 48 h of substrate conversion. Xylose concentrations: 10 g/L (this work; xylose phase in mixed glucose-xylose fermentation; Table 1), 15 g/L (unpublished results), 20 g/L ([8]), and 50 g/L (this work).
Click here for file
[http://www.biomedcentral.com/content/supplementary/1475-2859-9-16-S1.JPEG]

Additional file 2: Compilation of results from FBA.
Click here for file
[http://www.biomedcentral.com/content/supplementary/1475-2859-9-16-S2.XLS]

Additional file 3: Specific uptake and release rates as well as biomass yields obtained in anaerobic batch and fed-batch fermentations using strain BP10001. Rates were determined from data acquired in the first 42 h of batch fermentation and in the first 20 h of fed-batch reactions.
Click here for file
[http://www.biomedcentral.com/content/supplementary/1475-2859-9-16-S3.XLS]

Additional file 4: Optimization of the HPLC analytic procedure for determination of co-utilization of glucose and xylose. Panel A shows the refractive index trace for a sample from a typical batch fermentation (cf. Figure 2) analyzed using the Aminex HPX-87H column. Overlapping peaks for phosphate-glucose and glucose-xylose are clearly recognized. Therefore, this method was unsuitable for determination of sugar consumption in the phase of the fermentation where glucose and xylose are utilized simultaneously. Determination of q_{xylose} besides the larger $q_{glucose}$ was not reliable. Panel B shows the improved separation when using an Aminex HPX-87C column. A concentration of phosphate of 22 mM did not interfere with determination of glucose. Xylose in a constant concentration of 10 g/L was compatible with measurement of glucose in the concentration range 1 - 10 g/L. The standard deviation on the measured xylose value was 0.02 g/L.
Click here for file
[http://www.biomedcentral.com/content/supplementary/1475-2859-9-16-S4.JPEG]

Acknowledgements
Financial support from the Austrian Science Fund FWF (P18275-B09 to BN) is gratefully acknowledged. The authors would like to thank Prof. Uwe Sauer (Institute of Molecular Systems Biology, ETH Zurich) for providing the genome-scale metabolic model of *S. cerevisiae*.

Authors' contributions
BN, MK and SK designed research; BP, KL, MW and SK performed and analyzed mixed glucose-xylose batch fermentations. KL and SK performed and analyzed fed-batch fermentations. MK performed flux balance analysis. BN, MK and SK wrote the paper. All authors have read and approved the final version of the manuscript.

Competing interests
The authors declare that they have no competing interests.

Received: 1 December 2009 Accepted: 10 March 2010
Published: 10 March 2010

References

1. Chu BC, Lee H: **Genetic improvement of *Saccharomyces cerevisiae* for xylose fermentation.** *Biotechnol Adv* 2007, **25(5)**:425-441.
2. Jeffries TW, Jin YS: **Metabolic engineering for improved fermentation of pentoses by yeasts.** *Appl Microbiol Biotechnol* 2004, **63(5)**:495-509.
3. Van Vleet JH, Jeffries TW: **Yeast metabolic engineering for hemicellulosic ethanol production.** *Curr Opin Biotechnol* 2009, **20(3)**:300-306.
4. Nevoigt E: **Progress in metabolic engineering of *Saccharomyces cerevisiae*.** *Microbiol Mol Biol Rev* 2008, **72(3)**:379-412.
5. Hahn-Hägerdal B, Karhumaa K, Fonseca C, Spencer-Martins I, Gorwa-Grauslund MF: **Towards industrial pentose-fermenting yeast strains.** *Appl Microbiol Biotechnol* 2007, **74(5)**:937-953.
6. Hahn-Hägerdal B, Karhumaa K, Jeppsson M, Gorwa-Grauslund MF: **Metabolic engineering for pentose utilization in *Saccharomyces cerevisiae*.** *Adv Biochem Eng Biotechnol* 2007, **108**:147-177.
7. Jeffries TW: **Engineering yeasts for xylose metabolism.** *Curr Opin Biotechnol* 2006, **17(3)**:320-326.
8. Petschacher B, Nidetzky B: **Altering the coenzyme preference of xylose reductase to favor utilization of NADH enhances ethanol yield from xylose in a metabolically engineered strain of *Saccharomyces cerevisiae*.** *Microb Cell Fact* 2008, **7**:9.
9. Krahulec S, Klimacek M, Nidetzky B: **Engineering of a matched pair of xylose reductase and xylitol dehydrogenase for xylose fermentation by *Saccharomyces cerevisiae*.** *Biotechnol J* 2009, **4(5)**:684-694.
10. Watanabe S, Abu Saleh A, Pack SP, Annaluru N, Kodaki T, Makino K: **Ethanol production from xylose by recombinant *Saccharomyces cerevisiae* expressing protein-engineered NADH-preferring xylose reductase from *Pichia stipitis*.** *Microbiology* 2007, **153(Pt 9)**:3044-3054.
11. Jeppsson M, Bengtsson O, Franke K, Lee H, Hahn-Hägerdal B, Gorwa-Grauslund MF: **The expression of a *Pichia stipitis* xylose reductase mutant with higher K_M for NADPH increases ethanol production from xylose in recombinant *Saccharomyces cerevisiae*.** *Biotechnol Bioeng* 2006, **93(4)**:665-673.
12. Matsushika A, Watanabe S, Kodaki T, Makino K, Inoue H, Murakami K, Takimura O, Sawayama S: **Expression of protein engineered NADP +-dependent xylitol dehydrogenase increases ethanol production from xylose in recombinant *Saccharomyces cerevisiae*.** *Appl Microbiol Biotechnol* 2008, **81(2)**:243-255.
13. Hou J, Shen Y, Li XP, Bao XM: **Effect of the reversal of coenzyme specificity by expression of mutated *Pichia stipitis* xylitol dehydrogenase in recombinant *Saccharomyces cerevisiae*.** *Lett Appl Microbiol* 2007, **45(2)**:184-189.
14. Wahlbom CF, Eliasson A, Hahn-Hägerdal B: **Intracellular fluxes in a recombinant xylose-utilizing *Saccharomyces cerevisiae* cultivated anaerobically at different dilution rates and feed concentrations.** *Biotechnol Bioeng* 2001, **72(3)**:289-296.
15. Pitkänen JP, Aristidou A, Salusjärvi L, Ruohonen L, Penttilä M: **Metabolic flux analysis of xylose metabolism in recombinant *Saccharomyces cerevisiae* using continuous culture.** *Metab Eng* 2003, **5(1)**:16-31.
16. Meinander NQ, Hahn-Hägerdal B: **Influence of cosubstrate concentration on xylose conversion by recombinant, XYL1-expressing *Saccharomyces cerevisiae* : a comparison of different sugars and ethanol as cosubstrates.** *Appl Environ Microbiol* 1997, **63(5)**:1959-1964.
17. Meinander NQ, Boels I, Hahn-Hägerdal B: **Fermentation of xylose/glucose mixtures by metabolically engineered *Saccharomyces cerevisiae* strains expressing XYL1 and XYL2 from *Pichia stipitis* with and without overexpression of TAL1.** *Bioresour Technol* 1999, **68(1)**:79-87.
18. Kötter P, Ciriacy M: **Xylose fermentation by *Saccharomyces cerevisiae*.** *Appl Microbiol Biotechnol* 1993, **38(6)**:776-783.
19. Kuyper M, Hartog MM, Toirkens MJ, Almering MJ, Winkler AA, van Dijken JP, Pronk JT: **Metabolic engineering of a xylose-isomerase-expressing *Saccharomyces cerevisiae* strain for rapid anaerobic xylose fermentation.** *FEMS Yeast Res* 2005, **5(4-5)**:399-409.
20. Souto-Maior AM, Runquist D, Hahn-Hägerdal B: **Crabtree-negative characteristics of recombinant xylose-utilizing *Saccharomyces cerevisiae*.** *J Biotechnol* 2009, **143(2)**:119-123.
21. Olofsson K, Bertilsson M, Lidén G: **A short review on SSF - an interesting process option for ethanol production from lignocellulosic feedstocks.** *Biotechnol Biofuels* 2008, **1(1)**:7.
22. Verduyn C, Postma E, Scheffers WA, van Dijken JP: **Physiology of *Saccharomyces cerevisiae* in anaerobic glucose-limited chemostat cultures.** *J Gen Microbiol* 1990, **136(3)**:395-403.
23. Nookaew I, Jewett MC, Meechai A, Thammarongtham C, Laoteng K, Cheevadhanarak S, Nielsen J, Bhumiratana S: **The genome-scale metabolic model iIN800 of *Saccharomyces cerevisiae* and its validation: a scaffold to query lipid metabolism.** *BMC Syst Biol* 2008, **2**:71.
24. Nissen TL, Schulze U, Nielsen J, Villadsen J: **Flux distributions in anaerobic, glucose-limited continuous cultures of *Saccharomyces cerevisiae*.** *Microbiology* 1997, **143(Pt 1)**:203-218.
25. Jouhten P, Rintala E, Huuskonen A, Tamminen A, Toivari M, Wiebe M, Ruohonen L, Penttilä M, Maaheimo H: **Oxygen dependence of metabolic fluxes and energy generation of *Saccharomyces cerevisiae* CEN.PK113-1A.** *BMC Syst Biol* 2008, **2**:60.
26. Petschacher B, Nidetzky B: **Engineering *Candida tenuis* Xylose reductase for improved utilization of NADH: antagonistic effects of multiple side chain replacements and performance of site-directed mutants under simulated in vivo conditions.** *Appl Environ Microbiol* 2005, **71(10)**:6390-6393.
27. Madhavan A, Tamalampudi S, Srivastava A, Fukuda H, Bisaria VS, Kondo A: **Alcoholic fermentation of xylose and mixed sugars using recombinant *Saccharomyces cerevisiae* engineered for xylose utilization.** *Appl Microbiol Biotechnol* 2009, **82(6)**:1037-1047.
28. Hamacher T, Becker J, Gárdonyi M, Hahn-Hägerdal B, Boles E: **Characterization of the xylose-transporting properties of yeast hexose**

transporters and their influence on xylose utilization. *Microbiology* 2002, **148(Pt 9)**:2783-2788.
29. Gárdonyi M, Jeppsson M, Lidén G, Gorwa-Grauslund MF, Hahn-Hägerdal B: **Control of xylose consumption by xylose transport in recombinant *Saccharomyces cerevisiae*.** *Biotechnol Bioeng* 2003, **82(7)**:818-824.
30. Kuyper M, Toirkens MJ, Diderich JA, Winkler AA, van Dijken JP, Pronk JT: **Evolutionary engineering of mixed-sugar utilization by a xylose-fermenting *Saccharomyces cerevisiae* strain.** *FEMS Yeast Res* 2005, **5(10)**:925-934.
31. Karhumaa K, Fromanger R, Hahn-Hägerdal B, Gorwa-Grauslund MF: **High activity of xylose reductase and xylitol dehydrogenase improves xylose fermentation by recombinant *Saccharomyces cerevisiae*.** *Appl Microbiol Biotechnol* 2007, **73(5)**:1039-1046.
32. Bengtsson O, Hahn-Hägerdal B, Gorwa-Grauslund MF: **Xylose reductase from *Pichia stipitis* with altered coenzyme preference improves ethanolic xylose fermentation by recombinant *Saccharomyces cerevisiae*.** *Biotechnol Biofuels* 2009, **2**:9.
33. Eliasson A, Hofmeyr JS, Pedler S, Hahn-Hägerdal B: **The xylose reductase/xylitol dehydrogenase/xylulokinase ratio affects product formation in recombinant xylose-utilising *Saccharomyces cerevisiae*.** *Enzyme Microb Technol* 2001, **29(4-5)**:288-297.
34. Petschacher B, Leitgeb S, Kavanagh KL, Wilson DK, Nidetzky B: **The coenzyme specificity of *Candida tenuis* xylose reductase (AKR2B5) explored by site-directed mutagenesis and X-ray crystallography.** *Biochem J* 2005, **385(Pt 1)**:75-83.
35. Matsushika A, Sawayama S: **Efficient bioethanol production from xylose by recombinant *Saccharomyces cerevisiae* requires high activity of xylose reductase and moderate xylulokinase activity.** *J Biosci Bioeng* 2008, **106(3)**:306-309.
36. Sedlak M, Ho NW: **Characterization of the effectiveness of hexose transporters for transporting xylose during glucose and xylose co-fermentation by a recombinant *Saccharomyces* yeast.** *Yeast* 2004, **21(8)**:671-684.
37. Runquist D, Hahn-Hägerdal B, Bettiga M: **Increased expression of the oxidative pentose phosphate pathway and gluconeogenesis in anaerobically growing xylose-utilizing *Saccharomyces cerevisiae*.** *Microb Cell Fact* 2009, **8**:49.
38. Öhgren K, Bengtsson O, Gorwa-Grauslund MF, Galbe M, Hahn-Hägerdal B, Zacchi G: **Simultaneous saccharification and co-fermentation of glucose and xylose in steam-pretreated corn stover at high fiber content with *Saccharomyces cerevisiae* TMB3400.** *J Biotechnol* 2006, **126(4)**:488-498.
39. Olofsson K, Rudolf A, Lidén G: **Designing simultaneous saccharification and fermentation for improved xylose conversion by a recombinant strain of *Saccharomyces cerevisiae*.** *J Biotechnol* 2008, **134(1-2)**:112-120.
40. Olofsson K, Wiman M, Lidén G: **Controlled feeding of cellulases improves conversion of xylose in simultaneous saccharification and co-fermentation for bioethanol production.** *J Biotechnol* 2010, **145(2)**:168-175.
41. Lee J: **Biological conversion of lignocellulosic biomass to ethanol.** *J Biotechnol* 1997, **56(1)**:1-24.
42. Boles E, Müller S, Zimmermann FK: **A multi-layered sensory system controls yeast glycolytic gene expression.** *Mol Microbiol* 1996, **19(3)**:641-642.
43. Salusjärvi L, Kankainen M, Soliymani R, Pitkänen JP, Penttilä M, Ruohonen L: **Regulation of xylose metabolism in recombinant *Saccharomyces cerevisiae*.** *Microb Cell Fact* 2008, **7**:18.
44. Zaldivar J, Borges A, Johansson B, Smits HP, Villas-Bôas SG, Nielsen J, Olsson L: **Fermentation performance and intracellular metabolite patterns in laboratory and industrial xylose-fermenting *Saccharomyces cerevisiae*.** *Appl Microbiol Biotechnol* 2002, **59(4-5)**:436-442.
45. Doran PM: **Bioprocess engineering principles.** London: Academic Press, 5 2000.
46. Kuepfer L, Sauer U, Blank LM: **Metabolic functions of duplicate genes in *Saccharomyces cerevisiae*.** *Genome Res* 2005, **15(10)**:1421-1430.
47. de Groot MJ, Daran-Lapujade P, van Breukelen B, Knijnenburg TA, de Hulster EA, Reinders MJ, Pronk JT, Heck AJ, Slijper M: **Quantitative proteomics and transcriptomics of anaerobic and aerobic yeast cultures reveals post-transcriptional regulation of key cellular processes.** *Microbiology* 2007, **153(Pt 11)**:3864-3878.
48. ter Linde JJ, Liang H, Davis RW, Steensma HY, van Dijken JP, Pronk JT: **Genome-wide transcriptional analysis of aerobic and anaerobic chemostat cultures of *Saccharomyces cerevisiae*.** *J Bacteriol* 1999, **181(24)**:7409-7413.
49. Salusjärvi L: **Transcriptome and proteome analysis of xylose-metabolising *Saccharomyces cerevisiae*.** Helsinki: University of Helsinki 2008.
50. Salusjärvi L, Poutanen M, Pitkänen JP, Koivistoinen H, Aristidou A, Kalkkinen N, Ruohonen L, Penttilä M: **Proteome analysis of recombinant xylose-fermenting *Saccharomyces cerevisiae*.** *Yeast* 2003, **20(4)**:295-314.
51. Lange HC, Heijnen JJ: **Statistical reconciliation of the elemental and molecular biomass composition of *Saccharomyces cerevisiae*.** *Biotechnol Bioeng* 2001, **75(3)**:334-344.

doi:10.1186/1475-2859-9-16
Cite this article as: Krahulec *et al.*: Fermentation of mixed glucose-xylose substrates by engineered strains of *Saccharomyces cerevisiae*: role of the coenzyme specificity of xylose reductase, and effect of glucose on xylose utilization. *Microbial Cell Factories* 2010 **9**:16.

List of publications

Diploma thesis:

Krahulec, S. Remodeling the active site of horse liver alcohol dehydrogenase and utilization of the enzyme for catalysis to lyase-type reactions. Graz University of Technology, Graz, 2006.

Publications in peer-reviewed journals:

1. Krahulec, S.; Petschacher, B.; Wallner, M.; Longus, K.; Klimacek, M.; Nidetzky, B., Fermentation of mixed glucose-xylose substrates by engineered strains of *Saccharomyces cerevisiae*: role of the coenzyme specificity of xylose reductase, and effect of glucose on xylose utilization. *Microb. Cell Fact.* **2010,** 9, (1), 16.

2. Krahulec, S.; Klimacek, M.; Nidetzky, B., Engineering of a matched pair of xylose reductase and xylitol dehydrogenase for xylose fermentation by *Saccharomyces cerevisiae*. *Biotechnol. J.* **2009,** 4, (5), 684-694.

3. Krahulec, S.; Armao, G. C.; Bubner, P.; Klimacek, M.; Nidetzky, B., Polyol-specific long-chain dehydrogenases/reductases of mannitol metabolism in *Aspergillus fumigatus*: biochemical characterization and pH studies of mannitol 2-dehydrogenase and mannitol-1-phosphate 5-dehydrogenase. *Chem. Biol. Interact.* **2009,** 178, (1-3), 274-82.

4. Krahulec, S.; Armao, G. C.; Weber, H.; Klimacek, M.; Nidetzky, B., Characterization of recombinant *Aspergillus fumigatus* mannitol-1-phosphate 5-dehydrogenase and its application for the stereoselective synthesis of protio and deuterio forms of D-mannitol 1-phosphate. *Carbohydr. Res.* **2008,** 343, (9), 1414-23.

5. Winkler, M.; Martínková, L.; Knall, A. C.; Krahulec, S.; Klempier, N., Synthesis and microbial transformation of β-amino nitriles. *Tetrahedron* **2005,** 61, (17), 4249-4260.

Talks at workshops and scientific conferences:

1. Krahulec, S.; Klimacek, M.; Nidetzky, B., Pentose fermenting yeasts - objectives and limits. Workshop "Future Perspectives of Lignocellulosic Bioethanol", Wien: 07.10.2009

2. Krahulec, S.; Petschacher, B.; Klimacek, M.; Nidetzky, B., Engineering the Coenzyme Specificity of Xylose Reductase and Xylitol Dehydrogenase to Enhance Xylose Fermentation by Recombinant *Saccharomyces cerevisiae*. 15th European Carbohydrate Symposium, Wien: 24.07.2009

3. Nidetzky, B.; Klimacek, M.; Krahulec, S.; Petschacher, B., Development and characterization of xylose-fermenting strains of *Saccharomyces cerevisisae* based on structure-based engineering of key metabolic enzymes. 31st Symposium on Biotechnology for Fuels and Chemicals, San Francisco: 03.05.2009

4. Krahulec, S.; Petschacher, B.; Klimacek, M.; Nidetzky, B., Enhanced xylose fermentation by altering the coenzyme preference of xylose reductase in metabolically engineered *S. cerevisiae*. Life Sciences 2008, Graz: 23.09.2008

5. Krahulec, S.; Petschacher, B.; Klimacek, M.; Nidetzky, B., Enhanced xylose fermentation by altering the coenzyme preference of xylose reductase in metabolically enigineered *S. cerevisiae*. ESBES 7 - 7th European Symposium on Biochemical Engineering, Faro: 10.09.2008

6. Krahulec, S.; Armao, G. C.; Weber, H.; Klimacek, M.; Nidetzky, B., Mannitol-1-phosphate 5-dehydrogenase and mannitol 2-dehydrogenase of the human pathogen *Aspergillus fumigatus*. 12. Österreichischer Kohlenhydrat-Workshop, Wien: 21.02.2008

Poster:

1. Egger, S.; Krahulec, S.; Patel, I.; Ludwig, R.; Haltrich, D.; Nidetzky, B., Multi-step redox transformations on UDP-glucose. COST workshop Biocatalysis and Medicinal Chemistry: Crossroads and Synergies, Semmering: 18.-21.01.2010

2. Krahulec, S.; Petschacher, B.; Klimacek, M.; Nidetzky, B., Engineering the Cofactor Preference of Xylose Reductase and Xylitol Dehydrogenase to Enhance Xylose Fermentation by Recombinant *Saccharomyces cerevisiae*. 2009 AIChE Annual Meeting, Nashville: 11.11.2009

3. Müller, M.; Krahulec, S., Stroh im Tank – wir sorgen nachhaltig für Bewegung. Lange Nacht der Forschung, Graz: 07.11.2009

4. Krahulec, S.; Armao, G. C.; Klimacek, M.; Nidetzky, B., Biochemical characterization of mannitol-1-phosphate 5-dehydrogenase and mannitol 2-dehydrogenase from the human pathogen *Aspergillus fumigatus*. 14th International Meeting on Enzymology and Molecular Biology of Carbonyl Metabolism, Kranjska Gora: 08.07.2008

Appendix

Supporting Information:

Enzymes of mannitol metabolism in the human pathogen *Aspergillus fumigatus*: kinetic properties of mannitol 2-dehydrogenase and mannitol-1-phosphate 5-dehydrogenase, and their physiological implications

Stefan Krahulec, Guilliano Cem Armao, Mario Klimacek, Bernd Nidetzky§

Institute of Biotechnology and Biochemical Engineering, Graz University of Technology, Petersgasse 12/I, A-8010 Graz, Austria

§Corresponding author

Supplementary Figure 1: Double reciprocal plots of adenosine nucleotide inhibition on *Af*M1PDH at pH 7.1.

Supplementary Figure 2: Double reciprocal plots of adenosine nucleotide inhibition on *Af*M2DH at pH 7.1.

Supplementary Figure 3: Semi-logarithmic plots of residual activities of *Af*M1PDH (A, B) and *Af*M2DH (C, D) at different incubation temperatures.

Supplementary Figure 1: Double reciprocal plots of adenosine nucleotide inhibition on *Af*M1PDH at pH 7.1. Panel A, C, E show inhibition on Fru6*P* reduction with varying concentration of NADH and Panel C, D, E on Man-ol1*P* oxidation with varying concentrations of NAD^+ in the presence of AMP (A, B), ADP (C, D) and ATP (E, F). Adenosine nucleotide concentrations: 5 mM (full squares), 2.5 mM (empty triangles), 1.25 mM (full triangles), 0.625 mM (empty circles) and 0 mM (full circles).

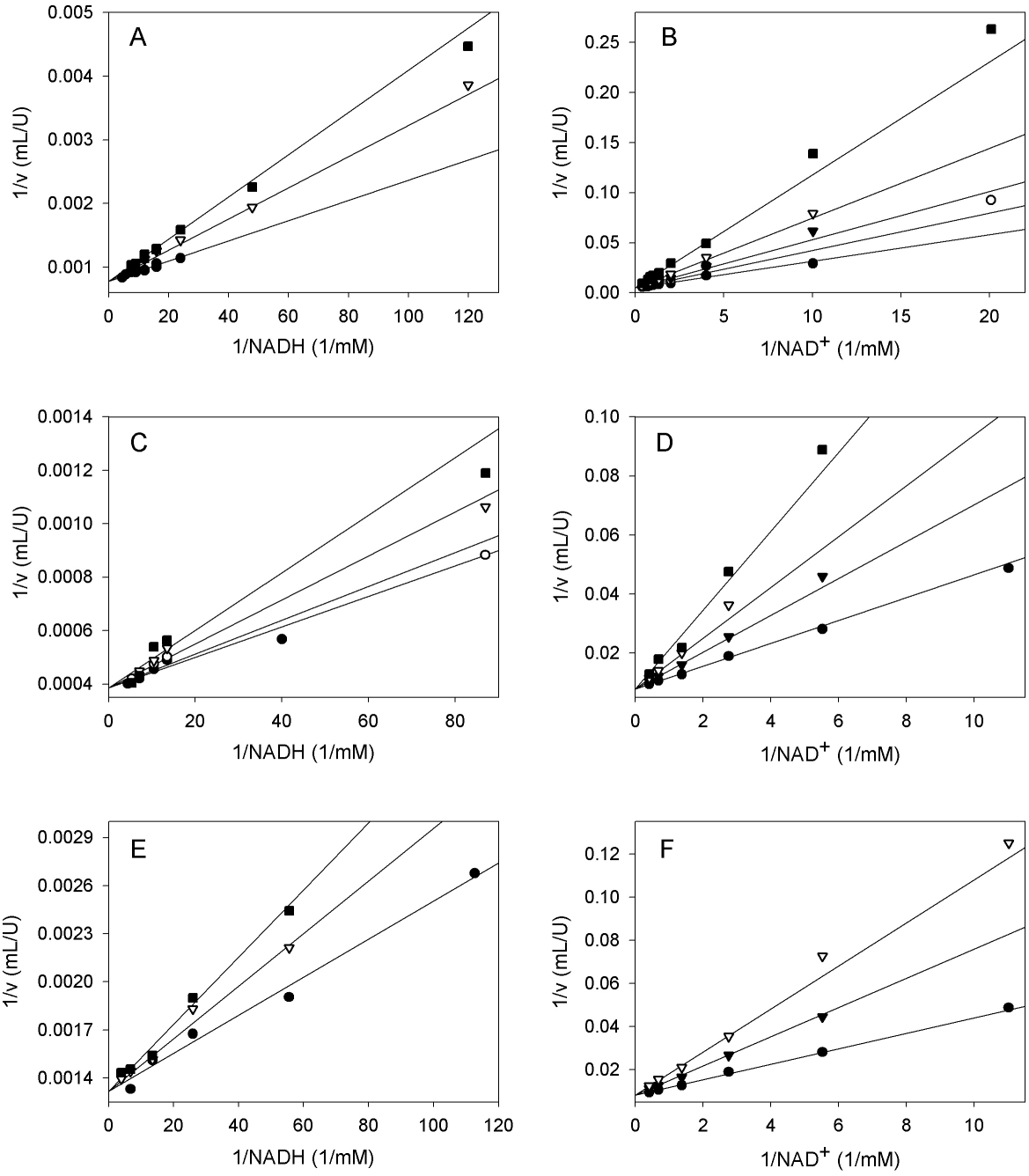

Supplementary Figure 2: Double reciprocal plots of adenosine nucleotide inhibition on *Af*M2DH at pH 7.1. Panel A, C, E show inhibition on fructose reduction with varying concentration of NADH and Panel C, D, E on mannitol oxidation with varying concentrations of NAD^+ in the presence of AMP (A, B), ADP (C, D) and ATP (E, F). Adenosine nucleotide concentrations: 5 mM (full squares), 2.5 mM (empty triangles), 1.25 mM (full triangles) and 0 mM (full circles).

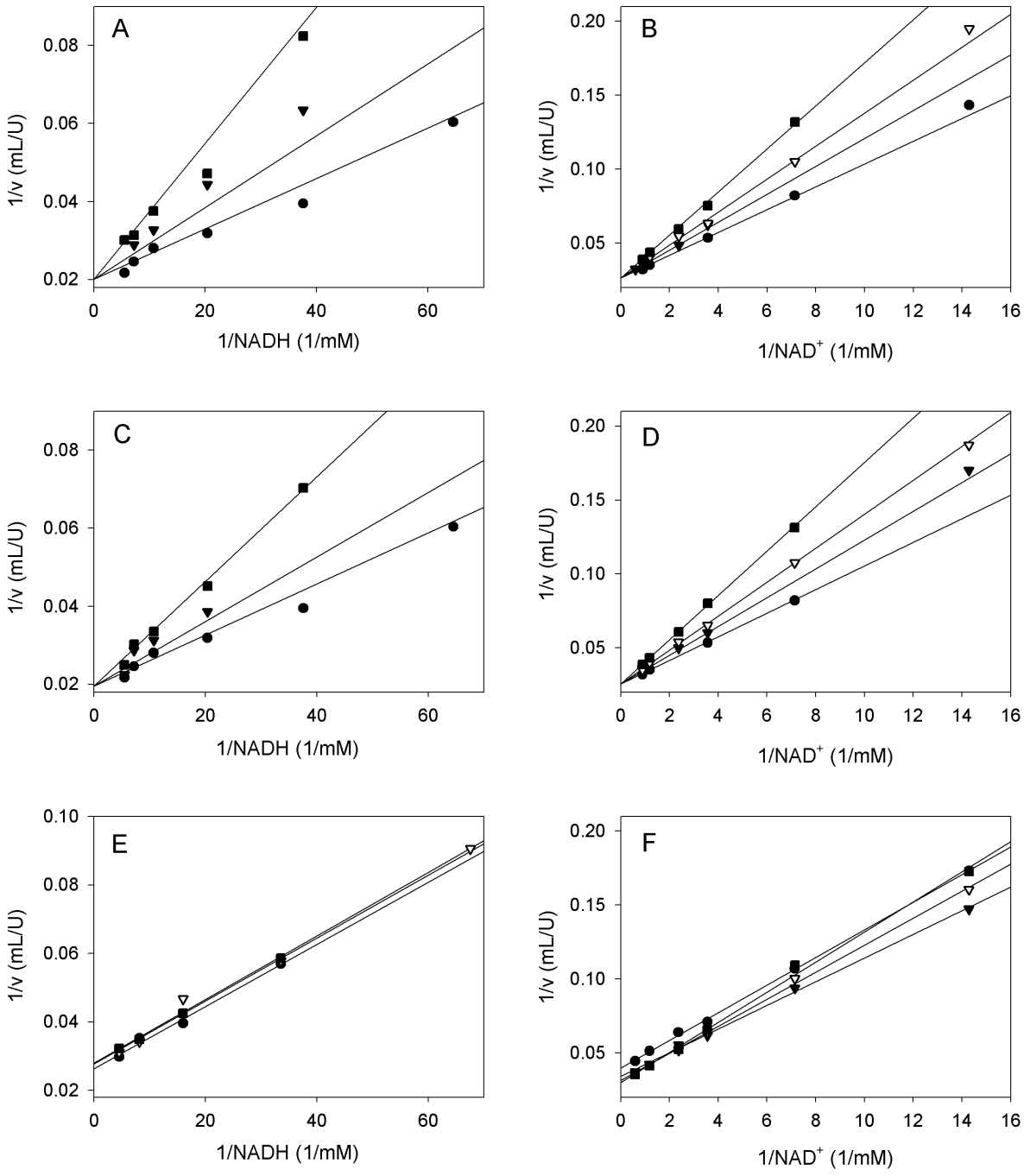

Supplementary Figure 3: Semi-logarithmic plots of residual activities of *Af*M1PDH (A, B) and *Af*M2DH (C, D) at different incubation temperatures.

Panel A and C display the entire time course of the inactivation studies while Panel B and D are close ups of the initial hours. Full symbols represent higher protein concentrations (*Af*M1PDH 0.26 mg/ml; *Af*M2DH: 0.5 mg/ml) empty symbols refer to lower protein concentrations (*Af*M1PDH 6 µg/ml, *Af*M2DH 3 µg/ml). Inactivation was assayed with *Af*M1PDH at 30°C (circles), 40°C (triangles), 50°C (squares) and with *Af*M2DH at 0°C (circles), 25°C (triangles), 30°C (squares).

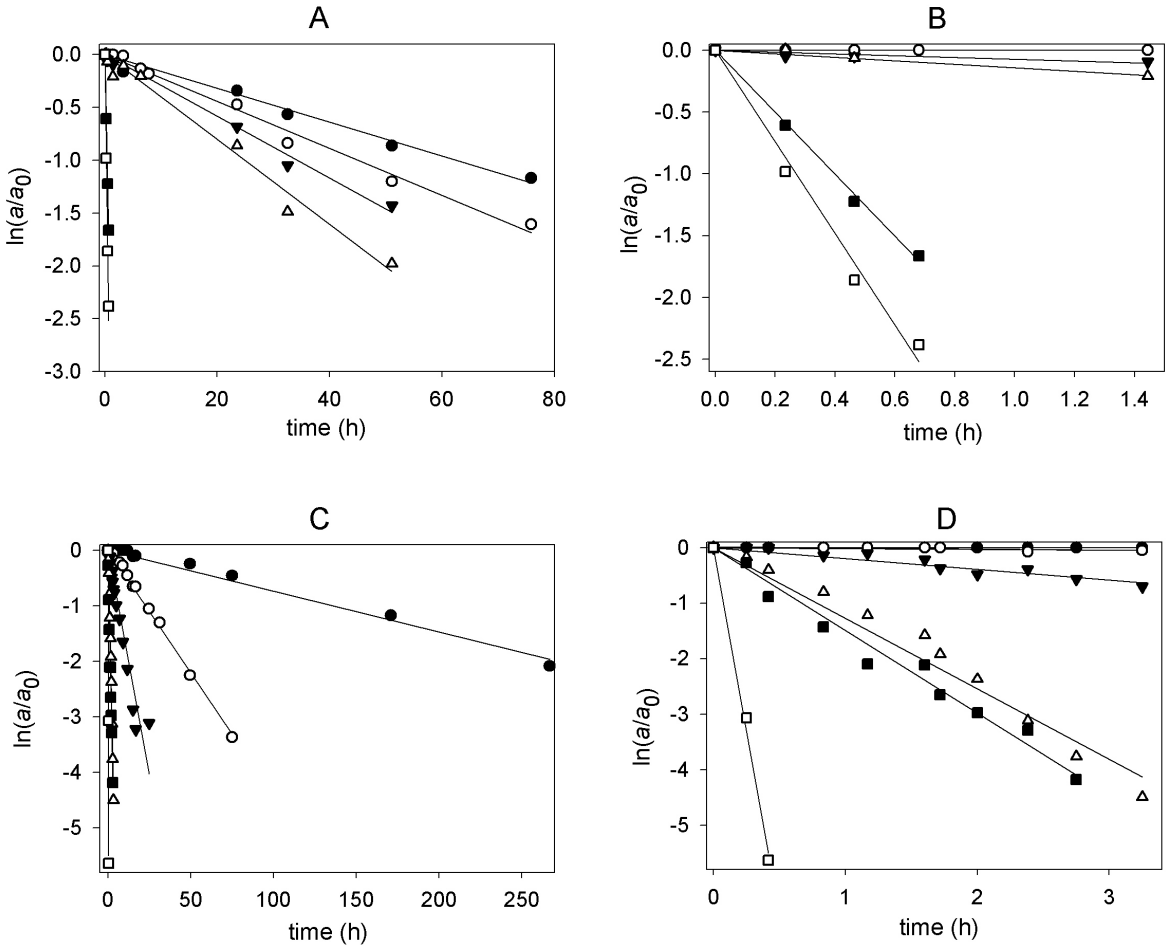

Supporting Information:

Fermentation of mixed glucose-xylose substrates by engineered strains of *Saccharomyces cerevisiae*: role of the coenzyme specificity of xylose reductase, and effect of glucose on xylose utilization

Stefan Krahulec, Barbara Petschacher, Michael Wallner, Karin Longus, Mario Klimacek[§], Bernd Nidetzky[§]

Institute of Biotechnology and Biochemical Engineering, Graz University of Technology, Petersgasse 12/I, A-8010 Graz, Austria

[§]Corresponding authors

Additional file 1: Dependence of q_{xylose} on xylose concentration for strain BP10001.

Additional file 2: Compilation of results from FBA.

Additional file 3: Specific uptake and release rates as well as biomass yields obtained in anaerobic batch and fed-batch fermentations using strain BP10001.

Additional file 4: Optimization of the HPLC analytic procedure for determination of co-utilization of glucose and xylose.

Additional file 1: Dependence of q_{xylose} on xylose concentration for strain BP10001. Data are from 5 independent fermentations using varied initial concentrations of xylose. q_{xylose} was determined from the first 48 h of substrate conversion. Xylose concentrations: 10 g/L (this work; xylose phase in mixed glucose-xylose fermentation; Table 1), 15 g/L (unpublished results), 20 g/L*, and 50 g/L (this work).

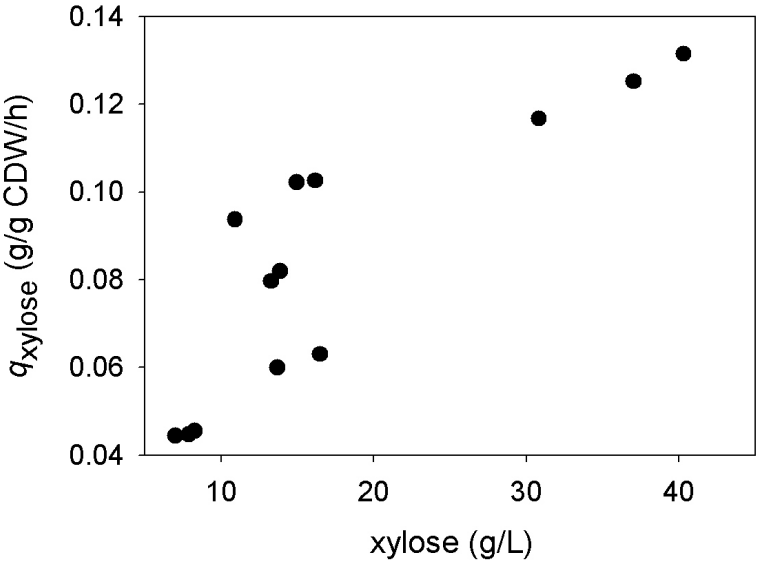

*Petschacher, B.; Nidetzky, B., Altering the coenzyme preference of xylose reductase to favor utilization of NADH enhances ethanol yield from xylose in a metabolically engineered strain of *Saccharomyces cerevisiae*. *Microb. Cell Fact.* **2008,** 7, 9.

Additional file 2: Compilation of results from FBA.

Coenzyme usage of XR		Glucose Fed Batch		Glucose / Xylose Fed Batch			Xylose Batch; objective function: CO2		
				vNADPH=vXylitol	NADPH_only	NADH_only	vNADPH=vXylitol	NADPH_max	NADH_only
Reactions	Gene	rates [mmol/gCDW/h]	relative rates	rates [mmol/gCDW/h]	rates [mmol/gCDW/h]	rates [mmol/gCDW/h]	rates [mmol/gCDW/h]	rates [mmol/gCDW/h]	rates [mmol/gCDW/h]
GLC + ATP -> G6P + ADP	GLK1 (GLC)	4.50	100.0	3.50	3.50	3.50	0.000	0.000	0.000
MAN + ATP -> MAN6P + ADP	GLK1 (MAN)	0.00	0.0	0.00	0.00	0.00	0.000	0.000	0.000
GLC + ATP -> G6P + ADP	HXK1 (GLC)	0.00	0.0	0.00	0.00	0.00	0.000	0.000	0.000
MAN + ATP -> MAN6P + ADP	HXK1 (MAN)	0.00	0.0	0.00	0.00	0.00	0.000	0.000	0.000
ATP + FRU -> ADP + F6P	HXK1 (FRU)	0.00	0.0	0.00	0.00	0.00	0.000	0.000	0.000
GLC + ATP -> G6P + ADP	HXK2 (GLC)	0.00	0.0	0.00	0.00	0.00	0.000	0.000	0.000
MAN + ATP -> MAN6P + ADP	HXK2 (MAN)	0.00	0.0	0.00	0.00	0.00	0.000	0.000	0.000
ATP + FRU -> ADP + F6P	HXK2 (FRU)	0.00	0.0	0.00	0.00	0.00	0.000	0.000	0.000
G6P <-> F6P	PGI1 (full)	0.00	0.0	0.00	0.00	0.00	0.000	0.000	0.000
G6P <-> bDG6P	PGI1 (half1)	4.14	92.1	2.72	1.25	3.14	-0.032	-0.309	-0.015
bDG6P <-> F6P	PGI1 (half2)	4.14	92.1	2.72	1.25	3.14	-0.032	-0.309	-0.015
F6P + ATP -> FDP + ADP	PFK1/2	4.22	93.7	3.89	3.42	4.03	0.496	0.352	0.502
F6P + ATP -> FDP + ADP	PFK1	0.00	0.0	0.00	0.00	0.00	0.000	0.000	0.000
FDP <-> DHAP + GAP	FBA1	4.22	93.7	3.89	3.42	4.03	0.496	0.352	0.502
DHAP <-> GAP	TPI1	3.43	76.3	3.50	3.03	3.64	0.408	0.292	0.414
GAP + PI + NAD <-> NADH + 13BPG	TDH1	0.00	0.0	0.00	0.00	0.00	0.000	0.000	0.000
GAP + PI + NAD <-> NADH + 13BPG	TDH2	7.72	171.5	8.00	7.56	8.14	1.168	0.973	1.174
GAP + PI + NAD <-> NADH + 13BPG	TDH3	0.00	0.0	0.00	0.00	0.00	0.000	0.000	0.000
13BPG + ADP <-> 3PG + ATP	PGK1	7.72	171.5	8.00	7.56	8.14	1.168	0.973	1.174
3PG <-> 2PG	GPM1	0.00	0.0	0.00	0.00	0.00	0.000	0.000	0.000
3PG <-> 2PG	GPM2	7.68	170.7	8.00	7.56	8.13	1.168	0.973	1.174
3PG <-> 2PG	GPM3	0.00	0.0	0.00	0.00	0.00	0.000	0.000	0.000
2PG <-> PEP	ENO1	0.00	0.0	0.00	0.00	0.00	0.000	0.000	0.000
2PG <-> PEP	ENO2	7.68	170.7	8.00	7.56	8.13	1.168	0.973	1.174
2PG <-> PEP	ERR3	0.00	0.0	0.00	0.00	0.00	0.000	0.000	0.000
2PG <-> PEP	ERR2	0.00	0.0	0.00	0.00	0.00	0.000	0.000	0.000
2PG <-> PEP	ERR1	0.00	0.0	0.00	0.00	0.00	0.000	0.000	0.000
PEP + ADP -> PYR + ATP	CDC19	7.64	169.7	7.96	7.53	8.08	1.168	0.973	1.174
PEP + ADP -> PYR + ATP	PYK2	0.00	0.0	0.00	0.00	0.00	0.000	0.000	0.000
PYRm + COAm + NADm -> NADHm + CO2m + ACCOAm	PDHcomp	0.17	3.8	0.15	0.00	0.15	0.000	0.000	0.000
ACCOAm + OAm -> COAm + CITm	CIT1	0.09	2.0	0.08	0.07	0.08	0.000	0.000	0.006
ACCOA + OA -> COA + CIT	CIT2	0.00	0.0	0.00	0.00	0.00	0.000	0.000	0.000
ACCOAm + OAm -> COAm + CITm	CIT3	0.00	0.0	0.00	0.00	0.00	0.000	0.000	0.000
CITm <-> ICITm	ACO1 (m)	0.00	0.0	0.00	0.00	0.00	0.000	0.000	0.000
CIT <-> ICIT	ACO1	0.09	2.0	0.08	0.07	0.08	0.000	0.000	0.006
CITm <-> ICITm	ACO2	0.00	0.0	0.00	0.00	0.00	0.000	0.000	0.000
ICITm + NADm -> CO2m + NADHm + AKGm	IDH1 / 2	0.00	0.0	0.00	0.00	0.00	0.000	0.000	0.000
ICITm + NADPm -> NADPHm + OSUCCm	IDP1 (ICIT)	0.00	0.0	0.00	0.00	0.00	0.000	0.000	0.000
ICIT + NADP -> NADPH + OSUCC	IDP2 (ICIT)	0.00	0.0	0.00	0.00	0.00	0.000	0.000	0.000
ICIT + NADP -> NADPH + OSUCC	IDP3 (ICIT)	0.09	2.0	0.08	0.07	0.08	0.000	0.000	0.000
OSUCCm -> CO2m + AKGm	IDP1 (OSUCCm)	0.00	0.0	0.00	0.00	0.00	0.000	0.000	0.000
OSUCC -> CO2 + AKG	IDP2 (OSUCC)	0.09	2.0	0.08	0.07	0.08	0.000	0.000	0.000
OSUCC -> CO2 + AKG	IDP3 (OSUCC)	0.00	0.0	0.00	0.00	0.00	0.000	0.000	0.000
AKGm + NADm + COAm -> CO2m + NADHm + SUCCCOAm	KGD1 / 2	0.00	0.0	0.00	0.00	0.00	0.000	0.000	0.000
ADPm + PIm + SUCCCOAm -> ATPm + SUCCm + COAm	LSC1 / 2	0.00	0.0	0.00	0.00	0.00	0.000	0.000	0.000
SUCCm + FADm <-> FUMm + FADH2m	SDHcomp (SUCC_half)	0.00	0.0	0.00	0.00	0.00	0.000	0.000	0.000
NADHm + FUMm -> SUCCm + NADm	YEL047C (m)	0.00	0.0	0.00	0.00	0.00	0.000	0.000	0.000
NADHm + FUMm -> SUCCm + NADm	OSM1	0.00	0.0	0.00	0.00	0.00	0.000	0.000	0.000
FUMm <-> MALm	FUM1	0.00	0.0	0.00	0.00	0.00	0.000	0.000	0.000
MALm + NADm <-> NADHm + OAm	MDH1 (NADH)	-0.04	-0.9	-0.05	-0.04	-0.05	-0.200	-0.135	-0.071
MAL + NAD <-> NADH + OA	MDH3	0.00	0.0	0.00	0.00	0.00	0.000	0.000	0.000
MAL + NAD <-> NADH + OA	MDH2	-0.09	-2.0	-0.08	-0.13	-0.08	0.000	-0.004	0.000
ICIT -> GLX + SUCC	ICL1	0.00	0.0	0.00	0.00	0.00	0.000	0.000	0.000
ICIT -> GLX + SUCC	ICL2	0.00	0.0	0.00	0.00	0.00	0.000	0.000	0.006
ACCOA + GLX -> COA + MAL	DAL7	0.00	0.0	0.00	0.00	0.00	0.000	0.000	0.006
ACCOA + GLX -> COA + MAL	MLS1	0.00	0.0	0.00	0.00	0.00	0.000	0.000	0.000
OA + ATP -> PEP + CO2 + ADP	PCK1	0.00	0.0	0.00	0.00	0.00	0.000	0.000	0.000
FDP -> F6P + PI	FBP1	0.00	0.0	0.00	0.00	0.00	0.000	0.000	0.000
PYR + ATP + CO2 -> ADP + OA + PI	PYC1	0.38	8.4	0.68	1.67	0.40	0.206	0.275	0.077
PYR + ATP + CO2 -> ADP + OA + PI	PYC2	0.00	0.0	0.00	0.00	0.00	0.000	0.000	0.000
MALm + NADPm -> CO2m + NADPHm + PYRm	MAE1	0.13	2.9	0.13	0.11	0.13	0.200	0.135	0.077
G6P + NADP <-> D6PGL + NADPH	ZWF1	0.26	5.7	0.70	2.17	0.27	0.032	0.230	0.015
D6PGL -> D6PGC	SOL1	0.00	0.0	0.00	0.00	0.00	0.000	0.000	0.000
D6PGL -> D6PGC	SOL2	0.00	0.0	0.00	0.00	0.00	0.000	0.000	0.000
D6PGL -> D6PGC	SOL3	0.00	0.0	0.00	0.00	0.00	0.000	0.000	0.000
D6PGL -> D6PGC	SOL4	0.26	5.7	0.70	2.17	0.27	0.032	0.230	0.015

D6PGC + NADP -> NADPH + CO2 + RL5P	GND2	0.00	0.0	0.00	0.00	0.00	0.000	0.000	0.000
D6PGC + NADP -> NADPH + CO2 + RL5P	GND1	0.26	5.7	0.70	2.17	0.27	0.032	0.230	0.015
RL5P <-> X5P	RPE1	0.14	3.2	0.04	1.03	-0.24	-0.232	-0.100	-0.244
RL5P <-> R5P	RKI1	0.11	2.5	0.66	1.14	0.51	0.264	0.330	0.258
R5P + X5P <-> GAP + S7P	TKL2 (R5P)	0.00	0.0	0.00	0.00	0.00	0.000	0.000	0.000
X5P + E4P <-> F6P + GAP	TKL2 (X5P)	0.00	0.0	0.00	0.00	0.00	0.000	0.000	0.000
R5P + X5P <-> GAP + S7P	TKL1 (R5P)	0.08	1.9	0.63	1.12	0.49	0.264	0.330	0.258
X5P + E4P <-> F6P + GAP	TKL1 (X5P)	0.06	1.4	0.61	1.10	0.47	0.264	0.330	0.258
GAP + S7P <-> E4P + F6P	TAL1	0.00	0.0	0.00	0.00	0.00	0.000	0.000	0.000
GAP + S7P <-> E4P + F6P	YGR043C	0.08	1.9	0.63	1.12	0.49	0.264	0.330	0.258
RIB + ATP -> R5P + ADP	RBK1	0.00	0.0	0.00	0.00	0.00	0.031	0.000	0.000
G1P <-> G6P	PGM1	0.00	0.0	0.00	0.00	0.00	0.000	0.000	0.000
G1P <-> G6P	PGM2	-0.10	-2.2	-0.09	-0.08	-0.09	0.000	-0.039	0.000
MAN6P <-> F6P	PMI40	-0.07	-1.6	-0.06	-0.06	-0.06	0.000	0.000	0.000
MAN6P <-> MAN1P	SEC53	0.07	1.6	0.06	0.06	0.06	0.000	0.000	0.000
GTP + MAN1P -> PPI + GDPMAN	PSA1	0.07	1.6	0.06	0.06	0.06	0.000	0.000	0.000
ATP + F6P -> ADP + F26P	PFK26	0.00	0.0	0.00	0.00	0.00	0.000	0.000	0.000
ATP + F6P -> ADP + F26P	PFK27	0.00	0.0	0.00	0.00	0.00	0.000	0.000	0.000
F26P -> F6P + PI	FBP26	0.00	0.0	0.00	0.00	0.00	0.000	0.000	0.000
GLAC + ATP -> GAL1P + ADP	GAL1	0.00	0.0	0.00	0.00	0.00	0.000	0.000	0.000
UDPGAL <-> UDPG	GAL10	0.00	0.0	0.00	0.00	0.00	0.000	0.000	0.000
G1P + UTP <-> UDPG + PPI	YHL012W	0.00	0.0	0.00	0.00	0.00	0.000	0.000	0.000
G1P + UTP <-> UDPG + PPI	UGP1	0.10	2.2	0.09	0.08	0.09	0.000	0.039	0.000
MLT -> 2 GLC	MAL32	0.00	0.0	0.00	0.00	0.00	0.000	0.000	0.000
MLT -> 2 GLC	YGR287C	0.00	0.0	0.00	0.00	0.00	0.000	0.000	0.000
MLT -> 2 GLC	MAL12	0.00	0.0	0.00	0.00	0.00	0.000	0.000	0.000
MLT -> 2 GLC	YJL216C	0.00	0.0	0.00	0.00	0.00	0.000	0.000	0.000
MLT -> 2 GLC	FSP2	0.00	0.0	0.00	0.00	0.00	0.000	0.000	0.000
MLT -> 2 GLC	YIL172C	0.00	0.0	0.00	0.00	0.00	0.000	0.000	0.000
MLT -> 2 GLC	YOL157C	0.00	0.0	0.00	0.00	0.00	0.000	0.000	0.000
UDPG + GAL1P <-> G1P + UDPGAL	GAL7	0.00	0.0	0.00	0.00	0.00	0.000	0.000	0.000
UDPG + G6P -> UDP + TRE6P	TPS1 / TSL1 / TPS3	0.00	0.0	0.00	0.00	0.00	0.000	0.039	0.000
TRE6P -> TRE + PI	TPS2	0.00	0.0	0.00	0.00	0.00	0.000	0.039	0.000
UDPG -> UDP + GLYCOGEN	GLC3	0.00	0.0	0.00	0.00	0.00	0.000	0.000	0.000
GLYCOGEN + PI -> G1P	GPH1 / GDB1	0.00	0.0	0.00	0.00	0.00	0.000	0.000	0.000
UDPG -> UDP + GLYCOGEN	GSY1	0.00	0.0	0.00	0.00	0.00	0.000	0.000	0.000
UDPG -> UDP + GLYCOGEN	GSY2	0.00	0.0	0.00	0.00	0.00	0.000	0.000	0.000
ATP + AC + COA -> AMP + PPI + ACCOA	ACS1	0.01	0.1	0.01	0.14	0.01	0.000	0.000	0.000
ATP + AC + COA -> AMP + PPI + ACCOA	ACS2	0.00	0.0	0.00	0.00	0.00	0.209	0.074	0.221
FALD + RGT + NAD <-> FGT + NADH	SFA1 (FALD)	0.00	0.0	0.00	0.00	0.00	0.000	0.000	0.000
FGT <-> RGT + FOR	YJL068C	0.00	0.0	0.00	0.00	0.00	0.000	0.000	0.000
PYR -> CO2 + ACAL	PDC6	7.06	156.9	7.23	6.46	7.52	1.162	0.898	1.174
PYR -> CO2 + ACAL	PDC5	0.00	0.0	0.00	0.00	0.00	0.000	0.000	0.000
PYR -> CO2 + ACAL	PDC1	0.00	0.0	0.00	0.00	0.00	0.000	0.000	0.000
+ ACCOAm	ACH1 (ACm)	0.00	0.0	0.00	0.00	0.00	0.000	0.000	0.000
ACCOA + AKG -> HCIT + COA	LYS21	0.02	0.6	0.02	0.02	0.02	0.000	0.000	0.000
ACCOA + AKG -> HCIT + COA	LYS20	0.00	0.0	0.00	0.00	0.00	0.000	0.000	0.000
HCIT <-> HCITm	U_1	0.02	0.6	0.02	0.02	0.02	0.000	0.000	0.000
ETH + NAD <-> ACAL + NADH	ADH4	0.00	0.0	0.00	0.00	0.00	0.000	0.000	0.000
ETHm + NADm <-> ACALm + NADHm	ADH3	-0.17	-3.8	-0.31	-0.64	-0.17	0.200	0.071	0.071
ETH + NAD <-> ACAL + NADH	ADH2	0.00	0.0	0.00	0.00	0.00	0.000	0.000	0.000
ETH + NAD <-> ACAL + NADH	ADH5	-6.93	-154.0	-7.29	-7.03	-7.43	-1.100	-0.971	-0.971
ETH + NAD <-> ACAL + NADH	ADH1	0.00	0.0	0.00	0.00	0.00	0.000	0.000	0.000
ETH + NAD <-> ACAL + NADH	SFA1 (ETH)	0.00	0.0	0.00	0.00	0.00	0.000	0.000	0.000
PPI -> 2 PI	IPP1	1.40	31.0	1.38	0.39	1.71	0.275	0.124	0.297
PPIm -> 2 PIm	PPA2	0.00	0.0	0.00	0.00	0.00	0.029	0.010	0.029
FOR + Qm -> QH2m + CO2 + 2 Hext	U_2	0.00	0.0	0.00	0.00	0.00	0.000	0.000	0.000
NADHm + Qm -> QH2m + NADm	NDI1	0.00	0.0	0.00	0.00	0.00	0.000	0.000	0.000
NADH + Qm -> QH2m + NAD	NDE2	0.00	0.0	0.00	0.00	0.00	0.000	0.000	0.000
NADH + Qm -> QH2m + NAD	NDE1	0.00	0.0	0.00	0.00	0.00	0.000	0.000	0.000
NADPH + 2 FERIm -> NADP + 2 FEROm	NCP1	0.00	0.0	0.00	0.00	0.00	0.000	0.000	0.000
FADH2m + Qm -> FADm + QH2m	SDHcomp (FADH2_half)	0.00	0.0	0.00	0.00	0.00	0.000	0.000	0.000
QH2m + 2 FERIm + 1.5 Hm -> Qm + 2 FEROm + 1.5 Hpump	CYTBcomp	0.00	0.0	0.00	0.00	0.00	0.000	0.000	0.000
4 FEROm + O2m + 2 Hm -> 4 FERIm + 2 Hpump	CYTCcomp	0.00	0.0	0.00	0.00	0.00	0.000	0.000	0.000
3 Hpump + ADPm + PIm -> ATPm + 3 Hm	ATPcomp	0.00	0.0	0.00	0.00	0.00	0.000	0.000	0.000
2 FERIm + LLAC -> PYR + 2 FEROm	CYB2	0.00	0.0	0.00	0.00	0.00	0.000	0.000	0.000
LLAC <-> LLAC	U_3	0.00	0.0	0.00	0.00	0.00	0.000	0.000	0.000
2 FERIm + LAC -> PYR + 2 FEROm	DLD1	0.00	0.0	0.00	0.00	0.00	0.000	0.000	0.000
2 FERIm + LACm -> PYRm + 2 FEROm	DLD2	0.00	0.0	0.00	0.00	0.00	0.000	0.000	0.000
2 FERIm + LAC -> PYR + 2 FEROm	DLD3	0.00	0.0	0.00	0.00	0.00	0.000	0.000	0.000
FOR + NAD -> CO2 + NADH	FDH2	0.00	0.0	0.00	0.00	0.00	0.000	0.000	0.000
FOR + NAD -> CO2 + NADH	FDH1	0.00	0.0	0.00	0.00	0.00	0.000	0.000	0.000
ATP + UREA + CO2 <-> ADP + PI + UREAC	DUR1,2 (UREA)	0.00	0.0	0.00	0.00	0.00	0.006	0.000	0.000
UREAC -> 2 NH3 + 2 CO2	DUR1,2 (UREAC)	0.00	0.0	0.00	0.00	0.00	0.006	0.000	0.000
H2SO3 + 3 NADPH <-> H2S + 3 NADP	MET10 / ECM17	0.01	0.1	0.01	0.00	0.01	0.000	0.000	0.000
C160COA + O2 -> TDEC160COA + H2O2	POX1 (C160COA)	0.00	0.0	0.00	0.00	0.00	0.000	0.000	0.000
TDEC160COA -> LHO160COA	FOX2 (TDEC160COA)	0.00	0.0	0.00	0.00	0.00	0.000	0.000	0.000
LHO160COA + NAD -> 3KETO160COA + NADH	FOX2 (LHO160COA)	0.00	0.0	0.00	0.00	0.00	0.000	0.000	0.000

3KETO160COA + COA -> ACCOA + C140COA	POT1 (3KETO160COA)	0.00	0.0	0.00	0.00	0.00	0.000	0.000	0.000
C140COA + O2 -> TDEC140COA + H2O2	POX1 (C140COA)	0.00	0.0	0.00	0.00	0.00	0.000	0.000	0.000
TDEC140COA -> LHO140COA	FOX2 (TDEC140COA)	0.00	0.0	0.00	0.00	0.00	0.000	0.000	0.000
LHO140COA + NAD -> 3KETO140COA + NADH	FOX2 (LHO140COA)	0.00	0.0	0.00	0.00	0.00	0.000	0.000	0.000
3KETO140COA + COA -> ACCOA + C120COA	POT1 (3KETO140COA)	0.00	0.0	0.00	0.00	0.00	0.000	0.000	0.000
C120COA + O2 -> TDEC120COA + H2O2	POX1 (C120COA)	0.00	0.0	0.00	0.00	0.00	0.000	0.000	0.000
TDEC120COA -> LHO120COA	FOX2 (TDEC120COA)	0.00	0.0	0.00	0.00	0.00	0.000	0.000	0.000
LHO120COA + NAD -> 3KETO120COA + NADH	FOX2 (LHO120COA)	0.00	0.0	0.00	0.00	0.00	0.000	0.000	0.000
3KETO120COA + 5 COA + 5 O2 + 5 NAD -> 6 ACCOA + 5 H2O2 + 5 NADH	POT1 (3KETO120COA)	0.00	0.0	0.00	0.00	0.00	0.000	0.000	0.000
C160COA + ACP <-> C160ACP + COA	FAS1 / 2 (C160COA)	0.00	0.0	0.00	0.00	0.00	-0.012	0.000	-0.016
C140COA + ACP <-> C140ACP + COA	FAS1 / 2 (C140COA)	0.00	0.0	0.00	0.00	0.00	0.000	0.000	-0.004
C120COA + ACP <-> C120ACP + COA	FAS1 / 2 (C120COA)	0.00	0.0	0.00	0.00	0.00	0.000	0.000	-0.004
C160AL + NAD -> C160 + NADH	U_4	0.00	0.0	0.00	0.00	0.00	0.000	0.000	0.000
C160 + ATP + COA -> C160COA + AMP + PPI	FAA1 (C160)	0.00	0.0	0.00	0.00	0.00	0.000	0.000	0.000
C160 + ATP + COA -> C160COA + AMP + PPI	FAA2 (C160)	0.00	0.0	0.00	0.00	0.00	0.000	0.000	0.000
C160 + ATP + COA -> C160COA + AMP + PPI	FAA3 (C160)	0.00	0.0	0.00	0.00	0.00	0.000	0.000	0.000
C160 + ATP + COA -> C160COA + AMP + PPI	FAA4 (C160)	0.00	0.0	0.00	0.00	0.00	0.000	0.000	0.000
2 ACCOA <-> COA + AACCOA	ERG10	0.00	0.0	0.00	0.00	0.00	0.000	0.000	0.000
ACCOA + ATP + CO2 -> MALCOA + ADP + PI	ACC1	0.00	0.1	0.00	0.00	0.00	0.090	0.000	0.151
ACCOAm + ATPm + CO2m -> MALCOAm + ADPm + PIm	HFA1	0.03	0.6	0.02	0.02	0.02	0.100	0.068	0.039
MALCOA + ACP <-> MALACP + COA	FAS1 / 2 (MALCOA)	0.00	0.1	0.00	0.00	0.00	0.090	0.000	0.151
ACCOA + ACP <-> ACACP + COA	FAS1 / 2 (ACCOA)	0.00	0.0	0.00	0.00	0.00	0.013	0.000	0.024
ACACP + 4 MALACP + 8 NADPH -> 8 NADP + C100ACP + 4 CO2 + 4 ACP	FATsyn (C100)	0.00	0.0	0.00	0.00	0.00	0.001	0.000	0.001
ACACP + 5 MALACP + 10 NADPH -> 10 NADP + C120ACP + 5 CO2 + 5 ACP	FATsyn (C120)	0.00	0.0	0.00	0.00	0.00	0.000	0.000	0.004
ACACP + 6 MALACP + 12 NADPH -> 12 NADP + C140ACP + 6 CO2 + 6 ACP	FATsyn (C140)	0.00	0.0	0.00	0.00	0.00	0.000	0.000	0.004
ACACP + 7 MALACP + 14 NADPH -> 14 NADP + C160ACP + 7 CO2 + 7 ACP	FATsyn (C160)	0.00	0.0	0.00	0.00	0.00	0.012	0.000	0.016
C160COA + NADPH + O2 -> C161COA + NADP	OLE1 (C161)	0.00	0.0	0.00	0.00	0.00	0.000	0.000	0.000
ACACP + 8 MALACP + 16 NADPH -> 16 NADP + C180ACP + 8 CO2 + 8 ACP	FATsyn (C180)	0.00	0.0	0.00	0.00	0.00	0.000	0.000	0.000
C180COA + NADPH + O2 -> C181COA + NADP	OLE1 (C181)	0.00	0.0	0.00	0.00	0.00	0.000	0.000	0.000
C181COA + NADPH + O2 -> C182COA + NADP	U_5	0.00	0.0	0.00	0.00	0.00	0.000	0.000	0.000
C140 + ATP + 7 COA + 6 FADm + 6 NAD -> AMP + PPI + 6 FADH2m + 6 NADH + 7 ACCOA	POX1 / FOX2 / POT1(C140)	0.00	0.0	0.00	0.00	0.00	0.000	0.000	0.000
C160 + ATP + 8 COA + 7 FADm + 7 NAD -> AMP + PPI + 7 FADH2m + 7 NADH + 8 ACCOA	POX1 / FOX2 / POT1(C160)	0.00	0.0	0.00	0.00	0.00	0.000	0.000	0.000
C180 + ATP + 9 COA + 8 FADm + 8 NAD -> AMP + PPI + 8 FADH2m + 8 NADH + 9 ACCOA	POX1 / FOX2 / POT1 (C180)	0.00	0.0	0.00	0.00	0.00	0.000	0.000	0.000
GL3P + 0.017 C100COA + 0.062 C120COA + 0.1 C140COA + 0.27 C160COA + 0.169 C161COA + 0.055 C180COA + 0.235 C181COA + 0.093 C182COA -> AGL3P + COA	SCT1 (GL3P)	0.00	0.0	0.00	0.00	0.00	0.029	0.010	0.029
DHAP + 0.017 C100COA + 0.062 C120COA + 0.1 C140COA + 0.27 C160COA + 0.169 C161COA + 0.055 C180COA + 0.235 C181COA + 0.093 C182COA -> ADHAP + COA	SCT1 (DHAP)	0.00	0.1	0.00	0.00	0.00	0.000	0.000	0.000
ADHAP + NADPH -> AGL3P + NADP	AYR1	0.00	0.1	0.00	0.00	0.00	0.000	0.000	0.000
AGL3P + 0.017 C100COA + 0.062 C120COA + 0.100 C140COA + 0.270 C160COA + 0.169 C161COA + 0.055 C180COA + 0.235 C181COA + 0.093 C182COA -> PA + COA	SLC1	0.00	0.1	0.00	0.00	0.00	0.029	0.010	0.029
PAm + CTPm <-> CDPDGm + PPIm	CDS1 (m)	0.00	0.0	0.00	0.00	0.00	0.029	0.010	0.029
PA <-> PAm	U_7	0.00	0.0	0.00	0.00	0.00	0.029	0.010	0.029
PA + CTP <-> CDPDG + PPI	CDS1	0.01	0.1	0.00	0.03	0.00	0.000	0.000	0.024
CTPm + RTHIOm -> DCTPm + OTHIOm	U_8	0.00	0.0	0.00	0.00	0.00	0.000	0.000	0.000
CDPDG + SER <-> CMP + PS	CHO1	0.00	0.0	0.00	0.00	0.00	0.000	0.000	0.000
CDPDGm + SERm <-> CMPm + PSm	CHO1 (m)	0.00	0.0	0.00	0.00	0.00	0.000	0.000	0.000
PS -> PE + CO2	PSD2	0.00	0.0	0.00	0.00	0.00	0.000	0.000	0.000
PSm -> PEm + CO2m	PSD1	0.00	0.0	0.00	0.00	0.00	0.000	0.000	0.000
SAM + PE -> SAH + PMME	CHO2	0.00	0.0	0.00	0.00	0.00	0.000	0.000	0.000
SAM + PMME -> SAH + PDME	OPI3 (PMME)	0.00	0.0	0.00	0.00	0.00	0.000	0.000	0.000
SAM + PDME -> SAH + PC	OPI3 (PDME)	0.00	0.0	0.00	0.00	0.00	0.000	0.000	0.000
PC -> CHO + PA	SPO14	0.00	0.1	0.00	0.02	0.00	0.000	0.000	0.024
ATP + CHO -> ADP + PCHO	CKI1 (CHO)	0.00	0.1	0.00	0.02	0.00	0.000	0.000	0.024
PCHO + CTP -> CDPCHO + PPI	PCT1	0.00	0.1	0.00	0.02	0.00	0.000	0.000	0.024

CDPCHO + DAGLY -> PC + CMP	CPT1	0.00	0.1	0.00	0.02	0.00	0.000	0.000	0.024
ATP + ETHAM -> ADP + PETHM	EKI1	0.00	0.0	0.00	0.00	0.00	0.000	0.000	0.000
ATP + ETHAM -> ADP + PETHM	CKI1 (ETHAM)	0.00	0.0	0.00	0.00	0.00	0.000	0.000	0.000
ETHAM <-> ACAL + NH3	U_10	0.00	0.0	0.00	0.00	0.00	0.000	0.000	0.000
PETHM + CTP -> CDPETN + PPI	MUQ1	0.00	0.0	0.00	0.00	0.00	0.000	0.000	0.000
CDPETN + DAGLY <-> CMP + PE	EPT1	0.00	0.0	0.00	0.00	0.00	0.000	0.000	0.000
G6P -> MI1P	INO1	0.00	0.0	0.00	0.00	0.00	0.000	0.000	0.000
MI1P -> MYOI + PI	INM1	0.00	0.0	0.00	0.00	0.00	0.000	0.000	0.000
MI1P -> MYOI + PI	YDR287W	0.00	0.0	0.00	0.00	0.00	0.000	0.000	0.000
CDPDG + MYOI -> CMP + PINS	PIS1	0.01	0.1	0.00	0.03	0.00	0.000	0.000	0.024
ATP + PINS -> ADP + PINS4P	PIK1	0.00	0.1	0.00	0.02	0.00	0.000	0.000	0.024
ATP + PINS -> ADP + PINS4P	STT4	0.00	0.0	0.00	0.00	0.00	0.000	0.000	0.000
ATP + PINS -> ADP + PINS4P	LSB6	0.00	0.0	0.00	0.00	0.00	0.000	0.000	0.000
PINS4P + ATP -> D45PI + ADP	MSS4	0.00	0.1	0.00	0.02	0.00	0.000	0.000	0.024
D45PI -> TPI + DAGLY	PLC1	0.00	0.1	0.00	0.02	0.00	0.000	0.000	0.024
CDPDGm + GL3Pm <-> CMPm + PGPm	PGS1	0.00	0.0	0.00	0.00	0.00	0.014	0.005	0.014
PGPm -> PIm + PGm	U_11	0.00	0.0	0.00	0.00	0.00	0.014	0.005	0.014
CDPDGm + PGm -> CMPm + CLm	CRD1	0.00	0.0	0.00	0.00	0.00	0.014	0.005	0.014
PA -> DAGLY + PI	DPP1	0.00	0.0	0.00	0.00	0.00	0.000	0.000	0.000
C160COA + SER -> COA + DHSPH + CO2	LCB1 / 2	0.00	0.0	0.00	0.00	0.00	0.000	0.000	0.000
DHSPH + NADH -> SPH + NAD	TSC10	0.00	0.0	0.00	0.00	0.00	0.000	0.000	0.000
SPH + O2 + NADPH -> PSPH + NADP	SUR2	0.00	0.0	0.00	0.00	0.00	0.000	0.000	0.000
SPH + C260COA -> CER2 + COA	LAG1 (SPH)	0.00	0.0	0.00	0.00	0.00	0.000	0.000	0.000
SPH + C260COA -> CER2 + COA	LAC1 (SPH)	0.00	0.0	0.00	0.00	0.00	0.000	0.000	0.000
CER2 + PINS -> IPC	AUR1 (CER2)	0.00	0.0	0.00	0.00	0.00	0.000	0.000	0.000
IPC + GDPMAN -> MIPC	SUR1 / CSG2 (IPC)	0.00	0.0	0.00	0.00	0.00	0.000	0.000	0.000
IPC + GDPMAN -> MIPC	CSH1 / CSG2 (IPC)	0.00	0.0	0.00	0.00	0.00	0.000	0.000	0.000
MIPC + PINS -> MIP2C	IPT1 (MIPC)	0.00	0.0	0.00	0.00	0.00	0.000	0.000	0.000
CER2 + NADPH + O2 -> CER3 + NADP	SCS7	0.00	0.0	0.00	0.00	0.00	0.000	0.000	0.000
CER3 + PINS -> IPC2	AUR1 (CER3)	0.00	0.0	0.00	0.00	0.00	0.000	0.000	0.000
IPC2 + GDPMAN -> MIPC2	SUR1 / CSG2 (IPC2)	0.00	0.0	0.00	0.00	0.00	0.000	0.000	0.000
IPC2 + GDPMAN -> MIPC2	CSH1 / CSG2 (IPC2)	0.00	0.0	0.00	0.00	0.00	0.000	0.000	0.000
MIPC2 + PINS -> MIP2C2	IPT1 (MIPC2)	0.00	0.0	0.00	0.00	0.00	0.000	0.000	0.000
SPH + ATP -> DHS1P + ADP	LCB4 (SPH)	0.00	0.0	0.00	0.00	0.00	0.000	0.000	0.000
SPH + ATP -> DHS1P + ADP	LCB5 (SPH)	0.00	0.0	0.00	0.00	0.00	0.000	0.000	0.000
DHS1P -> SPH + PI	LCB3 (DHS1P)	0.00	0.0	0.00	0.00	0.00	0.000	0.000	0.000
DHS1P -> SPH + PI	YSR3 (DHS1P)	0.00	0.0	0.00	0.00	0.00	0.000	0.000	0.000
PSPH + ATP -> PHS1P + ADP	LCB4 (PSPH)	0.00	0.0	0.00	0.00	0.00	0.000	0.000	0.000
PSPH + ATP -> PHS1P + ADP	LCB5 (PSPH)	0.00	0.0	0.00	0.00	0.00	0.000	0.000	0.000
PHS1P -> PSPH + PI	LCB3 (PHS1P)	0.00	0.0	0.00	0.00	0.00	0.000	0.000	0.000
PHS1P -> PSPH + PI	YSR3 (PHS1P)	0.00	0.0	0.00	0.00	0.00	0.000	0.000	0.000
DHS1P -> PETHM + C160AL	DPL1	0.00	0.0	0.00	0.00	0.00	0.000	0.000	0.000
C120ACP + 3 MALACP + 6 NADPH -> C180ACP + 3 ACP + 6 NADP + 3 CO2	ELO1(C120-C180)	0.00	0.0	0.00	0.00	0.00	0.000	0.000	0.000
C120ACP + 2 MALACP + 4 NADPH -> C160ACP + 2 ACP + 4 NADP + 2 CO2	ELO1 (C120-C160)	0.00	0.0	0.00	0.00	0.00	0.000	0.000	0.000
C140ACP + MALACP + 2 NADPH -> C160ACP + ACP + 2 NADP + CO2	ELO1 (C140-C160)	0.00	0.0	0.00	0.00	0.00	0.000	0.000	0.000
C180ACP + 4 MALACP + 8 NADPH + COA -> C260COA + 5 ACP + 8 NADP + 4 CO2	ELO3	0.00	0.0	0.00	0.00	0.00	0.000	0.000	0.000
H3MCOA + COA <-> ACCOA + AACCOA	ERG13	0.00	0.0	0.00	0.00	0.00	0.000	0.000	0.000
MVL + COA + 2 NADP <-> H3MCOA + 2 NADPH	HMG2	0.00	0.0	0.00	0.00	0.00	0.000	0.000	0.000
MVL + COA + 2 NADP <-> H3MCOA + 2 NADPH	HMG1	0.00	0.0	0.00	0.00	0.00	0.000	0.000	0.000
ATP + MVL -> ADP + PMVL	ERG12 (ATP)	0.00	0.0	0.00	0.00	0.00	0.000	0.000	0.000
CTP + MVL -> CDP + PMVL	ERG12 (CTP)	0.00	0.0	0.00	0.00	0.00	0.000	0.000	0.000
GTP + MVL -> GDP + PMVL	ERG12 (GTP)	0.00	0.0	0.00	0.00	0.00	0.000	0.000	0.000
UTP + MVL -> UDP + PMVL	ERG12 (UTP)	0.00	0.0	0.00	0.00	0.00	0.000	0.000	0.000
ATP + PMVL -> ADP + PPMVL	ERG8	0.00	0.0	0.00	0.00	0.00	0.000	0.000	0.000
ATP + PPMVL -> ADP + PI + IPPP + CO2	MVD1	0.00	0.0	0.00	0.00	0.00	0.000	0.000	0.000
IPPP <-> DMPP	IDI1	0.00	0.0	0.00	0.00	0.00	0.000	0.000	0.000
DMPP + IPPP -> GPP + PPI	ERG20 (DMPP)	0.00	0.0	0.00	0.00	0.00	0.000	0.000	0.000
GPP + IPPP -> FPP + PPI	ERG20 (GPP)	0.00	0.0	0.00	0.00	0.00	0.000	0.000	0.000
2 FPP + NADPH -> NADP + SQL + PPI	ERG9	0.00	0.0	0.00	0.00	0.00	0.000	0.000	0.000
SQL + O2 + NADPH -> S23E + NADP	ERG1	0.00	0.0	0.00	0.00	0.00	0.000	0.000	0.000
S23E -> LNST	ERG7	0.00	0.0	0.00	0.00	0.00	0.000	0.000	0.000
LNST + 3 NADPH + 3 O2 -> IGST + 3 NADP	ERG11	0.00	0.0	0.00	0.00	0.00	0.000	0.000	0.000
IGST + NADPH -> DMZYMST + NADP	ERG24	0.00	0.0	0.00	0.00	0.00	0.000	0.000	0.000
3 O2 + DMZYMST + 3 NADPH -> IMZYMST + 3 NADP	ERG25 (DMZYMST)	0.00	0.0	0.00	0.00	0.00	0.000	0.000	0.000
IMZYMST + NAD -> IIMZYMST + CO2 + NADH	ERG26 (IMZYMST)	0.00	0.0	0.00	0.00	0.00	0.000	0.000	0.000
IIMZYMST + NADPH -> MZYMST + NADP	ERG27(IIMZYMST)	0.00	0.0	0.00	0.00	0.00	0.000	0.000	0.000
3 O2 + MZYMST + 3 NADPH -> IZYMST + 3 NADP	ERG25 (MZYMST)	0.00	0.0	0.00	0.00	0.00	0.000	0.000	0.000
IZYMST + NAD -> IIZYMST + CO2 + NADH	ERG26 (IZYMST)	0.00	0.0	0.00	0.00	0.00	0.000	0.000	0.000
IIZYMST + NADPH -> ZYMST + NADP	ERG27 (IIZYMST)	0.00	0.0	0.00	0.00	0.00	0.000	0.000	0.000
ZYMST + SAM -> FEST + SAH	ERG6	0.00	0.0	0.00	0.00	0.00	0.000	0.000	0.000
FEST -> EPST	ERG2	0.00	0.0	0.00	0.00	0.00	0.000	0.000	0.000

EPST + O2 + NADPH -> NADP + ERTROL	ERG3	0.00	0.0	0.00	0.00	0.00	0.000	0.000	0.000
ERTROL + O2 + NADPH -> NADP + ERTEOL	ERG5	0.00	0.0	0.00	0.00	0.00	0.000	0.000	0.000
ERTEOL + NADPH -> ERGOST + NADP	ERG4	0.00	0.0	0.00	0.00	0.00	0.000	0.000	0.000
R5P + ATP <-> PRPP + AMP	PRS5	0.00	0.0	0.00	0.00	0.00	0.000	0.000	0.000
R5P + ATP <-> PRPP + AMP	PRS4	0.03	0.7	0.03	0.02	0.03	0.031	0.000	0.000
R5P + ATP <-> PRPP + AMP	PRS2	0.00	0.0	0.00	0.00	0.00	0.000	0.000	0.000
R5P + ATP <-> PRPP + AMP	PRS3	0.00	0.0	0.00	0.00	0.00	0.000	0.000	0.000
R5P + ATP <-> PRPP + AMP	PRS1	0.00	0.0	0.00	0.00	0.00	0.000	0.000	0.000
ATN <-> ATT	DAL1	0.00	0.0	0.00	0.00	0.00	0.000	0.000	0.000
ATT <-> UGC + UREA	DAL2	0.00	0.0	0.00	0.00	0.00	0.000	0.000	0.000
UGC <-> GLX + 2 NH3 + CO2	DAL3	0.00	0.0	0.00	0.00	0.00	0.000	0.000	0.000
ATP -> cAMP + PPI	CYR1	0.00	0.0	0.00	0.00	0.00	0.000	0.000	0.000
GMP + ATP <-> GDP + ADP	GUK1 (GMP+ATP)	0.00	0.0	0.00	0.00	0.00	0.000	0.000	0.000
DGMP + ATP <-> DGDP + ADP	GUK1 (DGMP+ATP)	0.00	0.0	0.00	0.00	0.00	0.000	0.000	0.000
GMP + DATP <-> GDP + DADP	GUK1 (GMP+DATP)	0.00	0.0	0.00	0.00	0.00	0.000	0.000	0.000
PRPP + GLN -> PPI + GLU + PRAM	ADE4	0.01	0.2	0.01	0.01	0.01	0.000	0.000	0.000
PRAM + ATP + GLY <-> ADP + PI + GAR	ADE5,7 (PRAM)	0.01	0.2	0.01	0.01	0.01	0.000	0.000	0.000
GAR + FTHF -> THF + FGAR	ADE8	0.01	0.2	0.01	0.01	0.01	0.000	0.000	0.000
FGAR + ATP + GLN -> GLU + ADP + PI + FGAM	ADE6	0.01	0.2	0.01	0.01	0.01	0.000	0.000	0.000
FGAM + ATP -> ADP + PI + AIR	ADE5,7 (FGAM)	0.01	0.2	0.01	0.01	0.01	0.000	0.000	0.000
CAIR <-> AIR + CO2	ADE2	-0.01	-0.2	-0.01	-0.01	-0.01	0.000	0.000	0.000
CAIR + ATP + ASP <-> ADP + PI + SAICAR	ADE1	0.01	0.2	0.01	0.01	0.01	0.000	0.000	0.000
SAICAR <-> FUM + AICAR	ADE13 (SAICAR)	0.01	0.2	0.01	0.01	0.01	0.000	0.000	0.000
AICAR + FTHF <-> THF + PRFICA	ADE16 (AICAR)	0.00	0.0	0.00	0.00	0.00	0.000	0.000	0.000
AICAR + FTHF <-> THF + PRFICA	ADE17 (AICAR)	0.02	0.3	0.01	0.01	0.01	0.000	0.000	0.000
PRFICA <-> IMP	ADE16 (PRFICA)	0.00	0.0	0.00	0.00	0.00	0.000	0.000	0.000
PRFICA <-> IMP	ADE17 (PRFICA)	0.02	0.3	0.01	0.01	0.01	0.000	0.000	0.000
IMP + GTP + ASP -> GDP + PI + ASUC	ADE12	0.01	0.2	0.01	0.01	0.01	0.000	0.006	0.000
ASUC <-> FUM + AMP	ADE13 (ASUC)	0.01	0.2	0.01	0.01	0.01	0.000	0.006	0.000
IMP + NAD -> NADH + XMP	IMD2	0.01	0.1	0.00	0.00	0.00	0.000	0.000	0.000
IMP + NAD -> NADH + XMP	IMD4	0.00	0.0	0.00	0.00	0.00	0.000	0.000	0.000
IMP + NAD -> NADH + XMP	IMD3	0.00	0.0	0.00	0.00	0.00	0.000	0.000	0.000
XMP + ATP + GLN -> GLU + AMP + PPI + GMP	GUA1	0.01	0.1	0.00	0.00	0.00	0.000	0.000	0.000
AMP -> IMP + NH3	AMD1	0.00	0.0	0.00	0.00	0.00	0.000	0.006	0.000
cAMP -> AMP	PDE1	0.00	0.0	0.00	0.00	0.00	0.000	0.000	0.000
cAMP -> AMP	PDE2	0.00	0.0	0.00	0.00	0.00	0.000	0.000	0.000
ADP + ATP -> PI + ATRP	APA2	0.00	0.0	0.00	0.00	0.00	0.000	0.000	0.000
ADP + ATP -> PI + ATRP	APA1	0.00	0.0	0.00	0.00	0.00	0.000	0.000	0.000
CAP + ASP -> CAASP + PI	URA2 (CAASP)	0.01	0.2	0.01	0.01	0.01	0.000	0.000	0.000
CAASP <-> DOROA	URA4	0.01	0.2	0.01	0.01	0.01	0.000	0.000	0.000
DOROA + FUM -> SUCC + OROA	URA1	0.01	0.2	0.01	0.01	0.01	0.000	0.000	0.000
OROA + PRPP <-> PPI + OMP	URA5	0.00	0.0	0.00	0.00	0.00	0.000	0.000	0.000
OROA + PRPP <-> PPI + OMP	URA10	0.01	0.2	0.01	0.01	0.01	0.000	0.000	0.000
OMP -> CO2 + UMP	URA3	0.01	0.2	0.01	0.01	0.01	0.000	0.000	0.000
ATP + UMP <-> ADP + UDP	URA6 (UMP)	0.00	0.1	0.00	0.00	0.00	0.000	0.000	0.000
URA + PRPP -> UMP + PPI	FUR1	0.00	0.0	0.00	0.00	0.00	0.000	0.000	0.000
CYTS -> URA + NH3	FCY1	0.00	0.0	0.00	0.00	0.00	0.000	0.000	0.000
DU + ATP -> DUMP + ADP	U_12	0.00	0.0	0.00	0.00	0.00	0.000	0.000	0.000
DT + ATP -> ADP + DTMP	U_13	0.00	0.0	0.00	0.00	0.00	0.000	0.000	0.000
URI + GTP -> UMP + GDP	URK1 (URI+GTP)	0.00	0.0	0.00	0.00	0.00	0.000	0.000	0.000
CYTD + GTP -> GDP + CMP	URK1 (CYTD+GTP)	0.00	0.0	0.00	0.00	0.00	0.000	0.000	0.000
URI + ATP -> ADP + UMP	URK1 (URI+ATP)	0.00	0.0	0.00	0.00	0.00	0.000	0.000	0.000
DU + PI <-> URA + DR1P	PNP1 (DU)	0.00	0.0	0.00	0.00	0.00	0.000	0.000	0.000
DT + PI <-> THY + DR1P	PNP1 (DT)	0.00	0.0	0.00	0.00	0.00	0.000	0.000	0.000
CYTD -> URI + NH3	CDD1 (CYTD)	0.00	0.0	0.00	0.00	0.00	0.000	0.000	0.000
DC -> NH3 + DU	CDD1 (DC)	0.00	0.0	0.00	0.00	0.00	0.000	0.000	0.000
DTMP + ATP <-> ADP + DTDP	CDC8	0.00	0.0	0.00	0.00	0.00	0.000	0.000	0.000
H2O2 + RTHIO -> OTHIO	TSA1	0.00	0.0	0.00	0.00	0.00	0.000	0.000	0.000
H2O2 + RTHIO -> OTHIO	TSA2	0.00	0.0	0.00	0.00	0.00	0.000	0.000	0.000
OTHIO + NADPH -> NADP + RTHIO	TRR1	0.01	0.1	0.01	0.00	0.01	0.000	0.000	0.000
OTHIOm + NADPHm -> NADPm + RTHIOm	TRR2	0.00	0.0	0.00	0.00	0.00	0.000	0.000	0.000
RTHIO + H2O2 -> OTHIO	TRX1	0.00	0.0	0.00	0.00	0.00	0.000	0.000	0.000
RTHIOm + H2O2m -> OTHIOm	TRX2	0.00	0.0	0.00	0.00	0.00	0.000	0.000	0.000
RTHIO + H2O2 -> OTHIO	TRX3	0.00	0.0	0.00	0.00	0.00	0.000	0.000	0.000
DUTP -> PPI + DUMP	DUT1	0.00	0.0	0.00	0.00	0.00	0.000	0.000	0.000
DUMP + MYLENTHF -> DHF + DTMP	CDC21	0.00	0.0	0.00	0.00	0.00	0.000	0.000	0.000
DCMP + ATP <-> ADP + DCDP	U_14	0.00	0.0	0.00	0.00	0.00	0.000	0.000	0.000
CMP + ATP <-> ADP + CDP	U_15	0.01	0.1	0.00	0.05	0.00	0.029	0.010	0.077
UTP + GLN + ATP -> GLU + CTP + ADP + PI	URA7	0.00	0.1	0.00	0.00	0.00	0.000	0.000	0.000
UTP + GLN + ATP -> GLU + CTP + ADP + PI	URA8	0.00	0.0	0.00	0.00	0.00	0.000	0.000	0.000
AD + PRPP -> PPI + AMP	APT1	0.00	0.0	0.00	0.00	0.00	0.000	0.000	0.000
ADN -> INS + NH3	AAH1 (ADN)	0.00	0.0	0.00	0.00	0.00	0.000	0.000	0.000
DA -> DIN + NH3	AAH1 (DA)	0.00	0.0	0.00	0.00	0.00	0.000	0.000	0.000
DIN + PI <-> HYXN + DR1P	PNP1 (DIN)	0.00	0.0	0.00	0.00	0.00	0.000	0.000	0.000
DA + PI <-> AD + DR1P	PNP1 (DA)	0.00	0.0	0.00	0.00	0.00	0.000	0.000	0.000
DG + PI <-> GN + DR1P	PNP1 (DG)	0.00	0.0	0.00	0.00	0.00	0.000	0.000	0.000
HYXN + R1P <-> INS + PI	PNP1 (HYXN)	0.00	0.0	0.00	0.00	0.00	0.000	0.000	0.000
AD + R1P <-> PI + ADN	PNP1 (AD)	0.00	0.0	0.00	0.00	0.00	0.000	0.000	0.000
GN + R1P <-> PI + GSN	PNP1 (GN)	0.00	0.0	0.00	0.00	0.00	0.000	0.000	0.000
XAN + R1P <-> PI + XTSINE	PNP1 (XAN)	0.00	0.0	0.00	0.00	0.00	-0.031	0.000	0.000
XAN + PRPP -> XMP + PPI	XPT1	0.00	0.0	0.00	0.00	0.00	0.031	0.000	0.000

CYTD -> CYTS + RIB	URH1 (CYTD)	0.00	0.0	0.00	0.00	0.00	0.000	0.000	0.000
URI -> URA + RIB	URH1 (URI)	0.00	0.0	0.00	0.00	0.00	0.031	0.000	0.000
ADN + ATP -> AMP + ADP	ADO1	0.00	0.0	0.00	0.00	0.00	0.000	0.000	0.000
ATP + AMP <-> 2 ADP	ADK1 (ATP)	1.30	28.8	1.30	0.27	1.62	0.275	0.090	0.249
GTP + AMP <-> ADP + GDP	ADK1 (GTP)	-0.08	-1.8	-0.07	-0.06	-0.07	0.000	-0.006	0.000
ITP + AMP <-> ADP + IDP	ADK1 (ITP)	0.00	0.0	0.00	0.00	0.00	0.000	0.000	0.000
ATPm + AMPm <-> 2 ADPm	ADK2	0.00	0.0	0.00	0.00	0.00	0.000	0.000	0.000
UDP + ATP <-> UTP + ADP	YNK1 (UDP)	0.10	2.3	0.09	0.08	0.09	0.000	0.039	0.000
CDP + ATP <-> CTP + ADP	YNK1 (CDP)	0.01	0.1	0.00	0.05	0.00	0.029	0.010	0.077
DGDP + ATP <-> DGTP + ADP	YNK1 (DGDP)	0.00	0.0	0.00	0.00	0.00	0.000	0.000	0.000
DUDP + ATP <-> DUTP + ADP	YNK1 (DUDP)	0.00	0.0	0.00	0.00	0.00	0.000	0.000	0.000
DCDP + ATP <-> DCTP + ADP	YNK1 (DCDP)	0.00	0.0	0.00	0.00	0.00	0.000	0.000	0.000
DTDP + ATP <-> DTTP + ADP	YNK1 (DTDP)	0.00	0.0	0.00	0.00	0.00	0.000	0.000	0.000
DADP + ATP <-> DATP + ADP	YNK1 (DADP)	0.00	0.0	0.00	0.00	0.00	0.000	0.000	0.000
GDP + ATP <-> GTP + ADP	YNK1 (GDP)	0.00	0.0	0.00	0.00	0.00	0.000	0.000	0.000
IDP + ATP <-> ITP + ADP	YNK1 (IDP)	0.00	0.0	0.00	0.00	0.00	0.000	0.000	0.000
DAMP + ATP <-> DADP + ADP	U_16	0.00	0.0	0.00	0.00	0.00	0.000	0.000	0.000
AD -> NH3 + HYXN	AAH1	0.00	0.0	0.00	0.00	0.00	0.000	0.000	0.000
INS + ATP -> IMP + ADP	U_17	0.00	0.0	0.00	0.00	0.00	0.000	0.000	0.000
GSN + ATP -> GMP + ADP	U_18	0.00	0.0	0.00	0.00	0.00	0.000	0.000	0.000
HYXN + PRPP -> PPI + IMP	HPT1 (HYXN)	0.00	0.0	0.00	0.00	0.00	0.000	0.000	0.000
GN + PRPP -> PPI + GMP	HPT1 (GN)	0.00	0.0	0.00	0.00	0.00	0.000	0.000	0.000
URI + PI <-> URA + R1P	U_19	0.00	0.0	0.00	0.00	0.00	-0.031	0.000	0.000
DUMP + ATP <-> DUDP + ADP	URA6 (DUMP)	0.00	0.0	0.00	0.00	0.00	0.000	0.000	0.000
CMP -> CYTS + R5P	U_20	0.00	0.0	0.00	0.00	0.00	0.000	0.000	0.000
DCMP -> DUMP + NH3	DCD1	0.00	0.0	0.00	0.00	0.00	0.000	0.000	0.000
DUMP -> DU + PI	U_21	0.00	0.0	0.00	0.00	0.00	0.000	0.000	0.000
DTMP -> DT + PI	U_22	0.00	0.0	0.00	0.00	0.00	0.000	0.000	0.000
DAMP -> DA + PI	U_23	0.00	0.0	0.00	0.00	0.00	0.000	0.000	0.000
DGMP -> DG + PI	U_24	0.00	0.0	0.00	0.00	0.00	0.000	0.000	0.000
DCMP -> DC + PI	U_25	0.00	0.0	0.00	0.00	0.00	0.000	0.000	0.000
CMP -> CYTD + PI	U_26	0.00	0.0	0.00	0.00	0.00	0.000	0.000	0.000
AMP -> PI + ADN	U_27	0.00	0.0	0.00	0.00	0.00	0.000	0.000	0.000
GMP -> PI + GSN	U_28	0.00	0.0	0.00	0.00	0.00	0.000	0.000	0.000
IMP -> PI + INS	U_29	0.00	0.0	0.00	0.00	0.00	0.000	0.000	0.000
XMP -> PI + XTSINE	U_30	0.00	0.0	0.00	0.00	0.00	0.031	0.000	0.000
UMP -> PI + URI	U_31	0.00	0.0	0.00	0.00	0.00	0.000	0.000	0.000
ADP + RTHIO -> DADP + OTHIO	RNR1 / 2 / 3 / 4 (ADP)	0.00	0.0	0.00	0.00	0.00	0.000	0.000	0.000
GDP + RTHIO -> DGDP + OTHIO	RNR1 / 2 / 3 / 4 (GDP)	0.00	0.0	0.00	0.00	0.00	0.000	0.000	0.000
CDP + RTHIO -> DCDP + OTHIO	RNR1 / 2 / 3 / 4 (CDP)	0.00	0.0	0.00	0.00	0.00	0.000	0.000	0.000
UDP + RTHIO -> DUDP + OTHIO	RNR1 / 2 / 3 / 4 (UDP)	0.00	0.0	0.00	0.00	0.00	0.000	0.000	0.000
ATP + RTHIO -> DATP + OTHIO	U_32 (ATP)	0.00	0.0	0.00	0.00	0.00	0.000	0.000	0.000
GTP + RTHIO -> DGTP + OTHIO	U_32 (GTP)	0.00	0.0	0.00	0.00	0.00	0.000	0.000	0.000
CTP + RTHIO -> DCTP + OTHIO	U_32 (CTP)	0.00	0.0	0.00	0.00	0.00	0.000	0.000	0.000
UTP + RTHIO -> DUTP + OTHIO	U_32 (UTP)	0.00	0.0	0.00	0.00	0.00	0.000	0.000	0.000
GTP -> GSN + 3 PI	U_36	0.00	0.0	0.00	0.00	0.00	0.000	0.000	0.000
DGTP -> DG + 3 PI	U_37	0.00	0.0	0.00	0.00	0.00	0.000	0.000	0.000
AMP -> AD + R5P	U_38	0.00	0.0	0.00	0.00	0.00	0.000	0.000	0.000
GLU -> GABA + CO2	GAD1	0.00	0.0	0.00	0.00	0.00	0.000	0.000	0.000
GABA + AKG -> SUCCSAL + GLU	UGA1	0.00	0.0	0.00	0.00	0.00	0.000	0.000	0.000
SUCCSAL + NADP -> SUCC + NADPH	UGA2	0.00	0.0	0.00	0.00	0.00	0.000	0.000	0.000
F6P + GLN -> GLU + GA6P	GFA1	0.00	0.0	0.00	0.00	0.00	0.000	0.000	0.000
ACCOA + GA6P <-> COA + NAGA6P	GNA1	0.00	0.0	0.00	0.00	0.00	0.000	0.000	0.000
NAGA1P <-> NAGA6P	PCM1	0.00	0.0	0.00	0.00	0.00	0.000	0.000	0.000
UTP + NAGA1P <-> UDPNAG + PPI	QRI1	0.00	0.0	0.00	0.00	0.00	0.000	0.000	0.000
UDPNAG -> CHIT + UDP	CHS3	0.00	0.0	0.00	0.00	0.00	0.000	0.000	0.000
UDPNAG -> CHIT + UDP	CHS2	0.00	0.0	0.00	0.00	0.00	0.000	0.000	0.000
UDPNAG -> CHIT + UDP	CHS1	0.00	0.0	0.00	0.00	0.00	0.000	0.000	0.000
GLUGSALm + NADPm -> NADPHm + GLUm	PUT2 (GLUGSAL+NADP)	0.00	0.0	0.00	0.00	0.00	0.000	0.000	0.000
P5Cm + NADm -> NADHm + GLUm	PUT2 (P5C+NAD)	0.00	0.0	0.00	0.00	0.00	0.000	0.000	0.000
AKG + GLN + NADH -> NAD + 2 GLU	GLT1	0.00	0.0	0.00	0.00	0.00	0.000	0.000	0.000
GLU + NAD -> AKG + NH3 + NADH	GDH2	0.00	0.0	0.00	0.00	0.00	0.000	0.000	0.000
AKG + NH3 + NADPH -> GLU + NADP	GDH3	0.45	10.0	0.71	1.63	0.44	0.006	0.135	0.000
AKG + NH3 + NADPH -> GLU + NADP	GDH1	0.00	0.0	0.00	0.00	0.00	0.000	0.000	0.000
GLU + NH3 + ATP -> GLN + ADP + PI	GLN1	1.19	26.5	1.20	0.06	1.52	0.006	0.000	0.000
GLN -> GLU + NH3	U_40	0.00	0.0	0.00	0.00	0.00	0.000	0.000	0.000
ARAB + NAD -> ARABLAC + NADH	ARA2	0.00	0.0	0.00	0.00	0.00	0.000	0.000	0.000
ARAB + NADP -> ARABLAC + NADPH	ARA1	0.00	0.0	0.00	0.00	0.00	0.000	0.000	0.000
ARABLACm + O2m -> DEACm + H2O2m	ALO1	0.00	0.0	0.00	0.00	0.00	0.000	0.000	0.000
XUL + ATP -> X5P + ADP	XKS1	0.00	0.0	1.20	1.20	1.20	0.760	0.760	0.760
OAm + GLUm -> ASPm + AKGm	AAT1 (OA)	0.00	0.0	0.00	0.00	0.00	0.000	0.000	0.000
OA + GLU <-> ASP + AKG	AAT2	0.16	3.5	0.47	1.43	0.19	0.006	0.135	0.000
PYR + GLU <-> AKG + ALA	ALT2	0.00	0.0	0.00	0.00	0.00	0.000	0.000	0.000
PYRm + GLUm <-> AKGm + ALAm	ALT1	0.04	0.9	0.04	0.03	0.04	0.000	0.000	0.000
ASP + ATP + GLN -> GLU + ASN + AMP + PPI	ASN1	1.12	24.9	1.13	0.01	1.46	0.000	0.000	0.000
ASP + ATP + GLN -> GLU + ASN + AMP + PPI	ASN2	0.00	0.0	0.00	0.00	0.00	0.000	0.000	0.000
SAM + HCYS -> SAH + MET	MHT1	0.00	0.0	0.00	0.00	0.00	0.000	0.000	0.000
SAM + HCYS -> SAH + MET	SAM4	0.00	0.0	0.00	0.00	0.00	0.000	0.000	0.000
ASN -> ASP + NH3	ASP3-1	0.00	0.0	0.00	0.00	0.00	0.000	0.000	0.000
ASN -> ASP + NH3	ASP3-2	0.00	0.0	0.00	0.00	0.00	0.000	0.000	0.000

ASN -> ASP + NH3	ASP3-3	0.00	0.0	0.00	0.00	0.00	0.000	0.000	0.000
ASN -> ASP + NH3	ASP3-4	1.11	24.7	1.12	0.00	1.45	0.000	0.000	0.000
ASN -> ASP + NH3	ASP1	0.00	0.0	0.00	0.00	0.00	0.000	0.000	0.000
3PG + NAD -> NADH + PHP	SER3	0.03	0.7	0.00	0.00	0.01	0.000	0.000	0.000
3PG + NAD -> NADH + PHP	SER33	0.00	0.0	0.00	0.00	0.00	0.000	0.000	0.000
PHP + GLU -> AKG + 3PSER	SER1	0.03	0.7	0.00	0.00	0.01	0.000	0.000	0.000
3PSER -> PI + SER	SER2	0.03	0.7	0.00	0.00	0.01	0.000	0.000	0.000
THFm + SERm <-> GLYm + MYLENTHFm	SHM1	0.01	0.3	-0.15	-0.64	-0.01	0.000	-0.065	0.000
THF + SER <-> GLY + MYLENTHF	SHM2	0.00	0.0	0.00	0.00	0.00	0.000	0.000	0.000
ALA + GLX <-> PYR + GLY	AGX1	0.00	0.0	0.00	0.00	0.00	0.000	0.000	0.000
MYLENTHFm + NADHm + CO2m + NH3m	GCV1 / GCV2	0.02	0.4	0.18	0.67	0.04	0.000	0.065	0.000
ASP + ATP -> ADP + BASP	HOM3	0.08	1.7	0.40	1.37	0.11	0.000	0.129	0.000
BASP + NADPH -> NADP + PI + ASPSA	HOM2	0.08	1.7	0.40	1.37	0.11	0.000	0.129	0.000
ASPSA + NADH -> NAD + HSER	HOM6 (NADH)	0.08	1.7	0.40	1.37	0.11	0.000	0.129	0.000
ASPSA + NADPH -> NADP + HSER	HOM6 (NADPH)	0.00	0.0	0.00	0.00	0.00	0.000	0.000	0.000
HSER + ATP -> ADP + PHSER	THR1	0.07	1.6	0.39	1.36	0.11	0.000	0.129	0.000
PHSER -> PI + THR	THR4	0.07	1.6	0.39	1.36	0.11	0.000	0.129	0.000
SER + HCYS -> LLCT	CYS4	0.00	0.0	0.00	0.00	0.00	0.000	0.000	0.000
CYS + OAHSER -> LLCT + AC	YML082W	0.00	0.0	0.00	0.00	0.00	0.000	0.000	0.000
THR -> GLY + ACAL	GLY1	0.04	0.9	0.36	1.34	0.08	0.000	0.129	0.000
THR -> NH3 + OBUT	CHA1 (THR)	0.02	0.4	0.02	0.01	0.02	0.000	0.000	0.000
THRm -> NH3m + OBUTm	ILV1 (THR)	0.00	0.0	0.00	0.00	0.00	0.000	0.000	0.000
SER -> PYR + NH3	CHA1 (SER)	0.00	0.0	0.13	0.63	0.00	0.000	0.065	0.000
LLCT -> HCYS + PYR + NH3	IRC7	0.00	0.0	0.00	0.00	0.00	0.000	0.000	0.000
SAH -> HCYS + ADN	SAH1	0.00	0.0	0.00	0.00	0.00	0.000	0.000	0.000
HCYS + MTHF -> THF + MET	MET6	0.01	0.1	0.01	0.00	0.01	0.000	0.000	0.000
LLCT -> CYS + NH3 + OBUT	CYS3	0.00	0.0	0.00	0.00	0.00	0.000	0.000	0.000
ACCOA + HSER <-> COA + OAHSER	MET2	0.00	0.1	0.00	0.00	0.00	0.000	0.000	0.000
OAHSER + H2S -> AC + HCYS	MET17	0.00	0.1	0.00	0.00	0.00	0.000	0.000	0.000
LLCT -> PYR + HCYS + NH3	STR3	0.00	0.0	0.00	0.00	0.00	0.000	0.000	0.000
CYS + OAHSER -> LLCT + AC	STR2	0.00	0.0	0.00	0.00	0.00	0.000	0.000	0.000
MET + ATP -> PPI + PI + SAM	SAM2	0.00	0.0	0.00	0.00	0.00	0.000	0.000	0.000
MET + ATP -> PPI + PI + SAM	SAM1	0.00	0.0	0.00	0.00	0.00	0.000	0.000	0.000
SLF + ATP -> PPI + APS	MET3	0.01	0.1	0.01	0.00	0.01	0.000	0.000	0.000
APS + ATP -> ADP + PAPS	MET14	0.01	0.1	0.01	0.00	0.01	0.000	0.000	0.000
H2SO3 + 3 NADPH <-> H2S + 3 NADP	MET10	0.00	0.0	0.00	0.00	0.00	0.000	0.000	0.000
SER + ACCOA -> COA + ASER	U_41	0.00	0.0	0.01	0.00	0.01	0.000	0.000	0.000
ASER + H2S -> AC + CYS	YGR012W	0.00	0.0	0.01	0.00	0.01	0.000	0.000	0.000
PAP -> AMP + PI	MET22	0.01	0.1	0.01	0.00	0.01	0.000	0.000	0.000
PAPS + RTHIO -> OTHIO + H2SO3 + PAP	MET16	0.01	0.1	0.01	0.00	0.01	0.000	0.000	0.000
OICAPm + GLUm <-> AKGm + LEUm	BAT1 (LEU)	0.03	0.6	0.02	0.02	0.02	0.000	0.000	0.000
OMVALm + GLUm <-> AKGm + ILEm	BAT1 (ILE)	0.02	0.4	0.02	0.01	0.02	0.000	0.000	0.000
OMVAL + GLU <-> AKG + ILE	BAT2 (ILE)	0.00	0.0	0.00	0.00	0.00	0.000	0.000	0.000
OIVALm + GLUm <-> AKGm + VALm	BAT1 (VAL)	-0.12	-2.7	-0.12	-0.11	-0.12	0.000	0.000	0.000
OIVAL + GLU <-> AKG + VAL	BAT2 (VAL)	0.14	3.2	0.14	0.12	0.14	0.000	0.000	0.000
OICAP + GLU <-> AKG + LEU	BAT2 (LEU)	0.00	0.0	0.00	0.00	0.00	0.000	0.000	0.000
OBUTm + HTPPm <-> ABUTm + TPPm	ILV2 / 6 (OBUT_ABUT)	0.02	0.4	0.02	0.01	0.02	0.000	0.000	0.000
2 PYRm <-> CO2m + ACLACm	ILV2 / 6 (2PYR_CO2+ACLAC)	0.07	1.5	0.06	0.05	0.06	0.000	0.000	0.000
ACLACm + NADPHm -> NADPm + DHIVALm	ILV5 (ACLAC whole)	0.05	1.1	0.04	0.04	0.04	0.000	0.000	0.000
ABUTm + NADPHm -> NADPm + DHMVALm	ILV5 (ABUT whole)	0.00	0.0	0.00	0.00	0.00	0.000	0.000	0.000
DHIVALm -> OIVALm	ILV3 (DHIVAL)	0.05	1.1	0.04	0.04	0.04	0.000	0.000	0.000
DHMVALm -> OMVALm	ILV3 (DHMVAL)	0.02	0.4	0.02	0.01	0.02	0.000	0.000	0.000
ACCOAm + OIVALm -> COAm + IPPMALm	LEU4 (m)	0.03	0.6	0.02	0.02	0.02	0.000	0.000	0.000
CHICAP <-> IPPMAL	LEU1 (whole)	0.00	0.0	0.00	0.00	0.00	0.000	0.000	0.000
CHICAP + NAD -> NADH + IPOSUCC	LEU2	0.03	0.6	0.02	0.02	0.02	0.000	0.000	0.000
HCITm <-> HACNm	LYS4 (first half)	0.02	0.6	0.02	0.02	0.02	0.000	0.000	0.000
HACNm <-> HICITm	LYS4 (second half)	0.02	0.6	0.02	0.02	0.02	0.000	0.000	0.000
HICITm + NADm <-> AKAm + CO2m + NADHm	LYS12	0.02	0.6	0.02	0.02	0.02	0.000	0.000	0.000
AKA + GLU <-> AMA + AKG	U_42	0.02	0.6	0.02	0.02	0.02	0.000	0.000	0.000
AMA + NADPH + ATP -> AMASA + NADP + AMP + PPI	LYS2 / 5	0.02	0.6	0.02	0.02	0.02	0.000	0.000	0.000
GLU + AMASA + NADPH <-> SACP + NADP	LYS9	0.02	0.6	0.02	0.02	0.02	0.000	0.000	0.000
SACP + NAD <-> LYS + AKG + NADH	LYS1	0.02	0.6	0.02	0.02	0.02	0.000	0.000	0.000
GLUm + ACCOAm -> COAm + NAGLUm	ARG2	0.00	0.0	0.00	0.00	0.00	0.000	0.000	0.000
GLUm + ACCOAm -> COAm + NAGLUm	ECM40 (ACCOA)	0.00	0.0	0.00	0.00	0.00	0.000	0.000	0.000
NAGLUm + ATPm -> ADPm + NAGLUPm	ARG5,6 (first half)	0.01	0.3	0.03	0.02	0.03	0.000	0.000	0.000
NAGLUPm + NADPHm -> NADPm + PIm + NAGLUSm	ARG5,6 (second half)	0.01	0.3	0.03	0.02	0.03	0.000	0.000	0.000
NAGLUSm + GLUm -> AKGm + NAORNm	ARG8	0.01	0.3	0.03	0.02	0.03	0.000	0.000	0.000
NAORNm + GLUm -> ORNm + NAGLUm	ECM40 (ORN)	0.01	0.3	0.03	0.02	0.03	0.000	0.000	0.000
GLN + 2 ATP + CO2 -> GLU + CAP + 2 ADP + PI	URA2 (GLN+CO2)	0.02	0.5	0.02	0.02	0.02	0.006	0.000	0.000
GLN + 2 ATP + CO2 -> GLU + CAP + 2 ADP + PI	CPA1 / 2	0.00	0.0	0.00	0.00	0.00	0.000	0.000	0.000
ORN + CAP -> CITR + PI	ARG3	0.01	0.3	0.01	0.01	0.01	0.006	0.000	0.000
ORN + AKG -> GLUGSAL + GLU	CAR2	0.00	0.0	0.01	0.01	0.01	0.000	0.000	0.000

CITR + ASP + ATP <-> AMP + PPI + ARGSUCC	ARG1	0.01	0.3	0.01	0.01	0.01	0.006	0.000	0.000
ARGSUCC <-> FUM + ARG	ARG4	0.01	0.3	0.01	0.01	0.01	0.006	0.000	0.000
ORN -> PTRSC + CO2	SPE1	0.00	0.0	0.00	0.00	0.00	0.000	0.000	0.000
SAM <-> DSAM + CO2	SPE2	0.00	0.0	0.00	0.00	0.00	0.000	0.000	0.000
PTRSC + DSAM -> SPRMD + 5MTA	SPE3	0.00	0.0	0.00	0.00	0.00	0.000	0.000	0.000
DSAM + SPRMD -> 5MTA + SPRM	SPE4	0.00	0.0	0.00	0.00	0.00	0.000	0.000	0.000
5MTA + GLN + ATP -> MET + AKG + ADP + PI	U_43	0.00	0.0	0.00	0.00	0.00	0.000	0.000	0.000
ARG -> ORN + UREA	CAR1	0.00	0.0	0.00	0.00	0.00	0.006	0.000	0.000
PRPP + ATP -> PPI + PRBATP	HIS1	0.01	0.1	0.01	0.00	0.01	0.000	0.000	0.000
PRBATP -> PPI + PRBAMP	HIS4 (first half)	0.01	0.1	0.01	0.00	0.01	0.000	0.000	0.000
PRBAMP -> PRFP	HIS4 (second half)	0.01	0.1	0.01	0.00	0.01	0.000	0.000	0.000
PRFP -> PRLP	HIS6	0.01	0.1	0.01	0.00	0.01	0.000	0.000	0.000
DIMGP -> IMACP	HIS3	0.01	0.1	0.01	0.00	0.01	0.000	0.000	0.000
IMACP + GLU -> AKG + HISOLP	HIS5 (IMACP)	0.01	0.1	0.01	0.00	0.01	0.000	0.000	0.000
HISOLP -> PI + HISOL	HIS2	0.01	0.1	0.01	0.00	0.01	0.000	0.000	0.000
HISOL + 2 NAD -> HIS + 2 NADH	HIS4 (HISOL)	0.01	0.1	0.01	0.00	0.01	0.000	0.000	0.000
PRLP + GLN -> GLU + AICAR + DIMGP	HIS7	0.01	0.1	0.01	0.00	0.01	0.000	0.000	0.000
E4P + PEP -> PI + 3DDAH7P	ARO4	0.02	0.5	0.02	0.02	0.02	0.000	0.000	0.000
E4P + PEP -> PI + 3DDAH7P	ARO3	0.00	0.0	0.00	0.00	0.00	0.000	0.000	0.000
3DDAH7P -> DQT + PI	ARO1 (3DDAH7P)	0.02	0.5	0.02	0.02	0.02	0.000	0.000	0.000
DQT -> DHSK	ARO1 (DQT)	0.02	0.5	0.02	0.02	0.02	0.000	0.000	0.000
DHSK + NADPH -> SME + NADP	ARO1 (DHSK)	0.02	0.5	0.02	0.02	0.02	0.000	0.000	0.000
SME + ATP -> ADP + SME3P	ARO1 (SME)	0.02	0.5	0.02	0.02	0.02	0.000	0.000	0.000
SME3P + PEP -> 3PSME + PI	ARO1 (SME3P)	0.02	0.5	0.02	0.02	0.02	0.000	0.000	0.000
3PSME -> PI + CHOR	ARO2	0.02	0.5	0.02	0.02	0.02	0.000	0.000	0.000
CHOR -> PHEN	ARO7	0.02	0.5	0.02	0.02	0.02	0.000	0.000	0.000
PHEN -> CO2 + PHPYR	PHA2	0.01	0.3	0.01	0.01	0.01	0.000	0.000	0.000
PHPYR + GLU <-> AKG + PHE	AAT1 (PHPYR)	0.00	0.0	0.00	0.00	0.00	0.000	0.000	0.000
PHPYR + GLU <-> AKG + PHE	HIS5 (PHPYR)	0.01	0.3	0.01	0.01	0.01	0.000	0.000	0.000
PHEN + NADP -> 4HPP + CO2 + NADPH	TYR1	0.01	0.2	0.01	0.01	0.01	0.000	0.000	0.000
4HPP + GLU -> AKG + TYR	ARO8	0.01	0.2	0.01	0.01	0.01	0.000	0.000	0.000
4HPP + GLU -> AKG + TYR	ARO9	0.00	0.0	0.00	0.00	0.00	0.000	0.000	0.000
PHEN + NAD -> 4HPP + CO2 + NADH	U_44	0.00	0.0	0.00	0.00	0.00	0.000	0.000	0.000
CHOR + GLN -> GLU + PYR + AN	TRP2	0.00	0.1	0.00	0.00	0.00	0.000	0.000	0.000
AN + PRPP -> PPI + NPRAN	TRP4	0.00	0.1	0.00	0.00	0.00	0.000	0.000	0.000
NPRAN -> CPAD5P	TRP1	0.00	0.1	0.00	0.00	0.00	0.000	0.000	0.000
CPAD5P -> CO2 + IGP	TRP3	0.00	0.1	0.00	0.00	0.00	0.000	0.000	0.000
IGP + SER -> GAP + TRP	TRP5	0.00	0.1	0.00	0.00	0.00	0.000	0.000	0.000
2 H2O2 -> O2	CTA1	0.00	0.0	0.00	0.00	0.00	0.000	0.000	0.000
2 H2O2 -> O2	CTT1	0.00	0.0	0.00	0.00	0.00	0.000	0.000	0.000
ACALm + NADm -> NADHm + ACm	ALD4 (NAD)	0.00	0.0	0.00	0.00	0.00	0.000	0.000	0.000
ACALm + NADPm -> NADPHm + ACm	ALD4 (NADP)	0.00	0.0	0.00	0.00	0.00	0.000	0.000	0.000
ACALm + NADPm -> NADPHm + ACm	ALD5	0.00	0.0	0.00	0.00	0.00	0.000	0.000	0.000
ACAL + NADP -> NADPH + AC	ALD6	0.00	0.0	0.00	0.13	0.00	0.262	0.127	0.274
TRP + O2 -> FKYN	BNA2	0.00	0.0	0.00	0.00	0.00	0.000	0.000	0.000
FKYN -> FOR + KYN	BNA3	0.00	0.0	0.00	0.00	0.00	0.000	0.000	0.000
KYN -> ALA + AN	BNA5 (KYN)	0.00	0.0	0.00	0.00	0.00	0.000	0.000	0.000
KYN + NADPH + O2 -> HKYN + NADP	BNA4	0.00	0.0	0.00	0.00	0.00	0.000	0.000	0.000
HKYN -> HAN + ALA	BNA5 (HKYN)	0.00	0.0	0.00	0.00	0.00	0.000	0.000	0.000
HAN + O2 -> CMUSA	BNA1	0.00	0.0	0.00	0.00	0.00	0.000	0.000	0.000
GLU + ATP -> ADP + GLUP	PRO1	0.01	0.3	0.00	0.00	0.00	0.000	0.000	0.000
GLU + ATP -> ADP + GLUP	YHR033W	0.00	0.0	0.00	0.00	0.00	0.000	0.000	0.000
GLUP + NADH -> NAD + PI + GLUGSAL	PRO2 (NAD)	0.00	0.0	0.00	0.00	0.00	0.000	0.000	0.000
GLUP + NADPH -> NADP + PI + GLUGSAL	PRO2 (NADP)	0.01	0.3	0.00	0.00	0.00	0.000	0.000	0.000
GLUGSAL <-> P5C	U_45	0.01	0.3	0.01	0.01	0.01	0.000	0.000	0.000
GLUGSALm <-> P5Cm	U_46	0.00	0.0	0.00	0.00	0.00	0.000	0.000	0.000
P5C + NADPH -> PRO + NADP	PRO3 (NADP)	0.00	0.0	0.00	0.00	0.00	0.000	0.000	0.000
PROm + NADm -> P5Cm + NADHm	PUT1	0.00	0.0	0.00	0.00	0.00	0.000	0.000	0.000
CYS + GLU + ATP -> GC + PI + ADP	GSH1	0.00	0.0	0.00	0.00	0.00	0.000	0.000	0.000
GLY + GC + ATP -> RGT + PI + ADP	GSH2	0.00	0.0	0.00	0.00	0.00	0.000	0.000	0.000
2 RGT + H2O2 <-> OGT	GPX2	0.00	0.0	0.00	0.00	0.00	0.000	0.000	0.000
2 RGT + H2O2 <-> OGT	HYR1	0.00	0.0	0.00	0.00	0.00	0.000	0.000	0.000
2 RGT + H2O2 <-> OGT	GPX1	0.00	0.0	0.00	0.00	0.00	0.000	0.000	0.000
2 RGT + H2O2 <-> OGT	GRX1	0.00	0.0	0.00	0.00	0.00	0.000	0.000	0.000
2 RGT + H2O2 <-> OGT	GRX2	0.00	0.0	0.00	0.00	0.00	0.000	0.000	0.000
2 RGT + H2O2 <-> OGT	GRX3	0.00	0.0	0.00	0.00	0.00	0.000	0.000	0.000
2 RGT + H2O2 <-> OGT	GRX4	0.00	0.0	0.00	0.00	0.00	0.000	0.000	0.000
2 RGT + H2O2 <-> OGT	GRX5	0.00	0.0	0.00	0.00	0.00	0.000	0.000	0.000
RGT + MTHGXL <-> LGT	GLO1	0.08	1.8	0.12	0.12	0.12	0.006	0.006	0.006
DHAP <-> MTHGXL + PI	U_47	0.08	1.8	0.12	0.12	0.12	0.006	0.006	0.006
LGT -> RGT + LAC	GLO2	0.08	1.8	0.12	0.12	0.12	0.006	0.006	0.006
LGTm -> RGTm + LACm	GLO4	0.00	0.0	0.00	0.00	0.00	0.000	0.000	0.000
LACAL + NADP <-> MTHGXL + NADPH	GRE2	0.00	0.0	0.00	0.00	0.00	0.000	0.000	0.000
NADPH + OGT -> NADP + 2 RGT	GLR1	0.00	0.0	0.00	0.00	0.00	0.000	0.000	0.000
UDPG -> 13GLUCAN + UDP	GSC2	0.10	2.2	0.09	0.08	0.09	0.000	0.000	0.000
UDPG -> 13GLUCAN + UDP	FKS1	0.00	0.0	0.00	0.00	0.00	0.000	0.000	0.000
UDPG -> 13GLUCAN + UDP	FKS3	0.00	0.0	0.00	0.00	0.00	0.000	0.000	0.000
13GLUCAN -> GLC	EXG2	0.00	0.0	0.00	0.00	0.00	0.000	0.000	0.000
13GLUCAN -> GLC	BGL2	0.00	0.0	0.00	0.00	0.00	0.000	0.000	0.000
13GLUCAN -> GLC	EXG1	0.00	0.0	0.00	0.00	0.00	0.000	0.000	0.000
13GLUCAN -> GLC	SPR1	0.00	0.0	0.00	0.00	0.00	0.000	0.000	0.000
GDPMAN + DOLP -> GDP + DOLMANP	DPM1	0.07	1.6	0.06	0.05	0.06	0.000	0.000	0.000
DOLMANP -> DOLP + MANNAN	PMT2	0.00	0.0	0.00	0.00	0.00	0.000	0.000	0.000
DOLMANP -> DOLP + MANNAN	PMT5	0.00	0.0	0.00	0.00	0.00	0.000	0.000	0.000
DOLMANP -> DOLP + MANNAN	PMT1	0.00	0.0	0.00	0.00	0.00	0.000	0.000	0.000

DOLMANP -> DOLP + MANNAN	PMT6	0.07	1.6	0.06	0.05	0.06	0.000	0.000	0.000
DOLMANP -> DOLP + MANNAN	PMT4	0.00	0.0	0.00	0.00	0.00	0.000	0.000	0.000
DOLMANP -> DOLP + MANNAN	PMT3	0.00	0.0	0.00	0.00	0.00	0.000	0.000	0.000
GL3P -> GL + PI	HOR2	0.70	15.6	0.27	0.27	0.27	0.039	0.039	0.039
GL3P -> GL + PI	RHR2	0.00	0.0	0.00	0.00	0.00	0.000	0.000	0.000
CHIT -> CHITO + AC	CDA1	0.00	0.0	0.00	0.00	0.00	0.000	0.000	0.000
CHIT -> CHITO + AC	CDA2	0.00	0.0	0.00	0.00	0.00	0.000	0.000	0.000
DHA + NADPH <-> GL + NADP	YPR1	0.00	0.0	0.00	0.00	0.00	0.000	0.000	0.000
DHA + NADPH <-> GL + NADP	GCY1	0.00	0.0	0.00	0.00	0.00	0.000	0.000	0.000
DHA + ATP -> DHAP + ADP	DAK2	0.00	0.0	0.00	0.00	0.00	0.000	0.000	0.000
DHA + ATP -> DHAP + ADP	DAK1	0.00	0.0	0.00	0.00	0.00	0.000	0.000	0.000
DHAP + NADH -> GL3P + NAD	GPD1	0.70	15.6	0.27	0.27	0.27	0.082	0.054	0.082
DHAP + NADH -> GL3P + NAD	GPD2	0.00	0.0	0.00	0.00	0.00	0.000	0.000	0.000
GL + ATP -> GL3P + ADP	GUT1	0.00	0.0	0.00	0.00	0.00	0.000	0.000	0.000
GL3P + FADm -> DHAP + FADH2m	GUT2	0.00	0.0	0.00	0.00	0.00	0.000	0.000	0.000
DAGLY + 0.017 C100COA + 0.062 C120COA + 0.100 C140COA + 0.270 C160COA + 0.169 C161COA + 0.055 C180COA + 0.235 C181COA + 0.093 C182COA -> TAGLY + COA	DGA1	0.00	0.0	0.00	0.00	0.00	0.000	0.000	0.000
ATP + THIAMIN -> AMP + TPP	THI80 (THIAMIN)	0.00	0.0	0.00	0.00	0.00	0.000	0.000	0.000
ATP + TPP -> ADP + TPPP	THI80 (TPP)	0.00	0.0	0.00	0.00	0.00	0.000	0.000	0.000
AIR -> AHM + GLAL	U_49	0.00	0.0	0.00	0.00	0.00	0.000	0.000	0.000
AHM + ATP -> AHMP + ADP	THI20 (AHM)	0.00	0.0	0.00	0.00	0.00	0.000	0.000	0.000
AHM + ATP -> AHMP + ADP	THI21	0.00	0.0	0.00	0.00	0.00	0.000	0.000	0.000
AHM + ATP -> AHMP + ADP	THI22	0.00	0.0	0.00	0.00	0.00	0.000	0.000	0.000
AHMP + ATP -> AHMPP + ADP	THI20 (AHMP)	0.00	0.0	0.00	0.00	0.00	0.000	0.000	0.000
GAP + PYR -> DTP + CO2	U_50	0.00	0.0	0.00	0.00	0.00	0.000	0.000	0.000
ASER + CYS + GLY + DTP -> GABA + THZP + AC + 4 CO2 + NH3	U_51	0.00	0.0	0.00	0.00	0.00	0.000	0.000	0.000
THZ + ATP -> THZP + ADP	THI6 (first half)	0.00	0.0	0.00	0.00	0.00	0.000	0.000	0.000
THZP + AHMPP -> THMP + PPI	THI6 (second half)	0.00	0.0	0.00	0.00	0.00	0.000	0.000	0.000
THMP + ATP <-> TPP + ADP	U_52	0.00	0.0	0.00	0.00	0.00	0.000	0.000	0.000
THMP -> THIAMIN + PI	U_53	0.00	0.0	0.00	0.00	0.00	0.000	0.000	0.000
GTP -> D6RSP5P + FOR + PPI	RIB1	0.00	0.0	0.00	0.00	0.00	0.000	0.000	0.000
D6RSP5P + NADPH -> D6RTP5P + NADP	RIB7	0.00	0.0	0.00	0.00	0.00	0.000	0.000	0.000
D6RTP5P -> A6RP5P2 + NH3	RIB2	0.00	0.0	0.00	0.00	0.00	0.000	0.000	0.000
RL5P -> DB4P + FOR	RIB3	0.00	0.0	0.00	0.00	0.00	0.000	0.000	0.000
DB4P + A6RP5P2 -> D8RL + PI	RIB4	0.00	0.0	0.00	0.00	0.00	0.000	0.000	0.000
2 D8RL -> RIBFLAV + RADP	RIB5	0.00	0.0	0.00	0.00	0.00	0.000	0.000	0.000
RIBFLAV + ATP -> FMN + ADP	FMN1	0.00	0.0	0.00	0.00	0.00	0.000	0.000	0.000
RIBFLAVm + ATPm -> FMNm + ADPm	FMN1 (m)	0.00	0.0	0.00	0.00	0.00	0.000	0.000	0.000
FMN + ATP -> FAD + PPI	FAD1	0.00	0.0	0.00	0.00	0.00	0.000	0.000	0.000
FMNm + ATPm -> FADm + PPIm	U_54	0.00	0.0	0.00	0.00	0.00	0.000	0.000	0.000
PYRDX + ATP -> PYRDXP + ADP	U_55	0.00	0.0	0.00	0.00	0.00	0.000	0.000	0.000
PYRDXA + ATP -> PYRDXAP + ADP	U_56	0.00	0.0	0.00	0.00	0.00	0.000	0.000	0.000
PYRDXL + ATP -> PYRDXLP + ADP	U_57	0.00	0.0	0.00	0.00	0.00	0.000	0.000	0.000
PYRDXAP + O2 -> PYRDXLP + H2O2 + NH3	PDX3 (PYRDXAP)	0.00	0.0	0.00	0.00	0.00	0.000	0.000	0.000
PYRDXP + O2 -> PYRDXLP + H2O2	PDX3 (PYRDXP)	0.00	0.0	0.00	0.00	0.00	0.000	0.000	0.000
PYRDX + O2 -> PYRDXL + H2O2	PDX3 (PYRDX)	0.00	0.0	0.00	0.00	0.00	0.000	0.000	0.000
PYRDXA + O2 -> PYRDXL + H2O2 + NH3	PDX3 (PYRDXA)	0.00	0.0	0.00	0.00	0.00	0.000	0.000	0.000
PYRDXAP -> PYRDXA + PI	U_58	0.00	0.0	0.00	0.00	0.00	0.000	0.000	0.000
3 MALCOA -> CHCOA + 2 COA + 2 CO2	U_59	0.00	0.0	0.00	0.00	0.00	0.000	0.000	0.000
ALA + CHCOA <-> CO2 + COA + AONA	U_60	0.00	0.0	0.00	0.00	0.00	0.000	0.000	0.000
SAM + AONA <-> SAMOB + DANNA	BIO3	0.00	0.0	0.00	0.00	0.00	0.000	0.000	0.000
CO2 + DANNA + ATP <-> DTB + PI + ADP	BIO4	0.00	0.0	0.00	0.00	0.00	0.000	0.000	0.000
DTB + CYS + 2 SAM <-> BT + ALA + 2 MET + 2 DA	BIO2	0.00	0.0	0.00	0.00	0.00	0.000	0.000	0.000
GTP -> FOR + AHTDPTP	FOL2	0.00	0.0	0.00	0.00	0.00	0.000	0.000	0.000
AHTDPTP -> PPI + DHNPTERP	U_61	0.00	0.0	0.00	0.00	0.00	0.000	0.000	0.000
AHTDPTP -> DHNPTER + 3 PI	PHO8	0.00	0.0	0.00	0.00	0.00	0.000	0.000	0.000
DHNPTERP -> DHNPTER + PI	U_62	0.00	0.0	0.00	0.00	0.00	0.000	0.000	0.000
DHNPTER -> AHHDP + GLAL	FOL1 (DHNPTER)	0.00	0.0	0.00	0.00	0.00	0.000	0.000	0.000
AHHDP + ATP -> AMP + AHHDPPP	FOL1 (AHHDP)	0.00	0.0	0.00	0.00	0.00	0.000	0.000	0.000
CHOR + GLN -> ADCHOR + GLU	ABZ1	0.00	0.0	0.00	0.00	0.00	0.000	0.000	0.000
ADCHOR -> PYR + PABA	ABZ2	0.00	0.0	0.00	0.00	0.00	0.000	0.000	0.000
PABA + AHHDPPP -> PPI + DHPTERA	FOL1 (AHHDPPP)	0.00	0.0	0.00	0.00	0.00	0.000	0.000	0.000
PABA + AHHDP -> DHPTERA	FOL1 (PABA+AHHDP)	0.00	0.0	0.00	0.00	0.00	0.000	0.000	0.000
DHPTERA + ATP + GLU -> ADP + PI + DHF	FOL3	0.00	0.0	0.00	0.00	0.00	0.000	0.000	0.000
DHFm + NADPHm -> NADPm + THFm	DFR1 (NADPm)	0.00	0.0	0.00	0.00	0.00	0.000	0.000	0.000
DHF + NADPH -> NADP + THF	DFR1 (NADP)	0.00	0.0	0.00	0.00	0.00	0.000	0.000	0.000
ATPm + FTHFm -> ADPm + PIm + MTHFm	U_63	0.00	0.0	0.00	0.00	0.00	0.000	0.000	0.000
ATP + FTHF -> ADP + PI + MTHF	U_64	0.01	0.1	0.00	0.00	0.00	0.000	0.000	0.000
THF + ATP + GLU -> ADP + PI + THFG	RMA1	0.00	0.0	0.00	0.00	0.00	0.000	0.000	0.000
THF + ATP + GLU -> ADP + PI + THFG	MET7	0.00	0.0	0.00	0.00	0.00	0.000	0.000	0.000
MYLENTHF + NADPH -> NADP + MTHF	MET12	0.00	0.0	0.01	0.00	0.01	0.000	0.000	0.000
MYLENTHFm + NADPHm -> NADPm + MTHFm	MET13	0.00	0.0	0.00	0.00	0.00	0.000	0.000	0.000
MYLENTHFm + NADPm <-> MENYLTHFm + NADPHm	MIS1 (MYLENTHFm)	0.00	0.0	0.00	0.00	0.00	0.000	0.000	0.000
MYLENTHF + NADP <-> MENYLTHF + NADPH	ADE3 (NADP)	0.03	0.7	0.02	0.02	0.02	0.000	0.000	0.000

THFm + FORm + ATPm -> ADPm + PIm + FTHFm	MIS1 (THFm)	0.00	0.0	0.00	0.00	0.00	0.000	0.000	0.000
FORm <-> FOR	U_65	0.00	0.0	0.00	0.00	0.00	0.000	0.000	0.000
THF + FOR + ATP -> ADP + PI + FTHF	ADE3 (THF)	0.00	0.0	0.00	0.00	0.00	0.000	0.000	0.000
MENYLTHFm <-> FTHFm	MIS1 (MENYLTHFm)	0.00	0.0	0.00	0.00	0.00	0.000	0.000	0.000
MENYLTHF <-> FTHF	ADE3 (MENYLTHF)	0.03	0.7	0.02	0.02	0.02	0.000	0.000	0.000
MYLENTHF + NAD -> MENYLTHF + NADH	MTD1	0.00	0.0	0.00	0.00	0.00	0.000	0.000	0.000
OIVAL + MYLENTHF -> DHPAN + THF	ECM31	0.00	0.0	0.00	0.00	0.00	0.000	0.000	0.000
DHPAN + NADPH -> NADP + PANT	PAN5	0.00	0.0	0.00	0.00	0.00	0.000	0.000	0.000
PANT + bALA + ATP -> AMP + PPI + PNTO	PAN6	0.00	0.0	0.00	0.00	0.00	0.000	0.000	0.000
PNTO + ATP -> ADP + 4PPNTO	YDR531W	0.00	0.0	0.00	0.00	0.00	0.000	0.000	0.000
4PPNTO + CTP + CYS -> CMP + PPI + 4PPNCYS	YIL083C	0.00	0.0	0.00	0.00	0.00	0.000	0.000	0.000
4PPNCYS -> CO2 + 4PPNTE	SIS2	0.00	0.0	0.00	0.00	0.00	0.000	0.000	0.000
4PPNCYS -> CO2 + 4PPNTE	VHS3	0.00	0.0	0.00	0.00	0.00	0.000	0.000	0.000
4PPNCYS -> CO2 + 4PPNTE	YKL088W	0.00	0.0	0.00	0.00	0.00	0.000	0.000	0.000
4PPNTE + ATP -> PPI + DPCOA	YGR277C	0.00	0.0	0.00	0.00	0.00	0.000	0.000	0.000
4PPNTEm + ATPm -> PPIm + DPCOAm	U_66	0.00	0.0	0.00	0.00	0.00	0.000	0.000	0.000
DPCOA + ATP -> ADP + COA	YDR196C	0.00	0.0	0.00	0.00	0.00	0.000	0.000	0.000
DPCOAm + ATPm -> ADPm + COAm	U_67	0.00	0.0	0.00	0.00	0.00	0.000	0.000	0.000
COA -> PAP + ACP	PPT2	0.00	0.0	0.00	0.00	0.00	0.000	0.000	0.000
SPRM + O2 -> SPRMD + 3AP + H2O2	FMS1	0.00	0.0	0.00	0.00	0.00	0.000	0.000	0.000
3AP + NAD -> bALA + NADH	ALD2	0.00	0.0	0.00	0.00	0.00	0.000	0.000	0.000
3AP + NAD -> bALA + NADH	ALD3	0.00	0.0	0.00	0.00	0.00	0.000	0.000	0.000
NAD -> AMP + NAMN	NPY1	0.00	0.0	0.00	0.00	0.00	0.000	0.000	0.000
NAMN -> R5P + NAM	U_68	0.00	0.0	0.00	0.00	0.00	0.000	0.000	0.000
NAM <-> NAC + NH3	PNC1	0.00	0.0	0.00	0.00	0.00	0.000	0.000	0.000
NAC + PRPP -> NACN + PPI	NPT1	0.00	0.0	0.00	0.00	0.00	0.000	0.000	0.000
CMUSA -> QA	U_69	0.00	0.0	0.00	0.00	0.00	0.000	0.000	0.000
QA + PRPP -> NACN + CO2 + PPI	BNA6	0.00	0.0	0.00	0.00	0.00	0.000	0.000	0.000
NAMN <-> NACN + NH3	U_70	0.00	0.0	0.00	0.00	0.00	0.000	0.000	0.000
NACN + ATP -> PPI + NAAD	NMA2	0.00	0.0	0.00	0.00	0.00	0.000	0.000	0.000
NACN + ATP -> PPI + NAAD	NMA1	0.00	0.0	0.00	0.00	0.00	0.000	0.000	0.000
NAAD + ATP + GLN -> NAD + AMP + PPI + GLU	QNS1	0.00	0.0	0.00	0.00	0.00	0.000	0.000	0.000
NAD + ATP -> NADP + ADP	UTR1	0.00	0.0	0.00	0.00	0.00	0.000	0.000	0.000
NAD + ATP -> NADP + ADP	YEF1	0.00	0.0	0.00	0.00	0.00	0.000	0.000	0.000
NADP -> NAD + PI	U_71	0.00	0.0	0.00	0.00	0.00	0.000	0.000	0.000
GSN + PI <-> GN + R1P	PNP1 (GSN)	0.00	0.0	0.00	0.00	0.00	0.000	0.000	0.000
QAm + PRPPm -> NACNm + CO2m + PPIm	BNA6 (m)	0.00	0.0	0.00	0.00	0.00	0.000	0.000	0.000
NACNm + ATPm -> PPIm + NAADm	NMA1 (m)	0.00	0.0	0.00	0.00	0.00	0.000	0.000	0.000
NAADm + ATPm + GLNm -> NADm + AMPm + PPIm + GLUm	QNS1 (m)	0.00	0.0	0.00	0.00	0.00	0.000	0.000	0.000
NADm + ATPm -> NADPm + ADPm	POS5	0.00	0.0	0.00	0.00	0.00	0.000	0.000	0.000
NADPm -> NADm + PIm	U_73	0.00	0.0	0.00	0.00	0.00	0.000	0.000	0.000
GSN + PI <-> GN + R1P	PNP1 (m)	0.00	0.0	0.00	0.00	0.00	0.000	0.000	0.000
SUCCCOAm + GLYm -> ALVm + COAm + CO2m	HEM1	0.00	0.0	0.00	0.00	0.00	0.000	0.000	0.000
ALV <-> ALVm	U_74	0.00	0.0	0.00	0.00	0.00	0.000	0.000	0.000
2 ALV -> PBG	HEM2	0.00	0.0	0.00	0.00	0.00	0.000	0.000	0.000
4 PBG -> HMB + 4 NH3	HEM3	0.00	0.0	0.00	0.00	0.00	0.000	0.000	0.000
HMB -> UPRG	HEM4	0.00	0.0	0.00	0.00	0.00	0.000	0.000	0.000
UPRG -> 4 CO2 + CPP	HEM12	0.00	0.0	0.00	0.00	0.00	0.000	0.000	0.000
O2 + CPP + NADPH -> 2 CO2 + PPPHG + NADP	HEM13	0.00	0.0	0.00	0.00	0.00	0.000	0.000	0.000
PPPHG <-> PPPHGm	U_75	0.00	0.0	0.00	0.00	0.00	0.000	0.000	0.000
3 O2m + 2 PPPHGm -> 2 PPPHm	HEM14	0.00	0.0	0.00	0.00	0.00	0.000	0.000	0.000
PPPHm -> PTHm	HEM15	0.00	0.0	0.00	0.00	0.00	0.000	0.000	0.000
FPPm + IPPPm -> GGPPm + PPIm	BTS1	0.00	0.0	0.00	0.00	0.00	0.000	0.000	0.000
GGPPm + IPPPm -> GFPPm + PPIm	U_76	0.00	0.0	0.00	0.00	0.00	0.000	0.000	0.000
GFPPm + IPPPm -> HPPm + PPIm	COQ1	0.00	0.0	0.00	0.00	0.00	0.000	0.000	0.000
FPP <-> FPPm	U_77	0.00	0.0	0.00	0.00	0.00	0.000	0.000	0.000
CHOR <-> CHORm	U_78	0.00	0.0	0.00	0.00	0.00	0.000	0.000	0.000
CHORm -> 4HBZm + PYRm	U_79	0.00	0.0	0.00	0.00	0.00	0.000	0.000	0.000
4HBZm + HPPm -> H4HBZm + PPIm	COQ2	0.00	0.0	0.00	0.00	0.00	0.000	0.000	0.000
H4HBZm + O2m + NADPHm -> D4HBZm + NADPm	U_80	0.00	0.0	0.00	0.00	0.00	0.000	0.000	0.000
D4HBZm + SAMm -> M4HBZm + SAHm	COQ3 (D4HBZ)	0.00	0.0	0.00	0.00	0.00	0.000	0.000	0.000
M4HBZm -> 2HPMPm + CO2m	U_81	0.00	0.0	0.00	0.00	0.00	0.000	0.000	0.000
2HPMPm + O2m -> 2HPMBm	COQ6	0.00	0.0	0.00	0.00	0.00	0.000	0.000	0.000
2HPMBm + SAMm -> 2HPMMBm + SAHm	COQ5	0.00	0.0	0.00	0.00	0.00	0.000	0.000	0.000
2HPMMBm + O2m + NADPHm -> 2HMHMBm + NADPm	CAT5	0.00	0.0	0.00	0.00	0.00	0.000	0.000	0.000
2HMHMBm + SAMm -> QH2m + SAHm	COQ3 (2HMHMB)	0.00	0.0	0.00	0.00	0.00	0.000	0.000	0.000
O2 <-> O2m	U_82	0.00	0.0	0.00	0.00	0.00	0.000	0.000	0.000
CO2 <-> CO2m	U_83	-0.41	-9.1	-0.55	-0.85	-0.40	-0.200	-0.200	-0.077
ETH <-> ETHm	U_84	-0.17	-3.8	-0.31	-0.64	-0.17	0.200	0.071	0.071
ACAL <-> ACALm	U_85	0.17	3.8	0.31	0.64	0.17	-0.200	-0.071	-0.071
NH3 <-> NH3m	U_86	-0.02	-0.4	-0.18	-0.67	-0.04	0.000	-0.065	0.000
THFm <-> THF	U_87	-0.03	-0.7	-0.03	-0.02	-0.03	0.000	0.000	0.000
MYLENTHFm <-> MYLENTHF	U_88	0.03	0.7	0.03	0.02	0.03	0.000	0.000	0.000
SERm <-> SER	U_89	-0.01	-0.3	0.15	0.64	0.01	0.000	0.065	0.000
GLYm <-> GLY	U_90	0.00	-0.1	-0.33	-1.31	-0.05	0.000	-0.129	0.000

OICAPm <-> OICAP	U_91	-0.03	-0.6	-0.02	-0.02	-0.02	0.000	0.000	0.000
PROm <-> PRO	U_92	0.00	0.0	0.00	0.00	0.00	0.000	0.000	0.000
CMPm <-> CMP	U_93	0.00	0.0	0.00	0.00	0.00	0.000	0.000	0.000
ACm <-> AC	ADY2 (ACm)	0.00	0.0	0.00	0.00	0.00	0.000	0.000	0.000
THRm <-> THR	U_95	0.00	0.0	0.00	0.00	0.00	0.000	0.000	0.000
AKAm -> AKA	U_96	0.00	0.0	0.00	0.00	0.00	0.000	0.000	0.000
VALm <-> VAL	U_97	-0.12	-2.7	-0.12	-0.11	-0.12	0.000	0.000	0.000
CITm + ICIT <-> CIT + ICITm	CTP1 (ICIT)	0.00	0.0	0.00	0.00	0.00	0.000	0.000	0.000
ADP + ATPm -> ADPm + ATP	AAC1	0.00	0.0	0.00	0.00	0.00	0.000	0.000	0.000
ADP + ATPm -> ADPm + ATP	PET9	0.00	0.0	0.00	0.00	0.00	0.000	0.000	0.000
ADP + ATPm <-> ADPm + ATP	AAC3	-0.04	-0.9	-0.05	-0.04	-0.05	-0.100	-0.068	-0.039
PI <-> PIm	MIR1	-0.04	-0.9	-0.05	-0.04	-0.05	-0.172	-0.093	-0.110
MAL + PIm -> MALm + PI	DIC1 (MAL)	0.00	0.0	0.00	0.00	0.00	0.000	0.000	0.000
SUCC + PIm -> SUCCm + PI	DIC1 (SUCC)	0.00	0.0	0.00	0.00	0.00	0.000	0.000	0.000
CIT + MALm <-> CITm + MAL	CTP1 (MAL)	-0.09	-2.0	-0.08	-0.07	-0.08	0.000	0.000	-0.006
IPPMAL <-> IPPMALm	U_99	-0.03	-0.6	-0.02	-0.02	-0.02	0.000	0.000	0.000
LAC <-> LACm	U_100	0.00	0.0	0.00	0.00	0.00	0.000	0.000	0.000
PYR <-> PYRm	YIA6	0.00	0.0	0.00	0.00	0.00	0.000	0.000	0.000
PYR <-> PYRm	YEA6	0.19	4.3	0.16	0.01	0.17	-0.200	-0.135	-0.077
GLUm <-> GLU	AGC1 (GLU)	0.01	0.2	0.00	0.00	0.00	0.000	0.000	0.000
ORN <-> ORNm	ORT1	-0.01	-0.3	-0.03	-0.02	-0.03	0.000	0.000	0.000
OIVAL <-> OIVALm	U_101	-0.14	-3.2	-0.14	-0.12	-0.14	0.000	0.000	0.000
OMVAL <-> OMVALm	U_102	0.00	0.0	0.00	0.00	0.00	0.000	0.000	0.000
FAD + FMNm -> FADm + FMN	FLX1	0.00	0.0	0.00	0.00	0.00	0.000	0.000	0.000
RIBFLAV <-> RIBFLAVm	U_103	0.00	0.0	0.00	0.00	0.00	0.000	0.000	0.000
4PPNTE <-> 4PPNTEm	U_104	0.00	0.0	0.00	0.00	0.00	0.000	0.000	0.000
PRPP <-> PRPPm	U_105	0.00	0.0	0.00	0.00	0.00	0.000	0.000	0.000
DHF <-> DHFm	U_106	0.00	0.0	0.00	0.00	0.00	0.000	0.000	0.000
QA <-> QAm	U_107	0.00	0.0	0.00	0.00	0.00	0.000	0.000	0.000
SAM <-> SAMm	U_108	0.00	0.0	0.00	0.00	0.00	0.000	0.000	0.000
SAH <-> SAHm	U_109	0.00	0.0	0.00	0.00	0.00	0.000	0.000	0.000
DCTPm -> DCTP	U_110	0.00	0.0	0.00	0.00	0.00	0.000	0.000	0.000
LGT -> LGTm	U_111	0.00	0.0	0.00	0.00	0.00	0.000	0.000	0.000
H2O2 <-> H2O2m	U_112	0.00	0.0	0.00	0.00	0.00	0.000	0.000	0.000
SUCC + FUMm -> SUCCm + FUM	SFC1	0.00	0.0	0.00	0.00	0.00	0.000	0.000	0.000
AKGm + AKA <-> AKG + AKAm	ODC1	0.00	0.0	0.00	0.00	0.00	0.000	0.000	0.000
AKGm + AKA <-> AKG + AKAm	ODC2	-0.02	-0.6	-0.02	-0.02	-0.02	0.000	0.000	0.000
ASP <-> ASPm	AGC1 (ASP)	0.00	0.0	0.00	0.00	0.00	0.000	0.000	0.000
ASP + GLUm <-> ASPm + GLU	AGC1 (ASP+GLU)	0.00	0.0	0.00	0.00	0.00	0.000	0.000	0.000
GL3P -> GL3Pm	U_113	0.00	0.0	0.00	0.00	0.00	0.014	0.005	0.014
CTP -> CTPm	U_114	0.00	0.0	0.00	0.00	0.00	0.000	0.000	0.000
ACCOAm -> COAm + ACm	ACH1 (ACCOAm)	0.00	0.0	0.00	0.00	0.00	0.000	0.000	0.000
ACCOAm + OIVALm -> COAm + IPPMALm	LEU9	0.00	0.0	0.00	0.00	0.00	0.000	0.000	0.000
ACCOA + OIVAL -> COA + IPPMAL	LEU4	0.00	0.0	0.00	0.00	0.00	0.000	0.000	0.000
ACCOA + COAm <-> ACCOAm + COA	CAT2, CRC1	-0.03	-0.6	-0.02	0.11	-0.03	0.116	0.078	0.050
OA <-> OAm	OAC1	0.13	2.9	0.13	0.11	0.13	0.200	0.135	0.077
ATP -> ADP + PI	U_116	0.00	0.0	0.00	0.00	0.00	0.000	0.000	0.000
ATP -> ADP + PI + Hext	PMP1	0.00	0.0	0.00	0.00	0.00	0.000	0.000	0.000
ATP -> ADP + PI + Hext	PMP2	0.00	0.0	0.00	0.00	0.00	0.000	0.000	0.000
ATP -> ADP + PI + Hext	PMA1	0.00	0.0	0.00	0.00	0.00	0.000	0.000	0.000
ATP -> ADP + PI + Hext	PMA2	0.00	0.0	0.00	0.00	0.00	0.023	0.000	0.095
MELI -> GLC + GLAC	YBR184W (MELI)	0.00	0.0	0.00	0.00	0.00	0.000	0.000	0.000
LACTOxt -> GLCxt + GLACxt	YBR184W (LACTO)	0.00	0.0	0.00	0.00	0.00	0.000	0.000	0.000
RAFxt -> GLACxt + SUCxt	YBR184W (RAF)	0.00	0.0	0.00	0.00	0.00	0.000	0.000	0.000
EPMxt <-> MANxt + GLACxt	YBR184W (EPM)	0.00	0.0	0.00	0.00	0.00	0.000	0.000	0.000
GGLxt <-> GLxt + GLACxt	YBR184W (GGL)	0.00	0.0	0.00	0.00	0.00	0.000	0.000	0.000
TRExt -> 2 GLCxt	ATH1	0.00	0.0	0.00	0.00	0.00	0.000	0.000	0.000
TRE -> 2 GLC	NTH2	0.00	0.0	0.00	0.00	0.00	0.000	0.000	0.000
TRE -> 2 GLC	NTH1	0.00	0.0	0.00	0.00	0.00	0.000	0.000	0.000
OBUT <-> OBUTm	U_117	0.02	0.4	0.02	0.01	0.02	0.000	0.000	0.000
GLCxt -> GLC	HXT4 (GLC)	4.50	100.0	3.50	3.50	3.50	0.000	0.000	0.000
GLCxt -> GLC	GAL2 (GLC)	0.00	0.0	0.00	0.00	0.00	0.000	0.000	0.000
GLCxt -> GLC	HXT11 (GLC)	0.00	0.0	0.00	0.00	0.00	0.000	0.000	0.000
GLCxt -> GLC	STL1 (GLC)	0.00	0.0	0.00	0.00	0.00	0.000	0.000	0.000
GLCxt -> GLC	HXT1 (GLC)	0.00	0.0	0.00	0.00	0.00	0.000	0.000	0.000
GLCxt -> GLC	HXT13 (GLC)	0.00	0.0	0.00	0.00	0.00	0.000	0.000	0.000
GLCxt -> GLC	HXT15 (GLC)	0.00	0.0	0.00	0.00	0.00	0.000	0.000	0.000
GLCxt -> GLC	HXT16 (GLC)	0.00	0.0	0.00	0.00	0.00	0.000	0.000	0.000
GLCxt -> GLC	HXT10 (GLC)	0.00	0.0	0.00	0.00	0.00	0.000	0.000	0.000
GLCxt -> GLC	HXT17 (GLC)	0.00	0.0	0.00	0.00	0.00	0.000	0.000	0.000
GLCxt -> GLC	HXT2 (GLC)	0.00	0.0	0.00	0.00	0.00	0.000	0.000	0.000
GLCxt -> GLC	HXT3 (GLC)	0.00	0.0	0.00	0.00	0.00	0.000	0.000	0.000
GLCxt -> GLC	HXT5 (GLC)	0.00	0.0	0.00	0.00	0.00	0.000	0.000	0.000
GLCxt -> GLC	HXT6 (GLC)	0.00	0.0	0.00	0.00	0.00	0.000	0.000	0.000
GLCxt -> GLC	HXT7 (GLC)	0.00	0.0	0.00	0.00	0.00	0.000	0.000	0.000
GLCxt -> GLC	HXT8 (GLC)	0.00	0.0	0.00	0.00	0.00	0.000	0.000	0.000
GLCxt -> GLC	HXT9 (GLC)	0.00	0.0	0.00	0.00	0.00	0.000	0.000	0.000
GLACxt -> GLAC	GAL2 (GLAC)	0.00	0.0	0.00	0.00	0.00	0.000	0.000	0.000
GLACxt -> GLAC	HXT10 (GLAC)	0.00	0.0	0.00	0.00	0.00	0.000	0.000	0.000
GLACxt -> GLAC	HXT11 (GLAC)	0.00	0.0	0.00	0.00	0.00	0.000	0.000	0.000
GLACxt -> GLAC	HXT14	0.00	0.0	0.00	0.00	0.00	0.000	0.000	0.000
GLACxt -> GLAC	HXT9 (GLAC)	0.00	0.0	0.00	0.00	0.00	0.000	0.000	0.000
GLACxt -> GLAC	STL1 (GLAC)	0.00	0.0	0.00	0.00	0.00	0.000	0.000	0.000
GLUxt <-> GLU	AGP3	0.00	0.0	0.00	0.00	0.00	0.000	0.000	0.000
GLUxt <-> GLU	GAP1	0.00	0.0	0.00	0.00	0.00	0.000	0.000	0.000
GLUxt <-> GLU	AGP1	0.00	0.0	0.00	0.00	0.00	0.000	0.000	0.000
GLUxt <-> GLU	DIP5	0.00	0.0	0.00	0.00	0.00	0.000	0.000	0.000
FRUxt -> FRU	HXT1 (FRU)	0.00	0.0	0.00	0.00	0.00	0.000	0.000	0.000

FRUxt -> FRU	HXT10 (FRU)	0.00	0.0	0.00	0.00	0.00	0.000	0.000	0.000
FRUxt -> FRU	HXT11 (FRU)	0.00	0.0	0.00	0.00	0.00	0.000	0.000	0.000
FRUxt -> FRU	HXT13 (FRU)	0.00	0.0	0.00	0.00	0.00	0.000	0.000	0.000
FRUxt -> FRU	HXT15 (FRU)	0.00	0.0	0.00	0.00	0.00	0.000	0.000	0.000
FRUxt -> FRU	HXT16 (FRU)	0.00	0.0	0.00	0.00	0.00	0.000	0.000	0.000
FRUxt -> FRU	HXT17 (FRU)	0.00	0.0	0.00	0.00	0.00	0.000	0.000	0.000
FRUxt -> FRU	HXT2 (FRU)	0.00	0.0	0.00	0.00	0.00	0.000	0.000	0.000
FRUxt -> FRU	HXT3 (FRU)	0.00	0.0	0.00	0.00	0.00	0.000	0.000	0.000
FRUxt -> FRU	HXT4 (FRU)	0.00	0.0	0.00	0.00	0.00	0.000	0.000	0.000
FRUxt -> FRU	HXT5 (FRU)	0.00	0.0	0.00	0.00	0.00	0.000	0.000	0.000
FRUxt -> FRU	HXT6 (FRU)	0.00	0.0	0.00	0.00	0.00	0.000	0.000	0.000
FRUxt -> FRU	HXT7 (FRU)	0.00	0.0	0.00	0.00	0.00	0.000	0.000	0.000
FRUxt -> FRU	HXT8 (FRU)	0.00	0.0	0.00	0.00	0.00	0.000	0.000	0.000
FRUxt -> FRU	HXT9 (FRU)	0.00	0.0	0.00	0.00	0.00	0.000	0.000	0.000
MANxt -> MAN	HXT1 (MAN)	0.00	0.0	0.00	0.00	0.00	0.000	0.000	0.000
MANxt -> MAN	HXT10 (MAN)	0.00	0.0	0.00	0.00	0.00	0.000	0.000	0.000
MANxt -> MAN	HXT11 (MAN)	0.00	0.0	0.00	0.00	0.00	0.000	0.000	0.000
MANxt -> MAN	HXT13 (MAN)	0.00	0.0	0.00	0.00	0.00	0.000	0.000	0.000
MANxt -> MAN	HXT15 (MAN)	0.00	0.0	0.00	0.00	0.00	0.000	0.000	0.000
MANxt -> MAN	HXT16 (MAN)	0.00	0.0	0.00	0.00	0.00	0.000	0.000	0.000
MANxt -> MAN	HXT17 (MAN)	0.00	0.0	0.00	0.00	0.00	0.000	0.000	0.000
MANxt -> MAN	HXT2 (MAN)	0.00	0.0	0.00	0.00	0.00	0.000	0.000	0.000
MANxt -> MAN	HXT3 (MAN)	0.00	0.0	0.00	0.00	0.00	0.000	0.000	0.000
MANxt -> MAN	HXT4 (MAN)	0.00	0.0	0.00	0.00	0.00	0.000	0.000	0.000
MANxt -> MAN	HXT5 (MAN)	0.00	0.0	0.00	0.00	0.00	0.000	0.000	0.000
MANxt -> MAN	HXT6 (MAN)	0.00	0.0	0.00	0.00	0.00	0.000	0.000	0.000
MANxt -> MAN	HXT7 (MAN)	0.00	0.0	0.00	0.00	0.00	0.000	0.000	0.000
MANxt -> MAN	HXT8 (MAN)	0.00	0.0	0.00	0.00	0.00	0.000	0.000	0.000
MANxt -> MAN	HXT9 (MAN)	0.00	0.0	0.00	0.00	0.00	0.000	0.000	0.000
SUCxt -> GLCxt + FRUxt	SUC2	0.00	0.0	0.00	0.00	0.00	0.000	0.000	0.000
MLTxt + Hext <-> MLT	MAL31	0.00	0.0	0.00	0.00	0.00	0.000	0.000	0.000
MALxt + AKG <-> MAL + AKGxt	U_118	0.00	0.0	0.00	-0.06	0.00	0.000	-0.004	0.000
ARABxt <-> ARAB	U_119	0.00	0.0	0.00	0.00	0.00	0.000	0.000	0.000
GL <-> GLxt	FPS1	0.70	15.6	0.27	0.27	0.27	0.039	0.039	0.039
GLxt -> GL	GUP1	0.00	0.0	0.00	0.00	0.00	0.000	0.000	0.000
GLxt -> GL	GUP2	0.00	0.0	0.00	0.00	0.00	0.000	0.000	0.000
LACxt + Hext -> LAC	JEN1 (LAC)	0.00	0.0	0.00	0.00	0.00	0.000	0.000	0.000
MELIxt + Hext -> MELI	U_120	0.00	0.0	0.00	0.00	0.00	0.000	0.000	0.000
RIBxt + Hext -> RIB	U_121	0.00	0.0	0.00	0.00	0.00	0.000	0.000	0.000
TRExt + Hext -> TRE	U_122	0.00	0.0	0.00	0.00	0.00	0.000	0.000	0.000
LLACxt + Hext -> LLAC	JEN1 (LLAC)	0.00	0.0	0.00	0.00	0.00	0.000	0.000	0.000
ALAxt + Hext <-> ALA	GAP1 (ALA)	0.00	0.0	0.00	0.00	0.00	0.000	0.000	0.000
ALAxt + Hext <-> ALA	DIP5 (ALA)	0.00	0.0	0.00	0.00	0.00	0.000	0.000	0.000
ALAxt + Hext <-> ALA	AGP1 (ALA)	0.00	0.0	0.00	0.00	0.00	0.000	0.000	0.000
ALAxt + Hext <-> ALA	TAT2 (ALA)	0.00	0.0	0.00	0.00	0.00	0.000	0.000	0.000
ALAxt + Hext <-> ALA	PUT4 (ALA)	0.00	0.0	0.00	0.00	0.00	0.000	0.000	0.000
ARGxt + Hext <-> ARG	GAP1 (ARG)	0.00	0.0	0.00	0.00	0.00	0.000	0.000	0.000
ARGxt + Hext <-> ARG	CAN1 (ARG)	0.00	0.0	0.00	0.00	0.00	0.000	0.000	0.000
ARGxt + Hext <-> ARG	ALP1	0.00	0.0	0.00	0.00	0.00	0.000	0.000	0.000
ASNxt + Hext <-> ASN	GAP1 (ASN)	0.00	0.0	0.00	0.00	0.00	0.000	0.000	0.000
ASNxt + Hext <-> ASN	AGP1 (ASN)	0.00	0.0	0.00	0.00	0.00	0.000	0.000	0.000
ASNxt + Hext <-> ASN	GNP1 (ASN)	0.00	0.0	0.00	0.00	0.00	0.000	0.000	0.000
ASNxt + Hext <-> ASN	DIP5 (ASN)	0.00	0.0	0.00	0.00	0.00	0.000	0.000	0.000
ASPxt + Hext <-> ASP	AGP3 (ASP)	0.00	0.0	0.00	0.00	0.00	0.000	0.000	0.000
ASPxt + Hext <-> ASP	GAP1 (ASP)	0.00	0.0	0.00	0.00	0.00	0.000	0.000	0.000
ASPxt + Hext <-> ASP	DIP5 (ASP)	0.00	0.0	0.00	0.00	0.00	0.000	0.000	0.000
CYSxt + Hext <-> CYS	GAP1 (CYS)	0.00	0.0	0.00	0.00	0.00	0.000	0.000	0.000
CYSxt + Hext <-> CYS	GNP1 (CYS)	0.00	0.0	0.00	0.00	0.00	0.000	0.000	0.000
CYSxt + Hext <-> CYS	BAP2 (CYS)	0.00	0.0	0.00	0.00	0.00	0.000	0.000	0.000
CYSxt + Hext <-> CYS	BAP3 (CYS)	0.00	0.0	0.00	0.00	0.00	0.000	0.000	0.000
CYSxt + Hext <-> CYS	TAT1 (CYS)	0.00	0.0	0.00	0.00	0.00	0.000	0.000	0.000
CYSxt + Hext <-> CYS	TAT2 (CYS)	0.00	0.0	0.00	0.00	0.00	0.000	0.000	0.000
GLYxt + Hext <-> GLY	GAP1 (GLY)	0.00	0.0	0.00	0.00	0.00	0.000	0.000	0.000
GLYxt + Hext <-> GLY	TAT2 (GLY)	0.00	0.0	0.00	0.00	0.00	0.000	0.000	0.000
GLYxt + Hext <-> GLY	DIP5 (GLY)	0.00	0.0	0.00	0.00	0.00	0.000	0.000	0.000
GLYxt + Hext <-> GLY	PUT4 (GLY)	0.00	0.0	0.00	0.00	0.00	0.000	0.000	0.000
GLNxt + Hext <-> GLN	GAP1 (GLN)	0.00	0.0	0.00	0.00	0.00	0.000	0.000	0.000
GLNxt + Hext <-> GLN	AGP1 (GLN)	0.00	0.0	0.00	0.00	0.00	0.000	0.000	0.000
GLNxt + Hext <-> GLN	GNP1 (GLN)	0.00	0.0	0.00	0.00	0.00	0.000	0.000	0.000
GLNxt + Hext <-> GLN	DIP5 (GLN)	0.00	0.0	0.00	0.00	0.00	0.000	0.000	0.000
HISxt + Hext <-> HIS	HIP1	0.00	0.0	0.00	0.00	0.00	0.000	0.000	0.000
HISxt + Hext <-> HIS	GAP1 (HIS)	0.00	0.0	0.00	0.00	0.00	0.000	0.000	0.000
HISxt + Hext <-> HIS	AGP1 (HIS)	0.00	0.0	0.00	0.00	0.00	0.000	0.000	0.000
HISxt + Hext <-> HIS	TAT1 (HIS)	0.00	0.0	0.00	0.00	0.00	0.000	0.000	0.000
ILExt + Hext <-> ILE	TAT1 (ILE)	0.00	0.0	0.00	0.00	0.00	0.000	0.000	0.000
ILExt + Hext <-> ILE	GAP1 (ILE)	0.00	0.0	0.00	0.00	0.00	0.000	0.000	0.000
ILExt + Hext <-> ILE	AGP1 (ILE)	0.00	0.0	0.00	0.00	0.00	0.000	0.000	0.000
ILExt + Hext <-> ILE	BAP2 (ILE)	0.00	0.0	0.00	0.00	0.00	0.000	0.000	0.000
ILExt + Hext <-> ILE	BAP3 (ILE)	0.00	0.0	0.00	0.00	0.00	0.000	0.000	0.000
ILExt + Hext <-> ILE	TAT1 (ILE, obsolete)	0.00	0.0	0.00	0.00	0.00	0.000	0.000	0.000
LEUxt + Hext <-> LEU	TAT1 (LEU)	0.00	0.0	0.00	0.00	0.00	0.000	0.000	0.000
LEUxt + Hext <-> LEU	GAP1 (LEU)	0.00	0.0	0.00	0.00	0.00	0.000	0.000	0.000
LEUxt + Hext <-> LEU	AGP1 (LEU)	0.00	0.0	0.00	0.00	0.00	0.000	0.000	0.000
LEUxt + Hext <-> LEU	BAP2 (LEU)	0.00	0.0	0.00	0.00	0.00	0.000	0.000	0.000
LEUxt + Hext <-> LEU	BAP3 (LEU)	0.00	0.0	0.00	0.00	0.00	0.000	0.000	0.000
LEUxt + Hext <-> LEU	obsolete)	0.00	0.0	0.00	0.00	0.00	0.000	0.000	0.000
LEUxt + Hext <-> LEU	GNP1 (LEU)	0.00	0.0	0.00	0.00	0.00	0.000	0.000	0.000
METxt + Hext <-> MET	GAP1 (MET)	0.00	0.0	0.00	0.00	0.00	0.000	0.000	0.000
METxt + Hext <-> MET	AGP1 (MET)	0.00	0.0	0.00	0.00	0.00	0.000	0.000	0.000

METxt + Hext <-> MET	GNP1 (MET)	0.00	0.0	0.00	0.00	0.00	0.000	0.000	0.000
METxt + Hext <-> MET	BAP2 (MET)	0.00	0.0	0.00	0.00	0.00	0.000	0.000	0.000
METxt + Hext <-> MET	BAP3 (MET)	0.00	0.0	0.00	0.00	0.00	0.000	0.000	0.000
METxt + Hext <-> MET	MUP1	0.00	0.0	0.00	0.00	0.00	0.000	0.000	0.000
METxt + Hext <-> MET	MUP3	0.00	0.0	0.00	0.00	0.00	0.000	0.000	0.000
PHExt + Hext <-> PHE	GAP1 (PHE)	0.00	0.0	0.00	0.00	0.00	0.000	0.000	0.000
PHExt + Hext <-> PHE	AGP1 (PHE)	0.00	0.0	0.00	0.00	0.00	0.000	0.000	0.000
PHExt + Hext <-> PHE	TAT2 (PHE)	0.00	0.0	0.00	0.00	0.00	0.000	0.000	0.000
PHExt + Hext <-> PHE	BAP2 (PHE)	0.00	0.0	0.00	0.00	0.00	0.000	0.000	0.000
PHExt + Hext <-> PHE	BAP3 (PHE)	0.00	0.0	0.00	0.00	0.00	0.000	0.000	0.000
PROxt + Hext <-> PRO	GAP1 (PRO)	0.00	0.0	0.00	0.00	0.00	0.000	0.000	0.000
PROxt + Hext <-> PRO	PUT4 (PRO)	0.00	0.0	0.00	0.00	0.00	0.000	0.000	0.000
TRPxt + Hext <-> TRP	TAT1 (TRP)	0.00	0.0	0.00	0.00	0.00	0.000	0.000	0.000
TRPxt + Hext <-> TRP	GAP1 (TRP)	0.00	0.0	0.00	0.00	0.00	0.000	0.000	0.000
TRPxt + Hext <-> TRP	TAT1 (TRP, obsolete)	0.00	0.0	0.00	0.00	0.00	0.000	0.000	0.000
TRPxt + Hext <-> TRP	TAT2 (TRP)	0.00	0.0	0.00	0.00	0.00	0.000	0.000	0.000
TRPxt + Hext <-> TRP	BAP2 (TRP)	0.00	0.0	0.00	0.00	0.00	0.000	0.000	0.000
TRPxt + Hext <-> TRP	BAP3 (TRP)	0.00	0.0	0.00	0.00	0.00	0.000	0.000	0.000
TYRxt + Hext <-> TYR	TAT1 (TYR)	0.00	0.0	0.00	0.00	0.00	0.000	0.000	0.000
TYRxt + Hext <-> TYR	GAP1 (TYR)	0.00	0.0	0.00	0.00	0.00	0.000	0.000	0.000
TYRxt + Hext <-> TYR	AGP1 (TYR)	0.00	0.0	0.00	0.00	0.00	0.000	0.000	0.000
TYRxt + Hext <-> TYR	BAP2 (TYR)	0.00	0.0	0.00	0.00	0.00	0.000	0.000	0.000
TYRxt + Hext <-> TYR	TAT1 (TYR, obsolete)	0.00	0.0	0.00	0.00	0.00	0.000	0.000	0.000
TYRxt + Hext <-> TYR	TAT2 (TYR)	0.00	0.0	0.00	0.00	0.00	0.000	0.000	0.000
TYRxt + Hext <-> TYR	BAP3 (TYR)	0.00	0.0	0.00	0.00	0.00	0.000	0.000	0.000
VALxt + Hext <-> VAL	GAP1 (VAL)	0.00	0.0	0.00	0.00	0.00	0.000	0.000	0.000
VALxt + Hext <-> VAL	AGP1 (VAL)	0.00	0.0	0.00	0.00	0.00	0.000	0.000	0.000
VALxt + Hext <-> VAL	BAP3 (VAL)	0.00	0.0	0.00	0.00	0.00	0.000	0.000	0.000
VALxt + Hext <-> VAL	TAT1 (VAL)	0.00	0.0	0.00	0.00	0.00	0.000	0.000	0.000
VALxt + Hext <-> VAL	BAP2 (VAL)	0.00	0.0	0.00	0.00	0.00	0.000	0.000	0.000
SERxt + Hext <-> SER	AGP3 (SER)	0.00	0.0	0.00	0.00	0.00	0.000	0.000	0.000
SERxt + Hext <-> SER	AGP1 (SER)	0.00	0.0	0.00	0.00	0.00	0.000	0.000	0.000
SERxt + Hext <-> SER	GNP1 (SER)	0.00	0.0	0.00	0.00	0.00	0.000	0.000	0.000
SERxt + Hext <-> SER	GAP1 (SER)	0.00	0.0	0.00	0.00	0.00	0.000	0.000	0.000
SERxt + Hext <-> SER	DIP5 (SER)	0.00	0.0	0.00	0.00	0.00	0.000	0.000	0.000
THRxt + Hext <-> THR	TAT1 (THR)	0.00	0.0	0.00	0.00	0.00	0.000	0.000	0.000
THRxt + Hext <-> THR	AGP1 (THR)	0.00	0.0	0.00	0.00	0.00	0.000	0.000	0.000
THRxt + Hext <-> THR	GAP1 (THR)	0.00	0.0	0.00	0.00	0.00	0.000	0.000	0.000
THRxt + Hext <-> THR	GNP1 (THR)	0.00	0.0	0.00	0.00	0.00	0.000	0.000	0.000
LYSxt + Hext <-> LYS	LYP1	0.00	0.0	0.00	0.00	0.00	0.000	0.000	0.000
LYSxt + Hext <-> LYS	GAP1 (LYS)	0.00	0.0	0.00	0.00	0.00	0.000	0.000	0.000
SAMxt + Hext -> SAM	SAM3	0.00	0.0	0.00	0.00	0.00	0.000	0.000	0.000
GABAxt + Hext -> GABA	PUT4 (GABA)	0.00	0.0	0.00	0.00	0.00	0.000	0.000	0.000
GABAxt + Hext -> GABA	UGA4 (GABA)	0.00	0.0	0.00	0.00	0.00	0.000	0.000	0.000
CHOxt + Hext -> CHO	HNM1	0.00	0.0	0.00	0.00	0.00	0.000	0.000	0.000
ALVxt + Hext -> ALV	UGA4 (ALV)	0.00	0.0	0.00	0.00	0.00	0.000	0.000	0.000
ORNxt + Hext <-> ORN	GAP1 (ORN)	0.00	0.0	0.00	0.00	0.00	0.000	0.000	0.000
ORNxt + Hext <-> ORN	CAN1 (ORN)	0.00	0.0	0.00	0.00	0.00	0.000	0.000	0.000
PTRSCxt + Hext -> PTRSC	AGP2 (PTRSC)	0.00	0.0	0.00	0.00	0.00	0.000	0.000	0.000
SPRMDxt + Hext -> SPRMD	AGP2 (SPRMD)	0.00	0.0	0.00	0.00	0.00	0.000	0.000	0.000
URAxt + Hext -> URA	FUR4	0.00	0.0	0.00	0.00	0.00	0.000	0.000	0.000
CYTSxt + Hext -> CYTS	FCY2 (CYTS)	0.00	0.0	0.00	0.00	0.00	0.000	0.000	0.000
ADxt + Hext -> AD	FCY2 (AD)	0.00	0.0	0.00	0.00	0.00	0.000	0.000	0.000
GNxt + Hext <-> GN	FCY2 (GN)	0.00	0.0	0.00	0.00	0.00	0.000	0.000	0.000
CYTSxt + Hext -> CYTS	FCY21 (CYTS)	0.00	0.0	0.00	0.00	0.00	0.000	0.000	0.000
ADxt + Hext -> AD	FCY21 (AD)	0.00	0.0	0.00	0.00	0.00	0.000	0.000	0.000
GNxt + Hext <-> GN	FCY21 (GN)	0.00	0.0	0.00	0.00	0.00	0.000	0.000	0.000
CYTSxt + Hext -> CYTS	FCY22 (CYTS)	0.00	0.0	0.00	0.00	0.00	0.000	0.000	0.000
ADxt + Hext -> AD	FCY22 (AD)	0.00	0.0	0.00	0.00	0.00	0.000	0.000	0.000
GNxt + Hext <-> GN	FCY22 (GN)	0.00	0.0	0.00	0.00	0.00	0.000	0.000	0.000
CYTSxt + Hext -> CYTS	TPN1 (CYTS)	0.00	0.0	0.00	0.00	0.00	0.000	0.000	0.000
ADxt + Hext -> AD	TPN1 (AD)	0.00	0.0	0.00	0.00	0.00	0.000	0.000	0.000
GNxt + Hext <-> GN	TPN1 (GN)	0.00	0.0	0.00	0.00	0.00	0.000	0.000	0.000
ADNxt + Hext -> ADN	U_126	0.00	0.0	0.00	0.00	0.00	0.000	0.000	0.000
GSNxt + Hext -> GSN	U_127	0.00	0.0	0.00	0.00	0.00	0.000	0.000	0.000
URIxt + Hext -> URI	FUI1	0.00	0.0	0.00	0.00	0.00	0.000	0.000	0.000
CYTDxt + Hext -> CYTD	U_128	0.00	0.0	0.00	0.00	0.00	0.000	0.000	0.000
INSxt + Hext -> INS	U_129	0.00	0.0	0.00	0.00	0.00	0.000	0.000	0.000
XTSINExt + Hext -> XTSINE	U_130	0.00	0.0	0.00	0.00	0.00	0.000	0.000	0.000
DTxt + Hext -> DT	U_131	0.00	0.0	0.00	0.00	0.00	0.000	0.000	0.000
DINxt + Hext -> DIN	U_132	0.00	0.0	0.00	0.00	0.00	0.000	0.000	0.000
DGxt + Hext -> DG	U_133	0.00	0.0	0.00	0.00	0.00	0.000	0.000	0.000
DAxt + Hext -> DA	U_134	0.00	0.0	0.00	0.00	0.00	0.000	0.000	0.000
DCxt + Hext -> DC	U_135	0.00	0.0	0.00	0.00	0.00	0.000	0.000	0.000
DUxt + Hext -> DU	U_136	0.00	0.0	0.00	0.00	0.00	0.000	0.000	0.000
MLTxt + Hext -> MLT	MAL11	0.00	0.0	0.00	0.00	0.00	0.000	0.000	0.000
HYXNxt + Hext <-> HYXN	U_138	0.00	0.0	0.00	0.00	0.00	0.000	0.000	0.000
LACALxt <-> LACAL	U_139	0.00	0.0	0.00	0.00	0.00	0.000	0.000	0.000
FALDxt -> FALD	U_140	0.00	0.0	0.00	0.00	0.00	0.000	0.000	0.000
XULxt + Hext -> XUL	U_141	0.00	0.0	0.00	0.00	0.00	0.000	0.000	0.000
XANxt <-> XAN	U_142	0.00	0.0	0.00	0.00	0.00	0.000	0.000	0.000
ACxt + Hext -> AC	ADY2 (AC)	0.00	0.0	0.00	0.00	0.00	0.000	0.000	0.000
FORxt <-> FOR	U_143	0.00	0.0	0.00	0.00	0.00	0.000	0.000	0.000
ETH <-> ETHxt	U_144	7.10	157.8	7.60	7.67	7.60	0.900	0.900	0.900
SUCC <-> SUCCxt + Hext	U_145	0.02	0.4	0.02	0.02	0.02	0.006	0.006	0.006
PYRxt + Hext -> PYR	JEN1 (PYR)	0.00	0.0	0.00	0.00	0.00	0.000	0.000	0.000
UREAxt + 2 Hext <-> UREA	DUR3	0.00	0.0	0.00	0.00	0.00	0.000	0.000	0.000

NH3xt <-> NH3	MEP1	-90.31	-2006.9	-90.36	-90.42	-90.36	-544.852	-544.852	-544.852
NH3xt <-> NH3	MEP2	45.40	1009.0	45.40	45.40	45.40	272.426	272.426	272.426
NH3xt <-> NH3	MEP3	45.40	1009.0	45.40	45.40	45.40	272.426	272.426	272.426
SLFxt -> SLF	SUL1	0.00	0.0	0.00	0.00	0.00	0.000	0.000	0.000
SLFxt -> SLF	SUL2	0.00	0.0	0.00	0.00	0.00	0.000	0.000	0.000
SLFxt -> SLF	YGR125W	0.01	0.1	0.01	0.00	0.01	0.000	0.000	0.000
PIxt + Hext <-> PI	PHO90	7.93	176.3	7.93	7.93	7.93	47.603	47.603	47.603
PIxt + Hext <-> PI	PHO87	7.93	176.3	7.93	7.93	7.93	47.603	47.603	47.603
PIxt + Hext <-> PI	PHO89	7.93	176.3	7.93	7.93	7.93	0.000	0.000	0.000
PIxt + Hext <-> PI	PHO91	-31.70	-704.5	-31.70	-31.65	-31.70	47.603	47.603	47.603
PIxt + Hext <-> PI	PHO84	7.93	176.3	7.93	7.93	7.93	-142.779	-142.798	-142.707
CIT <-> CITxt + Hext	U_146	0.00	0.0	0.00	0.00	0.00	0.000	0.000	0.000
FUM <-> FUMxt + Hext	U_147	0.02	0.3	0.02	0.01	0.02	0.000	0.000	0.000
C140xt -> C140	FAT1 (C140)	0.00	0.0	0.00	0.00	0.00	0.000	0.000	0.000
C160xt -> C160	FAT1 (C160)	0.00	0.0	0.00	0.00	0.00	0.000	0.000	0.000
C180xt -> C180	FAT1 (C180)	0.00	0.0	0.00	0.00	0.00	0.000	0.000	0.000
AKG <-> AKGxt + Hext	U_151	0.00	0.0	0.00	0.06	0.00	0.000	0.004	0.000
PNTOxt + Hext <-> PNTO	FEN2	0.00	0.0	0.00	0.00	0.00	0.000	0.000	0.000
GLAL <-> GLALxt	U_152	0.00	0.0	0.00	0.00	0.00	0.000	0.000	0.000
ACAL <-> ACALxt	U_153	0.00	0.0	0.00	0.00	0.00	0.000	0.000	0.000
THIAMINxt + Hext -> THIAMIN	THI7	0.00	0.0	0.00	0.00	0.00	0.000	0.000	0.000
THIAMINxt + Hext -> THIAMIN	THI71	0.00	0.0	0.00	0.00	0.00	0.000	0.000	0.000
THIAMINxt + Hext -> THIAMIN	THI72	0.00	0.0	0.00	0.00	0.00	0.000	0.000	0.000
ATNxt -> ATN	DAL4	0.00	0.0	0.00	0.00	0.00	0.000	0.000	0.000
ATTxt -> ATT	DAL5	0.00	0.0	0.00	0.00	0.00	0.000	0.000	0.000
PAPxt <-> PAP	U_154	0.00	0.0	0.00	0.00	0.00	0.000	0.000	0.000
DTTPxt <-> DTTP	U_155	0.00	0.0	0.00	0.00	0.00	0.000	0.000	0.000
THYxt <-> THY + Hext	U_156	0.00	0.0	0.00	0.00	0.00	0.000	0.000	0.000
GA6Pxt <-> GA6P	U_157	0.00	0.0	0.00	0.00	0.00	0.000	0.000	0.000
BTxt + Hext <-> BT	VHT1	0.00	0.0	0.00	0.00	0.00	0.000	0.000	0.000
AONAxt + Hext <-> AONA	BIO5	0.00	0.0	0.00	0.00	0.00	0.000	0.000	0.000
DANNAxt + Hext <-> DANNA	U_158	0.00	0.0	0.00	0.00	0.00	0.000	0.000	0.000
OGTxt -> OGT	U_159	0.00	0.0	0.00	0.00	0.00	0.000	0.000	0.000
SPRMxt -> SPRM	U_160	0.00	0.0	0.00	0.00	0.00	0.000	0.000	0.000
O2xt <-> O2	U_161	0.00	0.0	0.00	0.00	0.00	0.000	0.000	0.000
CO2 <-> CO2xt	U_162	7.47	165.9	7.90	7.90	7.90	1.188	1.054	1.188
ERGOSTxt <-> ERGOST	AUS1 (ERGOST)	0.00	0.0	0.00	0.00	0.00	0.000	0.000	0.000
ZYMSTxt <-> ZYMST	AUS1 (ZYMST)	0.00	0.0	0.00	0.00	0.00	0.000	0.000	0.000
RIBFLAVxt + Hext -> RIBFLAV	U_163	0.00	0.0	0.00	0.00	0.00	0.000	0.000	0.000
NACxt + Hext -> NAC	U_164	0.00	0.0	0.00	0.00	0.00	0.000	0.000	0.000
PYRDXxt + Hext -> PYRDX	TPN1	0.00	0.0	0.00	0.00	0.00	0.000	0.000	0.000
PABAxt + Hext -> PABA	U_166	0.00	0.0	0.00	0.00	0.00	0.000	0.000	0.000
ALA -> ALAt	U_167	0.00	0.0	0.00	0.00	0.00	0.000	0.000	0.000
ALAm -> ALAt	U_168	0.04	0.9	0.04	0.03	0.04	0.000	0.000	0.000
ARG -> ARGt	U_169	0.01	0.3	0.01	0.01	0.01	0.000	0.000	0.000
ASN -> ASNt	U_170	0.01	0.2	0.01	0.01	0.01	0.000	0.000	0.000
ASP -> ASPt	U_171	0.03	0.6	0.02	0.02	0.02	0.000	0.000	0.000
ASPm -> ASPt	U_172	0.00	0.0	0.00	0.00	0.00	0.000	0.000	0.000
CYS -> CYSt	U_173	0.00	0.0	0.00	0.00	0.00	0.000	0.000	0.000
GLU -> GLUt	U_174	0.03	0.6	0.02	0.02	0.02	0.000	0.000	0.000
GLUm -> GLUt	U_175	0.00	0.0	0.00	0.00	0.00	0.000	0.000	0.000
GLN -> GLNt	U_176	0.01	0.2	0.01	0.01	0.01	0.000	0.000	0.000
GLY -> GLYt	U_177	0.03	0.6	0.02	0.02	0.02	0.000	0.000	0.000
GLYm -> GLYt	U_178	0.00	0.0	0.00	0.00	0.00	0.000	0.000	0.000
HIS -> HISt	U_179	0.01	0.1	0.01	0.00	0.01	0.000	0.000	0.000
ILE -> ILEt	U_180	0.00	0.0	0.00	0.00	0.00	0.000	0.000	0.000
ILEm -> ILEt	U_181	0.02	0.4	0.02	0.01	0.02	0.000	0.000	0.000
LEU -> LEUt	U_182	0.00	0.0	0.00	0.00	0.00	0.000	0.000	0.000
LEUm -> LEUt	U_183	0.03	0.6	0.02	0.02	0.02	0.000	0.000	0.000
LYS -> LYSt	U_184	0.02	0.6	0.02	0.02	0.02	0.000	0.000	0.000
MET -> METt	U_185	0.00	0.1	0.00	0.00	0.00	0.000	0.000	0.000
PHE -> PHEt	U_186	0.01	0.3	0.01	0.01	0.01	0.000	0.000	0.000
PRO -> PROt	U_187	0.01	0.3	0.01	0.01	0.01	0.000	0.000	0.000
PROm -> PROt	U_188	0.00	0.0	0.00	0.00	0.00	0.000	0.000	0.000
SER -> SERt	U_189	0.02	0.4	0.01	0.01	0.01	0.000	0.000	0.000
SERm -> SERt	U_190	0.00	0.0	0.00	0.00	0.00	0.000	0.000	0.000
THR -> THRt	U_191	0.02	0.4	0.02	0.01	0.02	0.000	0.000	0.000
THRm -> THRt	U_192	0.00	0.0	0.00	0.00	0.00	0.000	0.000	0.000
TRP -> TRPt	U_193	0.00	0.1	0.00	0.00	0.00	0.000	0.000	0.000
TYR -> TYRt	U_194	0.01	0.2	0.01	0.01	0.01	0.000	0.000	0.000
VAL -> VALt	U_195	0.02	0.5	0.02	0.02	0.02	0.000	0.000	0.000
AMP -> AMPt	U_196	0.00	0.1	0.00	0.00	0.00	0.000	0.000	0.000
AMPm -> AMPt	U_197	0.00	0.0	0.00	0.00	0.00	0.000	0.000	0.000
GMP -> GMPt	U_198	0.00	0.1	0.00	0.00	0.00	0.000	0.000	0.000
UMP -> UMPt	U_199	0.01	0.1	0.01	0.00	0.01	0.000	0.000	0.000
CMP -> CMPt	U_200	0.00	0.1	0.00	0.00	0.00	0.000	0.000	0.000
CMPm -> CMPt	U_201	0.00	0.0	0.00	0.00	0.00	0.000	0.000	0.000
DAMP -> DAMPt	U_202	0.00	0.0	0.00	0.00	0.00	0.000	0.000	0.000
DCMP -> DCMPt	U_203	0.00	0.0	0.00	0.00	0.00	0.000	0.000	0.000
DGMP -> DGMPt	U_204	0.00	0.0	0.00	0.00	0.00	0.000	0.000	0.000
DTMP -> DTMPt	U_205	0.00	0.0	0.00	0.00	0.00	0.000	0.000	0.000
PA -> PAt	U_206	0.00	0.0	0.00	0.00	0.00	0.000	0.000	0.000
PAm -> PAt	U_207	0.00	0.0	0.00	0.00	0.00	0.000	0.000	0.000
PS -> PSt	U_208	0.00	0.0	0.00	0.00	0.00	0.000	0.000	0.000
PSm -> PSt	U_209	0.00	0.0	0.00	0.00	0.00	0.000	0.000	0.000
PE -> PEt	U_210	0.00	0.0	0.00	0.00	0.00	0.000	0.000	0.000
PEm -> PEt	U_211	0.00	0.0	0.00	0.00	0.00	0.000	0.000	0.000
MIPC -> MIP2Ct	U_212	0.00	0.0	0.00	0.00	0.00	0.000	0.000	0.000
MIPC2 -> MIP2Ct	U_213	0.00	0.0	0.00	0.00	0.00	0.000	0.000	0.000

MIP2C -> MIP2Ct	U_214	0.00	0.0	0.00	0.00	0.00	0.000	0.000	0.000
MIP2C2 -> MIP2Ct	U_215	0.00	0.0	0.00	0.00	0.00	0.000	0.000	0.000
ERGOST -> ERGOSTt	U_216	0.00	0.0	0.00	0.00	0.00	0.000	0.000	0.000
ATP -> ATPt	U_217	2.08	46.3	1.89	1.62	1.89	0.000	0.000	0.000
ATPm -> ATPt	U_218	0.00	0.0	0.00	0.00	0.00	0.000	0.000	0.000
ADPt -> ADP	U_219	2.08	46.3	1.89	1.62	1.89	0.000	0.000	0.000
ADPt -> ADPm	U_220	0.00	0.0	0.00	0.00	0.00	0.000	0.000	0.000
PIt -> PI	U_221	2.08	46.3	1.90	1.62	1.90	0.000	0.000	0.000
PIt -> PIm	U_222	0.00	0.0	0.00	0.00	0.00	0.000	0.000	0.000
0.459 ALAt + 0.161 ARGt + 0.102 ASNt + 0.297 ASPt + 0.007 CYSt + 0.302 GLUt + 0.105 GLNt + 0.290 GLYt + 0.066 HISt + 0.193 ILEt + 0.296 LEUt + 0.286 LYSt + 0.051 METt + 0.134 PHEt + 0.165 PROt + 0.185 SERt + 0.191 THRt + 0.028 TRPt + 0.102 TYRt + 0.265 VALt + 0.051 AMPt + 0.051 GMPt + 0.067 UMPt + 0.050 CMPt + 0.0036 DAMPt + 0.0024 DCMPt + 0.0024 DGMPt + 0.0036 DTMPt + 0.0066 TAGLY + 0.007 ERGOSTt + 0.005922 MIP2Ct + 0.0000182 CHIT + 0.0006 PAt + 0.005 PINS + 0.002 PSt + 0.002 PEt + 0.006 PC + 0.809 MANNAN + 1.136 13GLUCAN + 23.9166 ATPt + 0.000004 TPPP + 0.000001 RIBFLAV + 0.000001 COAt + 0.000001 PTHm + 0.000001 cAMP + 0.000001 THF + 0.000001 NAD + 0.000001 FAD + 0.000001 RGT + 0.000001 QH2m -> BM + 23.9166 ADPt + 23.9456 PIt	U_223	0.09	1.9	0.08	0.07	0.08	0.000	0.000	0.000
ACLACm <-> OHIVALm	ILV5 (ACLAC first half)	0.00	0.0	0.00	0.00	0.00	0.000	0.000	0.000
OHIVALm + NADPHm -> DHIVALm + NADPm	ILV5 (ACLAC second half)	0.00	0.0	0.00	0.00	0.00	0.000	0.000	0.000
ABUTm <-> HMOPm	ILV5 (ABUT first half)	0.02	0.4	0.02	0.01	0.02	0.000	0.000	0.000
HMOPm + NADPHm -> DHMVALm + NADPm	ILV5 (ABUT second half)	0.02	0.4	0.02	0.01	0.02	0.000	0.000	0.000
CHICAP <-> IPPMALE	LEU1 (first half)	-0.03	-0.6	-0.02	-0.02	-0.02	0.000	0.000	0.000
IPPMALE <-> IPPMAL	LEU1 (second half)	-0.03	-0.6	-0.02	-0.02	-0.02	0.000	0.000	0.000
C140ACP + 2 MALACP + 4 NADPH -> C180ACP + ACP + 4 NADP + 2 CO2	ELO1 (C140-C180)	0.00	0.0	0.00	0.00	0.00	0.000	0.000	0.000
C160ACP + MALACP + 2 NADPH -> C180ACP + ACP + 2 NADP + CO2	ELO1 (C160-C180)	0.00	0.0	0.00	0.00	0.00	0.000	0.000	0.000
C161ACP + MALACP + 2 NADPH -> C181ACP + ACP + 2 NADP + CO2	ELO1 (C161-C181)	0.00	0.0	0.00	0.00	0.00	0.000	0.000	0.000
DGMP + DATP <-> DGDP + DADP	GUK1 (DGMP+DATP)	0.00	0.0	0.00	0.00	0.00	0.000	0.000	0.000
CYTD + ATP -> ADP + CMP	URK1 (CYTD+ATP)	0.00	0.0	0.00	0.00	0.00	0.000	0.000	0.000
CYTD + UTP -> UDP + CMP	URK1 (CYTD+UTP)	0.00	0.0	0.00	0.00	0.00	0.000	0.000	0.000
CYTD + ITP -> IDP + CMP	URK1 (CYTD+ITP)	0.00	0.0	0.00	0.00	0.00	0.000	0.000	0.000
URI + UTP -> UDP + UMP	URK1 (URI+UTP)	0.00	0.0	0.00	0.00	0.00	0.000	0.000	0.000
URI + ITP -> IDP + UMP	URK1 (URI+ITP)	0.00	0.0	0.00	0.00	0.00	0.000	0.000	0.000
CYTD + DATP -> DADP + CMP	URK1 (CYTD+DATP)	0.00	0.0	0.00	0.00	0.00	0.000	0.000	0.000
URI + DATP -> DADP + UMP	URK1 (URI+DATP)	0.00	0.0	0.00	0.00	0.00	0.000	0.000	0.000
URI + DGTP -> DGDP + UMP	URK1 (URI+DGTP)	0.00	0.0	0.00	0.00	0.00	0.000	0.000	0.000
CYTD + DGTP -> DGDP + CMP	URK1 (CYTD+DGTP)	0.00	0.0	0.00	0.00	0.00	0.000	0.000	0.000
CYTD + DTTP -> DTDP + CMP	URK1 (CYTD+DTTP)	0.00	0.0	0.00	0.00	0.00	0.000	0.000	0.000
URI + DTTP -> DTDP + UMP	URK1 (URI+DTTP)	0.00	0.0	0.00	0.00	0.00	0.000	0.000	0.000
URI + DCTP -> DCDP + UMP	URK1 (URI+DCTP)	0.00	0.0	0.00	0.00	0.00	0.000	0.000	0.000
URI + DUTP -> DUDP + UMP	URK1 (URI+DUTP)	0.00	0.0	0.00	0.00	0.00	0.000	0.000	0.000
CYT + DCTP -> DCDP + CMP	URK1 (CYT+DCTP)	0.00	0.0	0.00	0.00	0.00	0.000	0.000	0.000
CYT + DUTP -> DUDP + CMP	URK1 (CYT+DUTP)	0.00	0.0	0.00	0.00	0.00	0.000	0.000	0.000
SERm -> PYRm + NH3m	ILV1 (SER)	0.00	0.0	0.00	0.00	0.00	0.000	0.000	0.000
ACLACm + TPPm <-> PYRm + HTPPm	ILV2 / 6 (ACLAC_PYR)	0.02	0.4	0.02	0.01	0.02	0.000	0.000	0.000
HTPPm + CO2m <-> PYRm + TPPm	ILV2 / 6 (CO2_PYR)	0.00	0.0	0.00	0.00	0.00	0.000	0.000	0.000
TPPm <-> TPP	U_224	0.00	0.0	0.00	0.00	0.00	0.000	0.000	0.000
P5C + NADH -> PRO + NAD	PRO3 (NAD)	0.01	0.3	0.01	0.01	0.01	0.000	0.000	0.000
P5Cm + NADm -> NADHm + GLUm	PUT2 (NADm)	0.00	0.0	0.00	0.00	0.00	0.000	0.000	0.000
P5Cm + NADPm -> NADPHm + GLUm	PUT2 (NADPm)	0.00	0.0	0.00	0.00	0.00	0.000	0.000	0.000
DHFm + NADHm -> NADm + THFm	DFR1 (NADm)	0.00	0.0	0.00	0.00	0.00	0.000	0.000	0.000
DHF + NADH -> NAD + THF	DFR1 (NAD)	0.00	0.0	0.00	0.00	0.00	0.000	0.000	0.000
C180 + ATP + COA -> C180COA + AMP + PPI	FAA1 (C180)	0.00	0.0	0.00	0.00	0.00	0.000	0.000	0.000
C180 + ATP + COA -> C180COA + AMP + PPI	FAA2 (C180)	0.00	0.0	0.00	0.00	0.00	0.000	0.000	0.000
C180 + ATP + COA -> C180COA + AMP + PPI	FAA3 (C180)	0.00	0.0	0.00	0.00	0.00	0.000	0.000	0.000
C180 + ATP + COA -> C180COA + AMP + PPI	FAA4 (C180)	0.00	0.0	0.00	0.00	0.00	0.000	0.000	0.000
C181 + ATP + COA -> C181COA + AMP + PPI	FAA1 (C181)	0.00	0.0	0.00	0.00	0.00	0.000	0.000	0.000
C181 + ATP + COA -> C181COA + AMP + PPI	FAA2 (C181)	0.00	0.0	0.00	0.00	0.00	0.000	0.000	0.000
C181 + ATP + COA -> C181COA + AMP + PPI	FAA3 (C181)	0.00	0.0	0.00	0.00	0.00	0.000	0.000	0.000
C181 + ATP + COA -> C181COA + AMP + PPI	FAA4 (C181)	0.00	0.1	0.00	0.00	0.00	0.029	0.010	0.029

C182 + ATP + COA -> C182COA + AMP + PPI	FAA1 (C182)	0.00	0.0	0.00	0.00	0.00	0.000	0.000	0.000
C182 + ATP + COA -> C182COA + AMP + PPI	FAA2 (C182)	0.00	0.0	0.00	0.00	0.00	0.000	0.000	0.000
C182 + ATP + COA -> C182COA + AMP + PPI	FAA3 (C182)	0.00	0.0	0.00	0.00	0.00	0.000	0.000	0.000
C182 + ATP + COA -> C182COA + AMP + PPI	FAA4 (C182)	0.00	0.0	0.00	0.00	0.00	0.000	0.000	0.000
MYOIxt -> MYOI	ITR1	0.00	0.0	0.00	0.00	0.00	0.000	0.000	0.000
NH3 -> NH3xt	ADY2 (NH3)	0.00	0.0	0.00	0.00	0.00	0.000	0.000	0.000
AC -> ACxt	U_225	0.00	0.0	0.00	0.00	0.00	0.053	0.053	0.053
MALCOAm + ACPm <-> MALACPm + COAm	FATsyn (MALCOAm)	0.03	0.6	0.02	0.02	0.02	0.100	0.068	0.039
ACCOAm + ACPm <-> ACACPm + COAm	FATsyn (ACCOAm)	0.00	0.1	0.00	0.00	0.00	0.016	0.010	0.005
ACACPm + 4 MALACPm + 8 NADPHm -> 8 NADPm + C100ACPm + 4 CO2m + 4 ACPm	FATsyn (C100m))	0.00	0.0	0.00	0.00	0.00	0.000	0.000	0.000
ACACPm + 5 MALACPm + 10 NADPHm -> 10 NADPm + C120ACPm + 5 CO2m + 5 ACPm	FATsyn (C120m)	0.00	0.0	0.00	0.00	0.00	0.004	0.001	0.000
ACACPm + 6 MALACPm + 12 NADPHm -> 12 NADPm + C140ACPm + 6 CO2m + 6 ACPm	FATsyn (C140m)	0.00	0.0	0.00	0.00	0.00	0.006	0.002	0.002
ACACPm + 7 MALACPm + 14 NADPHm -> 14 NADPm + C160ACPm + 7 CO2m + 7 ACPm	FATsyn (C160m)	0.00	0.1	0.00	0.00	0.00	0.003	0.006	0.000
ACACPm + 8 MALACPm + 16 NADPHm -> 16 NADPm + C180ACPm + 8 CO2m + 8 ACPm	FATsyn (C180m)	0.00	0.0	0.00	0.00	0.00	0.003	0.001	0.003
C161ACPm + MALACPm + 2 NADPHm -> 2 NADPm + C181ACPm + CO2m + ACPm	U_226	0.00	0.0	0.00	0.00	0.00	0.000	0.000	0.000
COAm -> PAPm + ACPm	PPT2 (m)	0.00	0.0	0.00	0.00	0.00	0.000	0.000	0.000
PYRm + LAC -> LACm + PYR	U_227	0.00	0.0	0.00	0.00	0.00	0.000	0.000	0.000
NAD -> NADm	YIA6 (NAD)	0.00	0.0	0.00	0.00	0.00	0.000	0.000	0.000
AMP-> AMPm	YIA6 (AMP)	0.00	0.0	0.00	0.00	0.00	0.000	0.000	0.000
NAD -> NADm	YEA6 (NAD)	0.00	0.0	0.00	0.00	0.00	0.000	0.000	0.000
AMP-> AMPm	YEA6 (AMP)	0.00	0.0	0.00	0.00	0.00	0.000	0.000	0.000
CMPm + CTP -> CMP + CTPm	RIM2	0.00	0.0	0.00	0.00	0.00	0.029	0.010	0.029
IPPP <-> IPPPm	U_228	0.00	0.0	0.00	0.00	0.00	0.000	0.000	0.000
NADH + FUM -> SUCC + NAD	YEL047C	0.01	0.2	0.01	0.01	0.01	0.006	0.006	0.000
GL3P + 0.017 C100COA + 0.062 C120COA + 0.1 C140COA + 0.27 C160COA + 0.169 C161COA + 0.055 C180COA + 0.235 C181COA + 0.093 C182COA -> AGL3P + COA	GPT2 (GL3P)	0.00	0.0	0.00	0.00	0.00	0.000	0.000	0.000
DHAP + 0.017 C100COA + 0.062 C120COA + 0.1 C140COA + 0.27 C160COA + 0.169 C161COA + 0.055 C180COA + 0.235 C181COA + 0.093 C182COA -> ADHAP + COA	GPT2 (DHAP)	0.00	0.0	0.00	0.00	0.00	0.000	0.000	0.000
C100COAm + COA <-> C100COA + COAm	U_229 (C100)	0.00	0.0	0.00	0.00	0.00	0.000	0.000	0.000
C120COAm + COA <-> C120COA + COAm	U_229 (C120)	0.00	0.0	0.00	0.00	0.00	0.004	0.001	0.000
C140COAm + COA <-> C140COA + COAm	U_229 (C140)	0.00	0.0	0.00	0.00	0.00	0.006	0.002	0.002
C160COAm + COA <-> C160COA + COAm	U_229 (C160)	0.00	0.1	0.00	0.00	0.00	0.003	0.006	0.000
C161COAm + COA <-> C161COA + COAm	U_229 (C161)	0.00	0.0	0.00	0.00	0.00	0.000	0.000	0.000
C180COAm + COA <-> C180COA + COAm	U_229 (C180)	0.00	0.0	0.00	0.00	0.00	0.003	0.001	0.003
C181COAm + COA <-> C181COA + COAm	U_229 (C181)	0.00	0.0	0.00	0.00	0.00	0.000	0.000	0.000
GLNm -> GLNt	U_230	0.00	0.0	0.00	0.00	0.00	0.000	0.000	0.000
IPOSUCC -> OICAP + CO2	U_231	0.03	0.6	0.02	0.02	0.02	0.000	0.000	0.000
MLTxt -> MLT	MPH2	0.00	0.0	0.00	0.00	0.00	0.000	0.000	0.000
MLTxt -> MLT	MPH3	0.00	0.0	0.00	0.00	0.00	0.000	0.000	0.000
NADPHm + OGTm -> NADPm + 2 RGTm	GLR1 (m)	0.00	0.0	0.00	0.00	0.00	0.000	0.000	0.000
2 RGTm + H2O2m <-> OGTm	GRX2 (m)	0.00	0.0	0.00	0.00	0.00	0.000	0.000	0.000
PYR -> PYRxt	U_232	0.01	0.2	0.01	0.01	0.01	0.000	0.000	0.000
LAC -> LACxt	U_233	0.08	1.8	0.12	0.12	0.12	0.006	0.006	0.006
LLAC -> LLACxt	U_234	0.00	0.0	0.00	0.00	0.00	0.000	0.000	0.000
C140 + ATP + COA -> C140COA + AMP + PPI	FAA1 (C140)	0.00	0.0	0.00	0.00	0.00	0.000	0.000	0.000
C140 + ATP + COA -> C140COA + AMP + PPI	FAA2 (C140)	0.00	0.0	0.00	0.00	0.00	0.000	0.000	0.000
C140 + ATP + COA -> C140COA + AMP + PPI	FAA3 (C140)	0.00	0.0	0.00	0.00	0.00	0.000	0.000	0.000
C140 + ATP + COA -> C140COA + AMP + PPI	FAA4 (C140)	0.00	0.0	0.00	0.00	0.00	0.000	0.000	0.000
C181ACP + COA <-> C181COA + ACP	U_235	0.00	0.0	0.00	0.00	0.00	0.000	0.000	0.000
C161ACP + COA <-> C161COA + ACP	U_236	0.00	0.0	0.00	0.00	0.00	0.000	0.000	0.000
C100COA + ACP <-> C100ACP + COA	FAS1 / 2 (C100COA)	0.00	0.0	0.00	0.00	0.00	-0.001	0.000	-0.001
C181COA + COA + 2 NAD -> 2 NADH + ACCOA + C161COA	U_237	0.00	0.0	0.00	0.00	0.00	0.010	0.003	0.010
C181COA -> C182COA	U_239	0.00	0.0	0.00	0.00	0.00	0.005	0.002	0.005
C100ACPm + COAm <-> C100COAm + ACPm	U_240	0.00	0.0	0.00	0.00	0.00	0.000	0.000	0.000

C120ACPm + COAm <-> C120COAm + ACPm	U_241	0.00	0.0	0.00	0.00	0.00	0.004	0.001	0.000
C140ACPm + COAm <-> C140COAm + ACPm	U_242	0.00	0.0	0.00	0.00	0.00	0.006	0.002	0.002
C161ACPm + COAm <-> C161COAm + ACPm	U_243	0.00	0.0	0.00	0.00	0.00	0.000	0.000	0.000
C160ACPm + COAm <-> C160COAm + ACPm	U_244	0.00	0.1	0.00	0.00	0.00	0.003	0.006	0.000
C180ACPm + COAm <-> C180COAm + ACPm	U_245	0.00	0.0	0.00	0.00	0.00	0.003	0.001	0.003
C181ACPm + COAm <-> C181COAm + ACPm	U_246	0.00	0.0	0.00	0.00	0.00	0.000	0.000	0.000
C181xt -> C181	U_247	0.00	0.1	0.00	0.00	0.00	0.029	0.010	0.029
PSPH + C260COA -> CER2 + COA	LAG1 (PSPH)	0.00	0.0	0.00	0.00	0.00	0.000	0.000	0.000
PSPH + C260COA -> CER2 + COA	LAC1 (PSPH)	0.00	0.0	0.00	0.00	0.00	0.000	0.000	0.000
PA -> DAGLY + PI	LPP1	0.00	0.0	0.00	0.00	0.00	0.000	0.000	0.000
PA -> DAGLY + PI	PAH1	0.00	0.0	0.00	0.00	0.00	0.000	0.000	0.000
MYOIxt -> MYOI	ITR2	0.01	0.1	0.00	0.03	0.00	0.000	0.000	0.024
COAm -> COAt	U_248	0.00	0.0	0.00	0.00	0.00	0.000	0.000	0.000
COA -> COAt	U_249	0.00	0.0	0.00	0.00	0.00	0.000	0.000	0.000
XYL + NADPH -> XYLOL + NADP	XYL1 (NADPH)	0.00	0.0	0.30	1.50	0.00	0.140	0.324	0.000
XYL + NADH -> XYLOL + NAD	XYL1 (NADH)	0.00	0.0	1.20	0.00	1.50	0.760	0.576	0.900
XYLOL + NADP <-> XUL + NADPH	XYL2 (NADPH)	0.00	0.0	0.00	0.00	0.00	0.000	0.000	0.000
XYLOL + NAD <-> XUL + NADH	XYL2 (NADH)	0.00	0.0	1.20	1.20	1.20	0.760	0.760	0.760
XYLOL <-> XYLOLxt	U_252	0.00	0.0	0.30	0.30	0.30	0.140	0.140	0.140
XYLxt -> XYL	U_253	0.00	0.0	1.50	1.50	1.50	0.900	0.900	0.900
	Objective Function	0.0871		0.0792	0.0677	0.0792	1.188	1.054	1.188

Additional file 3: Specific uptake and release rates as well as biomass yields obtained in anaerobic batch and fed-batch fermentations using strain BP10001. Rates were determined from data acquired in the first 42 h of batch fermentation and in the first 20 h of fed-batch reactions.

Rate [mmol/g CDW/h]	Xylose Batch	Glucose / xylose Fed-Batch	Glucose Fed-Batch
q_{xylose}	0.9 ± 0.1	1.5 ± 0.1	-
$q_{glucose}$	-	3.5 ± 0.3	4.5 ± 0.4
$q_{xylitol}$	0.14 ± 0.01	0.30 ± 0.04	-
$q_{glycerol}$	0.039 ± 0.003	0.27 ± 0.01	0.7 ± 0.1
$q_{acetate}$	0.053 ± 0.005	ND[b]	ND[b]
$q_{ethanol}$	0.9 ± 0.1	7.1 ± 0.3	7.1 ± 0.6
$q_{succinate}$	0.0058 ± 0.0003	0.016 ± 0.001	0.019 ± 0.005
$q_{lactate}$	0.0055 ± 0.0005	0.12 ± 0.01	0.08 ± 0.01
$q_{pyruvate}$	0.0002 ± 0.00005	0.01 ± 0.005	0.007 ± 0.001
q_{CO2}	1.1 ± 0.1	7.9 ± 0.3	7.9 ± 0.7
$Y_{X/S}$ [g/g][a]	0 (0)	0.094 ± 0.003 (0.093)	0.11 ± 0.03 (0.107)

[a] Resultant $Y_{X/S}$ from FBA are indicated in parentheses
[b] ND - not detectable

Additional file 4: Optimization of the HPLC analytic procedure for determination of co-utilization of glucose and xylose. Panel A shows the refractive index trace for a sample from a typical batch fermentation (cf. Figure 2) analyzed using the Aminex HPX-87H column. Overlapping peaks for phosphate-glucose and glucose-xylose are clearly recognized. Therefore, this method was unsuitable for determination of sugar consumption in the phase of the fermentation where glucose and xylose are utilized simultaneously. Determination of q_{xylose} besides the larger $q_{glucose}$ was not reliable. Panel B shows the improved separation when using an Aminex HPX-87C column. A concentration of phosphate of 22 mM did not interfere with determination of glucose. Xylose in a constant concentration of 10 g/L was compatible with measurement of glucose in the concentration range 1 - 10 g/L. The standard deviation on the measured xylose value was 0.02 g/L.